

Light-Driven Reductive Transformations by *Shewanellaceae*

Sam Francis Rowe

PhD thesis, September 2017

University of East Anglia

School of Chemistry

Norwich

United Kingdom

© Sam Francis Rowe, September 2017

This copy of the thesis has been supplied on condition that anyone who consults it is understood to recognise that its copyright rests with the author and that use of any information derived there from must be in accordance with the current UK Copyright Law. In addition, any quotation or extract must include full attribution.

Abstract

The use of finite fossil reserves within the energy and petrochemicals industries has harmful environmental impacts due to the release of CO₂ into the Earth's atmosphere. Consequently, new technologies that harness renewable forms of energy, such as solar energy, are required for the sustainable production of valuable chemicals including fuels. Taking inspiration from plants and photosynthetic micro-organisms, artificial systems are being developed for solar-chemicals production by combining light-harvesting photosensitisers, such as molecular dyes and semiconducting nanoparticles, with electrocatalysts such as purified enzymes and whole-cell bacteria. In particular, whole-cell bacteria have emerged as effective electrocatalysts because they provide opportunities to develop self-regenerating systems that can facilitate multiple chemical transformations.

The work presented in this thesis aimed to develop a cell-based approach to solar-chemicals production where a single micro-organism can act as a multi-faceted electrocatalyst without the requirement for costly and time-consuming enzyme purification. The approach was developed with the non-photosynthetic bacterium *Shewanella oneidensis* MR-1, a model micro-organism for extracellular electron transfer. The system uses methyl viologen as an electron shuttle to transfer photo-energised electrons from water-compatible photosensitisers to bacterial enzymes for H₂-evolution and the reduction of fumarate, pyruvate and CO₂ to succinate, lactate and formate, respectively. Preliminary experiments were also carried out to investigate the possibility of using new-generation carbon dot photosensitisers for light-driven H₂-evolution in the absence of an exogenous electron shuttle. The work was performed in a step-wise manner involving an assessment of the determinants of each system using a range of analytical techniques and the findings form a basis for sustainable cell-based photocatalysis with other species of bacteria or genetically-modified *Shewanella* strains.

Acknowledgements

First and foremost, I would like to thank my supervisor Prof. Julea Butt for her continued support and guidance throughout my PhD. She has consistently been full of excellent ideas for my experimental and written work and I feel I have really grown as a scientist under her supervision. I must also thank the other members of my supervisory team, Prof. Steve Meech and Dr. Nick Watmough, who provided their expertise on a vast range of scientific disciplines to make my PhD work as comprehensive as possible.

Next, I would like to thank the collaborators working on this project who have always provided valuable suggestions and feedback: I must thank Dr. Gwénaëlle Le Gall and Dr. Adam Elliston (Institute of Food Research, UK) for assistance with ^1H -NMR analysis. I must thank the group of Prof. Erwin Reisner (University of Cambridge, UK) including Dr. Bertrand Reuillard and Dr. Benjamin Martindale for providing samples of carbon dots, Dr. Manuela Gross for providing samples of RuP and Dr. Moritz Kuehnel for assistance with calculating quantum yields. I must also thank the group of Dr. Lars Jeuken (University of Leeds, UK) including Ania Wroblewska-Wolna for helpful discussions about quantum dots and light-driven H_2 -evolution. I would also like to acknowledge Dr. Liang Shi (China University of Geosciences, Wuhan) for providing the *Shewanella* mutants, HydA⁻/HyaB⁻ and Mtr⁻, for the work in this thesis.

I am also very grateful to have met and worked with so many wonderful scientists at the University of East Anglia during my PhD. I am especially thankful to Dr. Emma Ainsworth and Dr. Colin Lockwood for welcoming me to the research group and for their patience in getting me started with spectrophotometric assays and culturing bacteria. Beyond the lab work, I will always have great memories of the conferences we went to and the nights out we had to unwind after a long day in lab. I would also like to thank Jack Day for performing experiments during his MChem project which have formed an integral part of the work presented in chapter 6 of this thesis and Dr. Simone Payne for purification of MtrC. I must also thank all the other past and present residents of office 2.24 in CHE and lab 2.30 in BIO who have helped me with experimental work and provided me with some fantastic memories from lab socials. In particular, I would like to thank Michael Norman (who must also be acknowledged for being an amazing housemate during my PhD), Sophie Bennett, Jon Davies and Amy Easey for the great times in and out of lab during my time in Norwich.

Lastly, I must thank all my friends and family who I have undoubtedly taken for granted during my PhD, particularly during my final year when I was concentrating on thesis writing. I will always appreciate how you have been on hand to help me de-stress and I cannot wait to start spending more time with you again.

Table of Contents

Abbreviations and Symbols	9
Chapter 1 - Introduction	15
1.1 General overview	16
1.2 Global challenges associated with the use of finite fossil reserves	16
1.3 Solar energy as a sustainable route to electricity production	21
1.4 Natural photosynthesis as inspiration for the direct production of chemicals and fuels from solar energy	24
1.5 Artificial photosynthesis for H ₂ -evolution, CO ₂ -fixation and chemical synthesis	27
1.5.1 Purified hydrogenases and formate dehydrogenases as electrocatalysts	30
1.5.2 Transition metal complexes as electrocatalysts	34
1.5.3 Whole-cell bacteria as electrocatalysts	36
1.6 Opportunities for developing whole-cell bacteria approaches to artificial photosynthesis	38
1.6.1 Metabolic versatility of <i>Shewanella oneidensis</i> MR-1 may allow for the simultaneous presence of multiple enzymes that catalyse useful reductive transformations	39
1.6.1.1 Hydrogenases	41
1.6.1.2 Fumarate reductase	42
1.6.1.3 Lactate dehydrogenases	43
1.6.1.4 Formate dehydrogenases	45
1.6.2 Outer membrane spanning complexes may provide a route to deliver photo-energised electrons from the outside to the inside of the bacterium	46
1.7 Aims of this thesis	49
Chapter 2 - Materials and Methods	52
2.1 General reagent preparations	53
2.2 Characterisation of irradiation sources	54
2.3 Bacterial growth, characterisation and processing	55
2.3.1 Growth media preparations	55

2.3.2 Strains used in this study	56
2.3.3 Growth conditions	57
2.3.4 Bicinchoninic acid (BCA) assay	57
2.3.5 Colony forming units (CFU)	58
2.3.6 Protein gels and Western blotting	58
2.3.7 Harvesting and re-suspension in a defined buffer	60
2.4 H ₂ detection and quantification	61
2.4.1 Quantification of headspace H ₂ using gas chromatography (GC)	61
2.4.1.1 Method principle and calibration	61
2.4.1.2 Measurement of headspace H ₂	62
2.4.2 Quantification of dissolved H ₂ using a H ₂ -sensing electrode	63
2.4.2.1 Method principle and calibration	63
2.4.2.2 Measurement of dissolved H ₂	65
2.5 Spectrophotometric enzyme assays	66
2.5.1 H ₂ oxidation coupled to benzyl viologen reduction	67
2.5.2 Fumarate- and CO ₂ -reduction driven by dithionite-reduced methyl viologen	67
2.6 Quantification of carbon-based compounds using ¹ H and ¹³ C nuclear magnetic resonance (NMR)	68
Chapter 3 - Anaerobic growth of <i>Shewanella oneidensis</i> MR-1 to catalyse H₂-evolution and reduction of fumarate, pyruvate and CO₂	71
3.1 Introduction	72
3.2 Anaerobic growth of <i>Shewanella oneidensis</i> MR-1 under acceptor-limited conditions	72
3.3 Biochemical assays of hydrogenase, fumarate reductase, lactate dehydrogenase and formate dehydrogenase activities in anaerobically grown <i>Shewanella oneidensis</i> MR-1	74
3.3.1 Hydrogenase activity	75
3.3.2 Reduction of fumarate, pyruvate and CO ₂	79
3.4 Discussion	85
Chapter 4 - Light-driven H₂-evolution by <i>Shewanella oneidensis</i> MR-1	87
4.1 Introduction	88

4.2 Reductive photocatalysis	88
4.2.1 Photosensitisers used in this study	91
4.2.2 Sacrificial electron donors used in this study	94
4.3 Photoreduction of methyl viologen under conditions compatible with <i>Shewanella oneidensis</i> MR-1 enzyme activity	96
4.4 Light-driven H ₂ -evolution by <i>Shewanella oneidensis</i> MR-1 from photo-produced MV ⁺	102
4.4.1 Impact of photosensitiser identity	102
4.4.2 Effect of <i>Shewanella oneidensis</i> MR-1 cell density	105
4.4.3 Effect of pH, light intensity and methyl viologen concentration	106
4.4.4 Viability of <i>Shewanella oneidensis</i> MR-1 after incubation with reagents required for light-driven H ₂ -evolution	110
4.5 Sustained light-driven H ₂ -evolution by <i>Shewanella oneidensis</i> MR-1 from photo-produced MV ⁺	112
4.6 Investigation of the possible role of outer membrane porin:cytochrome complexes in light-driven H ₂ -evolution by <i>Shewanella oneidensis</i> MR-1 from photo-produced MV ⁺	118
4.7 Discussion	122
Chapter 5 - Light-driven reduction of fumarate, pyruvate and CO₂ by <i>Shewanella oneidensis</i> MR-1	128
5.1 Introduction	129
5.2 Effect of fumarate, pyruvate and CO ₂ on light-driven H ₂ -evolution by <i>Shewanella oneidensis</i> MR-1 from photo-produced MV ⁺	129
5.3 Light-driven reduction of fumarate, pyruvate and CO ₂ by <i>Shewanella oneidensis</i> MR-1 from photo-produced MV ⁺	133
5.3.1 Irradiation at an intensity of 0.7 kW m ⁻² for 30 min	137
5.3.2 Irradiation at an intensity of 0.02 kW m ⁻² for 24 hr	138
5.4 Enhancement of light-driven CO ₂ -reduction by <i>Shewanella oneidensis</i> MR-1 from photo-produced MV ⁺	141
5.5 Longevity of the <i>Shewanella oneidensis</i> MR-1 fumarate reductase over 96 hr	145
5.6 Discussion	147

Chapter 6 - Assessment of light-driven H₂-evolution by <i>Shewanellaceae</i> with carbon dot photosensitisers	151
6.1 Introduction	152
6.2 Carbon dot photosensitisers	153
6.2.1 Synthesis and physicochemical properties	153
6.2.2 Photoreduction of electron acceptors under conditions compatible with <i>Shewanella oneidensis</i> MR-1 enzyme activity	156
6.3 Evaluation of <i>Shewanella oneidensis</i> MR-1 and other species of <i>Shewanella</i> for light-driven H ₂ -evolution with carbon dot photosensitisers	158
6.3.1 Genomic comparison of <i>Shewanellaceae</i>	158
6.3.2 Hydrogenase activity of <i>Shewanellaceae</i> after anaerobic, acceptor-limited growth	160
6.3.3 Preliminary assessment of light-driven H ₂ -evolution by <i>Shewanellaceae</i>	162
6.4 Discussion	164
Chapter 7 - Summary and Future Perspectives	167
References	173

Abbreviations and Symbols

All potentials in this thesis are quoted versus the standard hydrogen electrode (SHE).

°	Degree
°C	Celsius
%	Percentage
≈	Approximately equal to
Å	Angstrom (10^{-10} m)
λ	Wavelength
λ _{em}	Emission wavelength of the photosensitiser excited state
ΔAbs _{396nm}	Change in absorbance at 396 nm
ΔAbs _{600nm}	Change in absorbance at 600 nm
ΔH	Change in enthalpy
ε	Extinction coefficient
ε _{BV⁺}	Extinction coefficient for BV ⁺
ε _{MV⁺}	Extinction coefficient for MV ⁺
μ	Micro (10^{-6})
μg	Microgram
μL	Microlitre
μm	Micrometer
μM	Micromolar
ν	Frequency
200	<i>Shewanella putrefaciens</i> 200
A	Absorbance / Amp / Irradiation area
AA	Ascorbic acid
AD	Anno Domini
ADH	Alcohol dehydrogenase
ADP	Adenosine diphosphate
ANA-3	<i>Shewanella</i> ANA-3
aq	Aqueous phase
AQ	Anthraquinone
AQDS	Anthraquinone-2,6-disulfonate

ATP	Adenosine triphosphate
a.u.	Arbitrary units
BCA	Bicinchoninic acid
BCIP	5-bromo-4-chloro-3'-indolylphosphate p-toluidine salt
bpy	2,2'-bipyridine
BSA	Bovine serum albumin
BV	Benzyl viologen
BV ⁺	One-electron reduced form of benzyl viologen
BV ²⁺	Oxidised benzyl viologen
c	Speed of light in a vacuum ($2.998 \times 10^8 \text{ m s}^{-1}$) / Centi (10^{-2}) / Concentration
CB	Conduction band
CDs	Carbon dots
CD-CO ₂ ⁻	Anionic carbon dots
CD-NHMe ₂ ⁺	Cationic carbon dots
CFU	Colony forming units
cm	Centimeter
CN-32	<i>Shewanella putrefaciens</i> CN-32
CoA	Coenzyme A
COSY	Correlation spectroscopy
Cp*	1,2,3,4,5-pentamethylcyclopentadiene
Cys	Cysteine
Cyt c ₆	Cytochrome c ₆
Da	Dalton (g mol^{-1})
DMSO	Dimethyl sulfoxide
DT	(sodium) Dithionite
e ⁻	Electron
<i>E. coli</i>	<i>Escherichia coli</i>
EDTA	Ethylenediaminetetraacetic acid
E _m	Reduction potential
EPS	Extracellular polymeric substances
eV	Electron volt
EY	Eosin Y
F	Oxidised flavin
FAD	Flavin adenine dinucleotide

F _{ald} DH	Formaldehyde dehydrogenase
FccA	Fumarate reductase
FDH, F _{ate} DH	Formate dehydrogenase
FH ₂	Reduced flavin
Fl	Fluorescein
FMN	Flavin mononucleotide
FNR	Ferredoxin-NADP ⁺ -reductase
FocA	Formate transporter
ft	Foot
FWHM	Full width at half maximum
g	Gram / Gaseous phase
<i>g</i>	Earth's gravitational force
GC	Gas chromatography
h	Planck's constant ($6.626 \times 10^{-34} \text{ m}^2 \text{ kg s}^{-1}$)
H ₂ ase	Hydrogenase
HEPES	4-(2-hydroxyethyl)piperazine-1-ethanesulfonic acid
His	Histidine
HMBC	Heteronuclear multiple-bond correlation spectroscopy
HMW	High molecular weight
HOMO	Highest occupied molecular orbital
hr	Hour
HSQC	Heteronuclear single-quantum correlation spectroscopy
hν	Energy from a photon [i.e. Planck's constant (h) x frequency (ν)]
Hz	Hertz
I	Intensity of transmitted light
I ₀	Intensity of incident light
IC	Internal conversion
IM	Inner membrane
IR	Infrared
ISC	Intersystem crossing
J	Joule
k	Kilo (10 ³)
kDa	Kilodalton
kg	Kilogram

kHz	Kilohertz
kJ	Kilojoule
kW	Kilowatt
L	Litre
LB	Lysogeny broth
LDH	Lactate dehydrogenase
LMW	Low molecular weight
LUMO	Lowest unoccupied molecular orbital
m	Meter
M	Molar (mol L ⁻¹) / Mega (10 ⁶)
mA	Milliamp
Me	Methyl group (CH ₃)
MES	2-(N-morpholino)ethanesulfonic acid
mg	Milligram
MHz	Megahertz
min	Minute
MK	Menaquinone
MKH ₂	Menaquinol
mL	Millilitre
mm	Millimeter
mM	Millimolar
mol	Avogadro's constant (6.022 x 10 ²³ mol ⁻¹)
MPA	3-mercaptopropionic acid
MR-1	<i>Shewanella oneidensis</i> MR-1
MR-4	<i>Shewanella oneidensis</i> MR-4
MR-7	<i>Shewanella oneidensis</i> MR-7
ms	Millisecond
mV	Millivolt
MV	Methyl viologen
MV ⁰	Fully reduced methyl viologen
MV ⁺	One-electron reduced form of methyl viologen
MV ²⁺	Oxidised methyl viologen
MW	Molecular weight
n	Nano (10 ⁻⁹)

nA	Nanoamp
N _A	Avogadro's constant (6.022 x 10 ²³ mol ⁻¹)
n/a	Not available
NADH	Nicotinamide adenine dinucleotide
NADPH	Nicotinamide adenine dinucleotide phosphate
NBT	Nitro-blue tetrazolium chloride
N-CD	Nitrogen-doped anionic carbon dots
nd	Not detected
nm	Nanometer
nmol	Nanomol
NMR	Nuclear magnetic resonance
OD _{590nm}	Optical density at 590 nm
OM	Outer membrane
OS185	<i>Shewanella baltica</i> OS185
OS195	<i>Shewanella baltica</i> OS195
OS223	<i>Shewanella baltica</i> OS223
P680	Chlorophyll reaction centre of photosystem II
P700	Chlorophyll reaction centre of photosystem I
PDB ID	Protein data bank (http://www.rcsb.org/pdb) identification number
PF	Proflavine
PfIB	Pyruvate-formate lyase
P _i	Phosphate
PMF	Proton motive force
PMS	Phenazine methosulfate
ppm	Parts per million
PS	Photosensitiser
PS ⁰	Ground state of the photosensitiser
PS*	Photo-excited state of the photosensitiser
PS ⁺	One-electron oxidised state of the photosensitiser
PS ⁻	One-electron reduced state of the photosensitiser
Pta-AckA	Phosphotransacetylase-acetate kinase
PTFE	Polytetrafluoroethylene
PV-4	<i>Shewanella loihica</i> PV-4
PVDF	Polyvinylidene fluoride

rpm	Revolutions per minute
RuP	[Ru(bpy) ₂ (4,4-(PO ₃ H ₂) ₂ bpy)]Br ₂
s	Second
S ₀	Ground state
S ₁ , S ₂	Excited singlet states
SB2B	<i>Shewanella amazonensis</i> SB2B
SDS-PAGE	Sodium dodecyl sulfate polyacrylamide gel electrophoresis
SED	Sacrificial electron donor
SHE	Standard hydrogen electrode
SS	Stainless steel
STC	Small tetraheme cytochrome
t	Irradiation time
T	Tera (10 ¹²)
T ₁ , T ₂	Excited triplet states
TCA	Tricarboxylic acid
TCD	Thermal conductivity detector
TCEP	Tris(2-carboxyethyl)phosphine
TEOA	Triethanolamine
TMAO	Trimethylamine N-oxide
TMBD	3,3',5,5'-tetramethylbenzidine dihydrochloride hydrate
TON	Turnover number
Tris	Tris(hydroxymethyl)aminomethane
TSP	Sodium 3-(trimethylsilyl)-propionate-d ₄
TW	Terawatt
UV	Ultraviolet
V	Volt
VB	Valence band
VR	Vibrational relaxation
[v/v]	[Volume/Volume]
W	Watt
W3-18-1	<i>Shewanella putrefaciens</i> W3-18-1
[w/w]	[Weight/Weight]

CHAPTER 1

Introduction

Chapter 1 - Introduction

1.1 General overview

Fossil reserves are important commodities that currently underpin the supply of global commercially traded energy and the petrochemicals industry. However, they are finite resources and their combustion has detrimental impacts on the environment meaning that sustainable routes to electricity and chemicals production are sought after. One way to achieve this is to harness the near-infinite supply of solar energy reaching the Earth from the sun by taking inspiration from plants and photosynthetic micro-organisms that capture sunlight for the production of complex chemicals including fuels. A variety of artificial systems aiming to improve upon the natural processes have been developed through the combination of light-absorbing photosensitisers and electrocatalysts such as purified enzymes, transition metal complexes and whole-cell bacteria. This chapter reviews the advantages and disadvantages of various approaches to artificial photosynthesis and then describes how the non-photosynthetic bacterium *Shewanella oneidensis* MR-1 (MR-1) is a promising candidate for cell-based photocatalysis because it can produce multiple enzymes that catalyse useful chemical transformations and outer membrane porin:cytochrome complexes that act as electron conduits between the outside and inside of the cell. If MR-1 can be cultured to produce the enzymes of interest, it should be possible to combine the bacterium with abiotic reagents that generate photo-excited electrons to drive the production of commercially-important chemicals.

1.2 Global challenges associated with the use of finite fossil reserves

One of the biggest technological challenges currently facing human civilisation is the requirement to supply enough energy to support a rapidly growing global population without adversely affecting the environment.¹ At the moment, global energy consumption is approximately 17.2 TW and is predicted to rise to 27 TW by 2050 in line with an increase in global population from 7 to 9.4 billion.¹⁻⁴ In 2015, almost 90 % of total global energy

usage was derived from carbon-based fossil reserves such as oil, coal and natural gas, as shown in **Fig. 1.1**.^{4,5}

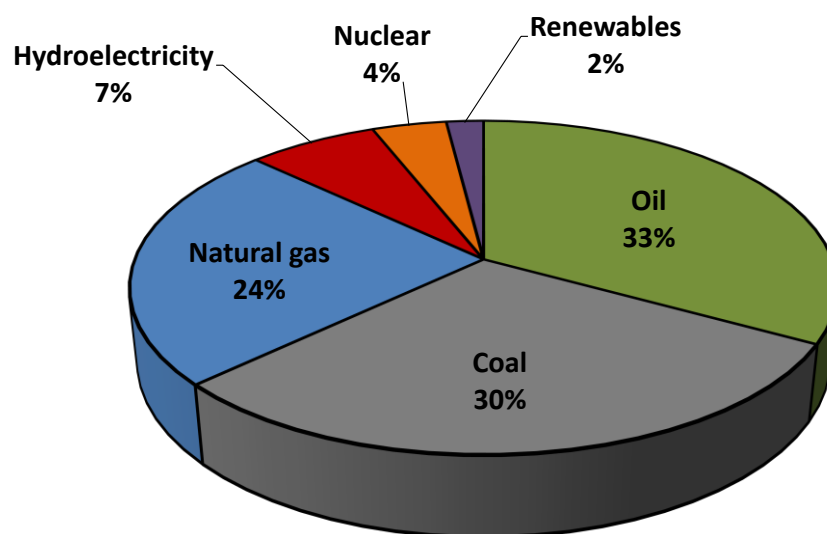


Figure 1.1 - Supply of global commercially traded energy in 2015 by origin. Renewables includes solar, wind, geothermal and biomass. Data from British Petroleum statistical review of world energy: June 2016 (<http://www.bp.com>).

Crude oil, coal and natural gas reserves are formed underground by the influence of extreme heat and pressure on the remains of dead plants and animals that have accumulated in sedimentary layers of rock over millions of years.⁶ As a consequence of the extremely long timescale over which they are created, fossil reserves are rendered non-renewable energy sources and are being consumed 500,000 times faster than they are being made naturally on Earth.² Based on current estimates, coal reserves would be able to cover the present global energy usage for > 110 years whereas oil and natural gas reserves would only cover the usage for approximately 53 and 54 years, respectively.⁴ Although these predictions are likely to fluctuate based on the discovery of new reserves, or the use of previously disregarded reserves such as oil sands in Canada,⁷ the fact remains that there will come a time when the use of oil, coal and natural gas will reach a maximum (known as “peaking”) then begin to decline due to the finite nature of these energy sources.⁸

The combustion of fossil reserves releases energy but also produces carbon dioxide (CO₂),⁹ as shown in **Eq. 1.1** for the combustion of methane (a major constituent of natural gas).^{10,11}



Atmospheric CO₂ levels have been rising since the Industrial Revolution, as shown in **Fig. 1.2A**, but widespread concern about the impact this has on the environment was only expressed after the 1950s due to the improvement of analytical techniques and increase in the number of scientific studies.^{12–15} CO₂ is a greenhouse gas meaning it allows sunlight to penetrate the Earth's atmosphere to reach the surface but blocks outgoing heat. This phenomenon increases surface temperatures and causes a rise in sea levels through ocean thermal expansion and the melting of glaciers and major ice sheets,¹⁶ as shown by the historical changes in globally-averaged temperature anomaly (i.e. change relative to the average global temperatures between 1951 and 1980) and sea level (relative to the level in 1990) presented in **Fig. 1.2B** and **1.2C**, respectively.^{16,17} Within the scientific community, there is an overwhelming consensus (shared by 90 to 100 % of publishing climate scientists) that humans are causing global warming.¹⁸ However, the challenge remains to communicate this information to the wider public and embed effective strategies to combat the detrimental impacts of this reality into future government policy.

The adverse effects of rising global temperatures and sea levels are increased risk of flooding, extreme weather, food insecurity and widespread extinction of plant and animal species.^{19–21} Additionally, elevated levels of CO₂ in the atmosphere have led to ocean acidification through air-sea gas exchange and subsequent chemical transformation to liberate H⁺ ions, as shown in **Eq. 1.2**. Since the pre-industrial era, the average pH of ocean surface water has decreased from 8.21 to 8.10, causing extensive damage to a range of marine organisms such as coral.²² Overall, there are clear, negative consequences related to the combustion of fossil reserves so it is imperative to develop more sustainable technologies for energy production to combat climate change.

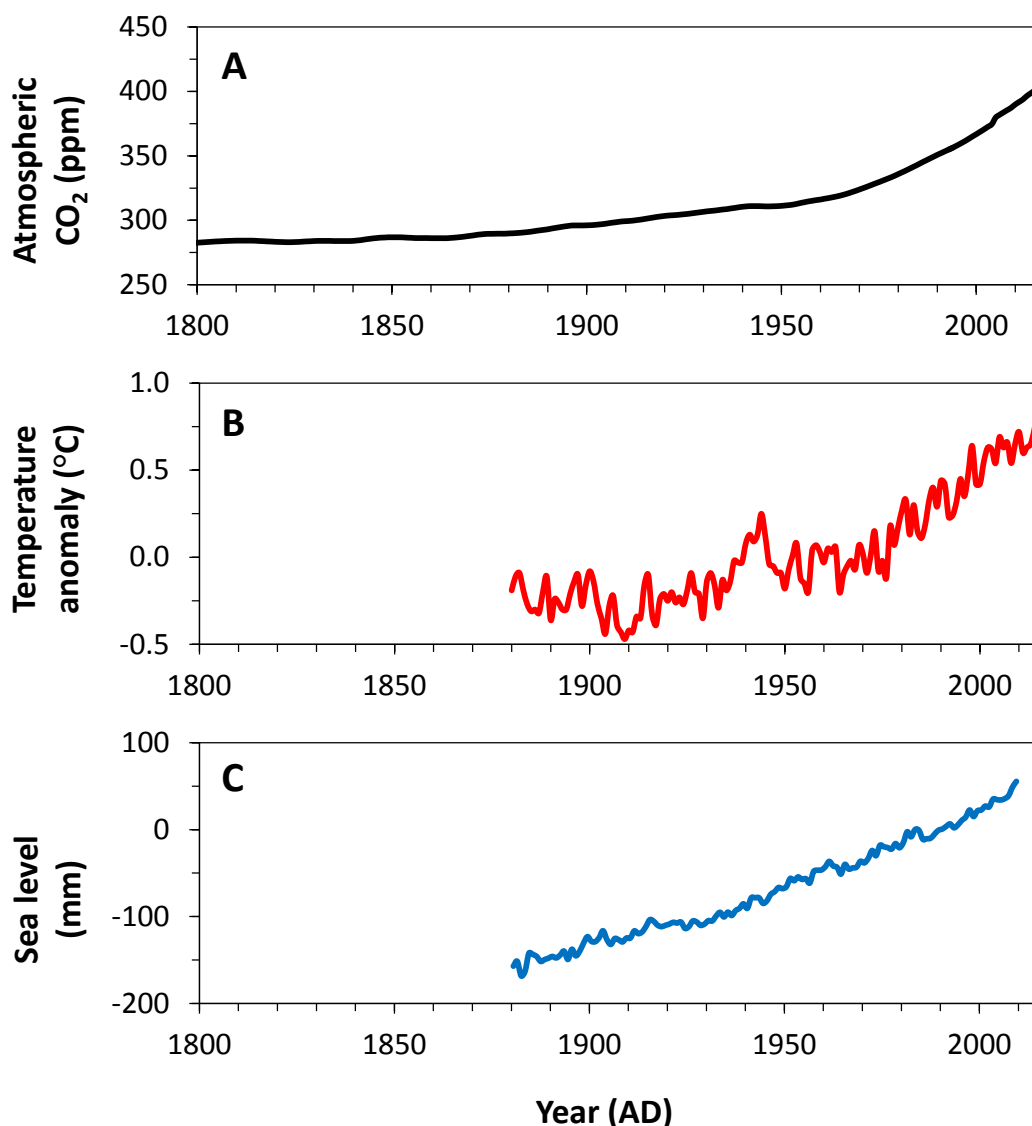
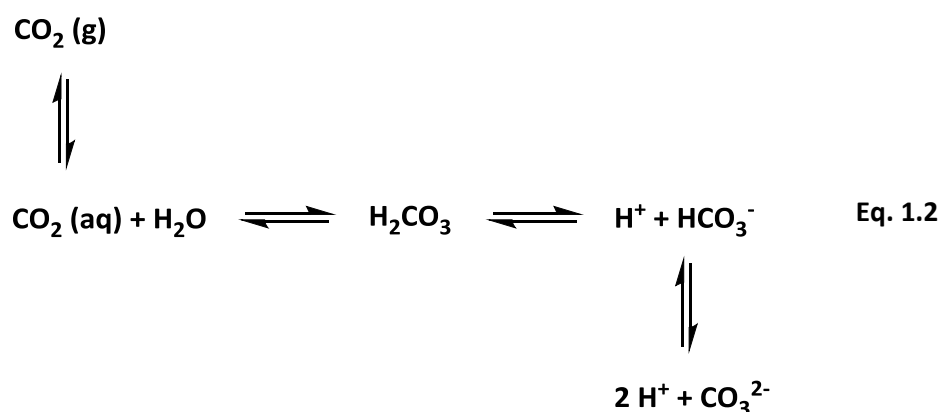


Figure 1.2 - Historical changes in atmospheric CO₂, temperature anomaly and sea level. A) Change in atmospheric CO₂ levels from 1800 to 2016. Data from ice core records (1800 to 2004) at Carbon Dioxide Information Analysis Centre (CDIAC, <http://cdiac.ornl.gov/>) and infrared absorption analysis (2005 to 2016) at National Oceanic and Atmospheric Administration (NOAA, <http://www.noaa.gov/>). B) Combined land (surface air) and sea (surface water) temperature anomaly (change relative to average temperatures between 1951 and 1980) from 1880 to 2016. Data from the NASA Goddard Institute for Space Studies (GISS, <https://www.giss.nasa.gov/>). C) Global average sea level from 1880 to 2009. Value at 1990 is set to zero. Data from Commonwealth Scientific and Industrial Research Organisation (CSIRO) oceans and atmosphere research (<http://www.csiro.au/en/Research/OandA>).



As well as underpinning the supply of global commercially traded energy, fossil reserves can also be transformed into valuable products as part of the petrochemicals industry.^{23,24} For example, crude oil can be refined and used to make plastics, lubricants, surfactants, insecticides and synthetic rubber.^{4,24} Although only 5 to 10 % of crude oil is used for the production of chemicals, these account for approximately 50 % of the profit made by conventional petrochemical refineries.²⁵ As such, it is vital that sustainable routes to chemicals production, in addition to energy production, are developed.

In 2015, only 9 % of global energy usage was derived from renewable sources (see **Fig. 1.1**) such as solar power, wind power, hydropower, geothermal power, biomass-derived power, ocean tidal power and wave power.^{4,5} By 2040, it is predicted that renewables will account for approximately 17 % of global energy usage through a combination of the sources listed above.^{8,26} Each energy source has a particular set of advantages and disadvantages and is typically suited to a specific climate or geographic location.²⁷ For example, wind power is relatively cheap to harvest and produces little air or water pollution but can contribute to soil erosion and is only viable in areas with substantial amounts of wind.²⁷ Similarly, hydropower is safe, abundant and offers the chance to develop recreational activities such as fishing and boating but dams can significantly influence the local hydrology and ecology.²⁷ Of all the renewable energy sources, solar energy is widely considered as one of the most promising due to its near-limitless supply and the fact that it can be used for the production of electricity as well as valuable chemicals including fuels.^{1,4,27} The next section describes the advantages of solar energy then introduces some of the ways in which it can be harnessed and converted into a usable form.

1.3 Solar energy as a sustainable route to electricity production

The sun provides the Earth with solar energy at a rate of approximately 120,000 TW.¹ This means that the energy reaching the planet over the course of two hours corresponds to more than the total annual energy usage of the entire global population. Solar energy is relatively well distributed over the planet and is practically inexhaustible based on the fact that the sun will endure for > 4 billion years.⁴ The average annual power of sunlight at the Earth's surface is 0.17 kW m⁻² and approximately 5 % of light is in the ultraviolet (UV, $\lambda < 400$ nm), 43 % of light is in the visible (400 to 700 nm) and 52 % of light is in the infrared (IR, $\lambda > 700$ nm) region of the electromagnetic spectrum.^{1,28} This is illustrated by the solar irradiance spectrum shown in **Fig. 1.3**.

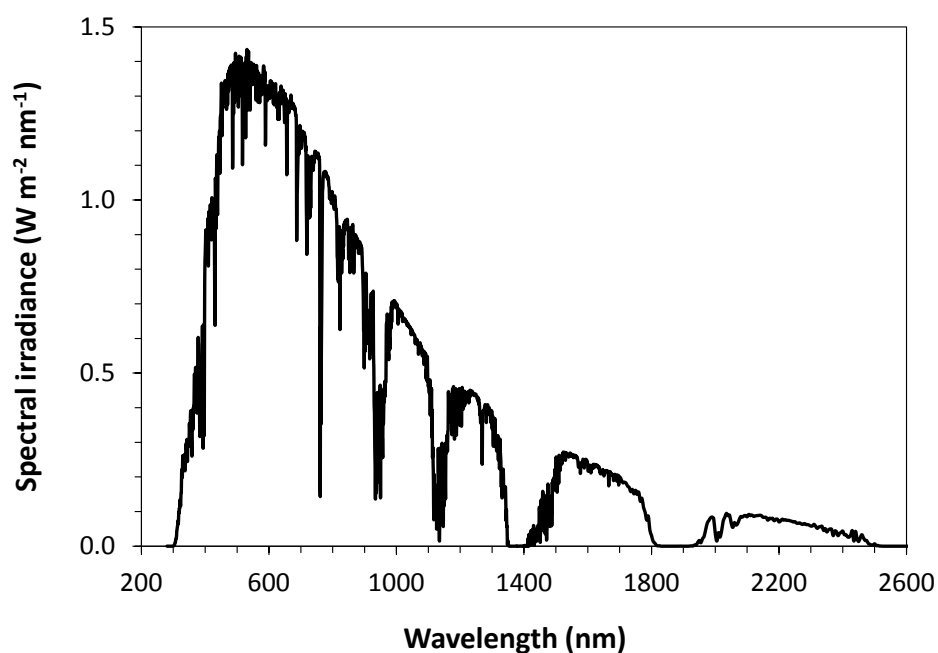


Figure 1.3 - Spectral distribution of sunlight at the Earth's surface. Data from National Renewable Energy Laboratory (NREL, https://www.nrel.gov/rredc/solar_resource.html).

There are a number of ways in which solar energy can be converted into a usable form, for example, through the use of solar water heaters, solar concentrators, photovoltaic devices (solar cells), natural photosynthesis and artificial photosynthesis, as described in **Table 1.1**. In the UK, the photovoltaics sector represents the main technology used for harnessing solar energy.²⁹ Photovoltaic devices work by using a thin layer of a semiconducting material to absorb photons in sunlight for the promotion of an electron to an excited energy state.

This results in the formation of a coulombically-bound electron-hole pair called an exciton which can be used to create an electrical current through charge separation followed by charge transfer to electrodes.³⁰⁻³² These processes are shown in **Fig. 1.4** for a generic light-absorbing donor material interfaced with an acceptor material.

Table 1.1 - Common ways in which solar energy can be captured and converted into a usable form.^{27,29,33,34}

Method	Description
Solar water heater	Panels attached to buildings that capture solar energy to heat water for circulation and/or storage as part of the central heating.
Solar concentrator	An array of lenses and mirrors that reflect sunlight on to a small area to heat molten salts or oils to high temperatures. The heat can be dissipated for electricity production as required.
Photovoltaic device	Semiconducting materials such as crystalline silicon that absorb photons in sunlight and transfer photo-generated charges to electrodes for electricity production (see Fig. 1.4).
Natural photosynthesis	Natural conversion of sunlight into lignocellulosic biomass by plants that can be harvested and either combusted (to release the stored energy) or processed (to create biofuels) (see section 1.4).
Artificial photosynthesis	Systems that mimic and attempt to improve upon the processes behind natural photosynthesis (e.g. light absorption, water-splitting, CO ₂ -reduction) for the production of complex chemicals including fuels (see section 1.5).

Of particular importance to the photovoltaics sector are crystalline silicon devices because they exhibit high photon-to-current conversion efficiencies even within commercially available modules (typical efficiencies are between 15 and 25 %).^{4,30,35} Examples of donor and acceptor materials are phosphorus-doped (n-type) and boron-doped (p-type) silicon, respectively.³⁶ The major drawback of silicon-based solar cells is the high cost of their production due to relatively low manufacturing throughput.^{32,37} As a consequence, organic solar cells containing polymers are being developed because they can be readily processed using solution-based techniques at relatively low temperatures.³⁷ Examples of acceptor materials are buckminsterfullerene (C₆₀) derivatives and donor materials are polymers that incorporate electron-donating moieties such as cyclopentadithiophene.^{30,38} If the current efficiencies of organic solar cells (8 to 11 %) continue to rise, it is likely that they will be able to compete with silicon-based devices on the commercial market for niche applications.^{4,35}

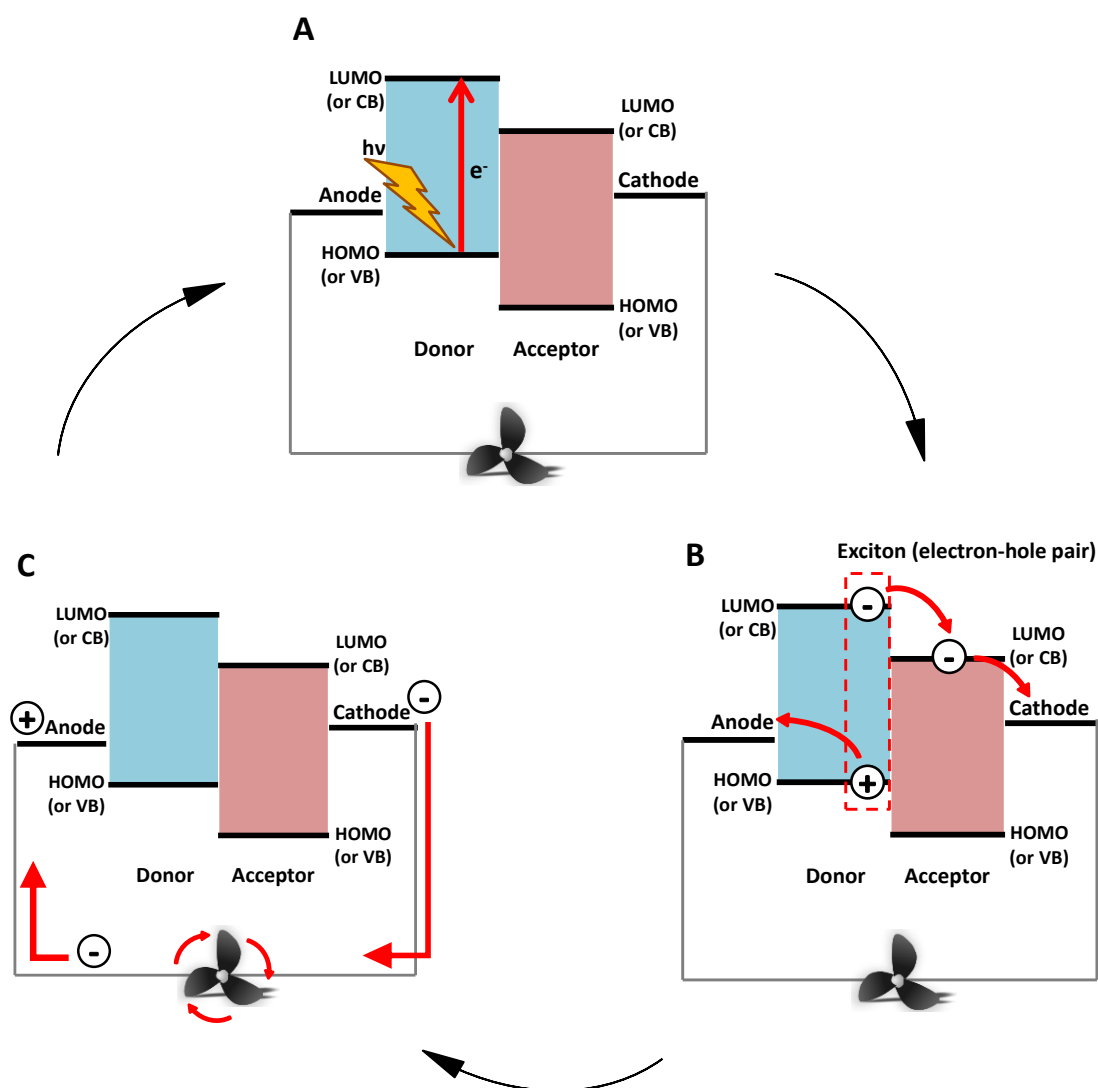
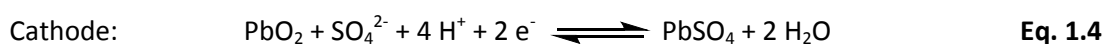
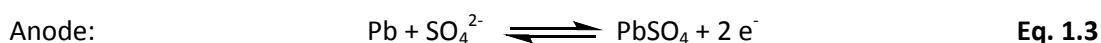


Figure 1.4 - Simplified diagrams for electricity generation using photovoltaic devices. A] Photon ($h\nu$) absorption by a generic donor (blue) promotes an electron from the highest occupied molecular orbital (HOMO), or valence band (VB), to the lowest unoccupied molecular orbital (LUMO), or conduction band (CB). B] Light absorption creates a coulombically-bound electron(-)/hole(+) pair which diffuses to the acceptor (pink) interface where charge separation occurs. Electrons and holes are then transferred to the cathode and anode, respectively. C] Charge recombination takes place after electrons flow from the cathode to the anode via an external circuit.

In the future, photovoltaic devices will undoubtedly be used to cover a major part of global energy usage due to increasing efficiencies and decreasing manufacturing costs.⁴ However, the output from these devices is intermittent as a result of day-night cycles and unpredictable weather meaning another process is typically required to store the electricity for when the sun is not shining.³⁹ One way to achieve this is to convert electrical energy into chemical energy by applying an external voltage to a battery (an electrochemical cell comprised of an electrolyte and two electrodes) to drive electrochemical reactions.⁴⁰

These reactions can then be reversed to discharge a flow of electrons by connecting the battery to a circuit. One of the oldest and most widely used batteries are lead-acid devices which contain lead metal and lead oxide electrodes with concentrated sulphuric acid as electrolyte.⁴¹ The electrochemical reactions that take place at the anode and cathode are shown in **Eq. 1.3** and **1.4**, respectively. Lead-acid batteries are versatile devices with typical efficiencies of > 60 %.⁴¹ However, they contain toxic materials and suffer from short life cycles and low energy densities.⁴¹ More recently, lithium-ion devices have shown great promise due to their superior energy densities and stabilities in comparison to traditional batteries and they are increasingly being used to power portable electronic devices as well as the next generation of electric vehicles.^{40,41} Current research in this area is focussed on the development of novel materials and device architectures to make large scale deployment as economically viable as possible.



Another way to overcome the problem of intermittent sunlight is to harvest solar energy for the direct conversion of cheap, abundant feedstocks into valuable chemicals and fuels which can be readily stored, distributed and consumed as required. These systems take inspiration from the natural processes performed by plants and photosynthetic micro-organisms.^{3,33} The next sections give an overview of natural photosynthesis then discuss artificial approaches to light-driven chemical synthesis.

1.4 Natural photosynthesis as inspiration for the direct production of chemicals and fuels from solar energy

During natural plant photosynthesis, solar energy is harvested for the generation of photo-energised electrons which drive the production of nicotinamide adenine dinucleotide phosphate (NADPH) and adenosine triphosphate (ATP). These molecules are then used to generate a multitude of complex chemicals via CO₂-fixation, as summarised in **Fig. 1.5**.³ Certain photosynthetic micro-organisms can also deliver photo-energised

electrons to enzymes that catalyse the production of versatile chemical fuels such as H_2 (the properties of which are described in greater detail in section 1.5).^{28,42}

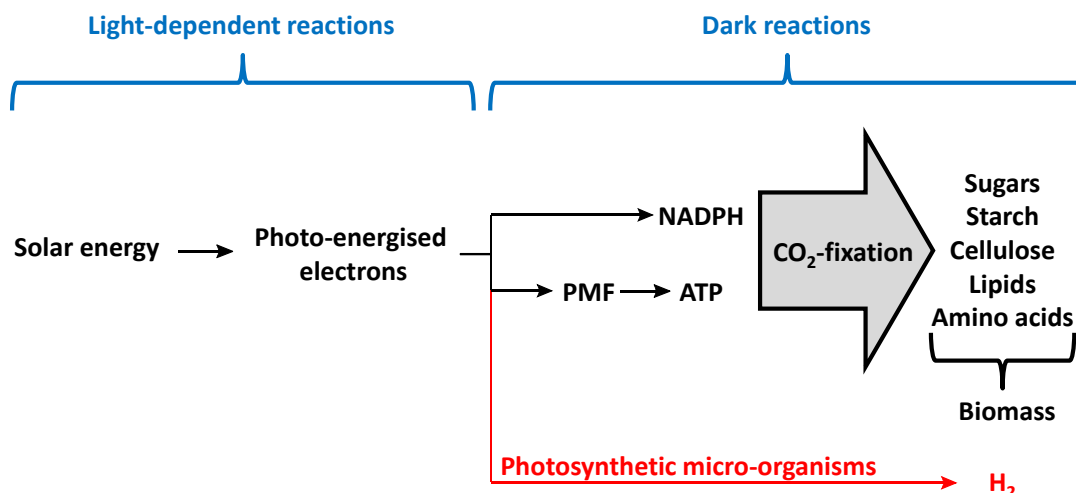


Figure 1.5 - Schematic diagram for the processes that underpin natural plant photosynthesis. Solar energy is used to produce photo-energised electrons which drive the formation of NADPH and a proton motive force (PMF) for ATP synthesis. NADPH and ATP are then used for CO_2 -fixation. Some photosynthetic micro-organisms can also catalyse the production of H_2 .

In plants, the light-dependent reactions occur within chloroplasts on thylakoid membranes containing protein complexes for photon absorption (photosystems I and II) and charge transport.³ Light-harvesting is achieved using an array of antennae molecules such as carotenoids (conjugated isoprene units)² and chlorophylls (magnesium(II) porphyrins and chlorins)⁴³ which transfer energy to specific chlorophyll reaction centres (called P700 and P680 for photosystems I and II, respectively) where charge separation occurs. Photo-excited electrons then initiate a series of redox reactions which result in the formation of NADPH and a proton motive force (PMF) for ATP synthesis (through the action of the ATP synthase).²⁸ Electrons are donated to the system through water-splitting which is facilitated by a catalytic cluster (embedded in photosystem II) comprised of four manganese ions and one calcium ion.³ The light-dependent processes can be summarised as a “Z-scheme”, as shown in **Fig. 1.6**. Photo-produced NADPH and ATP are then used within a series of light-independent (dark) reactions such as the Calvin cycle (where CO_2 is reduced to triose phosphates) to ultimately generate the diverse range of organic molecules that make up living organisms (collectively known as biomass).^{28,43} Overall, these processes represent a way to access complex chemicals from relatively simple feedstocks (i.e. H_2O and CO_2) through the capture and transformation of solar energy.

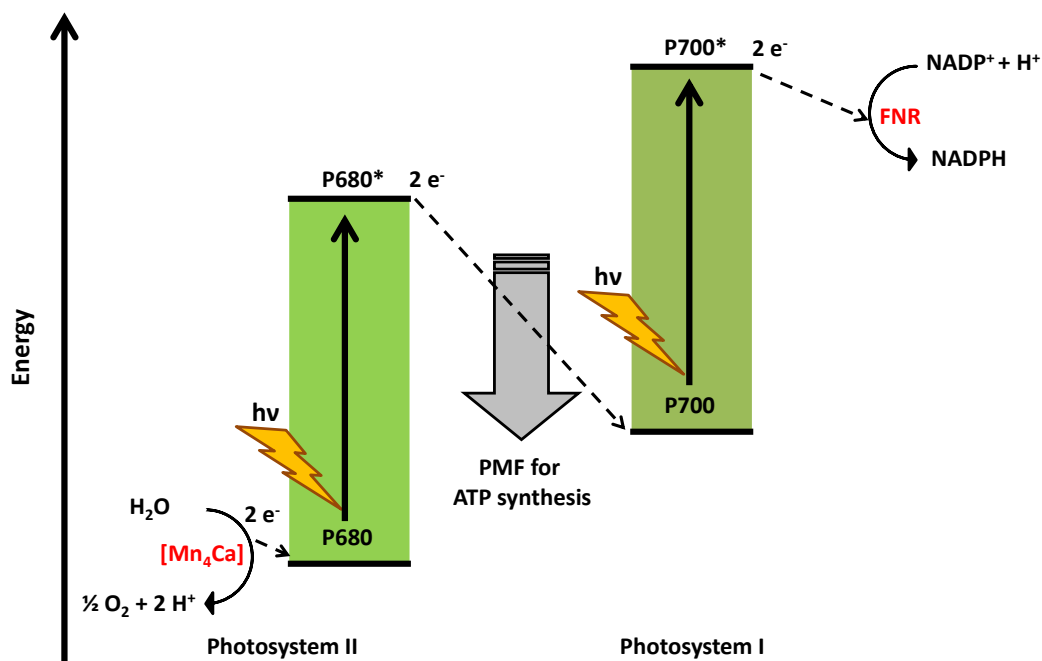


Figure 1.6 - Simplified Z-scheme for the light-driven electron transport chain in plant photosynthesis. Photosystems I and II absorb photons ($h\nu$) for charge separation at the P700 and P680 reaction centres, respectively. The ensuing redox cascades generate NADPH through the action of the ferredoxin-NADP⁺-reductase (FNR) and a proton motive force (PMF) for ATP synthesis. Electrons are donated to the system via a water-splitting manganese-calcium cluster $[Mn_4Ca]$ that forms part of photosystem II.

There are opportunities to exploit natural plant photosynthesis for the sustainable production of biomass (which can be combusted to produce heat or processed into biofuels such as bioethanol)²⁷ but there are some drawbacks associated with doing this. One disadvantage is the fact that the theoretical maximum efficiency of photosynthesis is only 4.6 % despite the quantum efficiencies (i.e. proportion of photons used to generate a charge-separated state) of the light-harvesting apparatus typically exceeding 90 %.^{2,44} In reality, however, it is unusual for dry matter yields to surpass 1 %, even under optimised conditions such as the intensive growth of sugar cane in tropical environments.³ This is because the energy required for water-splitting and CO_2 -fixation corresponds to photons with wavelengths in the red part of the electromagnetic spectrum (ca. 690 nm) and, although higher energy photons can be absorbed, surplus energy is dissipated as heat.³ This means that the growth of plants for biomass is rarely economically viable.²⁷ Furthermore, there are concerns that edible feedstocks such as grain are better used as food rather than for energy or biofuel production.⁴

It is also possible to exploit the natural processes performed by photosynthetic micro-organisms where solar energy is captured for the enzymatic production of chemical fuels such as H₂.^{28,42} For example, light-driven H₂-evolution by the green alga *Chlamydomonas reinhardtii* can be induced by removal of sulphur from growth medium, with maximal H₂ production rates of 11.1 mL H₂ hr⁻¹ (L culture)⁻¹ (reactor volumes ≤ 1.1 L) reported previously.^{45,46} However, these rates of H₂-evolution are not sustainable because sulphur-deprivation has negative effects on the survival, growth and light-harvesting capacity of the micro-organisms.^{46,47} Additionally, expanding the methodology for larger-scale H₂ production (reactor volumes > 50 L) is problematic due to decreases in efficiency under non-optimised conditions (e.g. natural sunlight vs. simulated irradiation) as well as strict requirements for anaerobicity, sterility and pH control.^{45,48}

To overcome the challenges described above, there has been a focus on the development of artificial systems that attempt to mimic and improve upon the outcomes of natural photosynthesis (i.e. light-driven chemical synthesis). The next section introduces artificial photosynthesis then describes two chemical transformations of particular importance to this area of research.

1.5 Artificial photosynthesis for H₂-evolution, CO₂-fixation and chemical synthesis

The general concept behind artificial photosynthesis can be visualised as an optimised redox cascade based on that which operates during natural photosynthesis, as shown in **Fig. 1.7**. A light-absorbing photosensitiser is used to harvest solar energy and transfer photo-energised electrons to an electrocatalyst that performs a reductive chemical transformation. For this process to take place, electrons are transferred to the photosensitiser from an electron donor such as an electrode, a catalyst that performs water-splitting or a chemical reducing agent referred to as a sacrificial electron donor (SED).^{1,2,49} The latter example is used extensively within systems for artificial photosynthesis because a range of small, simple molecules (such as tertiary aliphatic amines) can be employed as SEDs.⁴⁹ Two products of particular interest are H₂ (from the reduction of protons) and formate (from the reduction of CO₂) because they are both valuable fuels and platform chemicals derived from abundant substrates (see below).^{50,51}

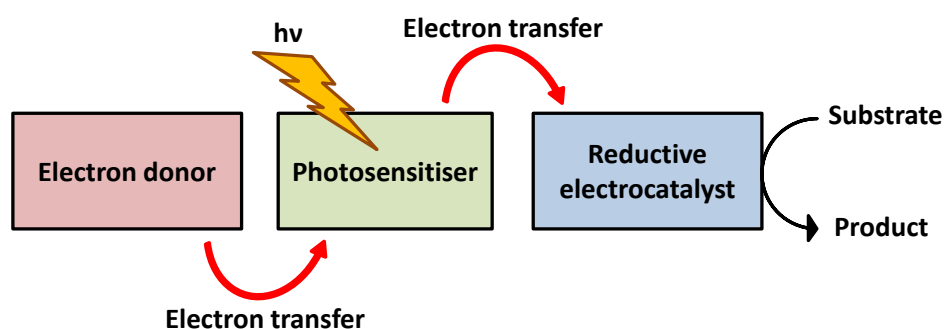


Figure 1.7 - Schematic diagram for artificial photosynthesis. A photosensitiser absorbs photons ($h\nu$) for promotion of an electron to an excited state. This is followed by electron transfer to an electrocatalyst that performs a reductive chemical transformation. Electrons are typically supplied to the photosensitiser by an electrode, a catalyst that splits water or a SED.

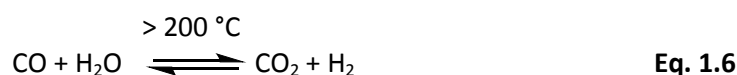
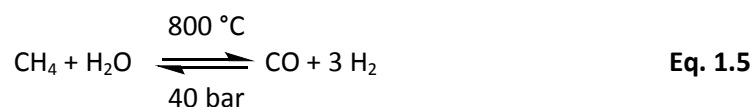
H_2 is a versatile energy carrier with the highest gravimetric energy density of any fuel, as highlighted in **Table 1.2**. It can act as a store for electricity (which can be released using a fuel cell, with water as the only byproduct) to overcome the problem of intermittent sunlight and is an important commodity for a number of industrial procedures.⁴ For example, H_2 can be combined with N_2 as part of the Haber-Bosch process to make ammonia for fertiliser production or combined with carbon monoxide to produce long chain hydrocarbons (such as synthetic petrol and diesel) through Fischer-Tropsch chemistry.^{4,42,52}

Table 1.2 - Approximate gravimetric energy densities of common fuels.¹¹

Fuel	Gravimetric energy density ($MJ\ kg^{-1}$)
Hydrogen	142
Methane	56
Gasoline	47
Diesel	45
Coal	15 - 27
Wood	15

H_2 is currently produced on a large scale through the steam reformation of methane followed by the water-gas shift reaction, shown in **Eq. 1.5** and **1.6**, respectively.^{4,42} These processes are relatively cost-effective but rely on a non-renewable feedstock and transition metal catalysts as well as high temperatures and pressures.^{4,42} The water-gas

shift reaction has the added disadvantage of producing CO₂ as a side product. As such, more sustainable routes to H₂ production need to be developed.



The light-driven reduction of CO₂ to formate is an important chemical transformation for a number of reasons. First, the reaction achieves the removal of a potent greenhouse gas from the atmosphere which could help to combat the detrimental effects of climate change caused by the combustion of fossil reserves (see section 1.2). Secondly, the reaction represents the storage of H₂ as a liquid which is easier to handle and transport than gaseous H₂.⁵³ Formate can be used directly in fuel cells to produce an electrical current or the H₂ stored within formate can be released on demand using transition metal catalysts.⁵⁴ Lastly, formate (or formic acid) is a versatile commodity with applications in the textiles industry and as an antibacterial additive in livestock feeds.⁵⁵ It can also be used to produce other chemicals. For example, the sequential reduction of CO₂ to methanol via formic acid and formaldehyde has been reported previously using three nicotinamide adenine dinucleotide (NADH)-dependent enzymes encapsulated within a porous matrix.⁵⁶ A schematic diagram for this system is shown in **Fig. 1.8**.

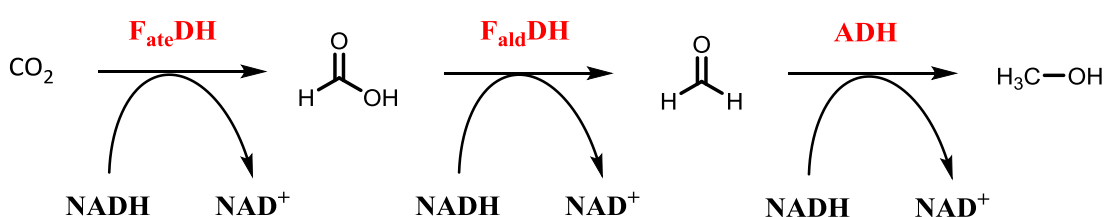


Figure 1.8 - Schematic diagram for the enzymatic reduction of CO₂ to methanol. F_{ate}DH = formate dehydrogenase, F_{alid}DH = formaldehyde dehydrogenase, ADH = alcohol dehydrogenase.

The predominant industrial process for the generation of formic acid involves the combination of carbon monoxide and methanol at high pressures and temperatures in the presence of a strong base.^{54,55} As a consequence, new technologies for formic acid production that operate under milder conditions are sought after.

Early approaches to artificial photosynthesis achieved light-driven reduction of protons to H_2 using homogeneous systems containing colloidal metal (e.g. platinum, palladium and gold) electrocatalysts.⁴³ SEDs such as ethylenediaminetetraacetic acid (EDTA) or N-phenylglycine were used as a source of electrons, photosensitisers such as $\text{Ru}(\text{bpy})_3^{2+}$ (where bpy is 2,2'-bipyridine) were used for light absorption and experiments were typically carried out in aqueous solutions due to the availability of protons.^{57,58} Many of these systems also used small, redox-active molecules such as methyl viologen (MV) which can cycle between the fully oxidised form (MV^{2+}) and one-electron reduced form (MV^+) to shuttle electrons from the photosensitiser to the electrocatalyst.⁵⁸ Recently, more sophisticated approaches to light-driven H_2 -evolution have been developed using purified enzymes or transition metal complexes as electrocatalysts to avoid the requirement for rare and expensive metal colloids.⁴³ These advances have also provided the opportunity to expand the repertoire of chemical transformations to include photocatalytic CO_2 -reduction to formate and other valuable products. The next sections describe the advantages and disadvantages of using purified enzymes and transition metal complexes as electrocatalysts for artificial photosynthesis then discuss how whole-cell bacteria may offer routes to improved solar-chemicals production. More detailed information about the role and function of photosensitisers and SEDs for reductive photocatalysis is provided at the beginning of chapter 4.

1.5.1 Purified hydrogenases and formate dehydrogenases as electrocatalysts

Hydrogenase and metal-dependent formate dehydrogenase enzymes underpin metabolism in a range of micro-organisms by catalysing the reversible interconversion of protons to H_2 and CO_2 to formate, respectively.^{59,60} Although the two enzymes catalyse different chemical transformations, they are similar with respect to their structural organisation, as shown in **Fig. 1.9** with representative enzymes. In general, the enzymes contain two distinct subunits: one with a series of iron-sulphur clusters for electron transfer and one with a buried active site for catalysis.^{60,61} Hydrogenases typically have active sites comprising a nickel atom and an iron atom ([NiFe]-hydrogenases) or two iron atoms ([FeFe]-hydrogenases) whereas metal-dependent formate dehydrogenases have active sites based on molybdenum or tungsten.^{60,62} Chemical structures of the different active sites are shown in **Fig. 1.10**.^{60,63,64} During reductive catalysis *in vivo*, electrons derived from

metabolism are delivered to the distal iron-sulphur cluster then rapidly transferred to the active site. In artificial systems, the purified enzymes must be combined with reagents that harvest solar energy and supply the chain of redox centres with photo-energised electrons.

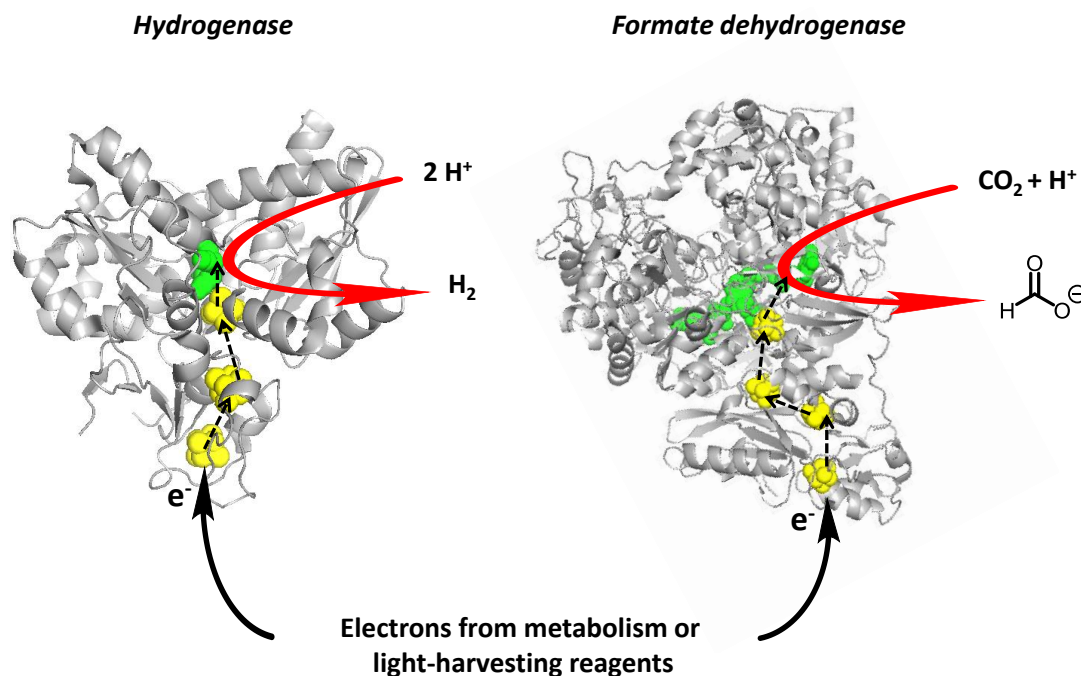


Figure 1.9 - Representative hydrogenase and formate dehydrogenase structures. Electrons derived from metabolism or light-harvesting reagents are transferred to the active site (green) via iron-sulphur clusters (yellow). Crystal structures for the [FeFe]-hydrogenase from *Desulfovibrio desulfuricans* (PDB ID: 1HFE) and the W-containing formate dehydrogenase from *Desulfovibrio gigas* (PDB ID: 1H0H). Images rendered with PyMOL software.

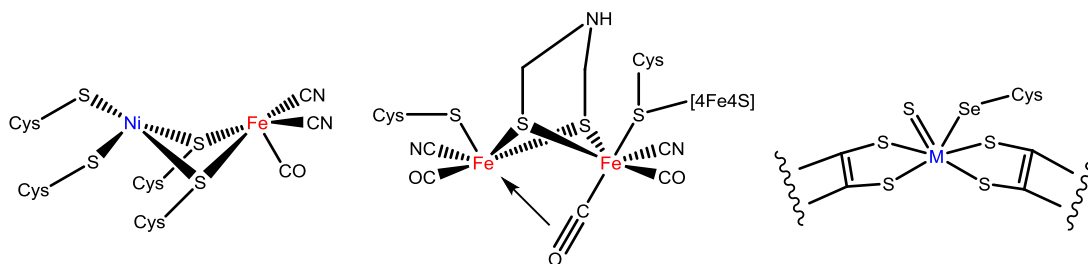


Figure 1.10 - Chemical structures for the active sites of [NiFe]-hydrogenases (left), [FeFe]-hydrogenases (middle) and metal-containing formate dehydrogenases (right). Cys = cysteine, [4Fe4S] = iron-sulphur cluster, M = Mo or W.

Examples of artificial photosynthesis with purified enzymes are described below to highlight some of the ways in which light-driven H_2 -evolution and CO_2 -reduction can be performed. This is followed by a more general overview of the advantages and disadvantages of such systems. Experimental details including schematic diagrams for each example are provided in **Table 1.3**. Example A⁶⁵ in **Table 1.3** involves a mediated approach

to photocatalytic formate production where electron transfer from the photosensitiser to the NADH-dependent formate dehydrogenase proceeds via multiple redox reactions involving regeneration of the NADH cofactor. This system is relatively complex and reliant on the diffusion of each component for electron exchange. Example B⁶⁶ in **Table 1.3** achieves direct electron transfer from the photosensitiser to the [FeFe]-hydrogenase for H₂-evolution by chemically-linking the two components. This system shows remarkable stability over 64 days (samples held at room temperature with ambient light under non-turnover conditions) but requires a combination of SEDs to achieve the highest rates of photocatalytic H₂ production as well as genetic manipulation of the photosensitiser and enzyme for attachment of the chemical linker. Example C⁶⁷ in **Table 1.3** achieves light-driven H₂-evolution through attachment of the photosensitiser to the [NiFe]-hydrogenase with only EDTA as the SED. Despite their close proximity, however, direct electron transfer between the photosensitiser and the enzyme does not occur and a high concentration of MV as an electron transfer mediator is required to facilitate photocatalytic H₂-evolution.

In general, the use of purified enzymes for artificial photosynthesis takes advantage of their high catalytic turnover rates and specificities which are displayed under relatively mild conditions (i.e. in aqueous solutions with near-neutral pH at ambient temperatures) and match or exceed those of noble metals.^{59,68} As an example, the rate of H₂ oxidation by the [NiFe]-hydrogenase from *Allochromatium vinosum* matches that of platinum.⁶⁹ Additionally, an increasing number of photocatalytic transformations can be targeted as new enzymes are isolated and interfaced with photosensitisers, as shown in a number of recent publications.^{1,42,62,68,70} This includes CO₂-reduction to carbon monoxide and methanol (both valuable fuels and feedstocks) using carbon monoxide dehydrogenases and alcohol dehydrogenases, respectively, as well as O-dealkylation reactions using cytochrome P450 enzymes (versatile mono-oxygenases involved in the synthesis of numerous complex chemicals including vitamins, steroids and fatty acids).^{62,70,71} However, there are a number of drawbacks associated with using purified enzymes for solar-chemicals production. For example, there is a time and cost associated with the isolation of enzymes and there may be a requirement for genetic manipulation or the addition of exogenous cofactors such as NADH to achieve photocatalysis.^{65,66,68} As a result, research has also focussed on the use of transition metal complexes as electrocatalysts because they can be readily created and modified using synthetic chemistry.^{1,33,43}

Table 1.3 - Examples of artificial photosynthesis with purified enzymes as electrocatalysts from Yadav et al. (2012) (A), Lubner et al. (2010) (B) and Zadornyy et al. (2012) (C). TEOA = triethanolamine, hv = photon, AQ = anthraquinone, $[\text{Rh}]^{\text{OX/RED}} = [\text{Cp}^*\text{Rh}(\text{bpy})\text{H}_2\text{O}]^{2+}$ where Cp* = 1,2,3,4,5-pentamethylcyclopentadiene, NADH = nicotinamide adenine dinucleotide, Cyt c₆^{OX/RED} = cytochrome c₆, AA = ascorbic acid, PMS = phenazine methosulfate, EDTA = ethylenediaminetetraacetic acid, MV = methyl viologen.

	Schematic diagram	pH	Irradiation conditions	Product formation rate
A		7	Visible light irradiation ($\lambda > 420 \text{ nm}$) for 2 hr with continuous flow of CO_2 (flow rate = 0.5 mL min^{-1})	$55 \mu\text{mol formate hr}^{-1}$
B		8.3	Broad spectrum white light	$30.3 \pm 0.8 \text{ mol H}_2 \text{ hr}^{-1}$ (mg chlorophyll) ⁻¹
C		5.5	150,000 lx Xenon lamp	$121 \pm 1 \text{ mol H}_2 \text{ min}^{-1}$ (mg hydrogenase) ⁻¹

1.5.2 Transition metal complexes as electrocatalysts

In this section, further examples of artificial photosynthesis for H₂-evolution and CO₂-reduction are described to showcase the use of transition metal complexes as electrocatalysts and highlight their advantages and disadvantages. Experimental details including schematic diagrams are shown in **Table 1.4**. Example A⁷² in **Table 1.4** uses a diffusion-controlled approach to photocatalytic H₂-evolution with a synthetic [FeFe]-hydrogenase mimic as an electrocatalyst. The complex is compatible with aqueous solutions through the attachment of long ether chains but does not operate effectively under pH neutral conditions. In contrast, example B⁷³ in **Table 1.4** achieves light-driven H₂-evolution by anchoring the photosensitiser and the cobalt electrocatalyst to titanium dioxide for rapid electron transfer via the conduction band of the nanoparticles. The system readily self-assembles and shows optimal performance at pH 7 but suffers from significant decreases in activity after 6 hr irradiation due to photo-instability of the metal complexes. Example C⁷⁴ in **Table 1.4** uses anchoring groups to connect the ruthenium electrocatalyst to light-harvesting photosensitiser nanoparticles which can directly transfer electrons to the electrocatalyst for the photo-production of formate.

In general, transition metal complexes are suitable electrocatalysts because they exhibit high catalytic turnover rates and are amenable to chemical synthesis such that a range of metal centres, structures and ligands can be readily evaluated to optimise performance, as highlighted in a number of recent review articles.^{1,2,43,75,76} Additionally, their photophysical properties can be assessed using kinetic and spectroscopic techniques to further understand the mechanisms of electron transfer and catalysis for the design of better systems. The main disadvantage of using transition metal complexes as electrocatalysts is the relative cost and scarcity of certain metals, such as ruthenium, meaning that carrying out light-driven chemical transformations on a large scale may not be economically viable.¹ Although transition metal complexes can also be based on Earth-abundant metals, such as iron, synthetic routes can be relatively time-consuming and the complexes may suffer from poor long-term stability.^{1,2} To overcome these problems, as well as the problems associated with using purified enzymes, recent work has focussed on the use of whole-cell bacteria as electrocatalysts. These systems are discussed in the next section to show how they provide opportunities for sustained light-driven chemical synthesis and the formation of a wide range of products.

Table 1.4 - Examples of artificial photosynthesis with transition metal complexes as electrocatalysts from Wang et al. (2011) (A), Lakadamyali et al. (2011) (B) and Sato et al. (2010) (C). AA = ascorbic acid, hv = photon, MPA-CdTe = 3-mercaptopropionic acid capped cadmium telluride, L = cyanide group attached to long ether chains, TEOA = triethanolamine, CB = conduction band, VB = valence band, N-Ta₂O₅ = nitrogen-doped tantalum oxide, TON = turnover number with respect to the amount of catalyst.

	Schematic diagram	pH	Irradiation conditions	TON
A		4	Visible light irradiation ($\lambda > 400$ nm) for 10 hr	505
B		7	Visible light irradiation ($\lambda > 420$ nm) for 8 hr at an intensity of 1 kW m^{-2}	53 ± 4
C		-	Visible light irradiation ($410 \leq \lambda \leq 750$ nm) for 8 hr	89

1.5.3 Whole-cell bacteria as electrocatalysts

Artificial photosynthesis with whole-cell bacteria draws on the fact that micro-organisms naturally produce a wealth of metabolic machinery (e.g. enzymes for catalysis, proteins for electron transfer) during growth.⁷⁷⁻⁸¹ This can be exploited for light-driven chemical synthesis by combining micro-organisms with reagents that generate photo-energised electrons (or photo-produce simple molecules such as H₂) and deliver them to intracellular enzymes. Examples of whole-cell photocatalysis are discussed below to show how this can be achieved. Experimental details including schematic diagrams are provided in **Table 1.5**.

Example A⁸² in **Table 1.5** uses a hydrogenase-producing *Escherichia coli* (*E. coli*) strain to facilitate light-driven H₂-evolution over 15 hr with extracellular titanium dioxide nanoparticles for absorption of UV light. Here, electron transfer from the photosensitiser to intracellular hydrogenases is mediated by MV that shuttles photo-excited electrons across the bacterial outer membrane. Example B⁷⁷ in **Table 1.5** uses *Moorella thermoacetica* for the production of acetic acid under visible light irradiation. Light absorption is achieved using biologically-precipitated cadmium sulphide nanoparticles and electron transfer is directly linked to central metabolism meaning that acetic acid can be generated without compromising on the survival of the micro-organism. Example C⁷⁹ in **Table 1.5** uses an inorganic water-splitting device and *Ralstonia eutropha* for the reduction of CO₂ to either biomass (with the wild-type bacterium) or isopropanol (with a genetically-engineered strain). H₂ generated by the water-splitting device is transferred to the bacterium then oxidised by intracellular hydrogenases to produce NADPH for CO₂-reduction. The main disadvantage of the system is the production of reactive O₂ species at the cathode which hinder bacterial growth. Recently, this problem has been overcome by using a biocompatible cathode made from a cobalt phosphorus alloy.⁸⁰ In combination with genetically-engineered strains of *Ralstonia eutropha*, the new system can generate fusel alcohols (such as isobutanol and 3-methyl-1-butanol) with solar-to-product (quantum) yields of > 7 % (assuming the electricity required for water-splitting came from a photovoltaic device with 18 % efficiency), exceeding those of natural photosynthesis.⁸⁰ Overall, these examples show that whole-cell bacteria provide an excellent platform for the sustainable production of valuable products. In the next section, the key aspects of these systems are summarised to introduce the approach to solar-chemicals production that was developed in this thesis.

Table 1.5 - Examples of artificial photosynthesis with whole-cell bacteria as electrocatalysts from Honda et al. (2016) (A), Sakimoto et al. (2016) (B) and Torella et al. (2015) (C). AA = ascorbic acid, hv = photon, MV = methyl viologen, H₂ase = hydrogenase, Cys = cysteine, P_i = phosphate, SS = stainless steel, NADPH = nicotinamide adenine dinucleotide phosphate.

	Schematic diagram	pH	Irradiation conditions	Quantum yield (%)
A	<p>Diagram A shows a TiO₂ photocatalyst under 2 photons (2 hv) generating 2 electrons (2 e⁻). These electrons reduce MV²⁺ to MV⁺. MV⁺ then reduces H₂ase in <i>Escherichia coli</i>, which produces H₂ from 2 H⁺. Ascorbic acid (AA) is oxidized to AA⁺.</p>	7	UV light irradiation (λ = 300 nm) for 15 hr	0.3
B	<p>Diagram B shows a CdS photocatalyst under 8 photons (8 hv) generating 8 electrons (8 e⁻). These electrons reduce S²⁻ to S⁰ and Cd²⁺ to Cd⁰. The electrons then enter the Wood-Jungdahl pathway in <i>Moorella thermoacetica</i>, which produces biomass and acetic acid. Cysteine (Cys) is oxidized to Cys⁺.</p>	-	Simulated solar irradiation for 2.5 days at an intensity of 0.002 kW m ⁻²	2
C	<p>Diagram C shows a photoelectrochemical cell. The anode (NiMoZn SS) produces 2 H₂ from 4 H⁺ and 2 H₂O. The cathode (CoPi) produces 2 H₂ from 4 H⁺ and 2 H₂O. The electrons from the anode are used to reduce H₂ase in <i>Ralstonia eutropha</i>, which produces biomass and isopropanol. NADPH and NADP⁺ are also shown in the Calvin cycle.</p>	7	Theoretical performance based on the assumption that electricity for water-splitting was provided by a photovoltaic device with 18 % efficiency	3.2 ± 0.2 (biomass) 0.7 ± 0.1 (isopropanol)

1.6 Opportunities for developing whole-cell bacteria approaches to artificial photosynthesis

As shown in section 1.5, a variety of SEDs, photosensitisers and electrocatalysts can be used for artificial photosynthesis with electron transfer from the photosensitiser to the electrocatalyst proceeding directly or via electron shuttles such as MV. Although systems containing purified enzymes or transition metal complexes have undoubtedly furthered our understanding of photocatalysis, there are clear advantages to using whole-bacteria as electrocatalysts. These include: (i) access to a diverse range of products using the natural, or genetically-enhanced, repertoire of bacterial enzymes, (ii) self-regeneration whereby intracellular enzymes are repaired by the living organism for enhanced longevity and (iii) product formation under relatively mild conditions. Taking this into account, prospective micro-organisms for artificial photosynthesis should be able to produce multiple enzymes that catalyse useful chemical transformations and be amenable to productive electron exchange with light-harvesting reagents. In particular, non-photosynthetic bacteria that cannot naturally harvest solar energy are of interest because the catalytic efficiencies of intracellular enzymes can be coupled with the well-studied photochemical and photophysical properties of biotic and abiotic photosensitisers such as molecular dyes, semiconducting nanoparticles and light-harvesting protein complexes (see examples in **Table 1.3, 1.4** and **1.5**).

Based on these requirements, the non-photosynthetic bacterium *Shewanella oneidensis* MR-1 (MR-1) is especially attractive to this area of research for two main reasons. First, the bacterium has been the subject of extensive research efforts aiming to understand its remarkable metabolic capabilities that allow it to survive in redox-stratified environments. As a consequence, much is known about the structure and localisation of the enzymes it produces during respiration, some of which could be targeted for light-driven reductive transformations. Secondly, it can produce protein complexes spanning the outer membrane that exchange electrons with extracellular redox partners. These act as natural electron conduits between the exterior and interior of the cell and may provide a route to deliver photo-excited electrons to bacterial enzymes. The next sections provide background information about MR-1 then describe how its unique characteristics make it suitable for assessing whether it can be utilised for light-driven chemical synthesis.

1.6.1 Metabolic versatility of *Shewanella oneidensis* MR-1 may allow for the simultaneous presence of multiple enzymes that catalyse useful reductive transformations

MR-1 (previously referred to as *Alteromonas putrefaciens* MR-1 and *Shewanella putrefaciens* MR-1) is a Gram-negative, γ -proteobacterium which was first isolated from the anoxic sediments of Lake Oneida, New York State in 1988.^{83,84} The bacterium is a facultative anaerobe renowned for its respiratory versatility with respect to the array of terminal electron acceptors it can utilise during respiration.⁸⁵ This includes O₂, fumarate, dimethyl sulfoxide (DMSO), trimethylamine N-oxide (TMAO), protons, nitrate, nitrite, thiosulfate, sulfite and elemental sulphur as well as insoluble iron (III) and manganese (IV) hydr(oxides) and electrodes.⁸⁵⁻⁹¹ Of particular significance are the final three examples because they are unable to cross the bacterial outer membrane.⁸⁵ The range of electron donors that can be utilised by MR-1 is much narrower and includes H₂, pyruvate, lactate and formate.⁹²⁻⁹⁴ Research into anaerobic respiration with these substrates allows the construction of the key metabolic pathways within the cytoplasm and periplasm of MR-1, as shown in **Fig. 1.11** with lactate as electron donor and fumarate as electron acceptor.⁹³⁻⁹⁵

In the cytoplasm, lactate is oxidised to pyruvate and then to acetyl coenzyme A (CoA) and formate by the lactate dehydrogenases and the pyruvate-formate lyase (PflB), respectively.⁹⁵ Pyruvate can also be oxidised by the pyruvate dehydrogenase to generate CO₂ and reduce NAD⁺ to NADH but this has not been included in **Fig. 1.11** for clarity.⁹³ Acetyl-CoA is then oxidised to acetate via the phosphotransacetylase-acetate kinase (Pta-AckA) pathway which results in the generation of ATP through substrate-level phosphorylation.⁹⁵ Formate is transferred across the inner membrane to the periplasm via a predicted bi-directional formate transporter (FocA) where it is oxidised to CO₂ and protons by the formate dehydrogenases.⁹⁴ This process releases electrons to the menaquinone (MK) pool for reduction of MK to menaquinol (MKH₂). Re-oxidation of MKH₂ can be facilitated by the tetraheme cytochrome CymA, a membrane-bound quinol dehydrogenase that acts as a hub for electron transfer to a range of terminal reductases in MR-1.^{89,96} The redox cycling of MK and MKH₂ leads to the generation of a PMF across the inner membrane. In the presence of fumarate, electrons can be transferred from CymA to the fumarate reductase to produce succinate.⁹⁴ In the absence of a terminal electron

acceptor, known as acceptor-limited conditions, MKH_2 can be re-oxidised by the hydrogenases for the reduction of protons to H_2 .⁹¹

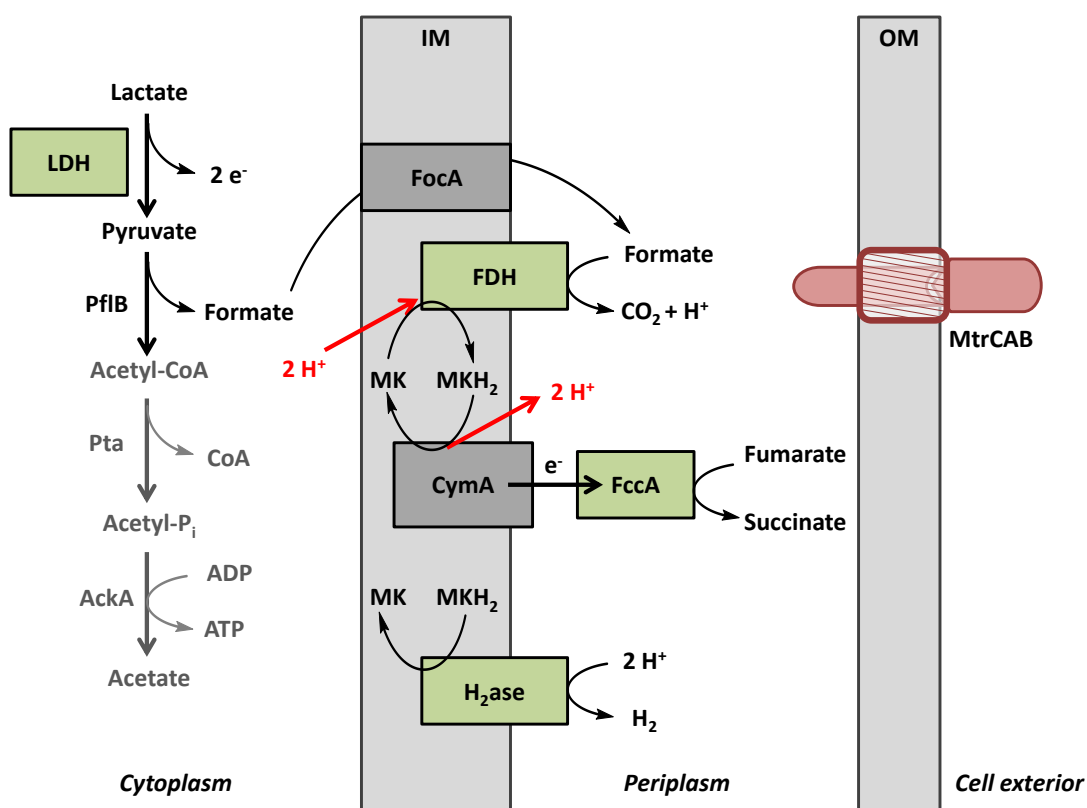


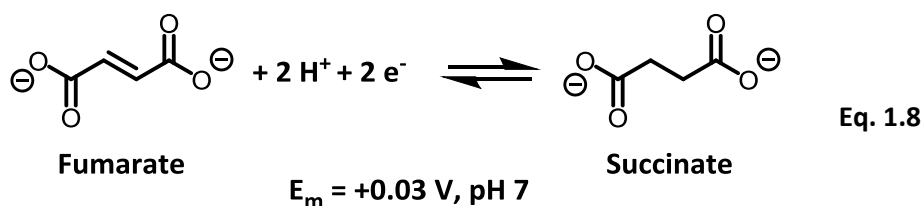
Figure 1.11 - Anaerobic respiration by MR-1 with lactate as electron donor and fumarate as electron acceptor. In the absence of another electron acceptor, menaquinol (MKH_2) is re-oxidised by the hydrogenases (H_2ase) for subsequent reduction of protons to H_2 . IM = inner membrane, OM = outer membrane, ADP = adenosine diphosphate, ATP = adenosine triphosphate, LDH = lactate dehydrogenase, CoA = coenzyme A, PflB = pyruvate-formate lyase, P_i = phosphate, Pta = phosphotransacetylase, AckA = acetate kinase, FDH = formate dehydrogenase, MK = menaquinone, FccA = fumarate reductase.

Based on the respiratory capabilities of MR-1, there are four key enzymes that could be exploited for light-driven reductive transformations to generate products of current interest. These are the hydrogenases (for reduction of protons to H_2),^{91,97,98} fumarate reductase (for reduction of fumarate to succinate, an example of C=C bond hydrogenation),⁹⁹ lactate dehydrogenases (for reduction of pyruvate to lactate, an example of C=O bond hydrogenation)⁹³ and formate dehydrogenases (for reduction of CO_2 to formate).⁹⁴ The reductive transformations and their mid-point potentials (E_m , all values quoted versus the standard hydrogen electrode in this thesis)^{100,101} are shown in Eq. 1.7 to 1.10 and further details about the enzymes are provided in the sections below. More information about the wider importance of these reductive transformations is given in

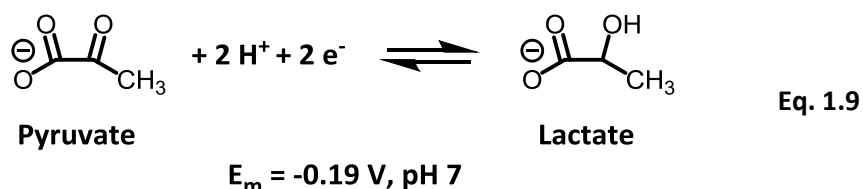
section 1.5 (for reduction of protons to H₂ and CO₂ to formate) and the sections below (for reduction of fumarate to succinate and pyruvate to lactate).



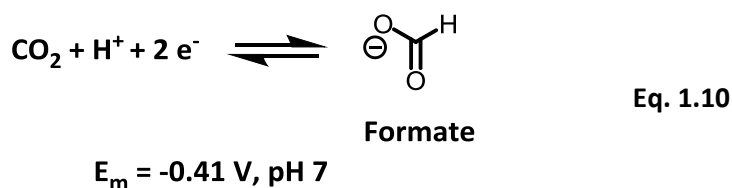
$$E_m = -0.41 \text{ V, pH 7}$$



$$E_m = +0.03 \text{ V, pH 7}$$



$$E_m = -0.19 \text{ V, pH 7}$$



$$E_m = -0.41 \text{ V, pH 7}$$

1.6.1.1 Hydrogenases

The genome sequence of MR-1 reveals that the bacterium possesses genes that encode for one [NiFe]-hydrogenase and one [FeFe]-hydrogenase, both of which are localised to the periplasm.^{91,102} The [NiFe]-hydrogenase is quinone-reactive and comprised of three subunits: HyaA (small subunit, SO2099), HyaB (large catalytic subunit, SO2098) and HyaC (cytochrome *b* subunit, SO2097).^{91,103} The [FeFe]-hydrogenase is comprised of HydA (large catalytic subunit, SO3920) and HydB (small subunit, SO3921) and is predicted to form a formate-hydrogen lyase complex because the *hydA* operon contains a putative formate dehydrogenase γ subunit (SO3922).^{91,94} Early reports that described H₂ metabolism by MR-1 suggested that the [NiFe]-hydrogenase was bi-directional (i.e. could catalyse the oxidation of H₂ in addition to the reduction of protons) and the [FeFe]-hydrogenase was solely involved in H₂-evolution.⁹¹ More recently, however, it has been shown that the

[FeFe]-hydrogenase can couple the oxidation of H₂ to the reduction of amaranth (an azo dye that is predicted to be reduced extracellularly).^{104,105}

1.6.1.2 Fumarate reductase

The MR-1 fumarate reductase (FccA, SO0974) is a soluble, uni-directional enzyme containing four bis-histidine ligated heme *c* groups and a non-covalently bound flavin adenine dinucleotide (FAD) catalytic cofactor.^{99,106} The crystal structure has been solved previously¹⁰⁶ and is shown in **Fig. 1.12**. The enzyme is comprised of three domains: the N-terminal domain contains the heme groups, the C-terminal domain contains the FAD group and the clamp domain joins the N- and C-terminal domains.¹⁰⁷ The enzyme is unique as a fumarate reductase because it is monomeric and localised to the periplasm. This is in contrast to other bacterial quinol-fumarate oxidoreductases which are typically membrane-bound and formed of multiple subunits containing iron-sulphur clusters.¹⁰⁸ FccA acts as a terminal reductase during MR-1 metabolism by receiving electrons from CymA for the reduction of fumarate to succinate (see **Fig. 1.11**) but has also been implicated in electron transfer across the periplasmic space during anaerobic growth with extracellular electron acceptors.^{89,109}

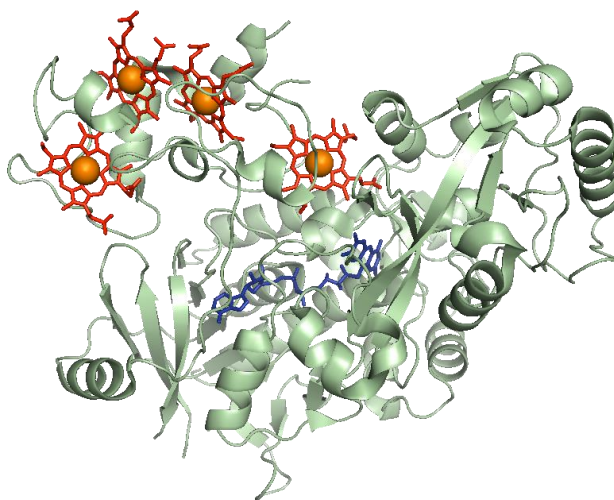


Figure 1.12 - Crystal structure of the MR-1 fumarate reductase (PDB ID: 1D4D). The FAD group is shown in blue and the heme groups are shown in red with the central iron atoms as orange spheres. Image rendered with PyMOL software.

The photocatalytic reduction of fumarate to succinate is an important reaction to target because it represents a fundamental transformation in organic chemistry (C=C bond hydrogenation) as well as the storage of H₂ within an organic molecule.^{110,111} Additionally, succinate (or succinic acid) has applications in the food industry as a flavour enhancer and is a key platform chemical for the generation of specialised polymers (such as polyesters and nylons) and high-value petrochemical products (such as tetrahydrofuran, 1,4-butanediol and γ -butyrolactone), the structures of which are shown in **Fig. 1.13**.^{112,113}

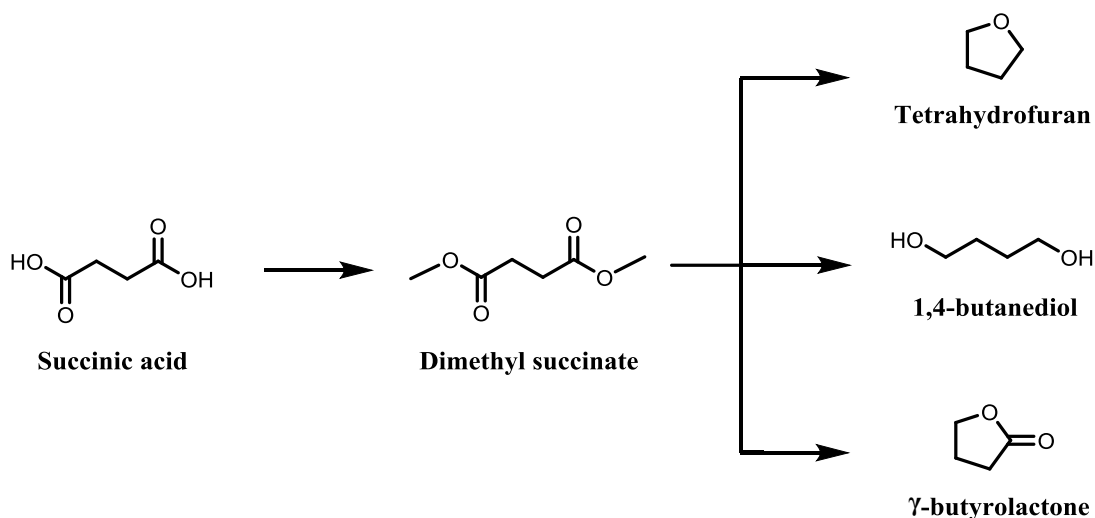


Figure 1.13 - Chemical structures of valuable chemicals that can be produced from succinic acid.

The commercial production of succinate has traditionally relied on technologies that require expensive metal catalysts such as palladium as well as high temperatures and pressures.¹¹² As a consequence, cheaper routes to succinate production that operate under milder conditions are sought after.

1.6.1.3 Lactate dehydrogenases

The oxidation of D- and L-lactate (the structures of which are shown in **Fig. 1.14**) by MR-1 is facilitated by two distinct lactate dehydrogenases (one for each lactate isomer) which are both membrane-bound enzymes on the cytoplasmic side of the inner membrane.^{93,114,115}

The first reports describing these enzymes found they were novel bacterial lactate dehydrogenases but subsequent analysis revealed there were homologous enzymes in other species of *Shewanella* as well as a range of α - and β -proteobacteria.¹¹⁴ Oxidation of D-lactate is performed by Dld-II (SO1521) which is a relatively distant homolog

(23 % sequence identity) of the D-lactate dehydrogenase from yeast and oxidation of L-lactate is carried out by LlDEFG (SO1518-SO1520) which is predicted to be a multi-subunit enzyme.¹¹⁴ Interestingly, D-lactate is preferentially utilised by MR-1 over L-lactate, presumably because D-lactate is able to inhibit the oxidation of L-lactate.¹¹⁵

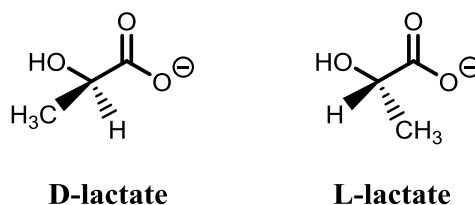


Figure 1.14 - Chemical structures of D- and L-lactate.

Lactate (or lactic acid) is a valuable commodity because it can be used as a platform chemical for the production of green solvents (such as lactate esters) and biodegradable fibres for biomedical applications.¹¹³ Additionally, there is an increasing interest in the polymerisation of lactic acid to give high molecular weight (HMW) poly-lactic acid which can be used as a sustainable alternative to polystyrene.¹¹³ The production of HMW polymers from lactic acid is most effective if the synthesis proceeds via a low molecular weight (LMW) pre-polymer and lactide, the structures of which are shown in **Fig. 1.15**.^{113,116}

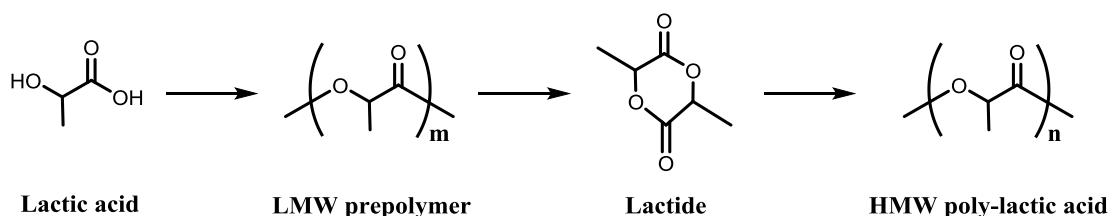


Figure 1.15 - Chemical conversions of lactic acid to produce high molecular weight (HMW) poly-lactic acid. LMW = low molecular weight, $m < n$.

On an industrial scale, lactic acid can be produced by chemical and biological routes.^{113,117} For example, the chemical synthesis of lactic acid can be achieved using hydrogen cyanide and acetaldehyde to produce a lactonitrile intermediate (in a reaction that proceeds in the liquid phase and requires high pressures) which can then be hydrolysed to lactic acid using concentrated hydrochloric or sulphuric acid.¹¹⁷ Lactic acid can also be produced under milder conditions through microbial fermentation of substrates such as glucose. Commercial fermentation yields are relatively high (approximately 90 % based on the

amount of supplied glucose) but the process results in the formation of calcium lactate which must be neutralised to give pure lactic acid.¹¹³ This neutralisation procedure leads to the formation of vast quantities of calcium sulfate as a waste product.¹¹³ As such, there is a desire for new routes to lactic acid production that proceed under ambient conditions and avoid the generation of unwanted byproducts.

1.6.1.4 Formate dehydrogenases

The genome of MR-1 contains gene clusters that encode for a total of three formate dehydrogenase complexes.⁹⁴ One of the gene clusters (SO0101-SO0103) encodes for a nitrate-inducible formate dehydrogenase.¹⁰² Transcription of the genes related to this enzyme is up-regulated during growth with nitrate as electron acceptor but the enzyme does not significantly contribute to formate oxidation during anaerobic growth with fumarate as electron acceptor.^{94,118} The other two gene clusters (SO4509-SO4511 and SO4513-SO4515) encode for related NADH-independent formate dehydrogenases (68 % sequence identity to each other) which have likely arisen from a gene duplication event.⁹⁴ Both enzymes are membrane-bound on the periplasmic side of the inner membrane and are comprised of three subunits: the α -subunits contain the catalytic active site, the β -subunits transfer electrons to the active site, and the γ -subunits anchor the enzyme to the inner membrane and exchange electrons with the MK pool.^{51,61,94} It is proposed that the ability to produce multiple formate dehydrogenases affords MR-1 with an evolutionary advantage for surviving in diverse environments where the concentration of formate is continuously fluctuating.⁹⁴

Overall, the respiratory flexibility of MR-1 makes the bacterium suitable for assessing whether it can be utilised for light-driven chemical synthesis because there are a range of enzymes that can be targeted for the generation of commercially-valuable products. As mentioned above, the bacterium is also suitable because it produces outer membrane protein complexes that can exchange electrons with insoluble redox partners such as metal hydr(oxides) and electrodes. The next section provides a description of how insoluble, extracellular electron acceptors are reduced by MR-1 during respiration then introduces recent work that acts as a direct platform to achieve the aims of this thesis.

1.6.2 Outer membrane spanning complexes may provide a route to deliver photo-energised electrons from the outside to the inside of the bacterium

To reduce extracellular electron acceptors that cannot enter the periplasm, MR-1 must transport electrons generated through central metabolism across the bacterial outer membrane, which typically acts as an insulating barrier.¹¹⁹ Electron transfer from the inside to the outside of the bacterium proceeds via porin:cytochrome complexes embedded in the outer membrane. MtrCAB is the most widely studied of these complexes but MR-1 can also produce a second complex called MtrDEF, the genes of which are highly expressed under aerobic aggregated (biofilm) growth.^{119,120} MtrCAB is comprised of three proteins in a 1:1:1 complex, as shown in **Fig. 1.16**. MtrC (≈ 75 kDa) is a decaheme cytochrome localised to the outer surface of MR-1 via a lipid anchor and MtrA (≈ 35 kDa) is a periplasmic decaheme cytochrome that forms a tight complex with MtrB (≈ 85 kDa), a 28-strand transmembrane β -barrel protein that creates a pore (3 to 4 nm in diameter) in the outer membrane.^{85,119,121} MtrC and MtrA each contain 10 bis-histidine ligated heme *c* groups which are covalently linked to the protein structure via the Cys-X-X-Cys-His motif (where Cys is cysteine, X is any residue and His is histidine).

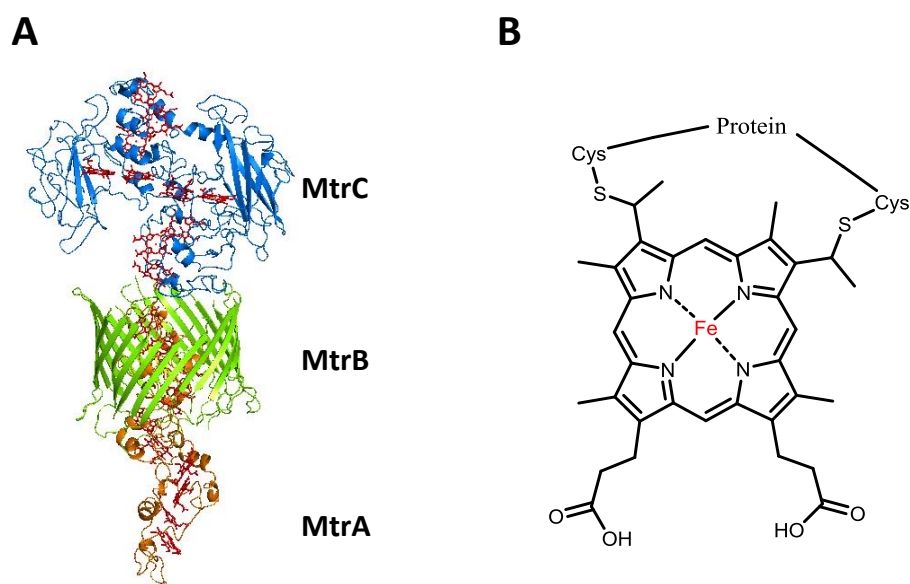


Figure 1.16 - Structure of the MR-1 outer membrane porin:cytochrome complex MtrCAB. A] Model of the MtrCAB complex rendered with PyMOL software by Dr. Marcus Edwards (University of East Anglia, UK) from the crystal structure of MtrC (PDB ID: 4LM8), a model of MtrA based on two NrfB (PDB ID: 2OZY) units and a model of MtrB generated using TMB_Pro_3D software. Heme groups within MtrC and MtrA are coloured in red. B] Chemical structure of heme *c*. Cys = cysteine residue.

The hemes of MtrC and MtrA are thought to be brought into close contact (≤ 11 Å edge-to-edge distances between porphyrin rings) with MtrA positioned inside MtrB to create a wire of iron centres that cycle between the oxidised (Fe(III), ferric) and reduced (Fe(II), ferrous) states to shuttle electrons across the outer membrane.^{122,123} With the purified complex adsorbed on a graphite electrode, the reduction potential of MtrCAB spans approximately -0.4 to +0.05 V.¹²⁴ Once electrons from the periplasm are transferred along the hemes of MtrA to reach MtrC, they are transferred to extracellular acceptors via direct, flavin-mediated and/or nanowire-assisted mechanisms, as summarised in **Fig. 1.17**.⁸⁵

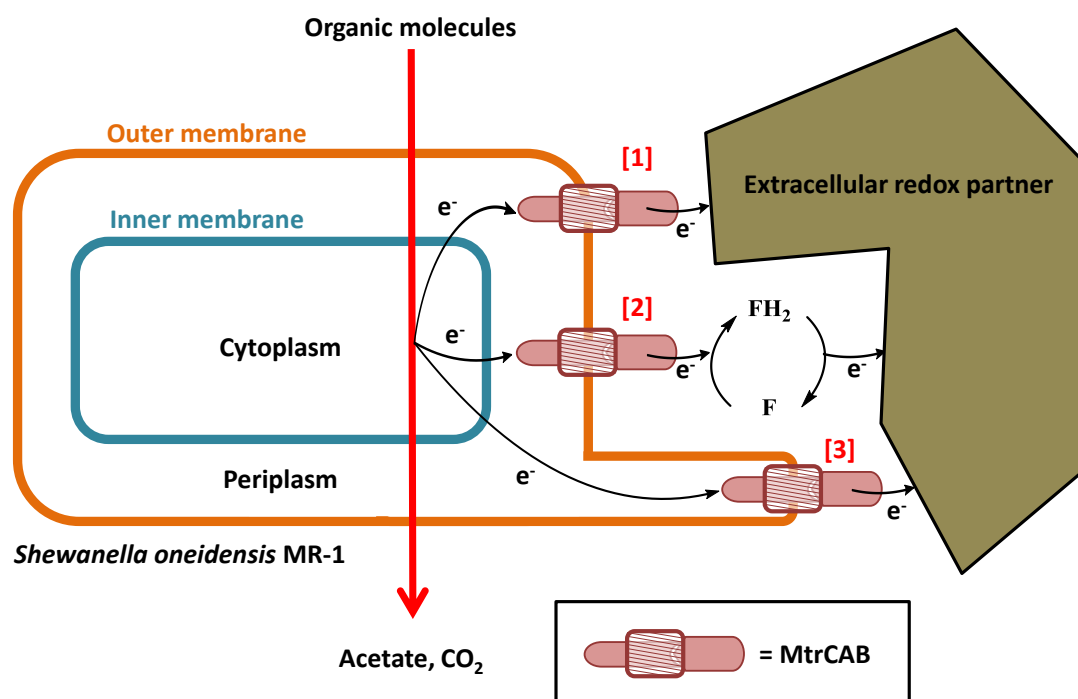


Figure 1.17 - Schematic diagram for the transfer of electrons from MR-1 central metabolism to an extracellular acceptor (e.g. an Fe(III) or Mn(IV) hydr(oxide) or an electrode) via MtrCAB. Electron transfer from MtrC to the acceptor can proceed via the direct [1], flavin-mediated [2] and/or nanowire-assisted [3] mechanisms. F = oxidised flavin, FH₂ = reduced flavin.

The direct mechanism of electron transfer has been supported by experiments where purified MtrCAB was re-constituted in spherical vesicles encapsulating MV. After reducing MV with a chemical reductant, the internalised pool of electrons could be released from the vesicles via MtrCAB through the addition of Fe(III) minerals (such as goethite, hematite and lepidocrocite) in the absence of an exogenous electron shuttle.^{125,126} The flavin-mediated mechanism has been supported by a number of previous studies, as reviewed in Brutinel et al. (2012).¹²⁷ For example, it was found that there was a dramatic decrease in current produced by electrode-grown bacterial biofilms (i.e. *Shewanella*

cultured with lactate as electron donor and an electrode poised at +0.24 V as electron acceptor) when the surrounding medium (containing flavin shuttles such as riboflavin) was exchanged with fresh medium.¹²⁸ The nanowire-assisted mechanism has been supported by immuno-labelling and live fluorescence imaging which revealed that electron transfer along bacterial appendages (typically referred to as nanowires) involved extensions of the outer membrane containing the MtrCAB complex.¹²⁹

By reversing the native flow of electrons through MtrCAB, it should be possible to drive reductive transformations in MR-1. This has been performed previously for the reduction of fumarate and chromate, although an electrode poised at a reducing potential provided electrons to the bacterium rather than a SED and photosensitiser.^{130,131} For example, Ross et al. (2011) reported that electrons could be transferred into MR-1 via MtrCAB for the reduction of fumarate to succinate using a graphite electrode poised at -0.36 V.¹³⁰ Further analysis revealed that approximately 85 % of electrons were transferred to the fumarate reductase via CymA and the MK pool with little direct electron transfer from MtrA.¹³⁰ More recently, the work reported in Ainsworth et al. (2016) assessed the photoreduction of purified MR-1 outer membrane cytochromes to evaluate the possibility of light-driven electron transfer into the bacterium.¹³² The key results from this work are described below to show how they provide a platform to achieve the aims of this thesis.

In Ainsworth et al. (2016), the photoreduction of purified MtrC, OmcA (a decaheme protein which is a homolog of MtrC) and MtrCAB was carried out using a range of photosensitisers including xanthene-dyes, an acridine-dye, flavins and ruthenium complexes.¹³² The proteins were combined with a SED and photosensitiser then samples were irradiated with a white light source ($\lambda > 390$ nm) at an intensity of 0.4 kW m^{-2} . The photoreduction of the proteins was monitored using a spectrophotometer to assess the increases in absorbance at 420, 523 and 552 nm corresponding to reduced heme. A schematic diagram for photoreduction of MtrC is shown in **Fig. 1.18A** and representative spectra for fully oxidised and fully reduced MtrC are given in **Fig. 1.18B**. The extent of heme photoreduction over 90 min irradiation was dependent on the photosensitiser and similar trends were seen for MtrC, OmcA and MtrCAB. With triethanolamine (TEOA) as SED, complete photoreduction was achieved with the xanthene- and acridine-dyes, approximately 61 % photoreduction was achieved using the flavins and ≤ 14 % photoreduction was achieved with the ruthenium complexes. However, it was found that the rate and extent of

photoreduction with the ruthenium complexes could be increased by co-adsorbing the photosensitiser and the protein on titanium dioxide nanoparticles with 2-(N-morpholino)ethanesulfonic acid (MES) as SED.¹³²

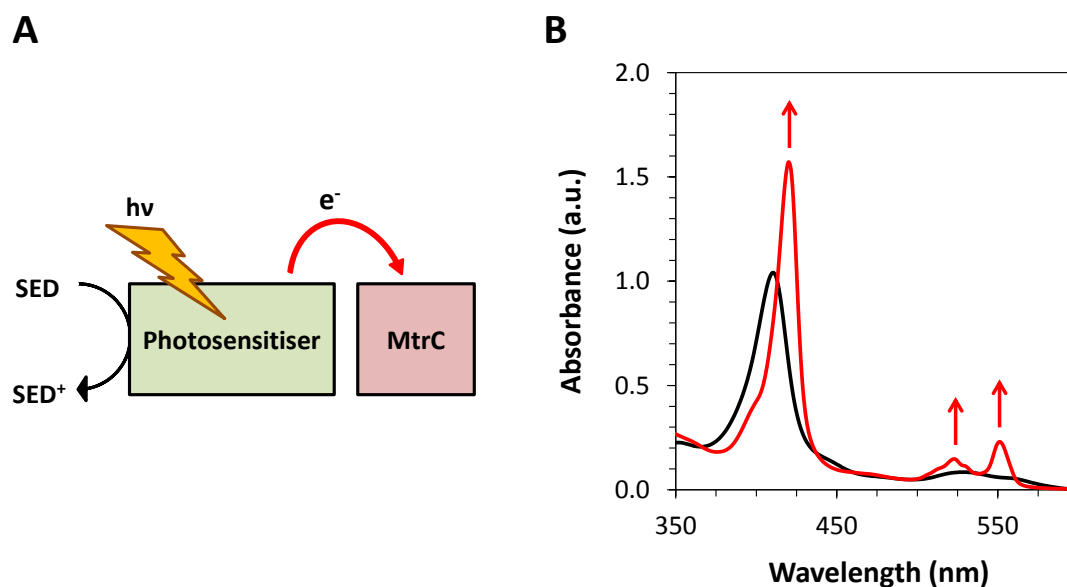


Figure 1.18 - Photoreduction of purified MtrC. A) Schematic diagram for photon ($h\nu$) absorption by a photosensitiser and transfer of photo-excited electrons to MtrC in the presence of a sacrificial electron donor (SED). B) Representative spectra showing fully oxidised (black) and fully reduced (red) MtrC in 50 mM HEPES, 100 mM NaCl, pH 7 at 4 °C. Arrows indicate the increase in absorbance at 420, 523 and 552 nm corresponding to heme reduction.

Overall, the findings in Ainsworth et al. (2016) provide a foundation for the work in this thesis through the evaluation of photosensitisers from a variety of chemical classes including a comprehensive assessment of their spectral properties, photoreduction potentials and relative photoreduction efficiencies in the presence of SEDs such as TEOA and 4-(2-hydroxyethyl)piperazine-1-ethanesulfonic acid (HEPES). Importantly, the work showed that photo-energised electrons can be rapidly transferred to isolated MR-1 outer membrane cytochromes under ambient conditions (i.e. in aqueous medium at pH 7) which should be compatible with bacteria for cell-based photocatalysis.

1.7 Aims of this thesis

The work presented in this thesis addressed two main objectives. The first objective was to establish whether MR-1 can be used for cell-based photocatalysis to generate multiple products. To achieve this, MR-1 was cultured to produce the enzymes of interest then

combined with a SED and photosensitiser (for generation of photo-excited electrons under irradiation by visible light) and MV (for effective electron transfer to bacterial enzymes). This approach has been summarised in **Fig. 1.19A**. The second objective was to evaluate whether outer membrane porin:cytochrome complexes can be used as electron conduits to transfer photo-excited electrons from photosensitisers to bacterial enzymes. This part of the work aimed to avoid the requirement for MV as an electron shuttle by exploiting the native electron transfer abilities of MR-1. This approach has been summarised in **Fig. 1.19B**. The objectives were pursued in a step-wise manner as described in the paragraphs below.

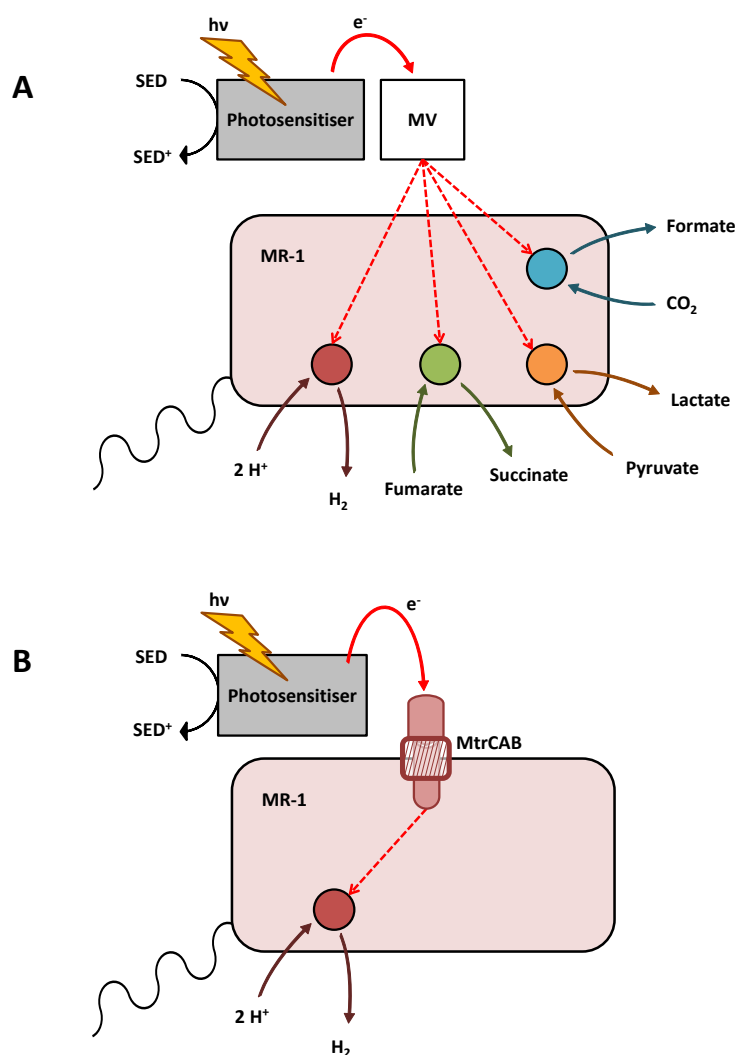


Figure 1.19 - Schematic diagrams showing the strategies for cell-based photocatalysis investigated in this work. Photon ($h\nu$) absorption by a photosensitiser in the presence of a SED leads to the transfer of photo-excited electrons to MR-1 enzymes via MV (A) or MtrCAB (B) for reductive chemical transformations. Red circle = hydrogenases, green circle = fumarate reductase, orange circle = lactate dehydrogenases, blue circle = formate dehydrogenases.

Chapter 3 describes how MR-1 growth conditions were established to facilitate the simultaneous presence of active hydrogenases, fumarate reductase, lactate

dehydrogenases and formate dehydrogenases. Enzyme assays with sodium dithionite (DT) as chemical reductant and MV as electron transfer mediator were performed after harvesting MR-1 from growth medium and re-suspending in a defined buffer to confirm the desired reductive transformations could be catalysed by the bacterium.

Chapter 4 describes the development of a system for photocatalytic reduction of protons to H₂ with MR-1. This reaction was selected for initial experiments because the formation of the product can be readily quantified using electrochemistry and gas chromatography. Water-compatible photosensitisers were assessed for their ability to photoreduce MV²⁺ under conditions compatible with MR-1 enzyme activity and then photoreduction of MV²⁺ was performed in the presence of MR-1 which had been cultured and processed as described in chapter 3. Determinants of the system such as MV concentration and pH were evaluated before the analysis was extended to assess sustained light-driven H₂-evolution.

Chapter 5 describes how the system for light-driven H₂-evolution presented in chapter 4 was used for the photocatalytic reduction of fumarate, pyruvate and CO₂ by providing MR-1 with the chosen carbon substrate prior to irradiation. This chapter also describes the competition between bacterial enzymes for electrons provided to MR-1 by photo-produced MV⁺, the ways in which light-driven CO₂-reduction can be enhanced, and the possibility of performing photocatalytic fumarate reduction over extended periods of time.

Chapter 6 describes preliminary work that evaluated cell-based photocatalysis using carbon dots (CDs) as photosensitisers without the need for MV as an electron shuttle. The CDs were first characterised by assessing their ability to photoreduce a range of electron acceptors in the presence of different SEDs. Combinations of CDs and SEDs were then used in experiments that aimed to achieve photo-production of H₂ by MR-1 and other species of *Shewanella*. Different strains were assessed in this work to exploit the different physicochemical properties associated with their outer surfaces.

Lastly, chapter 7 presents a wider summary and discussion of the work presented in this thesis. This includes an analysis of the future opportunities for cell-based photocatalysis with *Shewanellaceae* and other species of bacteria to achieve the sustainable production of commercially-valuable chemicals.

CHAPTER 2

Materials and Methods

Chapter 2 - Materials and Methods

2.1 General reagent preparations

Eosin Y (acid form), flavin mononucleotide (FMN, sodium salt), proflavine (3,6-diaminoacridine, hemisulfate salt), Ru(bpy)₃Cl₂ (where bpy is 2,2'-bipyridine), triethanolamine (TEOA), 1,1'-dimethyl-4,4'-bipyridinium dichloride (methyl viologen, MV), 1,1'-dibenzyl-4,4'-bipyridinium dichloride (benzyl viologen, BV), 4-(2-hydroxyethyl)-piperazine-1-ethanesulfonic acid (HEPES, acid form), casein digest of peptone, sodium fumarate (dibasic), ¹³C-formate (99 atom % ¹³C), ¹³C-sodium carbonate (anhydrous, 99 atom % ¹³C), sodium D,L-lactate solution (60 % [w/w]), sodium hydrosulfite (dithionite, DT), L-cysteine hydrochloride monohydrate, L-ascorbic acid (sodium salt), sodium sulfite, sodium azide, sodium chloride, potassium chloride, potassium chloride solution saturated with silver chloride, calcium chloride, nickel chloride, sodium phosphate (monobasic), potassium phosphate (dibasic), chloroplatinic acid hydrate and 2-(N-morpholino)ethanesulfonic acid hydrate (MES, acid form) were from Sigma-Aldrich. Fluorescein (acid form) was from Alfa Aesar. Papaic digest of soybean meal was from Neogen Corp. Tryptone and yeast extract were from Melford Laboratories Ltd. Glycerol, sodium pyruvate, sodium carbonate (anhydrous) and D-glucose were from Fischer Scientific. Sodium 3-(trimethylsilyl)-propionate-d₄ (TSP) was from Goss Scientific Instruments Ltd. Deuterium oxide was from Cambridge Isotope Laboratories. Sodium oxalate was from Lancaster Synthesis. Ethylenediaminetetraacetic acid solution (EDTA, 0.5 M, pH 8) was from Ambion Inc. The reagents listed above were used without further purification. [Ru(bpy)₂(4,4'-(PO₃H₂)₂bpy)]Br₂ (RuP) was kindly provided by Dr. Manuela Gross (University of Cambridge, UK) and was prepared as described previously.¹³³ Anionic carbon dots (CD-CO₂⁻), cationic carbon dots (CD-NHMe₂⁺, where Me = CH₃) and nitrogen-doped carbon dots (N-CDs) were kindly provided by Dr. Benjamin Martindale and Dr. Bertrand Reuillard (University of Cambridge, UK) and were prepared as described previously.¹³⁴⁻¹³⁶ MtrC was kindly provided by Dr. Simone Payne (University of East Anglia, UK) and was purified as described previously.¹³⁷

Aqueous solutions were prepared using Milli-Q water (resistivity 18.2 MΩ cm). Solution pH was confirmed using a Fisher Scientific accumet AE150 pH meter calibrated with standard

solutions at pH 4, 7 and 10 (Sigma-Aldrich). Stock solutions of photosensitisers were made by dissolving the appropriate mass in 50 mM HEPES, 2 mM CaCl₂, 10 mM KCl, pH 7. Solutions were then stored in the dark and their integrity confirmed using absorbance spectroscopy prior to use (extinction coefficients and absorbance spectra for photosensitisers are presented in chapters 4 and 6). Stock solutions of TEOA were made by dissolving the appropriate volume in 50 mM HEPES, 2 mM CaCl₂, 10 mM KCl and adjusting the pH to 7.8 using 5 M HCl. Stock solutions of MV, BV, DT, sodium fumarate, sodium pyruvate and (¹³C)-sodium carbonate were made by dissolving the appropriate mass in filter-sterilised (0.2 µm membrane, Sartorius Stedim Biotech) 50 mM HEPES, 50 mM NaCl, pH 7. H₂-saturated Milli-Q water was produced by purging 1 mL anaerobic Milli-Q water for 30 min with H₂ generated by a polymer electrolyte membrane electrolyser (Horizon Educational).

2.2 Characterisation of irradiation sources

Two irradiation sources were used for light-driven transformations. One was a KL5125 cold light source (Krüss) fitted with high-quality UV-filtering quartz glass and a 150 W (15 V) halogen lamp (Osram). The other irradiation source was a photosynthetic growth lamp within a New Brunswick Scientific Innova 44 shaker incubator. Relative spectral distributions of the irradiation sources are shown in **Fig. 2.1**.

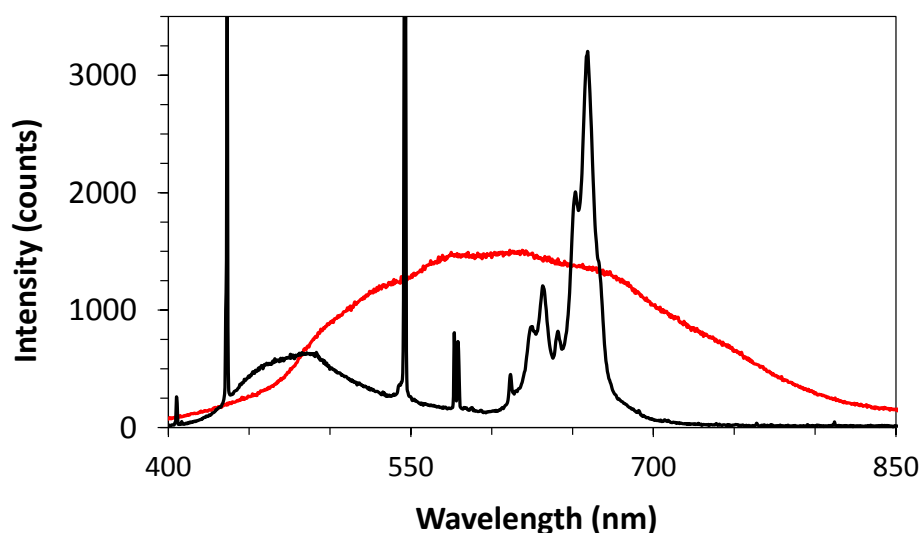


Figure 2.1 - Relative spectral distributions of the irradiation sources used in this study. Outputs from the cold light source (red) and the photosynthetic growth lamp (black) recorded using a HR2000CG-UV-NIR Ocean Optics fibre spectrometer.

Prior to each experiment, the light intensity at the sample was estimated using a SOLAR-100 Amprobe solar power meter (sensor wavelength 400 to 1100 nm) positioned an appropriate distance from the light source. Irradiation from the cold light source was provided at an intensity of 0.7 kW m^{-2} unless otherwise stated and irradiation from the photosynthetic growth lamp was provided at an intensity of 0.02 kW m^{-2} .

2.3 Bacterial growth, characterisation and processing

2.3.1 - Growth media preparations

The composition of lysogeny broth (LB) medium, M72 medium and anaerobic growth additions are shown in **Table 2.1**. The required components were dissolved in distilled water then the pH was adjusted to the indicated value with 10 M NaOH.

Table 2.1 - Growth media components.

LB medium (pH 7)	
Component	Concentration (g L^{-1})
Tryptone	10
Yeast extract	5
NaCl	10
M72 medium (pH 7.8) ¹³⁸	
Component	Concentration (g L^{-1})
Casein digest of peptone	15
Papaic digest of soybean meal	5
NaCl	5
Anaerobic growth additions for M72 medium (pH 7.9) ⁹⁸	
Component	Concentration (g L^{-1})
Sodium D,L-lactate	4.20
Sodium fumarate	3.00
NiCl ₂	0.45
HEPES	8.93

Liquid media were sterilised using an autoclave and anaerobic growth additions were filter-sterilised using a 0.2 µm membrane (Sartorius Stedim Biotech). To make LB-agar plates, 15 g L⁻¹ agar was added to LB medium before autoclave sterilisation. The LB-agar solid was then melted in a microwave, distributed between plastic Petri dishes and allowed to solidify within a laminar flow cabinet (Walker safety cabinets).

2.3.2 Strains used in this study

Descriptions of the *Shewanella* strains used in this study are given in **Table 2.2**. Wild-type strains were sourced from culture collections and mutant strains were kindly provided by Dr. Liang Shi (China University of Geosciences, Wuhan).

Table 2.2 - *Shewanella* strains used in this study.

<i>Shewanella</i> strain	Description [location of original isolation]	Ref.
<i>oneidensis</i> MR-1	Wild-type [Lake Oneida, New York, US]	83
HydA ⁻ /HyaB ⁻	$\Delta hydA$ (SO3920) and $\Delta hyaB$ (SO2098) in MR-1	139
Mtr ⁻	$\Delta mtrB$ - <i>mtrD</i> (SO1776-SO1782) in MR-1	140
<i>oneidensis</i> MR-4	Wild-type [Black Sea]	141
<i>oneidensis</i> MR-7	Wild-type [Black Sea]	141
<i>amazonensis</i> SB2B	Wild-type [Amapa River, Brazil]	142
ANA-3	Wild-type [Woods Hole, Massachusetts, US]	143
<i>baltica</i> OS185	Wild-type [Baltic Sea]	144
<i>baltica</i> OS195	Wild-type [Baltic Sea]	144
<i>baltica</i> OS223	Wild-type [Baltic Sea]	144
<i>loihica</i> PV-4	Wild-type [Hawaiian Seamount, US]	145
<i>putrefaciens</i> CN-32	Wild-type [Albuquerque, New Mexico, US]	146
<i>putrefaciens</i> 200	Wild-type [Alberta, Canada]	147
<i>putrefaciens</i> W3-18-1	Wild-type [Washington coast, Pacific Ocean]	148

The HydA⁻/HyaB⁻ mutant has the genes encoding the large subunits of the [FeFe]- and [NiFe]-hydrogenases (*hydA* and *hyaB*, respectively) deleted in *Shewanella oneidensis* MR-1 (MR-1).¹³⁹ The Mtr⁻ mutant has the genes encoding the entire *mtr* cluster (*mtrB*, *mtrA*, *mtrC*, *omcA*, *mtrF*, *mtrE*, *mtrD*) deleted in MR-1.¹⁴⁰

2.3.3 Growth conditions

Bacterial strains were stored at -80 °C in 25 % glycerol, 50 % LB medium, 25 % distilled water. Aliquots of the frozen strains were spread on to LB-agar plates and incubated for ≈24 hr at 30 °C. Single colonies were used to inoculate 10 mL LB medium which was then shaken aerobically at 200 rpm overnight (≈20 hr). The resultant cultures inoculated (2 % [v/v]) glass Hungate tubes (17 mL total volume) that contained 10 mL M72 medium supplemented with anaerobic growth additions (see **Table 2.1**). The additions contain 37.5 mM lactate as electron donor and 18.8 mM fumarate as electron acceptor with 1.9 mM NiCl₂ and 37.5 mM HEPES for production of active hydrogenases in *Shewanella*, as described previously.⁹⁸ The tubes were sealed, the headspaces (7 mL) were purged with N₂ for 5 min and the cultures were incubated with no shaking at 30 °C for the desired time period. Optical density at 590 nm (OD_{590nm}) was recorded with the tubes placed directly in a Fisher Scientific colorimeter (Model 45). A Hungate tube containing 10 mL distilled water was used as reference.

2.3.4 Bicinchoninic acid (BCA) assay

Total protein content of *Shewanella* samples was quantified using a bicinchoninic acid (BCA) assay (Sigma-Aldrich). In the assay, Cu²⁺ ions form complexes with protein in the sample and are reduced to Cu⁺. BCA then forms a blue-purple complex with Cu⁺ to give an increased absorbance at 562 nm which is proportional to the amount of protein present.¹⁴⁹ To prepare *Shewanella* samples, bacteria were harvested by centrifugation (5 min, 20000 x *g*, room temperature) from 1 mL of culture, re-suspended in 0.5 mL 100 mM HEPES, pH 7.2 and lysed by sonication (3 pulses each lasting 15 s with samples kept on ice between each pulse). Samples were then assayed according to the manufacturer's protocol by mixing them with BCA solution and copper (II) sulfate pentahydrate solution (4 %) in a 96-well plate (NUNC) and incubating at 37 °C for 30 min. After this time, the absorbance at 562 nm was recorded using a FLUOstar Omega plate

reader (BMG Labtech) under the control of Omega software (version 1.3). A calibration curve was generated using known quantities of bovine serum albumin (BSA) in 100 mM HEPES, pH 7.2. A representative calibration curve is shown in **Fig. 2.2**.

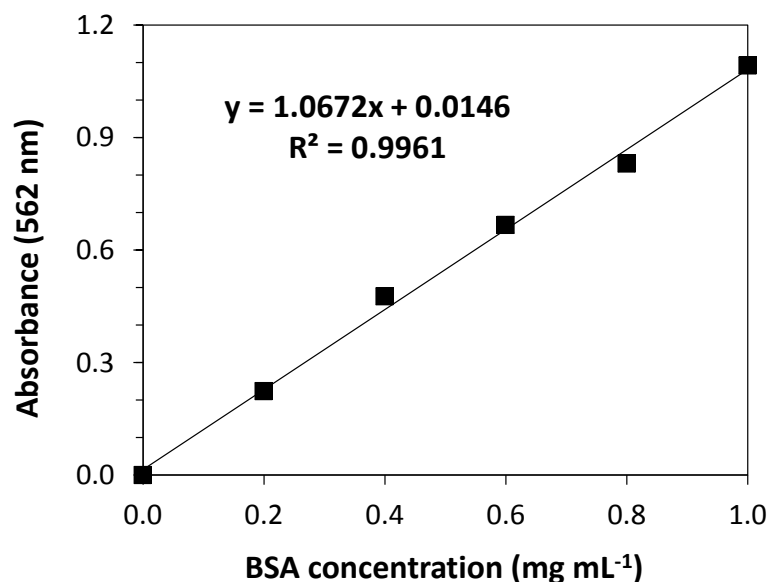


Figure 2.2 - Representative calibration curve for bicinchoninic acid assay. Absorbance at 562 nm for known concentrations of bovine serum albumin (BSA) in 100 mM HEPES, pH 7.2. Equation and R^2 value for linear trendline.

2.3.5 Colony forming units (CFU)

Viability of *Shewanella* strains was assessed by measuring colony forming units (CFU). Bacteria were harvested from reaction solutions by centrifugation (7 min, 20000 x *g*, room temperature) then supernatants were removed and cell pellets were gently re-suspended in LB medium. 10-fold serial dilutions of the re-suspended cells were prepared in LB medium and 0.1 mL of each dilution was spread on an LB-agar plate. Colonies were then counted manually after incubating the plates at 30 °C for 48 hr. For each reaction condition, three plates spread with different serial dilutions were used to calculate a mean value for CFU mL⁻¹ in the reaction solution.

2.3.6 Protein gels and Western blotting

Sodium dodecyl sulfate polyacrylamide gel electrophoresis (SDS-PAGE) was used to analyse proteins produced by *Shewanella* strains that had been cultured for 24 hr in

M72 medium as described in section 2.3.3. Bacteria were harvested by centrifugation (5 min, 20000 x *g*, room temperature) from 1 mL of culture, re-suspended in 32 μ L loading buffer (6 M urea, 5 % sodium dodecyl sulfate, 0.1 % glycerol, 0.05 % bromophenol blue) and heated at 90 °C for 15 min. Samples (15 μ L) were then loaded on a 10 % SDS-PAGE gel and proteins were separated based on their molecular weight by electrophoresis (\approx 1 hr, 100 V, 60 mA). To visualise all proteins in the sample, SDS-PAGE gels were washed with distilled water then incubated with a Coomassie staining solution (InstantBlue, Expedeon) for 15 min. The blue Coomassie dye associates with proteins in the gel via electrostatic interactions with protonated amino acids and via hydrophobic interactions with aromatic amino acids.¹⁵⁰ To specifically visualise heme-containing proteins in the sample, SDS-PAGE gels were washed with distilled water then incubated with 250 mM sodium acetate, pH 5 for 15 min before the addition of 3.2 mM 3,3',5,5'-tetramethylbenzidine dihydrochloride hydrate (TMBD) in methanol and incubation for a further 15 min. This was followed by the addition of 30 % H₂O₂ solution and incubation for 5 min. Gels were developed in the dark due to the light-sensitivity of TMBD. During the staining process, heme *c* groups (which remain covalently attached to proteins in the gel) catalyse the reduction of H₂O₂ with TMBD as reductant.^{151,152} Oxidised TMBD then forms a blue charge-transfer complex with another molecule of TMBD¹⁵³ to reveal the position of heme-containing proteins.

To specifically visualise MtrB and MtrC in the sample through Western blotting, proteins on the SDS-PAGE gel were transferred to a polyvinylidene fluoride (PVDF) membrane (GE Healthcare) which was then incubated overnight in blocking buffer (5 % skimmed milk, 20 mM Tris-HCl, 150 mM NaCl, 0.1 % Tween 20, pH 7.5) at 5 °C to prevent non-specific binding. After this time, the membrane was washed and incubated with 0.6 μ g mL⁻¹ of either anti-MtrB (specific to residues 23-42) or anti-MtrC (specific to residues 399-410) primary antibody in blocking buffer at room temperature. After 2 hr, the membrane was washed and incubated with 0.15 μ g mL⁻¹ goat anti-rabbit secondary antibody conjugated to alkaline phosphatase (Sigma-Aldrich) in 20 mM Tris-HCl, 150 mM NaCl, 0.1% Tween 20, pH 7.5 at room temperature. After 1 hr, proteins were visualised by incubating the membrane with nitro-blue tetrazolium chloride (NBT) / 5-bromo-4-chloro-3'-indolyphosphate *p*-toluidine salt (BCIP) solution (Thermo Fisher Scientific) for 10 min. During the visualisation process, alkaline phosphatase (localised at the protein of interest) catalyses the dephosphorylation of BCIP to form an intermediate that undergoes a redox reaction with NBT. This yields a blue-purple precipitate to reveal the position of MtrB

and MtrC.^{154,155} A schematic diagram for the Western blotting visualisation process is shown in **Fig. 2.3**.

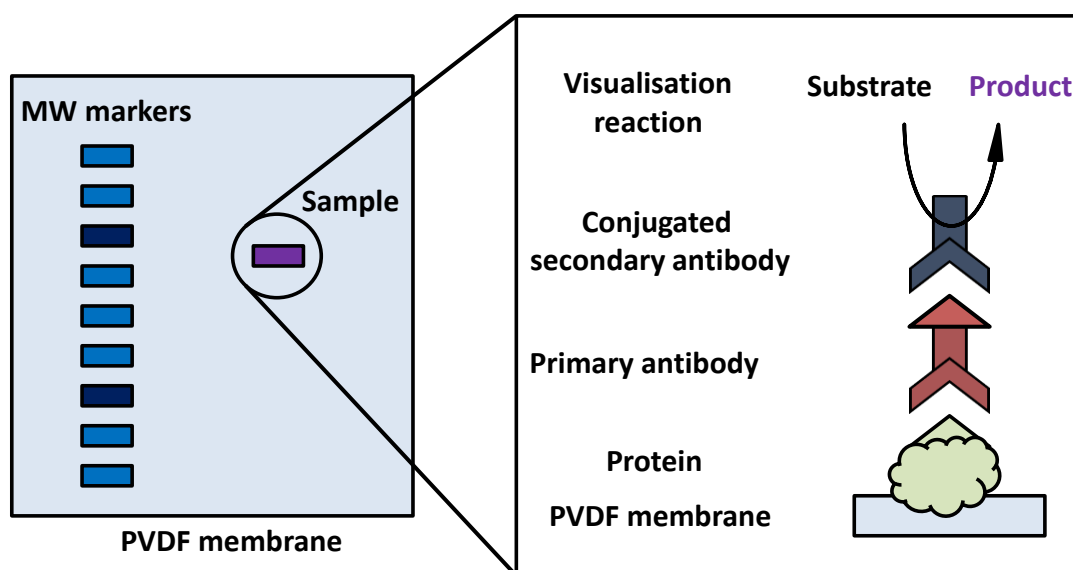


Figure 2.3 - Schematic diagram of processes and protein:protein interactions for visualisation in Western blotting after electrophoretic resolution. Proteins on a polyvinylidene fluoride (PVDF) membrane are visualised using a protein-specific primary antibody and a secondary antibody conjugated to alkaline phosphatase that catalyses the production of a coloured precipitate. MW = molecular weight.

2.3.7 Harvesting and re-suspension in a defined buffer

To prepare bacterial suspensions for enzyme assays and reductive transformations, *Shewanella* strains were cultured for the desired time period in M72 medium as described in section 2.3.3 then Hungate tubes were taken into a N₂-filled chamber (Belle Technology, clear acrylic chamber, atmospheric O₂ < 10 ppm) and the contents transferred to Eppendorf tubes. The tubes were removed from the chamber and bacteria were harvested by centrifugation (5 min, 13000 x g, 5 °C). The tubes were then returned to the chamber, the supernatants were removed and the cell pellets were gently re-suspended in anaerobic 50 mM HEPES, 50 mM NaCl (pH 6, 7 or 8). Suspensions were centrifuged as before and, inside the N₂-filled chamber, the cell pellets were gently re-suspended to the desired OD_{590nm} in anaerobic 50 mM HEPES, 50 mM NaCl (pH 6, 7 or 8). Bacterial suspensions in the defined buffer were then supplemented with the reagents required for the particular experiment (see below).

2.4 H₂ detection and quantification

2.4.1 Quantification of headspace H₂ using gas chromatography (GC)

2.4.1.1 Method principle and calibration

Headspace H₂ was quantified using a PerkinElmer Clarus 580 gas chromatograph with a thermal conductivity detector (TCD) and stainless steel molecular sieve column (PerkinElmer, 6 ft length, 2 mm internal diameter). The instrument used a TCD current of -40 mA, argon carrier gas at a flow rate of 25 mL min⁻¹ and internal temperatures of 80 °C for the oven housing the column and 100 °C for the packed injector and TCD. The instrument settings are summarised in **Fig. 2.4**. Mixtures of gases that are injected into the instrument are separated as individual components interact with the column differently and consequently reach the TCD at different rates. The detector monitors changes in the thermal conductivity of the column effluent versus pure carrier gas using heated filaments. The temperature, and hence resistance, of the filaments remains constant in the presence of pure carrier gas but changes when the sample, with a different thermal conductivity, flows through. The change in resistance is sensed by a bridge circuit which produces a voltage proportional to the amount of sample.

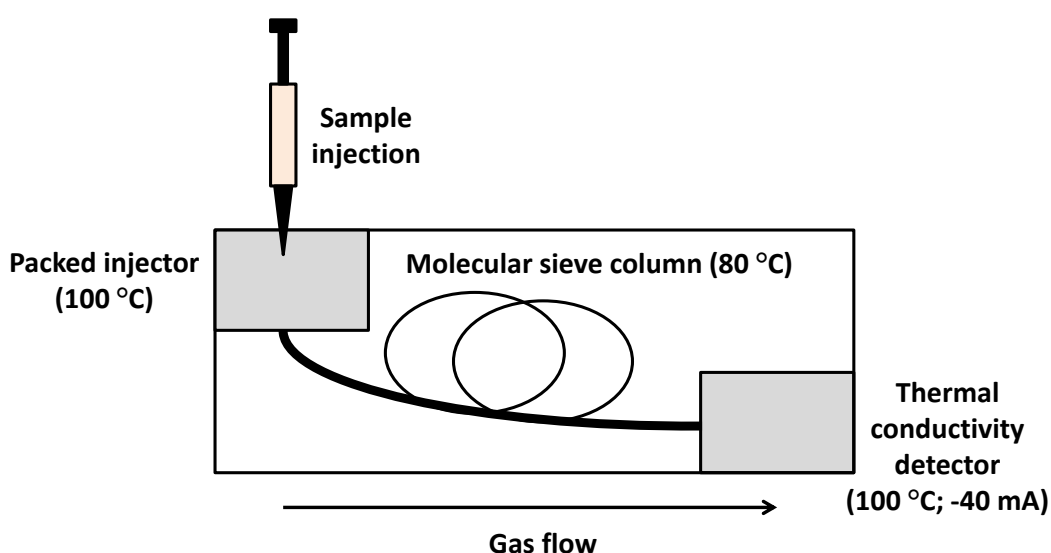


Figure 2.4 - Schematic diagram of gas chromatograph with thermal conductivity detector. Samples containing a mixture of gases are separated as they flow through the column. Individual components give a change in voltage as they reach the detector.

H₂, O₂ and N₂ were the only species detected by gas chromatography (GC) using the instrument settings and experimental conditions described in this chapter. Representative GC data showing voltage changes over time for an injection of 0.15 mL pure air (containing only O₂ and N₂) or 0.15 mL 10000 ppm H₂ in N₂ (containing no O₂) are presented in **Fig. 2.5A** to demonstrate typical peak positions. The H₂ peak area was converted to an amount of H₂ by regularly calibrating the instrument with a series of gas standards containing 100, 1000, 5000 or 10000 ppm H₂ in N₂ (Scientific and Technical Gases Ltd). A representative calibration curve is shown in **Fig. 2.5B**.

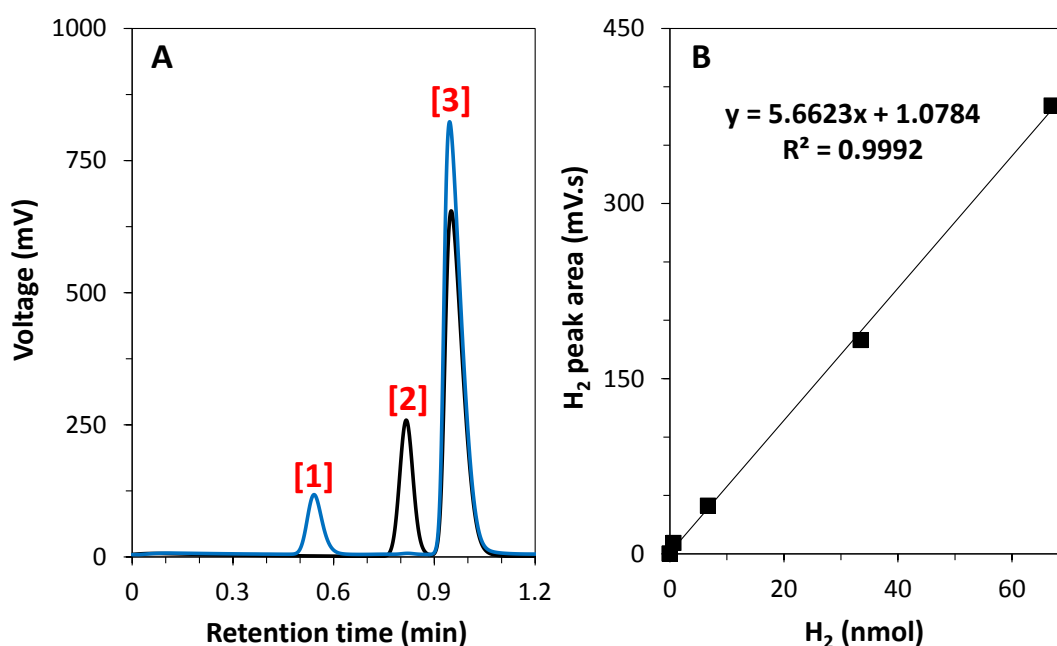


Figure 2.5 - Representative gas chromatography data. A) Relative positions of peaks corresponding to H₂ [1], O₂ [2] and N₂ [3] for an injection of 0.15 mL pure air (black) or 10000 ppm H₂ in N₂ (blue). B) Correlation between peak area and amount of H₂ determined using gas standards with known quantities of H₂ in N₂. Equation and R² value for linear trendline. See text for instrument settings.

2.4.1.2 Measurement of headspace H₂

GC was used to quantify headspace H₂ produced during microbial growth and by light-driven H₂-evolution over irradiation times of > 1 hr. To quantify H₂-evolution during microbial growth, *Shewanella* strains were cultured as described in section 2.3.3 then gaseous samples (0.15 mL) were extracted from Hungate tubes after the desired time period using a gas-tight syringe pre-purged with N₂ (destructive sampling from tubes). To quantify light-driven H₂-evolution, *Shewanella* strains were cultured and processed as described in sections 2.3.3 and 2.3.7, respectively, then cell pellets were gently

re-suspended to the desired OD_{590nm} in anaerobic 50 mM HEPES, 50 mM NaCl, pH 7 supplemented with a sacrificial electron donor (SED), MV and a photosensitiser as required. Reaction suspensions were transferred to clear, colourless glass vials (Supelco, 5 mL total volume) which were tightly sealed within the N_2 -filled chamber. Samples were then irradiated with the cold light source (room temperature, 0.7 kW m^{-2} light intensity unless otherwise stated) or the photosynthetic growth lamp ($25 \text{ }^\circ\text{C}$, 0.02 kW m^{-2} light intensity) with no stirring. Irradiation by the cold light source was provided with vials positioned inside the N_2 -filled chamber and the lamp positioned outside the chamber. The walls of the chamber served as an additional filter for light with $\lambda < 400 \text{ nm}$. Irradiation by the photosynthetic growth lamp was provided with vials positioned at a 45° angle on a foil-lined tray within the shaker incubator to maximise light absorption by the sample. Gaseous samples (0.15 mL) were extracted from glass vials after the desired time period using a gas-tight syringe pre-purged with N_2 (non-destructive sampling from vials).

2.4.2 Quantification of dissolved H_2 using a H_2 -sensing electrode

2.4.2.1 Method principle and calibration

Dissolved H_2 was quantified using a H_2 -sensing (Clark-type) electrode (Hansatech Oxygraph Plus) which measures a current proportional to the amount of dissolved H_2 in the sample. The instrument uses an electrode disk with a platinum anode positioned below the reaction solution and a silver cathode embedded in the insulating electrode base, as shown in **Fig. 2.6**. The anode is separated from the gently stirred reaction solution by an absorbent spacer (Rizla Blue) and a layer of polytetrafluoroethylene (PTFE). The absorbent spacer ensures a connection between the cathode and anode by trapping a thin layer of electrolyte (50 % saturated solution of KCl in Milli-Q water). The PTFE membrane is selectively permeable to dissolved gases meaning that other chemical species in the sample cannot reach the anode to contribute to the observed current. The lower portion of the electrode sample chamber was covered in duct tape to ensure that light from the cold light source only irradiated the reaction solution and not the exposed electrode surfaces. This was found to reduce the background signals observed when irradiating samples. The instrument was prepared for H_2 detection according to the manufacturer's protocol (Hansatech). Briefly, the anode was prepared by soaking in 2 M H_2SO_4 (to clean the surface) then platinum black was electrochemically deposited on the electrode surface from

a solution of 2 % $\text{H}_2\text{PtCl}_6(\text{H}_2\text{O})_6$ in Milli-Q water. The cathode was prepared by electrochemically depositing silver chloride on the electrode surface from an aqueous solution of 3 M KCl saturated with AgCl. Plating the electrodes and polarising at +0.7 V rendered the unit responsive to H_2 and unresponsive to O_2 .

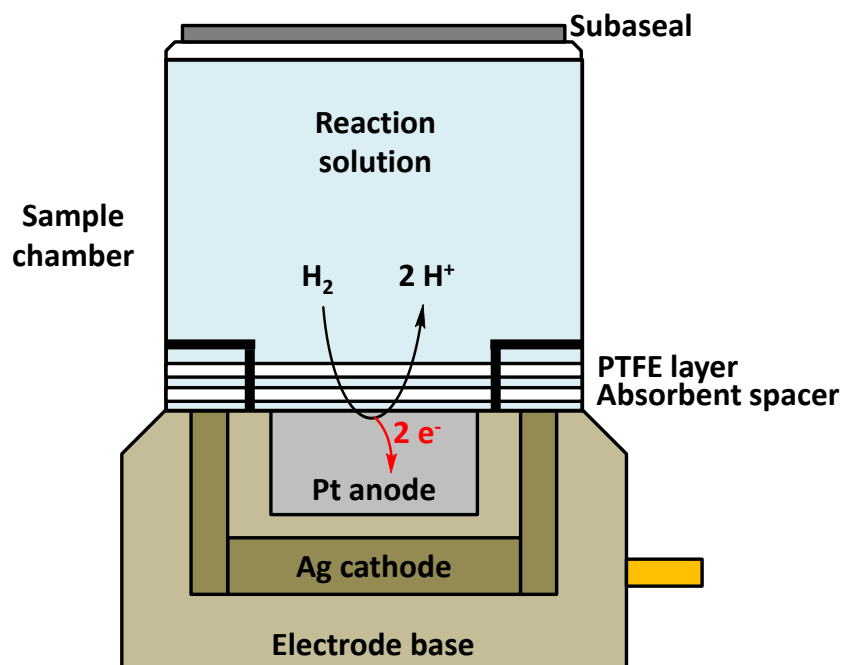


Figure 2.6 - Schematic diagram of H_2 -sensing electrode. The instrument consists of a platinum anode and silver cathode connected by an absorbent spacer saturated with electrolyte. Dissolved H_2 in the sample passes through the polytetrafluoroethylene (PTFE) layer to the anode where it is oxidised.

The observed current was converted to an amount of H_2 by regularly calibrating the instrument through the addition of aliquots of H_2 -saturated Milli-Q water (0.8 mM H_2 from Henry's Law,¹⁵⁶ prepared as described in section 2.1) to 1 mL anaerobic 50 mM HEPES, 50 mM NaCl, pH 7 within the electrode sample chamber. Representative data for the calibration of the H_2 -sensing electrode are shown in **Fig. 2.7**. Comparison of the H_2 -sensing electrode response under irradiation by the cold light source (0.7 kW m^{-2}) or in 50 mM HEPES, 50 mM NaCl at pH 6 or 8 showed no difference to that observed in 50 mM HEPES, 50 mM NaCl, pH 7 with no irradiation.

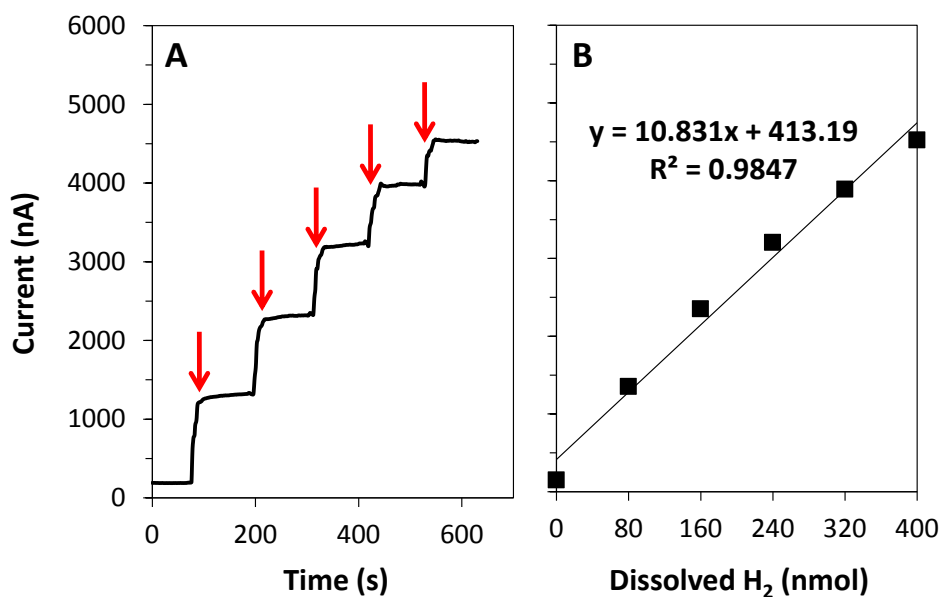


Figure 2.7 - Representative data showing calibration of the H₂-sensing electrode. A] Change in current over time in response to 5 additions (red arrows) of 0.1 mL H₂-saturated Milli-Q water to 1 mL anaerobic 50 mM HEPES, 50 mM NaCl, pH 7. B] Correlation between current and the amount of dissolved H₂. Equation and R² value for linear trendline.

2.4.2.2 Measurement of dissolved H₂

The H₂-sensing electrode was used for real-time quantification of dissolved H₂ produced by DT-driven H₂-evolution and light-driven H₂-evolution over irradiation times of < 1 hr. *Shewanella* strains were cultured and processed as described in sections 2.3.3 and 2.3.7, respectively, then cell pellets were gently re-suspended to the desired OD_{590nm} in anaerobic 50 mM HEPES, 50 mM NaCl (pH 6, 7 or 8). For DT-driven H₂-evolution, samples (1.29 mL) were supplemented with 0.3 mg mL⁻¹ DT and/or 0.3 mM MV as required then transferred to the H₂-sensing electrode which was sealed within the N₂-filled chamber with negligible headspace to ensure the majority of H₂ produced in the subsequent experiment remained in solution. Outside the N₂-filled chamber, the electrodes were connected to a potentiostat that poised the electrodes for H₂ detection. For light-driven H₂-evolution, samples (1.65 mL) were supplemented with TEOA, MV and a photosensitiser as required then transferred to the H₂-sensing electrode which was assembled and operated as described above. The system was allowed to equilibrate for 10 min under ambient light during which time the current fell to a constant low level. The sample was then periodically irradiated through the side of the electrode sample chamber (which transmits 90 % of light with $\lambda > 400$ nm) with the cold light source (room temperature, 0.7 kW m⁻² light intensity unless otherwise stated) for the desired time period(s).

2.5 Spectrophotometric enzyme assays

Spectrophotometric assays for the quantification of H₂ oxidation, fumarate-reduction and CO₂-reduction by bacterial enzymes were performed under anaerobic conditions inside a N₂-filled chamber with samples in sealed polystyrene cuvettes (STARLAB UK, 1 cm pathlength). Spectra were recorded using a Biochrom WPA Biowave II diode array spectrophotometer located inside the chamber. Absorbance changes were converted to concentration changes using the Beer-Lambert law shown in **Eq. 2.1**, where A is the absorbance, ϵ is the extinction coefficient in mM⁻¹ cm⁻¹, c is the concentration in mM, L is the pathlength of light in cm, I₀ is the intensity of incident light and I is the intensity of transmitted light. The extinction coefficients of redox indicators used in this study are provided in **Table 2.3**. Bacterial cell pellets for enzyme assays were harvested by centrifugation (5 min, 13000 x g, 5 °C) outside the N₂-filled chamber then supernatants were separated from cell pellets within the chamber and samples were supplemented with the reagents required for the particular assay (see below).

$$A = \epsilon \times c \times L = \log_{10} \left(\frac{I_0}{I} \right) \quad \text{Eq. 2.1}$$

Table 2.3 - Extinction coefficients of BV⁺, MV⁺ and MtrC used for spectrophotometric assays.

Redox indicator	Wavelength (nm)	Extinction coefficient (mM ⁻¹ cm ⁻¹)
BV ⁺	600	7.4 ¹⁵⁷
MV ⁺	396	42.1 ¹⁵⁸
	600	13.5 ¹⁵⁹
	606	13.7 ¹⁵⁸
MtrC (oxidised)	410	1260 ⁸⁴

The ability of different SEDs and photosensitisers to facilitate photoreduction of electron acceptors (MV²⁺, BV²⁺ and MtrC) under irradiation by visible light was also assessed using absorbance spectroscopy. Anaerobic samples containing a SED, an electron acceptor and a photosensitiser were prepared in sealed polystyrene cuvettes within a N₂-filled chamber then irradiated (0.7 kW m⁻², room temperature) through the side of the chamber by the cold light source with no stirring. Full details about the composition of samples for these experiments are provided in the relevant sections in chapters 4 and 6.

respectively). The absorbance at 600 nm was then recorded over 8 min with an addition of 0.1 mL of either 10 mM fumarate or 100 mM CO₂ (in 50 mM HEPES, 50 mM NaCl, pH 7) after approximately 1 min followed by gentle mixing and continued measurement.

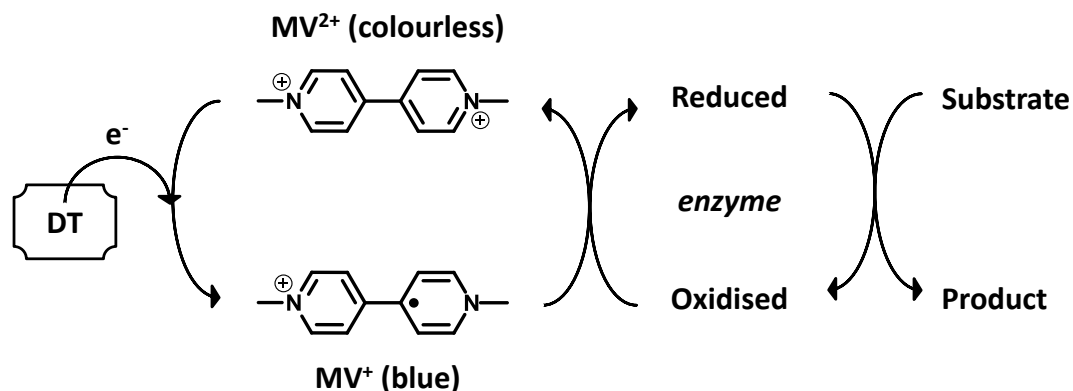


Figure 2.9 - Schematic diagram for assay of fumarate- and CO₂-reductase activity. Sodium dithionite (DT) is used to reduce oxidised methyl viologen (MV²⁺) to form MV⁺ which gives an increased absorbance at 600 nm. In the presence of functional enzyme, MV⁺ is re-oxidised and the absorbance at 600 nm decreases as electrons are transferred to the substrate.

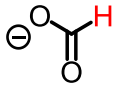
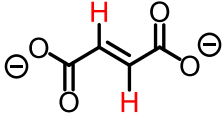
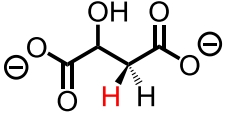
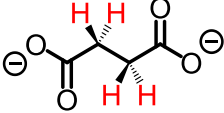
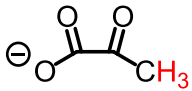
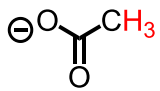
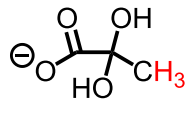
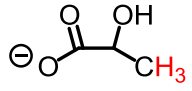
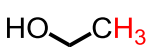
2.6 Quantification of carbon-based compounds using ¹H and ¹³C nuclear magnetic resonance (NMR)

Proton nuclear magnetic resonance (¹H-NMR) was used to quantify DT- and light-driven reduction of fumarate, pyruvate and CO₂. The technique draws on the fact that ¹H has a nuclear spin of ½ meaning it can align with or against an externally applied magnetic field to give two possible energy states with a difference in energy that is proportional to the strength of the applied field.^{160–162} Nuclei in the lower energy state (aligned with the field) can be excited into the higher energy state using radio frequency electromagnetic radiation. The release of energy as the nuclei return to the lower energy state (termed relaxation) can then be detected by a NMR spectrometer. The position (chemical shift) and shape (peak splitting) of the observed signals are characteristic of nuclei within particular chemical environments enabling the composition of the sample to be resolved from the NMR spectrum. Chemical shift is determined by the amount of electron density surrounding the nuclei because electrons induce a magnetic field that opposes the applied field. Consequently, electron-deficient nuclei experience a stronger overall field than electron-rich nuclei and absorb radiation at a higher frequency to give a greater chemical shift (relative to reference nuclei set at 0 ppm).^{160–162} Peak splitting is determined by magnetic interactions between vicinal nuclei in different chemical environments.

Peaks are split based on the “ $n + 1$ ” rule where n is the number of adjacent nuclei in a distinct chemical environment.^{160–162}

To prepare samples for ^1H NMR analysis, *Shewanella* strains were cultured and processed as described in sections 2.3.3 and 2.3.7, respectively, then cell pellets were gently re-suspended to $\text{OD}_{590\text{nm}} \approx 0.25$ in 1 mL 50 mM HEPES, 50 mM NaCl, pH 7 within clear, colourless glass vials (Supelco, 5 mL total volume). DT-driven transformations were performed by supplementing samples with 0.8 mg mL^{-1} DT, 0.5 mM MV and fumarate, pyruvate or CO_2 (initial concentrations between 2.2 and 5 mM) and incubating for 30 min in a N_2 -filled chamber. Light-driven transformations were performed by supplementing samples with 50 mM TEOA, 0.5 mM MV, 0.08 mM eosin Y and fumarate, pyruvate or CO_2 (initial concentrations between 8.1 and 11.7 mM) and irradiating with the cold light source (room temperature, 0.7 kW m^{-2}) for 30 min or the photosynthetic growth lamp ($25 \text{ }^\circ\text{C}$, 0.02 kW m^{-2}) for 24 hr. On completion of the desired incubations, cellular material was removed by centrifugation (7 min, $13000 \times g$, $5 \text{ }^\circ\text{C}$) and 0.4 mL of the supernatant was mixed with 0.4 mL NMR buffer (21.7 mM NaH_2PO_4 , 81 mM K_2HPO_4 , 1 mM TSP, 14.2 mM sodium azide in D_2O). Samples were then stored at $-20 \text{ }^\circ\text{C}$ until analysed at which point they were thawed at room temperature and 0.5 mL was transferred to a 5 mm NMR tube for spectral acquisition. Spectra were recorded at 600 MHz on a Bruker Avance spectrometer (Bruker BioSpin GmbH) running Topspin 2.0 software and fitted with a cryoprobe. Each spectrum was acquired with 64 scans, a spectral width of 12.3 kHz, an acquisition time of 2.7 s and a relaxation delay of 3.0 s. The “noesypr1d” pre-saturation sequence was used to suppress the residual water signal with low-power selective irradiation at the water frequency during the recycle delay and a mixing time of 10 ms. ^1H -NMR spectra were transformed with a 0.3 Hz line broadening, manually phased, baseline corrected and referenced by setting the TSP methyl signal to 0 ppm. Carbon-based compounds were quantified with Chenomx NMR suite 7.6TM software using resonances reported previously,^{163,164} the Human Metabolome Database (<http://www.hmdb.ca/>) and 2D-NMR methods: correlation spectroscopy (COSY), heteronuclear single-quantum correlation spectroscopy (HSQC) and heteronuclear multiple-bond correlation spectroscopy (HMBC). ^1H -NMR spectra were acquired and analysed in collaboration with Dr. Adam Elliston and Dr. Gwénaëlle Le Gall (Institute of Food Research, UK). The ^1H -NMR peaks used for quantification of carbon-based compounds are provided in **Table 2.4** with the protons corresponding to each peak shown in red on the chemical structures.

Table 2.4 - $^1\text{H-NMR}$ peaks used for quantification of carbon-based compounds. The protons corresponding to the observed signals are highlighted in red on the chemical structures.

Compound	Structure	Chemical shift (ppm)	Peak splitting
Formate		8.40	Singlet
Fumarate		6.50	Singlet
Malate		2.70	Doublet of doublets
Succinate		2.42	Singlet
Pyruvate		2.38	Singlet
Acetate		1.90	Singlet
Pyruvate hydrate		1.50	Singlet
Lactate		1.30	Doublet
Ethanol		1.20	Triplet

$^{13}\text{C-NMR}$ was used for quantification of ^{13}C -formate in supernatants after 24 hr irradiation (photosynthetic growth lamp at an intensity of 0.02 kW m^{-2}) of anaerobic samples containing MR-1 ($\text{OD}_{590\text{nm}} \approx 0.25$), 50 mM TEOA, 0.5 mM MV, 0.08 mM eosin Y and 10 mM ^{13}C -carbonate in 50 mM HEPES, 50 mM NaCl, pH 7 (1 mL) prepared as described above. Each $^{13}\text{C-NMR}$ spectrum was acquired with 5000 scans, a spectral width of 36000 Hz and an acquisition time of 0.91 s. The amount of ^{13}C -formate in samples was quantified by comparison to the spectra of defined concentrations (0, 0.25, 0.5, 1, 1.5, 2, 2.5, 10 and 100 mM) of ^{13}C -formate in 50 mM HEPES, 50 mM NaCl, pH 7.

CHAPTER 3

Anaerobic growth of *Shewanella oneidensis* MR-1 to catalyse H₂-evolution and reduction of fumarate, pyruvate and CO₂

Chapter 3 - Anaerobic growth of *Shewanella oneidensis* MR-1 to catalyse H₂-evolution and reduction of fumarate, pyruvate and CO₂

3.1 Introduction

As described in chapter 1, MR-1 is a suitable bacterium to be utilised for artificial photosynthesis because it can produce four key enzymes that catalyse reductive transformations of current interest. The enzymes are the hydrogenases, fumarate reductase, lactate dehydrogenases and formate dehydrogenases and the catalytic transformations are the reduction of protons, fumarate, pyruvate and CO₂ to H₂, succinate, lactate and formate, respectively. To best exploit this ability for light-driven chemical synthesis, a single growth condition must be established that leads to the simultaneous presence of all four enzymes in MR-1. This would allow the bacterium to act as a multi-faceted electrocatalyst with a tuneable product range determined by the presence of a particular substrate. In this chapter, results from biochemical assays are presented that assessed MR-1 enzyme activities after culturing the bacterium under anaerobic conditions with an excess of lactate as electron donor to fumarate as electron acceptor. Data are presented from spectrophotometric and electrochemical assays that were used to quantify hydrogenase activity and from ¹H-NMR analysis that was used to identify and quantify the products formed from the reduction of fumarate, pyruvate and CO₂. The work shown below forms the basis for cell-based photocatalysis with MR-1 developed in the next chapters where photo-excited electrons are delivered to bacterial enzymes to drive the desired reductive transformations.

3.2 Anaerobic growth of *Shewanella oneidensis* MR-1 under acceptor-limited conditions

Previous research into the metabolic pathways in MR-1 makes it possible to select culture conditions that should lead to the simultaneous presence of all four enzymes of interest to this study within the bacterium (see **Fig. 1.11**).^{91,93-95} With lactate as the electron donor and

fumarate as the electron acceptor, MR-1 should naturally produce the fumarate reductase, lactate dehydrogenases and formate dehydrogenases as these enzymes are required for the sequential oxidation of lactate to CO₂, with the liberated electrons used for reduction of fumarate to succinate. Furthermore, using an excess of lactate to fumarate should lead to acceptor-limited conditions once the fumarate has been completely depleted. Lactate oxidation should then become coupled to proton reduction as reducing equivalents are delivered to the hydrogenases. Lastly, the use of anaerobic growth conditions should avoid the (ir)reversible inhibition of the hydrogenases by O₂.⁶⁰ Growth of MR-1 under these conditions was reported previously in Meshulam-Simon et al. (2007) where it was found that depletion of fumarate led to the bacterium entering stationary phase and the onset of H₂ production.⁹¹ However, a comprehensive assessment of MR-1 enzyme activities was not performed in this previous study.

For the work in this thesis, MR-1 was cultured in nutrient-rich M72 medium containing 37.5 mM D,L-lactate, 18.8 mM fumarate, 37.5 mM HEPES and 1.88 mM NiCl₂ (see section 2.3.1), similar to the conditions reported previously for purification of the MR-1 [NiFe]-hydrogenase but with fumarate as the electron acceptor in place of DMSO.⁹⁸ M72 medium (10 mL) in glass Hungate tubes was inoculated (2 % [v/v]) with MR-1 then tubes were sealed and headspaces (7 mL) were purged with N₂ to remove atmospheric O₂. Cultures were incubated at 30 °C with periodic quantification of optical density at 590 nm (OD_{590nm}, a measure of scatter caused by and proportional to the size and number of bacteria in growth medium) and headspace H₂ content (see sections 2.3.3 and 2.4.1). Parallel control experiments were performed with the HydA⁻/HyaB⁻ strain lacking functional hydrogenases (see section 2.3.2)¹³⁹ and no bacteria. The changes in OD_{590nm} and headspace H₂ over 48 hr are shown in **Fig. 3.1**.

The OD_{590nm} of MR-1 and HydA⁻/HyaB⁻ cultures started increasing after the initial reading and plateaued after 8 and 12 hr, respectively, as the bacteria entered the stationary phase. Negligible changes in OD_{590nm} were seen for non-inoculated M72 medium showing that the growth curves produced with MR-1 and HydA⁻/HyaB⁻ correspond to the presence of bacteria. H₂ was first detected after 18 hr in headspaces of tubes containing MR-1 and the amount of H₂ increased between 18 and 48 hr to a total of 328 ± 35 nmol at the end of the experiment. H₂ was not detected in headspaces of tubes containing HydA⁻/HyaB⁻, or no bacteria, confirming that proton reduction resulted specifically from the activity of the

wild-type MR-1 [NiFe]- and/or [FeFe]-hydrogenases. Based on the predicted metabolic pathways in MR-1 (see **Fig. 1.11**), the increase in OD_{590nm} during incubation with an excess of lactate to fumarate and the presence of H₂ in culture headspaces after 18 hr suggest that MR-1 can produce the four key enzymes targeted in this study. However, the results do not indicate whether the enzymes can be exploited for reductive catalysis using an external source of electrons. As such, a series of biochemical assays were used to directly assess the activities of the enzymes after harvesting MR-1 from growth medium and re-suspending in a defined buffer.

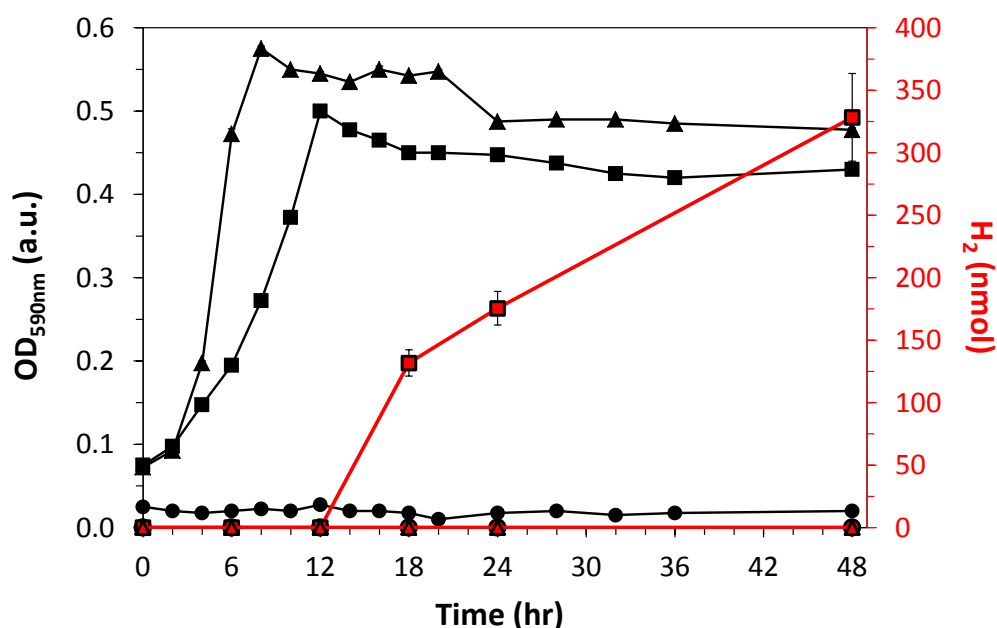


Figure 3.1 - Anaerobic growth of MR-1 and HydA⁻/HyaB⁻ with 37.5 mM lactate as electron donor and 18.8 mM fumarate as electron acceptor. Optical density at 590 nm (black, left axis) and headspace H₂ (red, right axis) for MR-1 (squares), HydA⁻/HyaB⁻ (triangles) and no bacteria (circles). Inoculation at 0 hr of M72 medium (10 mL) supplemented with anaerobic growth additions. Samples had 7 mL headspace (100 % N₂ at inoculation). Optical densities are mean values from 4 biological replicates, error bars indicate standard error. Headspace H₂ data are mean values from biological duplicates, error bars indicate maximum and minimum. Lines serve as a guide to the eye, the majority of error bars are too small to resolve.

3.3 Biochemical assays of hydrogenase, fumarate reductase, lactate dehydrogenase and formate dehydrogenase activities in anaerobically grown *Shewanella oneidensis* MR-1

For experimental tractability, *Shewanella* strains were routinely cultured for 24 hr under anaerobic, acceptor-limited conditions as described in section 3.2. Bacteria were then

harvested by centrifugation with minimal exposure to O₂ and gently re-suspended to the desired OD_{590nm} in anaerobic 50 mM HEPES, 50 mM NaCl, pH 7 within a N₂-filled chamber (see section 2.3.7). Washing and re-suspending bacteria removed residual growth medium to give a well-defined system that could be readily assessed for enzyme activities. The activity of the hydrogenases was evaluated using spectrophotometric H₂ oxidation assays and a H₂-sensing electrode that electrochemically detects dissolved H₂ in real-time. The activity of the fumarate reductase, lactate dehydrogenases and formate dehydrogenases was initially assessed by performing H₂-evolution assays in the presence of fumarate, pyruvate and CO₂ then formation of the desired products was quantified using ¹H-NMR analysis. Results from the experiments are presented in the sections below.

3.3.1 Hydrogenase activity

Spectrophotometric H₂ oxidation assays were performed with anaerobic bacterial suspensions at OD_{590nm} between 0.4 and 0.5. Samples were supplemented with BV as a colourimetric redox indicator ($E_m = -0.36\text{ V}$)¹⁶⁵ then the absorbance at 600 nm was recorded over 10 min with an addition of 0.1 mL H₂-saturated Milli-Q water after approximately 1 min. An increase in absorbance at 600 nm indicated the presence of functional hydrogenases capable of oxidising H₂ and transferring electrons to BV (see section 2.5.1). Representative data with MR-1, HydA⁻/HyaB⁻ and no bacteria are shown in **Fig. 3.2**.

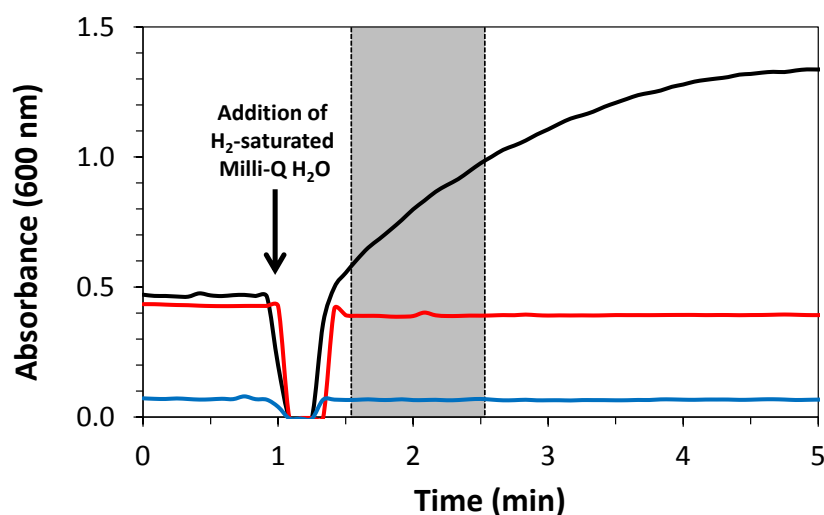


Figure 3.2 - Representative H₂ oxidation data. Absorbance at 600 nm for MR-1 (black), HydA⁻/HyaB⁻ (red) and no bacteria (blue). Samples contained 1 mM BV in 50 mM HEPES, 50 mM NaCl, pH 7 with an addition of 0.1 mL H₂-saturated Milli-Q water after 1 min. MR-1 and HydA⁻/HyaB⁻ OD_{590nm} ≈0.45. Pathlength 1 cm. Shaded area shows the time over which initial rates were calculated using **Eq. 3.1**.

The offset in absorbance at 0 min for MR-1 and HydA⁻/HyaB⁻ is due to scattering caused by the bacteria and the sharp decrease in absorbance around 1 min is due to removal of the cuvette from the spectrophotometer for mixing. Initial rates of H₂ oxidation were calculated over 1 min after the cuvette had been returned to the spectrophotometer (see **Fig. 3.2**, shaded area). Absorbance changes were converted to amounts of H₂ oxidised per min using **Eq. 3.1** where $\Delta\text{Abs}_{600\text{nm}}$ is the change in absorbance at 600 nm over 1 min, ϵ_{BV^+} is the extinction coefficient for the one-electron reduced form of BV (BV⁺, 7.4 mM⁻¹ cm⁻¹)¹⁵⁷ and division by a factor of two accounts for the fact that one molecule of H₂ liberates two electrons upon oxidation. Mean H₂ oxidation rates for MR-1, HydA⁻/HyaB⁻ and no bacteria are listed in **Table 3.1**. Results for MR-1 and HydA⁻/HyaB⁻ have been normalised to total protein content quantified using a BCA assay (see section 2.3.4) to allow a better comparison of the responses from different strains. Negligible H₂ oxidation rates were seen for samples containing HydA⁻/HyaB⁻ and no bacteria whereas an oxidation rate of 138 ± 34 nmol H₂ min⁻¹ mg⁻¹ was seen for samples containing MR-1. The results confirm that acceptor-limited growth conditions lead to the production of MR-1 hydrogenases that can oxidise H₂ and that these enzymes are responsible for the increase in absorbance at 600 nm during the spectrophotometric assays.

$$\frac{\Delta\text{Abs}_{600\text{nm}} \times 10^3}{\epsilon_{\text{BV}^+} \times 2} = \text{nmol H}_2 \text{ oxidised min}^{-1} \quad \text{Eq. 3.1}$$

Table 3.1 - Initial rates of H₂ oxidation coupled to BV reduction by MR-1, HydA⁻/HyaB⁻ and no bacteria. Rates with MR-1 and HydA⁻/HyaB⁻ are mean values from technical duplicates of 4 biological replicates with standard error (normalised to total protein). Rate with no bacteria is the mean value from technical duplicates, error indicates maximum and minimum. Anaerobic samples in 1 mM BV, 50 mM HEPES, 50 mM NaCl, pH 7.

Strain	H ₂ oxidation rate
MR-1	138 ± 34 nmol min ⁻¹ mg ⁻¹
HydA ⁻ /HyaB ⁻	2 ± 2 nmol min ⁻¹ mg ⁻¹
No bacteria	0.06 ± 0.02 nmol min ⁻¹

Of greater interest to this study is the opposite reaction catalysed by hydrogenases (i.e. the reduction of aqueous protons to H₂) because H₂ is a valuable and versatile chemical fuel (see section 1.5). To drive this transformation using MR-1, anaerobic bacterial suspensions (1.3 mL) at OD_{590nm} ≈ 0.25 were supplemented with 0.3 mg mL⁻¹ (≈ 1.7 mM) DT as a chemical reductant and 0.3 mM MV as an electron transfer mediator then formation of

H₂ was quantified electrochemically with samples placed within the chamber of a H₂-sensing electrode (see section 2.4.2). The use of DT and MV has been reported previously for H₂-evolution assays with whole-cell bacteria and purified enzymes.^{138,166–168} They are suitable reagents because DT ($E_m = -0.66$ V, pH 7)¹⁶⁹ can facilitate the reduction of MV²⁺ to MV⁺ ($E_m = -0.45$ V)¹⁶⁵ and MV is known to effectively cross the outer membrane of Gram-negative bacteria.^{82,170} Minimal gaseous headspace was allowed above samples within the chamber of the H₂-sensing electrode to ensure the majority of evolved H₂ remained in solution and reaction suspensions were gently stirred during measurement to afford homogeneity. Control experiments were carried out by systematically omitting or replacing components of the system detailed above. Representative H₂-evolution profiles for MR-1 and HydA⁻/HyaB⁻ with DT and MV are shown in **Fig. 3.3A** and are comparable to those reported previously with *E. coli*.¹⁶⁶ The amounts of dissolved H₂ in samples after 30 min are presented in **Fig. 3.3B**.

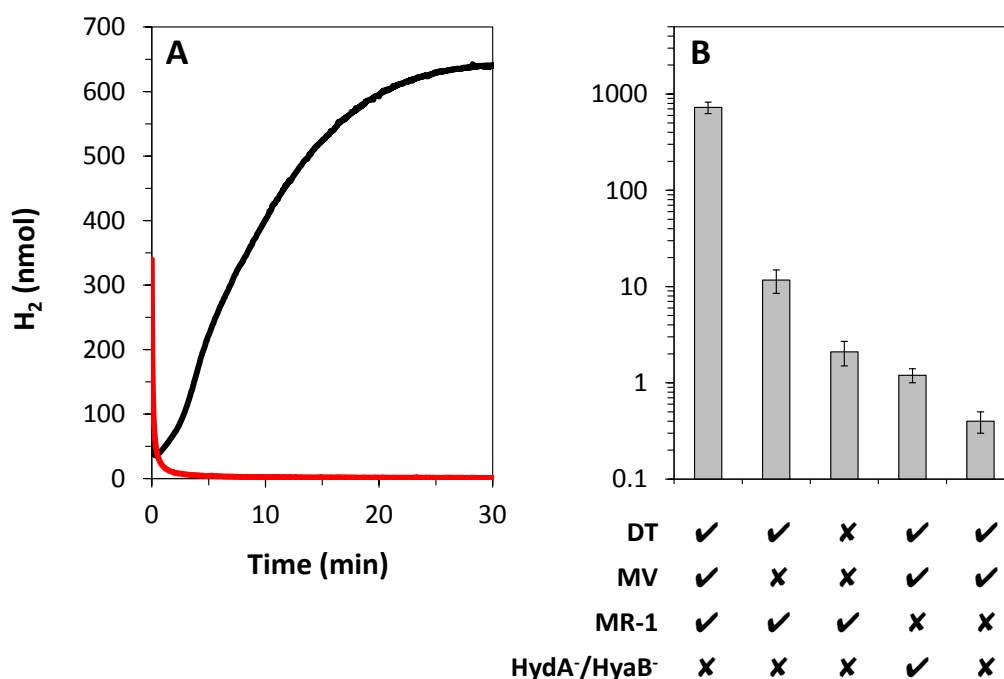


Figure 3.3 - DT-driven H₂-evolution by MR-1. A] Representative data for MR-1 (black) and HydA⁻/HyaB⁻ (red) at OD_{590nm} ≈ 0.25 in the presence of 0.3 mg mL⁻¹ DT and 0.3 mM MV. B] Dissolved H₂ produced after 30 min in suspensions (1.3 mL) of MR-1 or HydA⁻/HyaB⁻ (OD_{590nm} ≈ 0.25) with 0.3 mg mL⁻¹ DT and/or 0.3 mM MV as indicated. Mean value with standard error from 5 biological replicates for DT, MV and MR-1. Other values are the mean from duplicates, error bars indicate maximum and minimum. Anaerobic samples in 50 mM HEPES, 50 mM NaCl, pH 7 at room temperature.

MR-1 suspensions contained 725 ± 97 nmol H₂ after 30 min incubation with DT and MV. Approximately 60-fold less H₂ was produced in the absence of MV and less than 3 nmol H₂

was detected in samples where DT and MV or MR-1 were omitted, or where MR-1 was replaced with HydA⁻/HyaB⁻ at the same OD_{590nm}. The data confirm that acceptor-limited growth conditions lead to the production of MR-1 hydrogenases which can be exploited for DT-driven proton reduction. The control experiments show that electrons are exclusively provided to the hydrogenases by DT, as opposed to intracellular MR-1 metabolite reserves, and that MV can rapidly transfer electrons from DT to the hydrogenases.

Changing the OD_{590nm} of MR-1 suspensions was found to have a decisive impact on both the initial rate and total amount of DT-driven H₂-evolution, as shown in **Fig. 3.4** for MR-1 at OD_{590nm} ≈2.5, ≈0.25 or ≈0.03. The initial rate of H₂-evolution increased approximately 50-fold when the OD_{590nm} was raised from ≈0.03 to ≈0.25 and approximately 4-fold when raised from ≈0.25 to ≈2.5. These trends likely reflect the increase in hydrogenase content of the sample available to accept electrons from MV⁺ for proton reduction. However, total H₂ production after 40 min did not correlate with OD_{590nm} in the same way. For MR-1 at OD_{590nm} ≈2.5, the amount of dissolved H₂ plateaued after approximately 12 min then decreased such that net H₂ accumulation at the end of the experiment was around half as much as that seen with MR-1 at OD_{590nm} ≈0.25. This likely reflects the fact that the hydrogenases are reversible enzymes meaning that dissolved H₂ can be re-oxidised once DT has been depleted and there is no longer a driving force for proton reduction. Electrons could then be distributed amongst intracellular metabolites and enzymes with more positive redox potentials than the H⁺/H₂ couple ($E_m = -0.41$ V, pH 7).¹⁰⁰ It is possible that a closed system with no gaseous headspace (as is the case for the H₂-sensing electrode chamber) promotes H₂ re-oxidation as the product remains dissolved and readily accessible to the hydrogenases and it is likely that this process is more pronounced at the higher cell densities because of the greater quantity of intracellular electron acceptors in the sample.

Overall, the results presented in this section show that MR-1 contains functional, reversible hydrogenases after anaerobic growth under acceptor-limited conditions and that OD_{590nm} can significantly impact the rate and extent of DT-driven H₂-evolution. In the next section, data are shown from biochemical assays that evaluated whether MR-1 also contained fumarate reductase, lactate dehydrogenases and formate dehydrogenases active in the reduction of fumarate, pyruvate and CO₂, respectively, when cultured under acceptor-limited conditions.

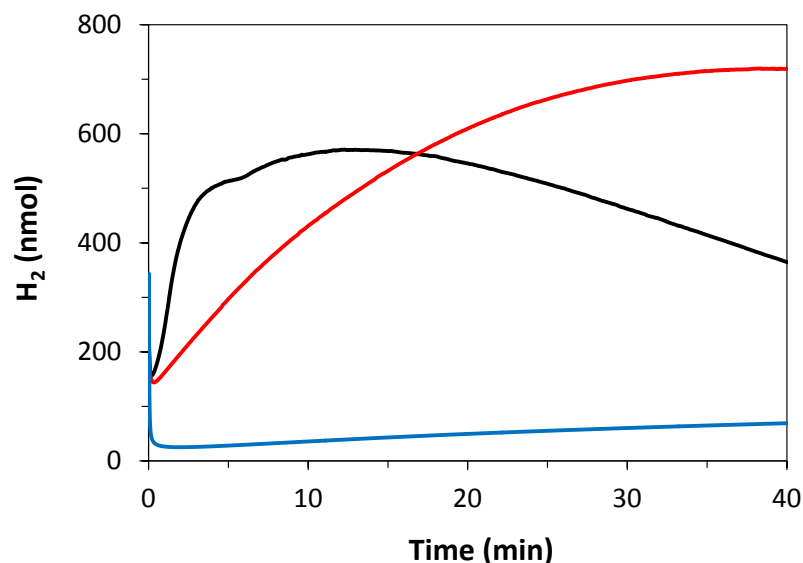


Figure 3.4 - DT-driven H₂-evolution by MR-1 at different cell densities. Dissolved H₂ in suspensions (1.3 mL) of MR-1 at OD_{590nm} ≈2.5 (black), ≈0.25 (red) or ≈0.03 (blue) with 0.3 mg mL⁻¹ DT and 0.3 mM MV. Anaerobic samples in 50 mM HEPES, 50 mM NaCl, pH 7 at room temperature.

3.3.2 Reduction of fumarate, pyruvate and CO₂

The reduction of carbon-based substrates by MR-1 was first assessed by performing DT-driven H₂-evolution assays in the presence of fumarate, pyruvate or CO₂ to see whether electrons could be re-directed away from the hydrogenases to the fumarate reductase, lactate dehydrogenases or formate dehydrogenases, respectively. Sodium carbonate dissolved in anaerobic 50 mM HEPES, 50 mM NaCl, pH 7 was used as a convenient source of CO₂ for the experiments and, for simplicity, the term “CO₂” is used in this thesis to refer to equilibrated solutions containing carbonic acid, bicarbonate and dissolved CO₂ (see **Eq. 1.2**).¹⁷¹ MR-1 was cultured and processed as described in sections 3.2 and 3.3 then bacterial suspensions (1.3 mL, OD_{590nm} ≈0.25) were supplemented with 0.3 mg mL⁻¹ DT, 0.3 mM MV and 5 mM fumarate, pyruvate or CO₂. Samples were transferred to the chamber of the H₂-sensing electrode and the amount of dissolved H₂ was monitored over 30 min. Representative data from the experiments are shown in **Fig. 3.5** and mean values for total H₂ production after 30 min are given in **Table 3.2**. In the presence of all three carbon substrates, less H₂ was produced compared to experiments with no added substrate suggesting that electrons provided to the bacterium by DT can be utilised for other reductive transformations. In the presence of pyruvate or CO₂, the amount of dissolved H₂ plateaued after approximately 13 or 21 min, respectively, and then started to decrease, presumably due to re-oxidation of H₂ by MR-1 as described above. The lack of detectable

H₂ in the presence of fumarate suggests that the reduction of fumarate proceeds to a significantly greater extent than the reduction of pyruvate and CO₂.

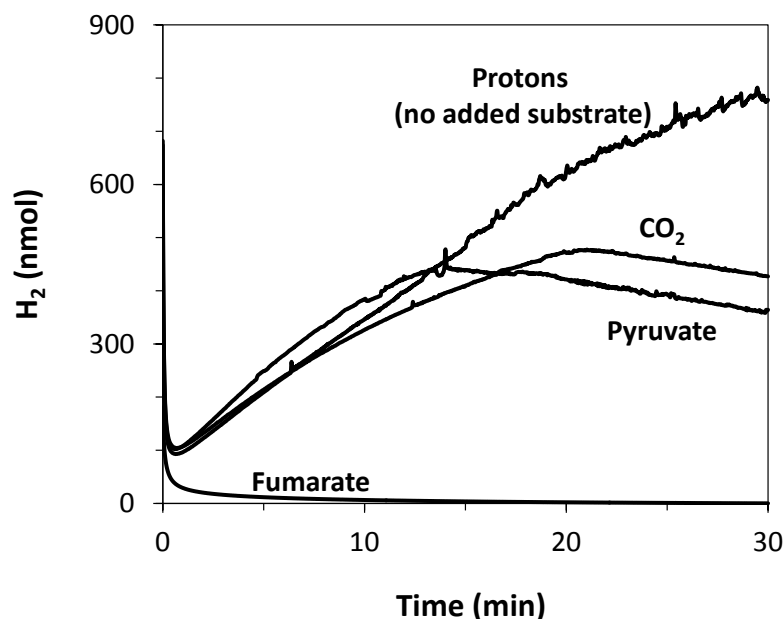


Figure 3.5 - DT-driven H₂-evolution by MR-1 in the presence of 5 mM fumarate, pyruvate or CO₂. Representative data for dissolved H₂ in MR-1 suspensions (OD_{590nm} ≈0.25) with 0.3 mg mL⁻¹ DT and 0.3 mM MV. Anaerobic samples (1.3 mL) in 50 mM HEPES, 50 mM NaCl, pH 7 at room temperature.

Table 3.2 - DT-driven H₂-evolution by MR-1 in the presence of fumarate, pyruvate or CO₂. Dissolved H₂ in samples incubated for 30 min with 0.3 mg mL⁻¹ DT, 0.3 mM MV and 5 mM fumarate, pyruvate or CO₂. MR-1 OD_{590nm} ≈0.25. Mean values from technical duplicates, error indicates maximum and minimum. Anaerobic samples (1.3 mL) in 50 mM HEPES, 50 mM NaCl, pH 7 at room temperature.

Added substrate	Dissolved H ₂ (nmol)
None	773 ± 14
Fumarate	0
Pyruvate	347 ± 18
CO ₂	450 ± 23

To quantify the formation of succinate, lactate and formate from reduction of fumarate, pyruvate and CO₂, respectively, anaerobic MR-1 suspensions (1 mL) at OD_{590nm} ≈0.25 were prepared in glass vials and a series of parallel assays were performed within a N₂-filled chamber. Samples contained 0.8 mg mL⁻¹ (≈4.6 mM) DT, 0.5 mM MV and fumarate, pyruvate or CO₂ (initial concentrations between 2.2 and 5 mM, see below). Greater initial concentrations of DT and MV were used compared to H₂-evolution assays to ensure a sufficient reservoir of electrons and rate of electron transfer for the reduction of carbon

substrates. After 30 min incubation, MR-1 was removed from samples by centrifugation and supernatants were mixed with deuterated phosphate buffer for $^1\text{H-NMR}$ analysis (see section 2.6). Control experiments were performed with no added carbon substrate and/or no bacteria. Representative $^1\text{H-NMR}$ spectra are shown in **Fig. 3.6** and supernatant compositions after 30 min are presented in **Table 3.3**. The peaks in **Fig. 3.6A** correspond to sodium 3-(trimethylsilyl)-propionate- d_4 (TSP, reference compound with methyl signal set to 0 ppm), MV (4.5, 8.5 and 9.1 ppm)¹⁷² and residual H_2O (4.8 ppm).¹⁷³ The broad series of peaks between 2.8 and 4.0 ppm corresponds to buffer components including HEPES¹⁷⁴ and trace metabolites produced by MR-1 (Human Metabolome Database, <http://www.hmdb.ca/>). Signals for carbon-based compounds were identified using a database of resonances in Chenomx NMR suite 7.6TM software (see section 2.6 and **Table 2.4**) and have been highlighted on the expanded spectra in **Fig. 3.6B**. Quantification of the compounds was performed by matching the area underneath the recorded peak to the area underneath a standard peak (corresponding to a known concentration of the chosen compound). Signals used for quantification were selected based on their clear position away from other resonances.

Key results from the $^1\text{H-NMR}$ analysis (see **Table 3.3**) have been summarised in **Fig. 3.7** to best compare the extents of each reductive transformation. With no added carbon substrate, the supernatants analysed after 30 min contained negligible quantities of carbon-based compounds both in the absence and presence of MR-1. The only exception was a slight enrichment of formate when MR-1 was incubated with DT and MV. This may be due to trace amounts of growth medium which were not removed during processing of MR-1 or the release of intracellular metabolite reserves upon bacterial lysis during incubation. Importantly, the control experiments show that buffer components do not contribute to the resonances of the compounds of interest and that incubation of MR-1 with DT and MV does not lead to substantial formation of carbon-based compounds. When MR-1 was incubated with DT, MV and fumarate (≈ 4721 nmol initially), the supernatants contained ≈ 3768 nmol succinate (80 % yield) and ≈ 976 nmol malate (21 % yield) after 30 min with only trace amounts of other compounds. Malate is likely formed from the hydration of the C=C bond in fumarate by the cytoplasmic fumarate hydratase (SO2222) which is part of the tricarboxylic acid (TCA) cycle.^{102,175} Transformation of fumarate did not take place in equivalent experiments performed with no bacteria.

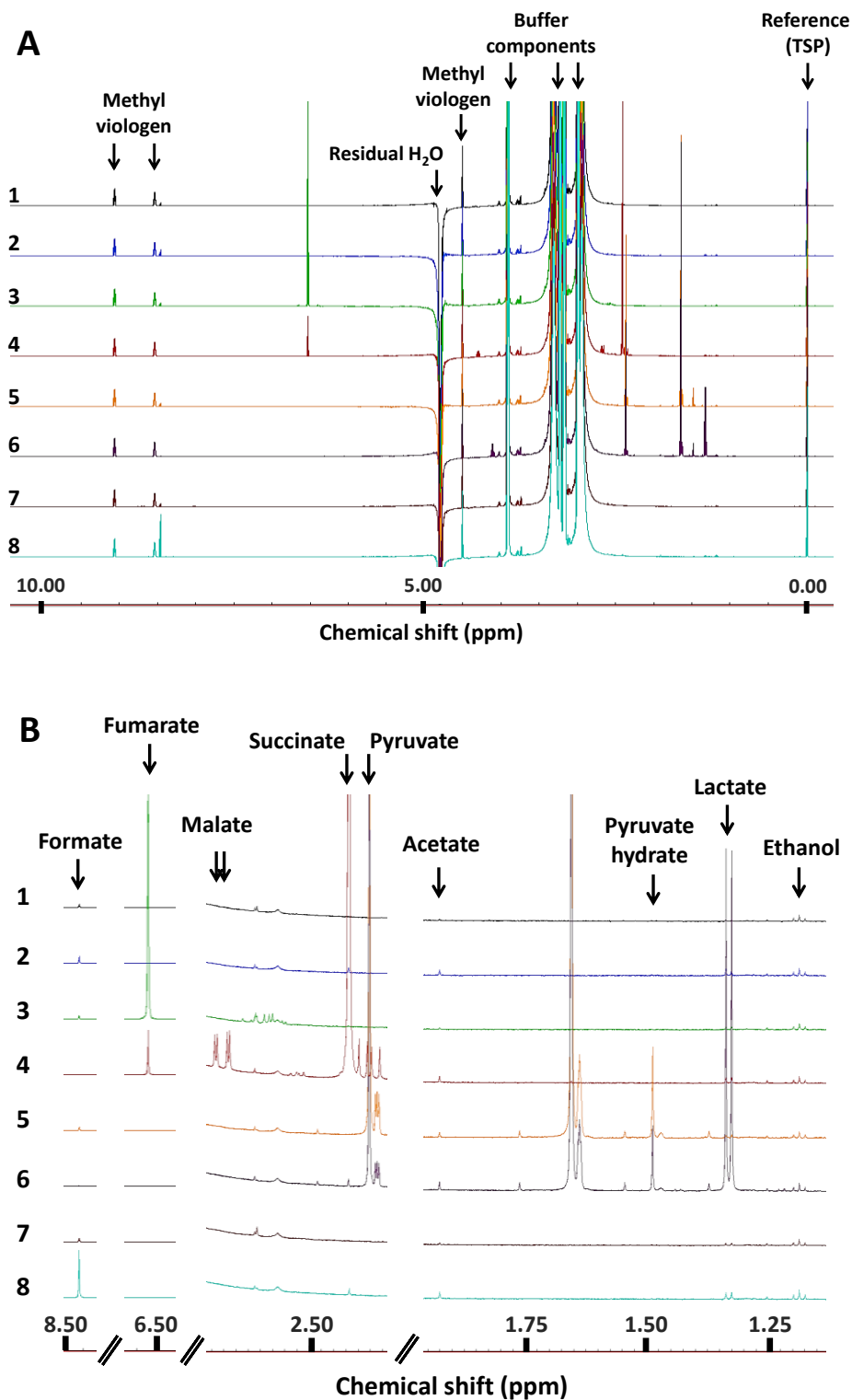


Figure 3.6 - Representative ^1H -NMR spectra for DT-driven reduction of fumarate, pyruvate and CO_2 by MR-1. A] Full spectra showing peak positions of buffer components and sodium 3-(trimethylsilyl)-propionate- d_4 (TSP) reference. B] Expanded view of spectra highlighting peaks used to quantify carbon-based compounds (see section 2.6). Numerical label for each spectrum refers to a set of conditions described in **Table 3.3**.

Table 3.3 - DT-driven reduction of fumarate, pyruvate and CO₂ by MR-1. ¹H-NMR derived quantification of the named compounds in supernatants recovered from samples (1 mL) incubated for 30 min with fumarate, pyruvate or CO₂ as indicated and 0.8 mg mL⁻¹ (ca. 4.6 mM) DT and 0.5 mM MV. Assays performed with or without MR-1 (OD_{590nm} ≈0.25). Anaerobic samples in 50 mM HEPES, 50 mM NaCl, pH 7 at room temperature. Samples had 4 mL headspace (initially 100 % N₂). nd = not detected, pyruvate is reported as the sum of pyruvate and pyruvate hydrate.

NMR spectra ref.	Added substrate	MR-1	Supernatant component (nmol)									
			Fumarate	Succinate	Malate	Pyruvate	Lactate	Formate	Acetate	Ethanol		
1	None	No	nd	nd	nd	nd	7 ± 2	116 ± 1	3	30 ± 1		
2		Yes	nd	9 ± 3	nd	nd	20	227	12 ± 2	31 ± 2		
3	Fumarate	No	4721 ± 15	1	nd	nd	7 ± 1	111 ± 3	4	29 ± 1		
4		Yes	623 ± 101	3768 ± 29	976 ± 82	nd	16	nd	12 ± 1	30 ± 1		
5	Pyruvate	No	nd	nd	nd	9 ± 1	108 ± 2	10 ± 1	28 ± 1			
6		Yes	nd	8	nd	1509 ± 3	926 ± 25	10 ± 5	15 ± 1	32 ± 1		
7	CO ₂	No	nd	nd	nd	6 ± 1	110 ± 3	4 ± 1	29 ± 2			
8		Yes	nd	8	nd	nd	24 ± 3	1474 ± 39	12 ± 1	37 ± 4		

Incubation of MR-1 with DT, MV and pyruvate (≈ 2220 nmol initially) for 30 min resulted in the formation of ≈ 926 nmol lactate (42 % yield) with no other major products. In the absence of MR-1, negligible quantities of lactate were detected. Lastly, incubation of MR-1 with DT, MV and CO_2 (≈ 5000 nmol initially) led to the production of ≈ 1474 nmol formate (29 % yield) after 30 min, with only trace amounts of other compounds. The yield of formate equates to approximately 6.5-fold more than what was detected in experiments with DT, MV, MR-1 and no added carbon substrate. In parallel experiments with no bacteria, the amount of formate detected was similar to that seen for all other abiotic assays. Overall, the yields of succinate, lactate and formate (80, 42 and 29 %, respectively) correlated well with the decreases in DT-driven H_2 -evolution caused by the presence of fumarate, pyruvate and CO_2 (100, 55 and 42 %, respectively, see **Table 3.2**).

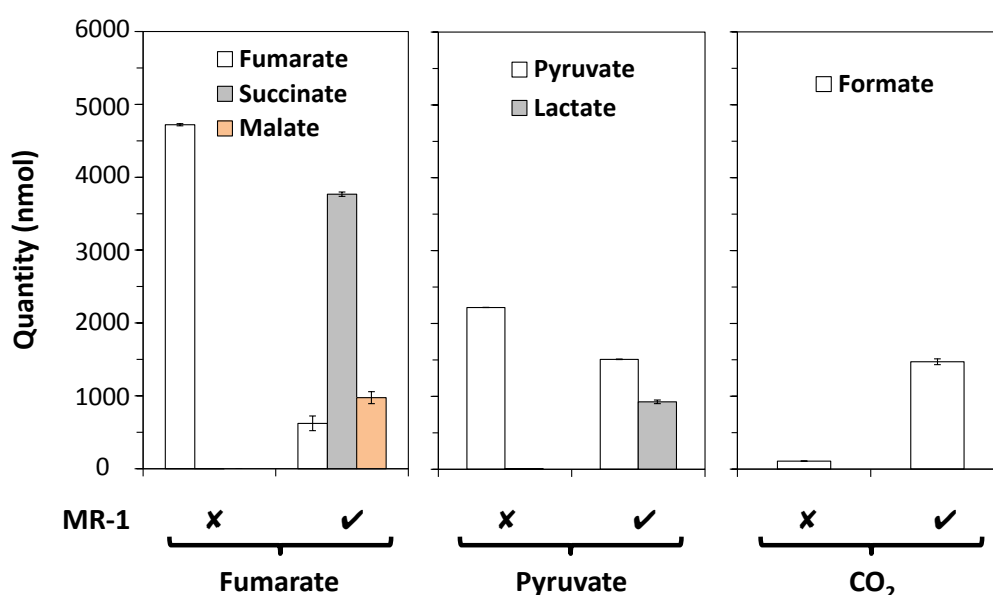


Figure 3.7 - DT-driven reduction of fumarate, pyruvate and CO_2 by MR-1. Composition of supernatants recovered from samples incubated for 30 min with 0.8 mg mL^{-1} DT, 0.5 mM MV, and fumarate (left), pyruvate (middle) or CO_2 (right). Assays performed with or without MR-1 ($\text{OD}_{590\text{nm}} \approx 0.25$) as indicated. Mean values from technical duplicates, error bars indicate maximum and minimum. Anaerobic samples (1 mL) in 50 mM HEPES, 50 mM NaCl, pH 7 at room temperature.

To summarise, the data shown in this section confirm that culturing MR-1 under anaerobic, acceptor-limited conditions leads to the presence of functional fumarate reductase, lactate dehydrogenases and formate dehydrogenases that can be exploited for reductive catalysis using DT and MV. Importantly, incubating MR-1 with DT, MV and a particular carbon substrate gave a distinct range of products and, with the exception of fumarate hydrolysis to malate, the majority of the enzymatic activity was associated with the desired reductive transformations.

3.4 Discussion

In this chapter, it was shown that MR-1 can be cultured to simultaneously contain hydrogenases, fumarate reductase, lactate dehydrogenases and formate dehydrogenases that can be readily assessed using biochemical assays. Spectrophotometric H₂ oxidation assays confirmed the presence of active hydrogenases after harvesting MR-1 from growth medium and re-suspending in a defined buffer. Although the assays did not assess the reductive transformation of interest, they represent a rapid and convenient method for comparing hydrogenase activity in different bacterial strains. Comparable assays with MR-1 have not been published previously but a H₂ oxidation rate of $17.4 \pm 2 \text{ nmol H}_2 \text{ min}^{-1} \text{ mg}^{-1}$ was reported for the purified MR-1 [NiFe]-hydrogenase in 50 mM HEPES, pH 7.8 with MV as the redox indicator.⁹⁸ The value is significantly lower than that reported here with MR-1 (see **Table 3.1**) considering that the results are normalised to total protein and only a small proportion of MR-1 cellular material is comprised of hydrogenases. This may reflect a loss of activity for the [NiFe]-hydrogenase during purification, the more positive reduction potential of the BV^{2+/+} couple versus the MV^{2+/+} couple¹⁶⁵ (which may have facilitated electron transfer during cell-based assays described in this chapter) and/or the possibility that the bacterium also contains [FeFe]-hydrogenases that contribute to H₂ oxidation.

The reduction of protons, fumarate, pyruvate and CO₂ to H₂, succinate, lactate and formate, respectively, by MR-1 was driven using DT-reduced MV. The H₂-sensing electrode allowed investigation of factors affecting DT-driven H₂-evolution including MR-1 OD_{590nm} and the presence of carbon-based substrates. Although experimental throughput for the detection of H₂ was low compared to GC, real-time H₂ production and consumption profiles could be obtained because DT and MV enable rapid electron transfer to the hydrogenases. This was highlighted by the fact that DT-driven proton reduction over 30 min gave greater yields of H₂ than those seen during natural MR-1 respiration (i.e. lactate oxidation coupled to proton reduction) over 48 hr (see **Fig. 3.1**). A key result from the H₂-evolution assays was evidence that MV is a suitable electron transfer mediator for bacterial enzymes, with negligible amounts of H₂ produced over 30 min in the absence of MV (see **Fig. 3.3**). Electron transfer from DT to the hydrogenases may still be taking place but these processes clearly occur over longer timescales. The use of MV affords a more rapid and direct approach to driving reductive transformations with MR-1 and permits electron transfer to soluble and membrane-bound enzymes localised to the periplasm and cytoplasm.

The transformation of carbon-based substrates was evaluated using $^1\text{H-NMR}$ spectroscopy coupled with software for the detection of microbial metabolites. The analysis allowed facile quantification of the compounds of interest and confirmed that other common metabolites such as acetate are only produced in small quantities (see **Table 3.3**). A comparable evaluation of multiple enzyme activities after culturing MR-1 under a single growth condition and the reduction of CO_2 to formate by the bacterium have not been reported previously at the time of writing. Based on the final amounts of succinate, lactate and formate after 30 min incubations, the rates of DT-driven fumarate-, pyruvate- and CO_2 -reduction by MR-1 were ≈ 126 , ≈ 31 and ≈ 49 nmol min^{-1} , respectively (see **Fig. 3.7**). The superior rates of fumarate-reduction most likely reflect the fact that the fumarate reductase is a soluble and highly abundant^{176,177} periplasmic enzyme with accessible redox cofactors (see **Fig. 1.12**)¹⁰⁶ whereas the hydrogenases, lactate dehydrogenases and formate dehydrogenases are predicted to be membrane-associated enzymes that exchange electrons with the MK pool, making it necessary for DT-driven electron transfer to proceed via intermediary redox partners.^{91,94,115} In all cases, complete consumption of the starting carbon substrate did not occur over 30 min. In part, it is likely that this is a result of electrons from DT being lost to alternative bacterial electron acceptors. For example, electrons are still transferred from MV^+ to the hydrogenases in the presence of pyruvate and CO_2 (see **Table 3.2**).

Overall, the results presented in this chapter are an important foundation to achieve the aims of this thesis because it was shown that MR-1 can act as a multi-faceted electrocatalyst with a selectable product range that can be quantified using a variety of analytical techniques. In the next chapter, results are shown from experiments that aimed to facilitate light-driven (rather than DT-driven) reduction of MV^{2+} to MV^+ using a SED and photosensitiser. Data are then presented from assays that quantified light-driven H_2 -evolution by anaerobically grown MR-1 from photo-produced MV^+ .

CHAPTER 4

Light-driven H₂-evolution by
Shewanella oneidensis MR-1

Chapter 4 - Light-driven H₂-evolution by *Shewanella oneidensis* MR-1

4.1 Introduction

In chapter 3, it was shown that MR-1 can be used to drive reductive transformations with DT as a chemical reductant and MV as an electron shuttle after culturing the bacterium under anaerobic, acceptor-limited conditions. To build upon the findings for cell-based photocatalysis with MR-1, it is of interest to exploit the ability of MV to rapidly transfer electrons to bacterial enzymes but replace DT with light-harvesting reagents that generate photo-excited electrons under irradiation by visible light. In this chapter, the photocatalytic reduction of protons to H₂ was targeted for the initial characterisation of such a system because the product can be readily quantified using a H₂-sensing electrode and GC. First, results are presented from spectrophotometric assays that were used to evaluate photoreduction of MV²⁺ to MV⁺ using a variety of water-soluble photosensitisers and SEDs under conditions compatible with MR-1 enzyme activity. Next, data are shown from experiments that aimed to drive H₂-evolution by performing photoreduction of MV²⁺ in the presence of anaerobically grown MR-1. Finally, results are presented from experiments that assessed the determinants of light-driven H₂-evolution, the longevity of the system and the role of porin:cytochrome complexes in electron transfer across the bacterial outer membrane. The results shown below provide a framework for the photoreduction of fumarate, pyruvate and CO₂ with MR-1 described in the next chapter.

4.2 Reductive photocatalysis

To develop a system for photocatalytic chemical synthesis with MR-1, the chemical reductant DT must be replaced by light-harvesting reagents that facilitate the reduction of MV²⁺ to MV⁺ for subsequent electron transfer to bacterial enzymes. As shown in section 1.5, it is possible to generate photo-energised electrons for reductive photocatalysis using a photosensitiser and a SED (see **Fig. 1.7** and examples in **Tables 1.3, 1.4** and **1.5**).^{1,2,49} More specifically, the absorption of light by a photosensitiser can promote an electron from the ground state (S₀) to an excited singlet state (S₁). After photo-excitation, excess energy is

rapidly lost to the surroundings through vibrational relaxation (VR) until the molecule relaxes to the lowest energy vibrational level of the excited state. It is also possible for an electron to be promoted to higher-energy excited singlet states (S_2). If this happens, VR takes place until the molecule is in the lowest energy vibrational level then internal conversion (IC) can occur whereby the molecule transitions to a lower-energy excited state (i.e. from S_2 to S_1). This is followed by further VR to the lowest energy vibrational level. At this point, energy can be lost through the emission of a photon. This process is termed fluorescence for relaxation from S_1 to S_0 with no change in electron spin during emission. Alternatively, intersystem crossing (ISC) can occur whereby the molecule transitions to an excited triplet state (T_1 , T_2) which will typically be longer-lived and have a lower energy than the corresponding singlet state. Once the lowest energy vibrational level is attained through VR, energy can be lost through the emission of a photon. This process is termed phosphorescence for relaxation from T_1 to S_0 with a corresponding change in electron spin during emission. The processes described above are summarised as a simplified Jablonski diagram in **Fig. 4.1**.^{178–180}

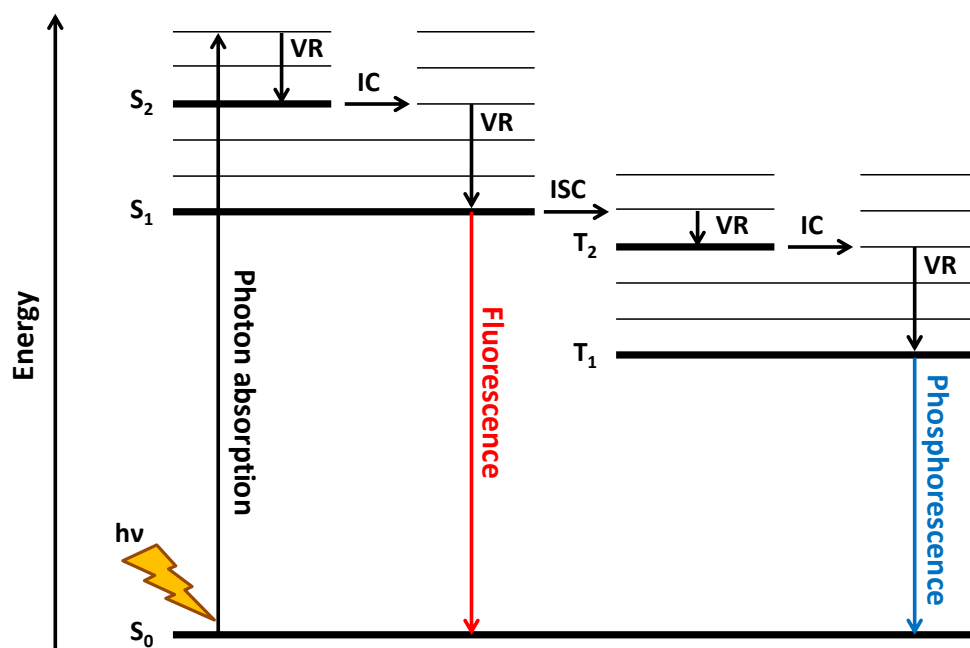


Fig. 4.1 - Simplified Jablonski diagram showing the fate of a photo-excited molecule following absorption of light ($h\nu$) in an isolated system. Vibrational levels within excited states are shown as horizontal lines and the lowest energy vibrational levels are highlighted in bold. S_0 = ground state, S_1 , S_2 = excited singlet states, T_1 , T_2 = excited triplet states, VR = vibrational relaxation, IC = internal conversion, ISC = intersystem crossing. See text for further details.

Alternatively, rather than energy loss by energy transfer, as above, this may occur by electron transfer. If the photo-excited state is sufficiently long-lived then it can act as an

electron donor and/or acceptor in the presence of other molecules. Excited state electron transfer is referred to as quenching and can proceed via a reductive or oxidative pathway, as summarised in **Fig. 4.2** for a generic photosensitiser and SED with MV as an electron acceptor.^{2,49,132} The first step in both cycles is absorption of a photon by the photosensitiser to form the photo-excited state (PS^*). During reductive quenching, PS^* oxidises the SED to form a one-electron reduced state of the photosensitiser (PS^-) which can then reduce MV^{2+} to regenerate the photosensitiser ground state (PS^0). During oxidative quenching, PS^* reduces MV^{2+} to form a one-electron oxidised state of the photosensitiser (PS^+) which can then oxidise the SED to regenerate PS^0 . The likelihood of each pathway depends on a variety of factors including the solvent and pH as well as the identity of the photosensitiser and SED.⁴⁹ These factors influence the (photo-)reduction potentials associated with each step of the process (see **Fig. 4.2**, red text) and hence the feasibility of each mechanism to achieve photoreduction of MV^{2+} .

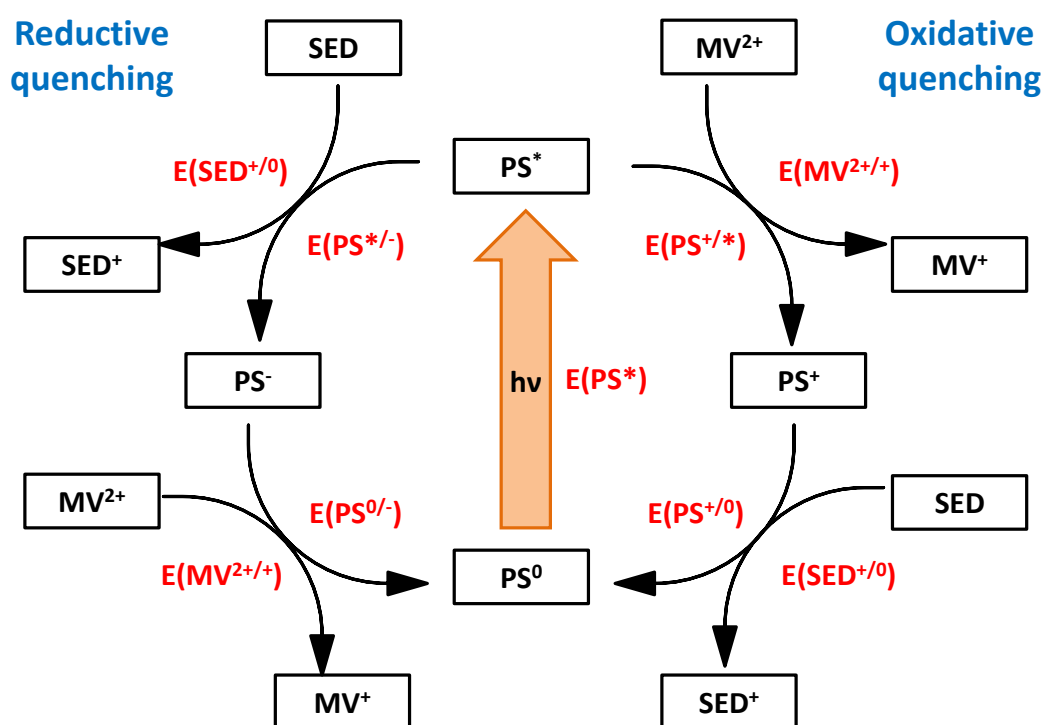


Fig. 4.2 - Reductive (left) and oxidative (right) quenching mechanisms after absorption of light ($h\nu$) by a photosensitiser showing the ground (PS^0), photo-excited (PS^*), one-electron reduced (PS^-) and one-electron oxidised (PS^+) states of the photosensitiser with their corresponding (photo-)reduction couples. SED = sacrificial electron donor, MV = methyl viologen.

A range of photosensitisers and SEDs can be used to generate and transfer photo-energised electrons via the mechanisms described above. Commonly used photosensitisers include molecular dyes, (sensitised-)semiconducting nanoparticles and

light-harvesting protein complexes^{1,68,180} whilst commonly used SEDs include aliphatic and aromatic amines, carboxylic acids, thiols and sugars (see examples in section 1.5).⁴⁹ The next sections give an overview of the photosensitisers and SEDs that were chosen for this study including their key structural and chemical properties.

4.2.1 Photosensitisers used in this study

Six photosensitisers were assessed in this study. Chemical structures and the available (photo-)reduction potentials from the literature are given in **Table 4.1**. Absorbance spectra for 10 μ M photosensitiser in 50 mM HEPES, 50 mM NaCl, pH 7 are shown in **Fig. 4.3** and the corresponding absorbance maxima and extinction coefficients are given in **Table 4.2**. Excited state energies, $E(\text{PS}^*)$, are calculated using **Eq. 4.1** (where h is Planck's constant and c is the speed of light) from the emission wavelength (λ_{em}) of the excited state as it decays to the ground state.¹⁷⁹ The oxidation and reduction potentials of the ground state, $E(\text{PS}^{+/0})$ and $E(\text{PS}^{0/-})$ respectively, are determined using cyclic voltammetry.¹⁸¹ Taken together, these values can be used to estimate the photoreduction potentials of the excited state, $E(\text{PS}^{+/*})$ and $E(\text{PS}^{* /-})$, using **Eq. 4.2** and **4.3**, respectively.^{179,181}

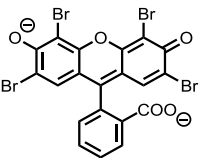
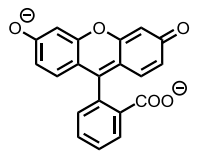
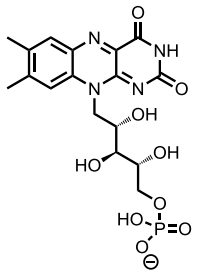
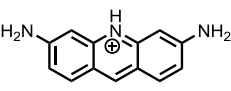
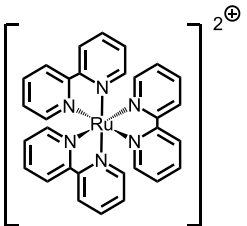
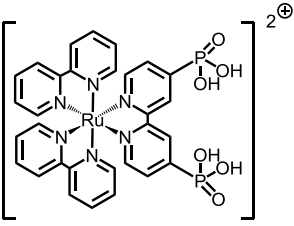
$$\frac{h \times c}{\lambda_{\text{em}}} = E(\text{PS}^*) \quad \text{Eq. 4.1}$$

$$E(\text{PS}^{+/*}) = E(\text{PS}^{+/0}) - E(\text{PS}^*) \quad \text{Eq. 4.2}$$

$$E(\text{PS}^{* /-}) = E(\text{PS}^{0 /-}) + E(\text{PS}^*) \quad \text{Eq. 4.3}$$

The values of $E(\text{PS}^{+/0})$ and $E(\text{PS}^{+/*})$ for FMN are not included in **Table 4.1** because the reductive quenching pathway is the predominant mechanism by which light-driven electron transfer takes place with this photosensitiser.^{182,183} Reductive quenching leads to formation of hydroquinone, PS^{2-} (via disproportionation of semiquinone), which can perform a two-electron reduction to regenerate the FMN ground state. The value of $E(\text{PS}^{+/*})$ for proflavine is not included in **Table 4.1** because the oxidative quenching pathway with this photosensitiser involves more complex photochemistry than that shown in **Fig. 4.2**.^{184–186} Oxidative quenching involves absorption of multiple photons and leads to the production of solvated electrons that can reduce an available electron acceptor or re-combine with oxidised proflavine to regenerate the photo-excited state.

Table 4.1 - Chemical structures and (photo-)reduction potentials of photosensitisers used in this study. Ionisation state shown for predominant form at pH 7. Potentials at pH 7 vs. SHE. PS⁰, PS*, PS⁻ and PS⁺ refer to the photosensitiser states shown in **Fig. 4.2**. ^aFor FMN, the relevant couples are E(PS^{0/2-}) and E(PS^{*-/2-}). n/a = not available.

Photosensitiser	E(PS*) (eV)	E(PS ⁺⁰) (V)	E(PS ^{+/*}) (V)	E(PS ^{0/-}) ^a (V)	E(PS ^{*-/}) ^a (V)	Ref.
Eosin Y 	1.89	+1.03	-0.86	-0.81	+1.08	187,188
Fluorescein 	1.96	+0.95	-1.01	-0.97	+0.99	187,188
FMN^a 	2.07	n/a	n/a	-0.22	+1.85	132,182,189
Proflavine 	2.14	+1.31	n/a	-0.78	+1.36	184,185
Ru(bpy)₃²⁺ 	2.10	+1.26	-0.84	-1.26	+0.84	190
RuP 	2.21	+1.26	-0.95	-1.09	+1.12	132,191,192

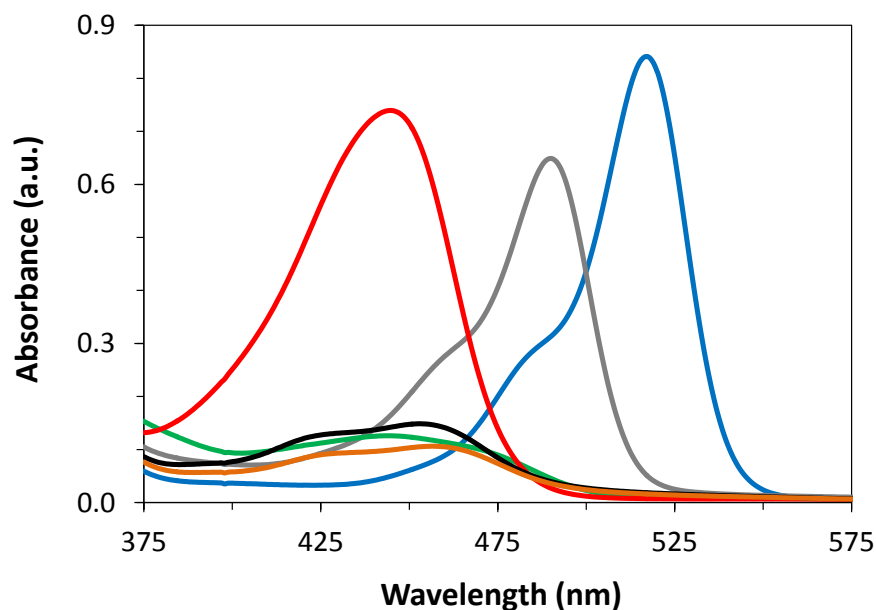


Figure 4.3 - Absorbance spectra of photosensitisers used in this study. 10 μM eosin Y (blue), fluorescein (grey), FMN (green), proflavine (red), $\text{Ru}(\text{bpy})_3^{2+}$ (black) and RuP (orange) in 50 mM HEPES, 50 mM NaCl, pH 7 (pathlength 1 cm).

Table 4.2 - Absorbance maxima and extinction coefficients of photosensitisers used in this study. λ_{max} given as maximum electronic absorbance at wavelengths > 400 nm for 10 μM photosensitiser in 50 mM HEPES, 50 mM NaCl, pH 7, see **Fig. 4.3**. *Extinction coefficients were determined by Dr. Emma Ainsworth (University of East Anglia, UK) using the Beer-Lambert law, see **Eq. 2.1**.

Photosensitiser	λ_{max} (nm)	ϵ_{max} ($\text{mM}^{-1} \text{cm}^{-1}$)
Eosin Y	520	80.4*
Fluorescein	490	64.6*
FMN	445	12.5 ¹⁹³
Proflavine	445	76.1*
$\text{Ru}(\text{bpy})_3^{2+}$	452	14.4 ¹⁹¹
RuP	455	10.2 ¹⁹¹

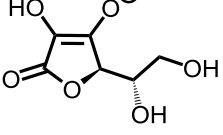
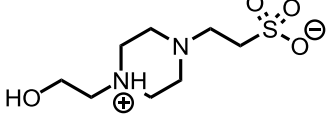
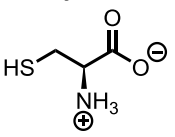
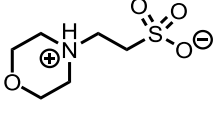
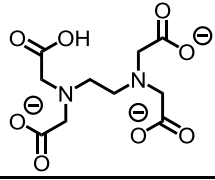
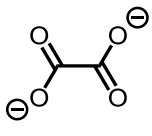
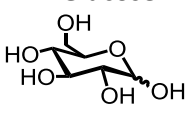
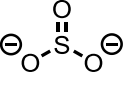
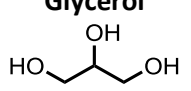
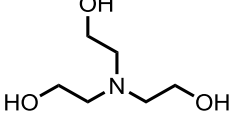
Eosin Y, fluorescein and proflavine are light-harvesting reagents with structures analogous to redox active molecules associated with microbial electron transfer, such as pycocyanin and anthraquinone-2,6-disulfonate (AQDS).¹⁹⁴ FMN is a flavin molecule secreted naturally by MR-1 up to concentrations of 0.5 μM in culture supernatants¹⁹⁵ and has been implicated in extracellular electron transfer to insoluble redox partners (see section 1.6.2).^{127,189} $\text{Ru}(\text{bpy})_3^{2+}$ and RuP are light-absorbing inorganic complexes with chemical structures comparable to iron (III) chelates which can be used by MR-1 as terminal electron

acceptors.^{84,88,196} These six photosensitisers were selected because they are water-compatible and their absorbance maxima fall within the visible region of the electromagnetic spectrum. Additionally, they have been used for photoreduction of purified MR-1 outer membrane cytochromes (see section 1.6.2)¹³² and photoreduction of MV has been reported previously for all photosensitisers, except FMN, in aqueous medium.^{186,197–200}

4.2.2 Sacrificial electron donors used in this study

Ten SEDs were assessed in this study. Chemical structures and the available reduction potentials from the literature are given in **Table 4.3**. TEOA and EDTA are two of the most widely used SEDs because they are compatible with many organic and inorganic photosensitisers,^{49,68,201,202} although EDTA is typically able to operate at more acidic pH than TEOA.⁴⁹ HEPES and MES are common Good's buffers that can also be employed as SEDs.¹³² In particular, the use of MES has been reported recently in systems comprised of purified protein and RuP co-adsorbed on titanium dioxide nanoparticles.^{110,132,203} Glucose and glycerol represent relatively sustainable SEDs^{204,205} because the former can be produced through natural photosynthesis as part of biomass and the latter is a waste product from the esterification of vegetable oils to biodiesel. Ascorbate is a versatile SED that can be used at acidic to neutral pH and shows promise as a recyclable proton/electron relay in photocatalytic systems with tris(2-carboxyethyl)phosphine (TCEP) as co-SED.^{49,206} Oxalate is considered a useful SED because its oxidation produces CO₂ and a CO₂ radical.^{49,207} CO₂ is an undesirable side product because of its detrimental impacts on the environment (see section 1.2) but its formation reduces the likelihood of charge recombination as the gaseous molecule can escape the reaction solution. The CO₂ radical is a powerful reductant capable of performing additional, potentially productive, electron transfer processes. Sulfite is typically used as a SED in combination with sulfide, for example, in systems containing cadmium-based semiconductors for light-driven H₂ production from H₂S.²⁰⁸ Lastly, thiols such as cysteine are used as SEDs because their oxidation can release multiple electrons and leads to the formation of inert disulfide-bridged dimers.^{49,209} More generally, these molecules were chosen as SEDs because they are water-soluble and their reported reduction potentials, $E(\text{SED}^{+/0})$, make them suitable for reductive and/or oxidative quenching with the majority of the photosensitisers described above.

Table 4.3 - Chemical structures and reduction potentials of SEDs used in this study. Ionisation state shown for predominant form at pH 7. Potentials vs. SHE: values for cysteine, EDTA, HEPES, MES, sulfite and TEOA were determined in aqueous solutions and values for ascorbate and oxalate were determined in solutions of acetonitrile/water (50:50). n/a = not available.

SED	E(SED ^{+ / 0}) (V)	SED	E(SED ^{+ / 0}) (V)
<p>L(+)-Ascorbate</p> 	+0.70 ²¹⁰	<p>HEPES</p> 	+0.80 ²¹¹
<p>L-Cysteine</p> 	+0.92 ²¹²	<p>MES</p> 	+0.95 ²¹³
<p>EDTA</p> 	+0.82-1.17 ^{49,214}	<p>Oxalate</p> 	+1.05 ²¹⁵
<p>D-Glucose</p> 	+1.00 ²¹⁶	<p>Sulfite</p> 	+0.75 ²¹⁷
<p>Glycerol</p> 	n/a	<p>TEOA</p> 	+0.82-1.07 ^{198,214}

The (photo-)reduction potentials of the photosensitisers and SEDs have been summarised as an energy level diagram in **Fig. 4.4** to show the feasibility of light-driven H₂-evolution with MR-1 using MV as an electron transfer mediator. In the majority of cases, the reduction potentials of the SEDs are more negative than those associated with the PS^{* / -} and PS^{0 / -} couples. Similarly, most of the reduction potentials associated with the PS^{0 / -} and PS^{+ / *} couples are more negative than the reduction potential of the MV^{2+ / +} couple. Taken together, this should make electron transfer from the SEDs to the photosensitisers and from the photosensitisers to MV²⁺ thermodynamically favourable. Once MV⁺ has been

generated, it should then be possible to deliver electrons to bacterial hydrogenases for proton reduction, as shown by the work presented in chapter 3.

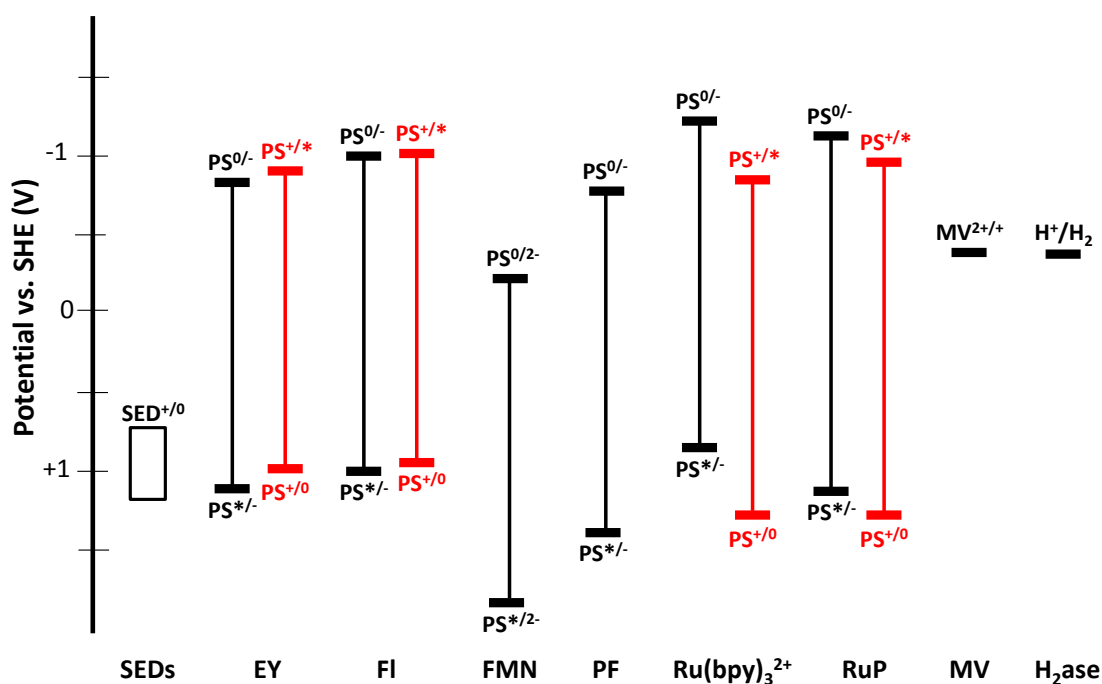


Figure 4.4 - Summary of photochemistry relevant to light-driven H₂-evolution with MR-1. (Photo-)reduction potentials for eosin Y (EY), fluorescein (FI), FMN, proflavine (PF), Ru(bpy)₃²⁺ and RuP related to reductive (black) and oxidative (red) quenching, see **Fig. 4.2** and **Table 4.1**. Potentials for the MV^{2+/+} and H⁺/H₂ couples as well as those spanned by the SEDs in **Table 4.3** are indicated. SED = sacrificial electron donor, MV = methyl viologen, H₂ase = hydrogenase.

In the next section, data are shown from experiments that evaluated different combinations of photosensitisers and SEDs for their ability to facilitate reduction of MV²⁺ to MV⁺ under irradiation by visible light. Results from the assays informed the choice of reagents used for photo-production of MV⁺ in the presence of MR-1 to drive H₂-evolution.

4.3 Photoreduction of methyl viologen under conditions compatible with *Shewanella oneidensis* MR-1 enzyme activity

First, experiments were performed to compare photoreduction of MV²⁺ using different photosensitisers and a chosen SED. For the assays, TEOA was selected as the SED because of its widespread use in photocatalytic systems including those containing purified enzymes and whole-cell bacteria.^{78,199,218} Photoreduction of MV²⁺ was evaluated in 50 mM HEPES, 50 mM NaCl, pH 7 because this buffer was shown to be compatible with MR-1 enzyme

activities in chapter 3. Anaerobic 50 mM HEPES, 50 mM NaCl, pH 7 (1 mL) was supplemented with 12 mM TEOA, 0.06 mM MV and 0.02 mM photosensitiser within a N₂-filled chamber then irradiated with the cold light source at an intensity of 0.7 kW m⁻² (see section 2.2). The amount of photo-produced MV⁺ was quantified spectrophotometrically by analysing the peaks appearing over time at 396 and 606 nm (see section 2.5). Representative spectra for experiments with each photosensitiser after 0, 10, 20 and 30 min irradiation are presented in **Fig. 4.5**.

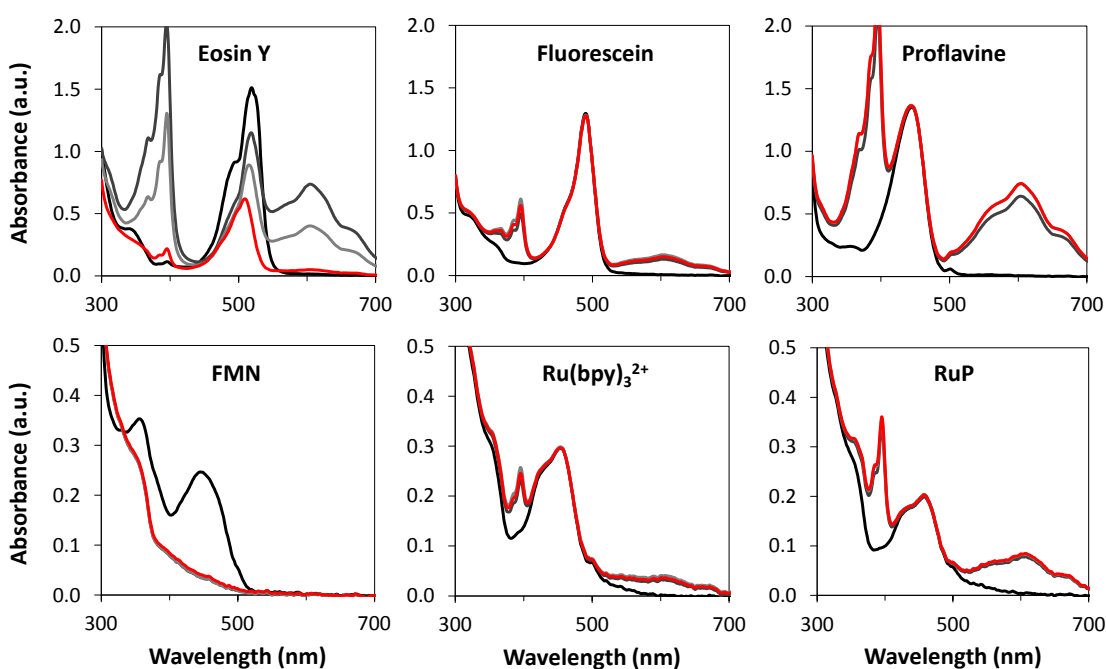


Figure 4.5 - Photoreduction of MV²⁺ by xanthene-, acridine- and Ru(II)-dyes. Representative spectra for 0.02 mM of the indicated photosensitiser with 12 mM TEOA recorded after 0 (black), 10 (dark grey), 20 (light grey) and 30 min (red) irradiation with the cold light source (0.7 kW m⁻²). The majority of spectra cannot be seen due to overlap. Starting concentration of MV²⁺ was 0.06 mM. Anaerobic samples (1 mL) in 50 mM HEPES, 50 mM NaCl, pH 7 (pathlength 1 cm).

FMN was the only photosensitiser that did not photoreduce MV²⁺. This reflects the fact that its reduction potential ($E_m = -0.22$ V) is more positive than the MV^{2+/+} couple ($E_m = -0.45$ V), making electron transfer thermodynamically unfavourable (see **Fig. 4.4**). The spectral changes seen in the assays instead correspond to formation of reduced FMN which has a lower extinction coefficient than oxidised FMN.²¹⁹ With eosin Y, fluorescein, proflavine, Ru(bpy)₃²⁺ and RuP, clear peaks at 396 and 606 nm appeared after 10 min irradiation. The peaks remained relatively stable over 30 min irradiation for all photosensitisers except eosin Y. In the case of eosin Y, the peaks corresponding to both MV⁺ and the photosensitiser diminished over time. This is likely due to photo-degradation of the

photosensitiser which has been reported previously in the absence of an electron acceptor²²⁰ (conditions which are attained once all available MV^{2+} has been photoreduced to MV^+). Eosin Y may also facilitate further reduction of bright blue MV^+ to pale yellow MV^0 ($E_m = -0.88\text{ V}$)²²¹ causing a change in the spectral properties of the solution. The absorbance changes at 396 nm (for $Ru(bpy)_3^{2+}$ and RuP) or 606 nm (for eosin Y, fluorescein and proflavine) after 10 min irradiation were converted to concentrations of MV^+ in the sample using the Beer-Lambert law (see **Eq. 2.1**) and the reported extinction coefficients for MV^+ (see section 2.5). Results from the analysis and equivalent experiments performed in the absence of TEOA are shown in **Fig. 4.6**. The concentration of MV^+ after 10 min irradiation decreased in the order eosin Y > proflavine >> fluorescein > RuP > $Ru(bpy)_3^{2+}$ and, in all cases, more MV^+ was formed when TEOA was present in the sample. Overall, the results show that a variety of photosensitisers can facilitate the reduction of MV^{2+} using visible light irradiation under conditions compatible with MR-1 enzyme activity.

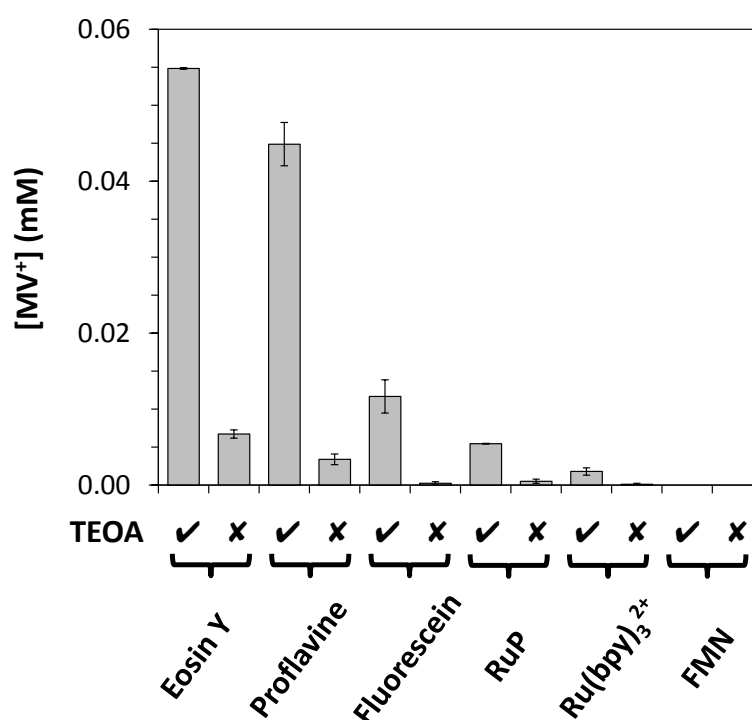


Figure 4.6 - Photoreduction of MV^{2+} by xanthene-, acridine- and Ru(II)-dyes. Concentration of MV^+ after 10 min irradiation (0.7 kW m^{-2}) of 0.06 mM MV and 0.02 mM of the indicated photosensitiser in the presence or absence of 12 mM TEOA. Mean values from technical duplicates, error bars indicate maximum and minimum. Anaerobic samples (1 mL) in 50 mM HEPES, 50 mM NaCl, pH 7. Irradiation provided by the cold light source.

In the next set of experiments, photoreduction of MV^{2+} was performed using eosin Y and $Ru(bpy)_3^{2+}$ as representative photosensitisers with different SEDs (see **Table 4.3**) to compare their effectiveness against TEOA. The concentrations of MV^+ after 10 min

irradiation with the cold light source (0.7 kW m^{-2}) are shown in **Fig. 4.7**. Eosin Y and $\text{Ru}(\text{bpy})_3^{2+}$ were used as representative photosensitisers for the assays to compare different chemical classes with different photochemical properties. Despite being able to photoreduce MV^{2+} to similar extents, eosin Y was chosen over proflavine as the latter is an anti-microbial agent^{222–224} and inclusion of $10 \text{ }\mu\text{M}$ proflavine, but not $10 \text{ }\mu\text{M}$ eosin Y or $\text{Ru}(\text{bpy})_3^{2+}$, in M72 medium during anaerobic, acceptor-limited growth of MR-1 resulted in limited change of $\text{OD}_{590\text{nm}}$ over 48 hr, as shown in **Fig. 4.8**. $\text{Ru}(\text{bpy})_3^{2+}$ was chosen over RuP because the former is more widely available from commercial suppliers.

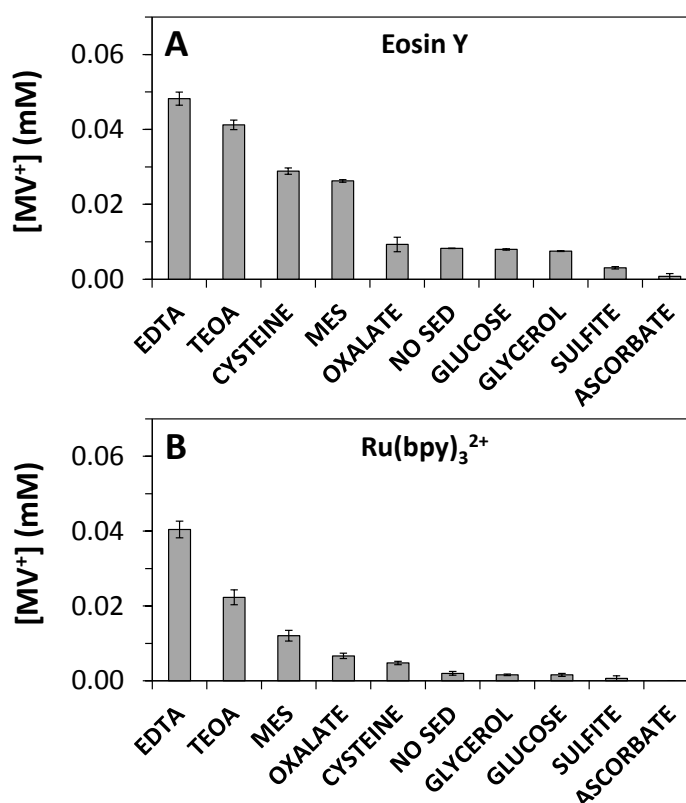


Figure 4.7 - Photoreduction of MV^{2+} by eosin Y and $\text{Ru}(\text{bpy})_3^{2+}$ with different SEDs. A) Concentration of MV^+ after 10 min irradiation (0.7 kW m^{-2}) of 0.02 mM eosin Y and either L(+)-ascorbate, L-cysteine, EDTA, D-glucose, oxalate, sulfite or TEOA at 10 mM or 30 mM MES or 27 mM glycerol. B) Concentration of MV^+ after 10 min irradiation (0.7 kW m^{-2}) of 0.04 mM $\text{Ru}(\text{bpy})_3^{2+}$ and either L(+)-ascorbate, L-cysteine, EDTA, D-glucose, oxalate, sulfite or TEOA at 25 mM or 75 mM MES or 69 mM glycerol. Starting concentration of MV^{2+} was 0.06 mM with eosin Y and 0.15 mM with $\text{Ru}(\text{bpy})_3^{2+}$. Mean values from technical duplicates, error bars indicate maximum and minimum. Anaerobic samples (1 mL) in 50 mM HEPES, 50 mM NaCl, pH 7. Irradiation provided by the cold light source.

The effectiveness of each SED is best evaluated against experiments with no added SED (which reflect the ability of HEPES in the buffer to act as a SED). In all cases, similar trends were seen with both eosin Y and $\text{Ru}(\text{bpy})_3^{2+}$. Relative to assays with no added SED,

ascorbate and sulfite were found to hinder photo-production of MV^+ , glucose and glycerol gave similar concentrations of MV^+ , and cysteine, EDTA, MES, oxalate and TEOA facilitated MV^{2+} photoreduction to greater extents. Overall, EDTA and TEOA were the most effective SEDs for photoreduction of MV^{2+} making them the most suitable reagents for experiments aiming to achieve light-driven H_2 -evolution with MR-1. Of the two, TEOA was chosen for subsequent work because it has been shown previously that EDTA adversely impacts anaerobic growth of MR-1 when present at low concentrations (0.25 mM), presumably due to destabilisation of the outer membrane.²²⁵

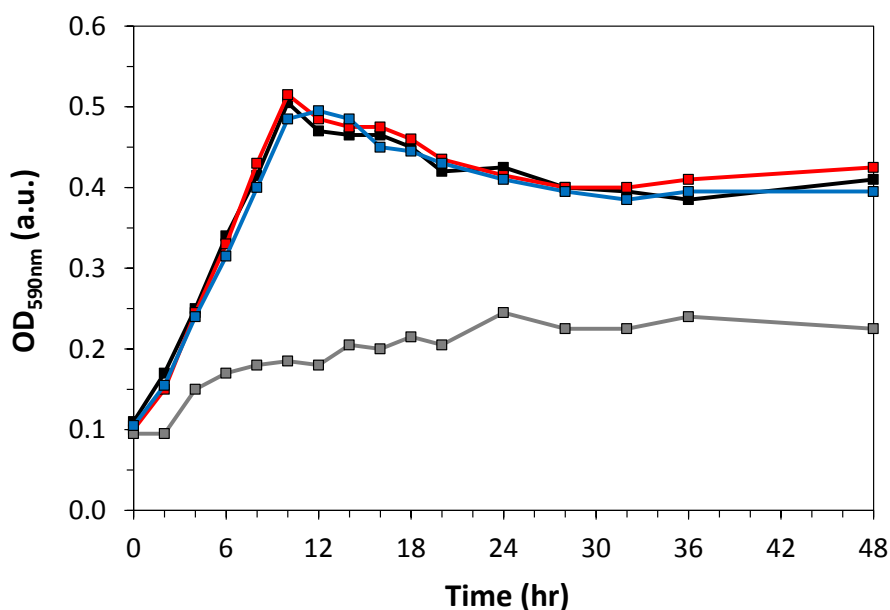


Figure 4.8 - Anaerobic growth of MR-1 with 37.5 mM lactate as electron donor and 18.8 mM fumarate as electron acceptor in the presence of eosin Y, proflavine or $Ru(bpy)_3^{2+}$. Optical density at 590 nm for MR-1 in the presence of no added photosensitizer (black) or 10 μ M eosin Y (red), proflavine (grey) or $Ru(bpy)_3^{2+}$ (blue). Inoculation at 0 hr of M72 medium (10 mL) supplemented with anaerobic growth additions. Samples had 7 mL headspace (100 % N_2 at inoculation). Optical densities are mean values from biological duplicates, error bars indicate maximum and minimum. Lines serve as a guide to the eye, the majority of error bars are too small to resolve.

To further quantify the photoreduction of MV^{2+} by eosin Y and $Ru(bpy)_3^{2+}$ in the presence of TEOA, quantum yields were calculated to show the proportion of incident light used in productive electron transfer (i.e. for reduction of MV^{2+} to MV^+). The external quantum yield of a photocatalytic system is defined by **Eq. 4.4** and considers all light falling incident on the sample. The internal quantum yield of a photocatalytic system is defined by **Eq. 4.5** and only considers light that has been absorbed by the photosensitizer to generate the photo-excited state. If the photosensitizer concentration is sufficiently high then it can be

assumed that all incident light is absorbed and that the external quantum yield equals the internal quantum yield.

$$\frac{\begin{array}{l} \text{(total number of electrons used} \\ \text{in productive electron transfer)} \\ \times 100 \% \end{array}}{\begin{array}{l} \text{(total number of photons} \\ \text{incident on the sample)} \end{array}} = \text{external quantum yield} \quad \text{Eq. 4.4}$$

$$\frac{\begin{array}{l} \text{(total number of electrons used} \\ \text{in productive electron transfer)} \\ \times 100 \% \end{array}}{\begin{array}{l} \text{(total number of photons} \\ \text{absorbed by the photosensitiser)} \end{array}} = \text{internal quantum yield} \quad \text{Eq. 4.5}$$

To irradiate samples with a defined number of photons, bandpass interference filters (Edmund Optics, 10 nm FWHM) that only transmit light at a particular wavelength were placed directly in front of the beam of light coming from the cold light source. The total number of incident photons over a known time and surface area was estimated from the light intensity and the energy of a single photon at the wavelength defined by the filter according to **Eq. 4.6**, where I_0 is the incident light intensity in kW m^{-2} , A is the area being irradiated in m^2 , t is the duration of the experiment in s , λ is the wavelength of light in m , h is Planck's constant and c is the speed of light. This calculation makes the assumption that all light incident on the sample is at a single wavelength.

$$\frac{I_0 \times A \times t \times \lambda \times 10^3}{h \times c} = \text{total photons} \quad \text{Eq. 4.6}$$

Stirred anaerobic samples (2 mL, 1 cm pathlength) containing 0.06 mM photosensitiser, 0.15 mM MV and 30 mM TEOA in 50 mM HEPES, 50 mM NaCl, pH 7 were irradiated for 10 min with light from the cold light source (0.01 kW m^{-2} , $1.2 \times 10^{-4} \text{ m}^2$ irradiation area) passing through a bandpass filter at 450 or 500 nm for experiments with $\text{Ru}(\text{bpy})_3^{2+}$ or eosin Y, respectively. At the end of the irradiation period, the total number of photo-excited electrons used in productive electron transfer was calculated using **Eq. 4.7**, where $\Delta\text{Abs}_{396\text{nm}}$ is the change in absorbance at 396 nm after 10 min, N_A is Avogadro's

constant, ϵ_{MV^+} is the extinction coefficient of MV^+ ($42.1 \text{ mM}^{-1} \text{ cm}^{-1}$)¹⁵⁸ and the factor of 5×10^5 accounts for the volume of the reaction solution.

$$\frac{\Delta \text{Abs}_{396\text{nm}} \times N_A}{\epsilon_{MV^+} \times 5 \times 10^5} = \text{total electrons} \quad \text{Eq. 4.7}$$

Based on the Beer-Lambert law (see **Eq. 2.1**) and the extinction coefficients of the photosensitisers (see **Table 4.2**), 0.06 mM eosin Y or $\text{Ru}(\text{bpy})_3^{2+}$ would give an absorbance of 4.82 or 0.86, respectively, at λ_{max} . This corresponds to the absorption of 99.99 or 86.20 % of incident light by eosin Y or $\text{Ru}(\text{bpy})_3^{2+}$, respectively. As such, it can be assumed that solutions containing eosin Y absorb all incident photons and the external quantum yield equals the internal quantum yield whereas solutions containing $\text{Ru}(\text{bpy})_3^{2+}$ only absorb 86.20 % of incident photons such that the external and internal quantum yields are different. Using **Eq. 4.4** to **4.7** and the experimental parameters described above, the quantum yields for photoreduction of MV^{2+} were 2.16 ± 0.22 % for eosin Y and 0.98 ± 0.04 (external) and 1.13 ± 0.05 (internal) % for $\text{Ru}(\text{bpy})_3^{2+}$ (all mean values from technical triplicates, error indicates standard error).

4.4 Light-driven H_2 -evolution by *Shewanella oneidensis* MR-1 from photo-produced MV^+

4.4.1 Impact of photosensitiser identity

To investigate light-driven H_2 -evolution, photo-production of MV^+ was carried out in the presence of MR-1 which had been cultured for 24 hr under anaerobic, acceptor-limited conditions then re-suspended in anaerobic 50 mM HEPES, 50 mM NaCl, pH 7 (see sections 2.3.3 and 2.3.7). Bacterial suspensions ($\text{OD}_{590\text{nm}} \approx 0.25$) were supplemented with 60 mM TEOA, 0.3 mM MV and 0.11 mM photosensitiser then stirred samples (1.7 mL, no gaseous headspace above reaction suspensions, room temperature) within the chamber of the H_2 -sensing electrode were irradiated (0.7 kW m^{-2}) periodically with the cold light source after a 10 min equilibration period (see section 2.4.2). Results from experiments with each of the six photosensitisers introduced above are presented in **Fig. 4.9A**. Equivalent experiments in the absence of MV are shown in **Fig. 4.9B**.

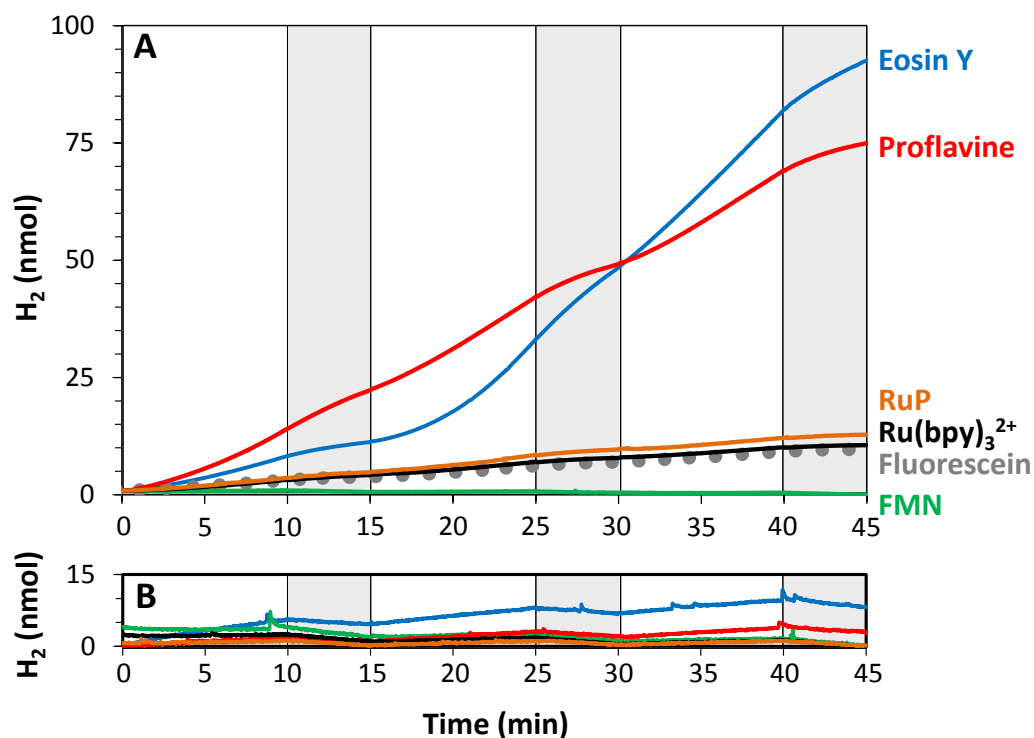


Figure 4.9 - Light-driven H₂ production by MR-1 with xanthene-, acridine- and Ru(II)-dyes. A] Dissolved H₂ in samples that experienced ambient light throughout and high intensity irradiation by the cold light source (0.7 kW m⁻²) between 0-10, 15-25 and 30-40 min (white panels). MR-1 suspensions (OD_{590nm} ≈ 0.25) with 60 mM TEOA, 0.3 mM MV and 0.11 mM of the indicated photosensitiser. B] As for A] but in the absence of MV. Anaerobic samples (1.7 mL) in 50 mM HEPES, 50 mM NaCl, pH 7 at room temperature.

At the end of experiments in the presence of MV, suspensions contained approximately 93, 75, 13, 11, 10 and 0 nmol dissolved H₂ with eosin Y, proflavine, RuP, Ru(bpy)₃²⁺, fluorescein and FMN, respectively. The final quantities of H₂ correlate with the relative extents of MV²⁺ photoreduction supported by each photosensitiser shown in **Fig. 4.6**. Identical experiments in the absence of MV gave approximately 8 (eosin Y), 3 (proflavine) and 0 (all other photosensitisers) nmol dissolved H₂ showing that direct electron transfer from the photosensitisers to the hydrogenases does not occur to a significant extent under these conditions. This is consistent with H₂-evolution assays using the chemical reductant DT as the source of electrons (see **Fig. 3.3**). In both cases, the addition of MV as electron shuttle afforded a more rapid approach to H₂-evolution with MR-1.

In the presence of MV and all photosensitisers except FMN, irradiation of the sample with high intensity light led to an increase in dissolved H₂ after a delay of approximately 30 sec to 1 min. The amount of dissolved H₂ increased for the duration of the irradiation period then continued to increase at a slower rate once the sample was returned to ambient light

conditions. The same trend of faster and slower H₂-evolution was seen during two further cycles of irradiation with high intensity light and then ambient light. Continuation of H₂-evolution after removal of the high intensity light source is due to accumulation of MV⁺ in the sample which corresponded to the gradual appearance of a deep blue colour in reaction suspensions over the course of the experiment. Formation of MV⁺ was confirmed by recording the absorbance spectrum of samples at the end of experiments described in Fig. 4.9A. The resultant spectra from assays with eosin Y or Ru(bpy)₃²⁺ as the photosensitiser are presented in Fig. 4.10. Peaks corresponding to formation of MV⁺ can be seen at 396 nm (with both photosensitisers) and 606 nm (with eosin Y only) superimposed on a background of scatter caused by the presence of MR-1. The relative amounts of MV⁺ seen with each photosensitiser correlate with the extents of MV²⁺ photoreduction achieved in abiotic assays (see Fig. 4.6). The build-up of MV⁺ during experiments means that proton reduction can continue in the absence of high intensity irradiation because there is a pool of electrons available for continued transfer to MR-1 hydrogenases.

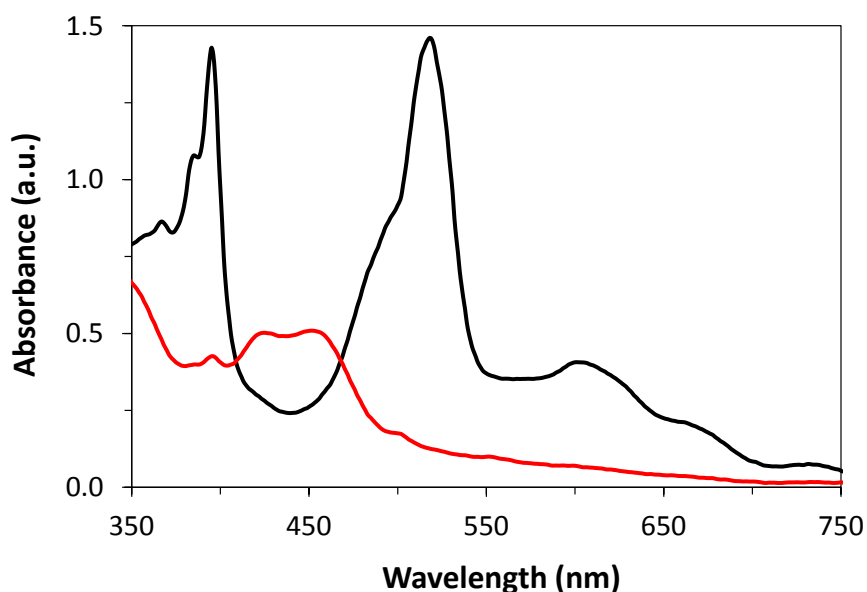


Figure 4.10 - Accumulation of MV⁺ in reactions suspensions during light-driven H₂ production by MR-1. Absorbance spectra recorded at the end of experiments described in Fig. 4.9A with eosin Y (black) or Ru(bpy)₃²⁺ (red) as photosensitiser. Reaction suspensions diluted 4-fold in anaerobic 50 mM HEPES, 50 mM NaCl, pH 7 for clearer spectra (pathlength 1 cm).

Overall, the work presented in this section shows that light-driven H₂-evolution can be achieved by carrying out the photoreduction of MV²⁺ to MV⁺ in the presence of anaerobically grown MR-1. To further understand the determinants of H₂ production,

eosin Y and $\text{Ru}(\text{bpy})_3^{2+}$ were used as representative photosensitisers in experiments which varied the cell density, buffer pH, light intensity and MV concentration.

4.4.2 Effect of *Shewanella oneidensis* MR-1 cell density

The first set of experiments assessed how changing MR-1 cell density and systematically omitting MR-1, functional hydrogenases, TEOA, the photosensitiser or irradiation affected light-driven H_2 production. MR-1 was cultured and processed as described in section 4.4.1 and a H_2 -sensing electrode was used to quantify H_2 production. Results from the experiments are shown in Fig. 4.11.

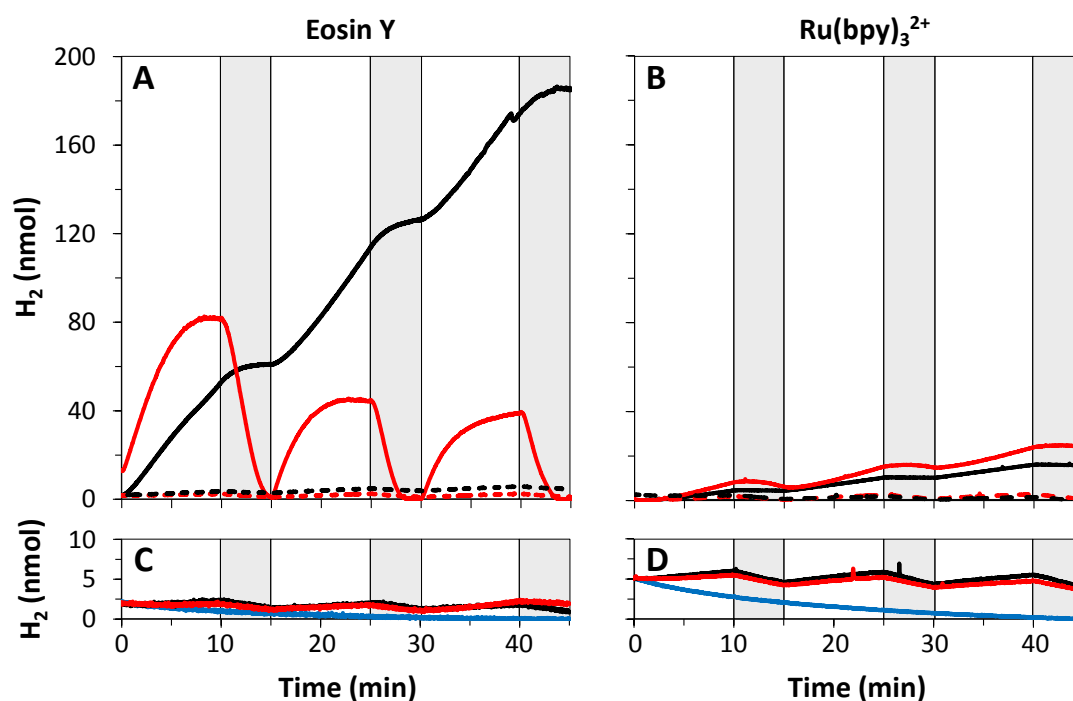


Figure 4.11 - Impact of MR-1 cell density and omission of MR-1, functional hydrogenases, TEOA, the photosensitiser or irradiation on light-driven H_2 production. Dissolved H_2 in samples that experienced ambient light throughout and high intensity irradiation (0.7 kW m^{-2}) between 0-10, 15-25 and 30-40 min (white panels). A] 0.11 mM eosin Y, 60 mM TEOA and 0.3 mM MV with MR-1 at $\text{OD}_{590\text{nm}} \approx 0.25$ (solid black line), MR-1 at $\text{OD}_{590\text{nm}} \approx 2.5$ (solid red line), no bacteria (dashed black line) or *HydA⁻/HyaB⁻* at $\text{OD}_{590\text{nm}} \approx 0.25$ (dashed red line). B] As for A] but with 0.11 mM $\text{Ru}(\text{bpy})_3^{2+}$ in place of eosin Y as photosensitiser. C] As for solid black line in A] but with omission of TEOA (black), eosin Y (red) or irradiation at 0.7 kW m^{-2} (blue). D] As for solid black line in B] but with omission of TEOA (black), $\text{Ru}(\text{bpy})_3^{2+}$ (red) or irradiation at 0.7 kW m^{-2} (blue). Anaerobic samples (1.7 mL) in 50 mM HEPES, 50 mM NaCl, pH 7 at room temperature. Irradiation provided by the cold light source.

For both photosensitisers, negligible amounts of H_2 were produced in experiments performed with no bacteria or with the *HydA⁻/HyaB⁻* strain in place of MR-1. This confirms

that light-driven H₂-evolution is a direct result of proton reduction by wild-type MR-1 hydrogenases and that abiotic processes do not significantly contribute to the formation of H₂. When experiments were performed with MR-1 at OD_{590nm} ≈0.25, eosin Y and Ru(bpy)₃²⁺ gave similar relative performances to those shown in **Fig. 4.9A**. With MR-1 at OD_{590nm} ≈2.5, very different trends were seen with the two photosensitisers. During experiments with eosin Y, there was no net accumulation of H₂ due to complete depletion of the product under ambient light conditions. This is most likely caused by re-oxidation of H₂ followed by distribution of electrons between intracellular electron acceptors. Comparable results were seen during H₂-evolution assays with MR-1 at OD_{590nm} ≈2.5 using the chemical reductant DT as the source of electrons (see section 3.3.1 and **Fig. 3.4**). However, this did not occur during experiments with Ru(bpy)₃²⁺ and approximately 50 % more H₂ was produced by the end of the experiment with MR-1 at OD_{590nm} ≈2.5 compared to OD_{590nm} ≈0.25. The different trends with each photosensitiser for MR-1 at OD_{590nm} ≈2.5 could be due to there being considerably more dissolved H₂ in experiments with eosin Y compared to those with Ru(bpy)₃²⁺. This may shift the equilibrium of the hydrogenase-catalysed reaction towards H₂ oxidation. Lastly, in experiments omitting TEOA, the photosensitiser or irradiation, only negligible amounts of H₂ were produced with both photosensitisers. The slight increases and decreases in dissolved H₂ may be caused by heating and cooling of the sample under irradiation and/or minor levels of proton reduction by MR-1 hydrogenases.

Overall, the results in this section confirm that MR-1, functional hydrogenases, TEOA, the photosensitiser and irradiation are all essential to achieve light-driven H₂ production and that cell density can greatly affect accumulation of the product. The next set of experiments extended the evaluation of the determinants of light-driven H₂-evolution with MR-1 by varying the buffer pH, light intensity and concentration of MV.

4.4.3 Effect of pH, light intensity and methyl viologen concentration

The effect of pH was evaluated using 50 mM HEPES, 50 mM NaCl at pH 6, 7 or 8 for washing and re-suspending MR-1 harvested after 24 hr anaerobic growth in M72 medium. The effect of light intensity was evaluated by irradiating samples with the cold light source at an intensity of 0.3, 0.5 or 0.7 kW m⁻². The effect of mediator concentration was evaluated by including MV in MR-1 suspensions to an initial concentration of 0, 0.3 or

1.2 mM. Only one parameter was changed at a time and irradiation of samples within the H₂-sensing electrode was provided continuously over 30 min to avoid significant changes to the rate of H₂-evolution, as seen in **Fig. 4.9A** and **4.11**. Samples (1.7 mL) were prepared as described in section 4.4.1 and all experiments contained MR-1 at OD_{590nm} ≈0.25, 60 mM TEOA and 0.11 mM photosensitiser. Results from the experiments are presented in **Fig. 4.12** and have been normalised to those collected with pH 7 buffer, 0.7 kW m⁻² light intensity and 0.3 mM MV to assess relative differences related to the change of a single parameter. The 100 % values correspond to 242 ± 24 or 33 ± 5 nmol dissolved H₂ in samples after 30 min irradiation with eosin Y or Ru(bpy)₃²⁺ as the photosensitiser, respectively.

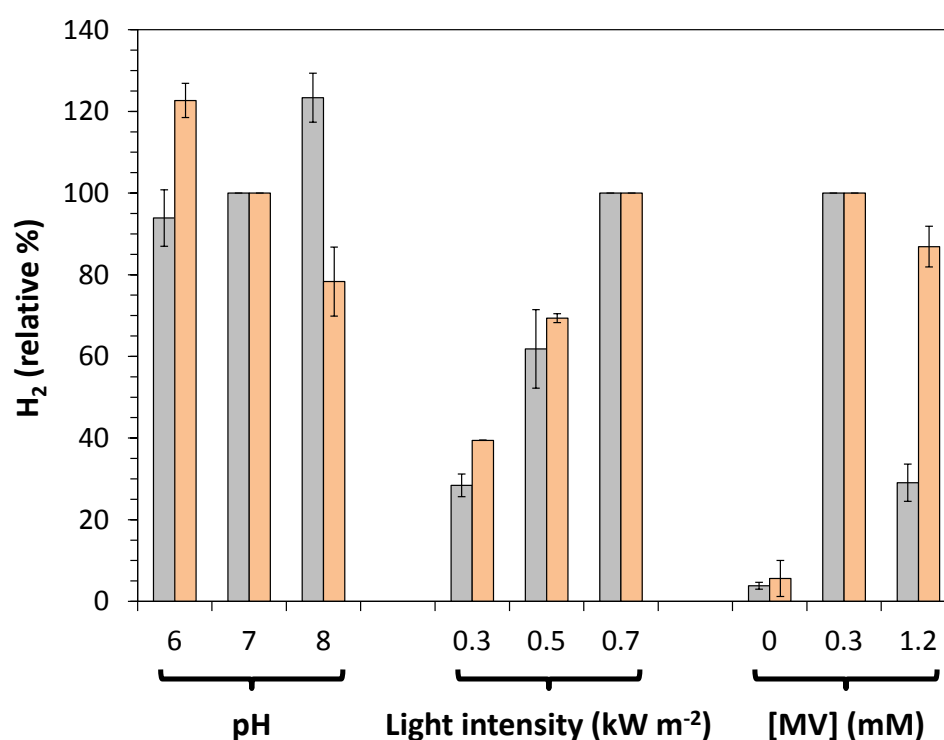


Figure 4.12 - Impact of pH, light intensity and MV concentration on light-driven H₂ production by MR-1. Dissolved H₂ after 30 min continuous irradiation of MR-1 suspensions (OD_{590nm} ≈0.25) with 0.11 mM eosin Y (grey) or Ru(bpy)₃²⁺ (orange). Buffer was pH 7, light intensity was 0.7 kW m⁻², and [MV] was 0.3 mM unless otherwise stated. Mean values from biological duplicates, error bars indicate maximum and minimum. Results normalised to those collected with pH 7 buffer, irradiation at 0.7 kW m⁻² and a starting concentration of 0.3 mM MV for each photosensitiser. 100 % dissolved H₂ was 242 ± 24 nmol with eosin Y (6 biological replicates) and 33 ± 5 nmol with Ru(bpy)₃²⁺ (5 biological replicates). Anaerobic samples (1.7 mL) with 60 mM TEOA in 50 mM HEPES, 50 mM NaCl at room temperature. Irradiation provided by the cold light source.

Normalising the results in **Fig. 4.12** overcomes the problem of comparing absolute amounts of H₂ produced by different MR-1 cultures due to day-to-day variations of biological samples. Representative sample variations are shown in **Fig. 4.13** for light-driven

H₂-evolution by MR-1 ($OD_{590nm} \approx 0.25$) in the presence of 60 mM TEOA, 0.3 mM MV and 0.11 mM photosensitiser. Dissolved H₂ was quantified with the H₂-sensing electrode and irradiation (0.7 kW m^{-2}) was provided by the cold light source continuously for 30 min. Each line represents a sample prepared on a different day from a different anaerobic culture of MR-1. Despite the changes in the final quantities of dissolved H₂ after 30 min, the relative effectiveness of eosin Y compared to $Ru(bpy)_3^{2+}$ in supporting light-driven H₂-evolution is consistent throughout all experiments.

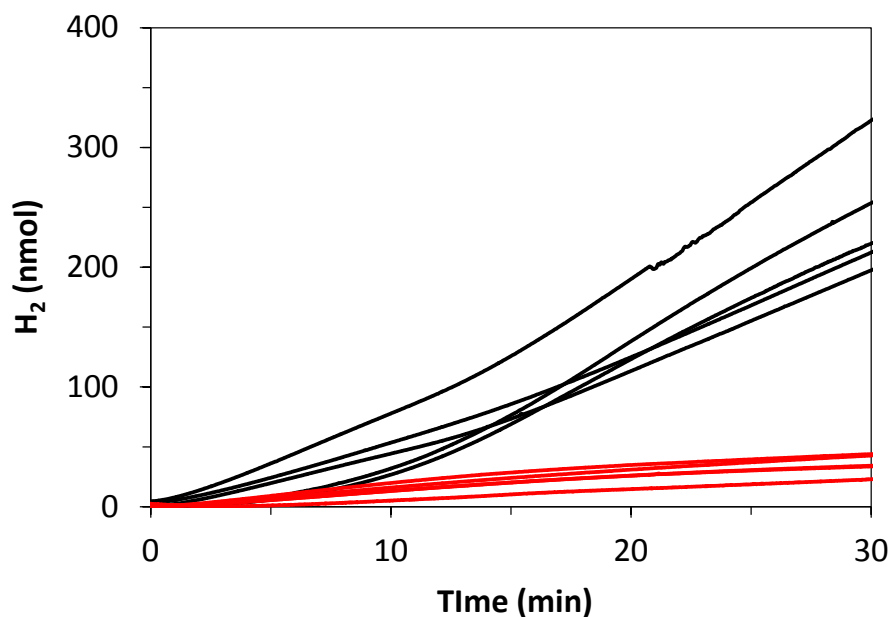


Figure 4.13 - Day-to-day variations in light-driven H₂ production by MR-1. Representative data for dissolved H₂ in MR-1 suspensions ($OD_{590nm} \approx 0.25$) with 60 mM TEOA, 0.3 mM MV and 0.11 mM eosin Y (black) or $Ru(bpy)_3^{2+}$ (red). Each line represents an experiment performed on a different day using a sample prepared from a different MR-1 culture. Anaerobic samples (1.7 mL) in 50 mM HEPES, 50 mM NaCl, pH 7 at room temperature. Irradiation (0.7 kW m^{-2}) was provided by the cold light source continuously for 30 min.

Changing the pH had little effect on light-driven H₂ production by MR-1. With eosin Y, the amount of dissolved H₂ after 30 min irradiation increased slightly with increasing buffer pH whereas with $Ru(bpy)_3^{2+}$ the amount of dissolved H₂ decreased slightly with increasing buffer pH. Hydrogenases typically exhibit more rapid proton reduction at lower pH²²⁶ but this was not observed to a significant extent here suggesting that the rate-defining events are not hydrogenase-dependent. Additionally, the spectral properties of the photosensitisers were found to be pH-independent, as shown by the absorbance profiles for eosin Y and $Ru(bpy)_3^{2+}$ in 50 mM HEPES, 50 mM NaCl at pH 6, 7 or 8 presented in **Fig. 4.14**. Instead, it is likely that changing the pH slightly alters the (photo-)reduction potentials of TEOA and/or the photosensitisers (see **Fig. 4.4**) and hence the feasibility of

light-driven electron transfer. With both photosensitisers, a lower light intensity led to less dissolved H_2 present in reaction suspensions after 30 min. This is likely due to fewer photons striking the sample leading to fewer photo-excited electrons being generated and transferred to MV for proton reduction. Of the three parameters assessed in the experiments described above, MV concentration had the greatest influence on total H_2 production. With both photosensitisers, negligible quantities of H_2 were produced with 0 mM MV confirming the key role of this reagent in light-driven electron transfer to MR-1 hydrogenases. Increasing the initial concentration of MV from 0.3 to 1.2 mM led to a decrease in H_2 production by approximately 71 and 13 % for experiments with eosin Y and $Ru(bpy)_3^{2+}$, respectively. A decrease in light-driven H_2 production caused by an increase in MV concentration was also reported in Gurunathan et al. (1997)¹⁹⁷ for a system comprised of sensitised- SnO_2 loaded with platinum in the presence of EDTA as SED. This observation was attributed to increased formation of the MV^+ dimer which has a more positive reduction potential than the MV^+ monomer, making proton reduction less thermodynamically favourable. Alternatively, increasing the concentration of MV may increase the likelihood of non-productive electron transfer pathways such as re-oxidation of MV^+ to MV^{2+} through electron donation to the highly oxidising PS^+ species (see **Fig. 4.2** and **Table 4.1**) generated during oxidative quenching of the photosensitiser excited state.

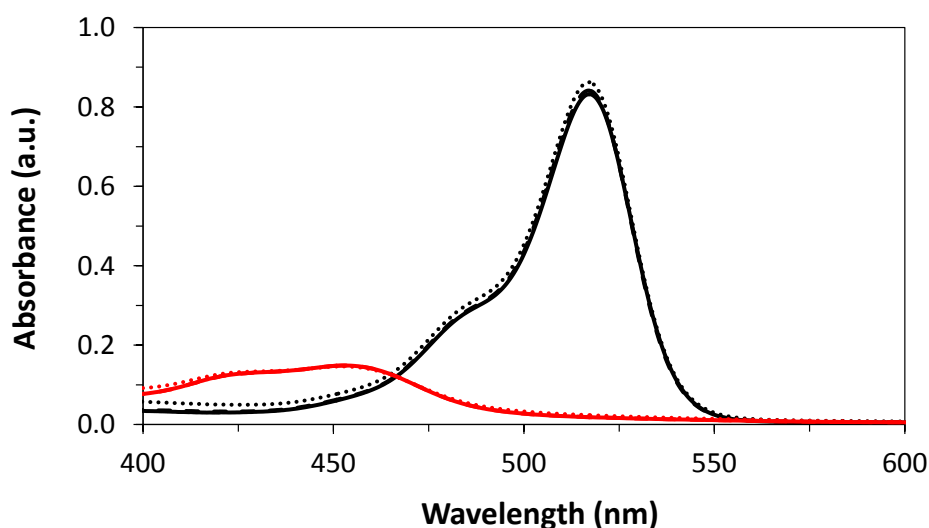


Figure 4.14 - Absorbance spectra of 10 μM eosin Y (black) and $Ru(bpy)_3^{2+}$ (red) in 50 mM HEPES, 50 mM NaCl at pH 6 (solid line), 7 (dashed line) or 8 (dotted line). Pathlength 1 cm. The majority of spectra cannot be seen due to overlap.

Overall, the findings in this section show that light-driven H_2 -evolution by MR-1 is predominantly influenced by the photosensitiser and MV. This suggests that the system is

highly dependent on photo-production of MV^+ and subsequent electron transfer to bacterial enzymes. In the next section, the implications of these processes on the viability of MR-1 were evaluated after incubating the bacterium with reagents required for light-driven H_2 -evolution. It is of interest to assess the viability of MR-1 to determine whether the system could be self-regenerating over extended periods of time with the opportunity for the bacterium to repair and/or replace enzymes as required.

4.4.4 Viability of *Shewanella oneidensis* MR-1 after incubation with reagents required for light-driven H_2 -evolution

Bacterial viability was assessed by measuring CFU mL^{-1} (see section 2.3.5) after incubating MR-1 (previously cultured under acceptor-limited conditions for 24 hr) in buffer only (1.7 mL anaerobic 50 mM HEPES, 50 mM NaCl, pH 7 with MR-1 at $OD_{590nm} \approx 0.25$) or buffer supplemented with 60 mM TEOA, 0.3 mM MV and either 0.11 mM eosin Y or $Ru(bpy)_3^{2+}$. Incubations were performed for 30 min in the dark or with irradiation (0.7 kW m^{-2}) by the cold light source. Results from the experiments are shown in **Fig. 4.15A**. Equivalent experiments were performed with reagents required for DT-driven H_2 -evolution where MR-1 was incubated with $26.4 \mu\text{g mL}^{-1}$ DT and/or 0.3 mM MV for 30 min in the dark. Results from the assays are shown in **Fig. 4.15B**.

When MR-1 was incubated in buffer only (with no added reagents) the samples contained $\approx 10^8$ CFU mL^{-1} after 30 min regardless of whether they were kept in the dark or irradiated by the cold light source. This shows that MR-1 remains viable after harvesting from M72 medium and processing for enzyme assays and that irradiation has little impact on bacterial survival in buffer only. When MR-1 was incubated with TEOA, MV and eosin Y, the samples contained $\approx 8 \times 10^4$ or 0 CFU mL^{-1} after 30 min in the dark or under irradiation, respectively. When MR-1 was incubated with TEOA, MV and $Ru(bpy)_3^{2+}$, the samples contained $\approx 3 \times 10^4$ or ≈ 77 CFU mL^{-1} after 30 min in the dark or under irradiation, respectively. The results show that the light-harvesting reagents have an intrinsic toxicity in the dark which is amplified under irradiation, particularly with eosin Y as photosensitiser. Based on the results shown in **Fig. 4.15B** for incubation with reagents required for DT-driven H_2 -evolution, it is likely that the loss of viability in the presence of TEOA, MV and a photosensitiser is primarily caused by the toxicity of MV and the generation of MV^+ under reducing conditions. However, additional factors may also be responsible for the further

decrease in viability under irradiation. For example, decomposition of TEOA after electron donation proceeds via carbon-centred radicals to eventually form a secondary amine and glycoaldehyde,⁴⁹ as shown in **Fig. 4.16**. Furthermore, it has been reported that (photo-)degradation of eosin Y can result in the formation of aromatic compounds such as diphenylmethane, 2,6-dibromophenol and benzoic acid²²⁷ whilst photo-damage of $\text{Ru}(\text{bpy})_3^{2+}$ can cause aquation of the ruthenium centre and release of the 2,2'-bipyridine ligands.²²⁸ Taken together, it is possible that under irradiation there is an accumulation of numerous chemical species in the sample which are potentially harmful to MR-1.

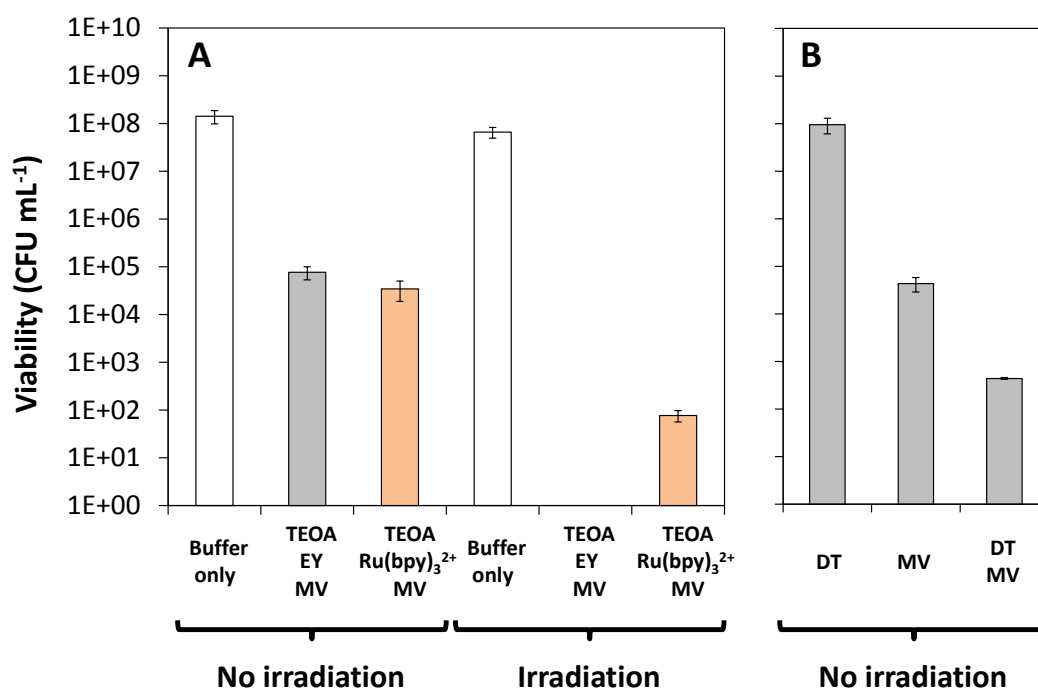


Figure 4.15 - Viability of MR-1 after incubation with reagents required for light-driven and DT-driven H_2 -evolution. A) CFU mL^{-1} after 30 min incubation in buffer only or buffer containing 60 mM TEOA, 0.3 mM MV and either 0.11 mM eosin Y (EY) or $\text{Ru}(\text{bpy})_3^{2+}$. B) CFU mL^{-1} after 30 min incubation in buffer containing 26.4 $\mu\text{g mL}^{-1}$ DT and/or 0.3 mM MV. Samples were kept in the dark or irradiated (0.7 kW m^{-2}) with the cold light source as indicated. Mean values from biological duplicates, error bars indicate maximum and minimum. Anaerobic samples (1.7 mL) with MR-1 at $\text{OD}_{590\text{nm}} \approx 0.25$ in 50 mM HEPES, 50 mM NaCl, pH 7 at room temperature.

Overall, the findings in this section indicate that light-driven H_2 -evolution has a detrimental impact on the viability of MR-1. The system can clearly be used to generate H_2 under irradiation by visible light (see sections 4.4.1, 4.4.2 and 4.4.3) but proton reduction after 30 min irradiation is predominantly performed by hydrogenases associated with non-viable bacteria. Despite these observations, it was of interest to evaluate the longevity of light-driven H_2 -evolution by MR-1 to see whether the hydrogenases remain active in the sample following the decrease in bacterial viability.

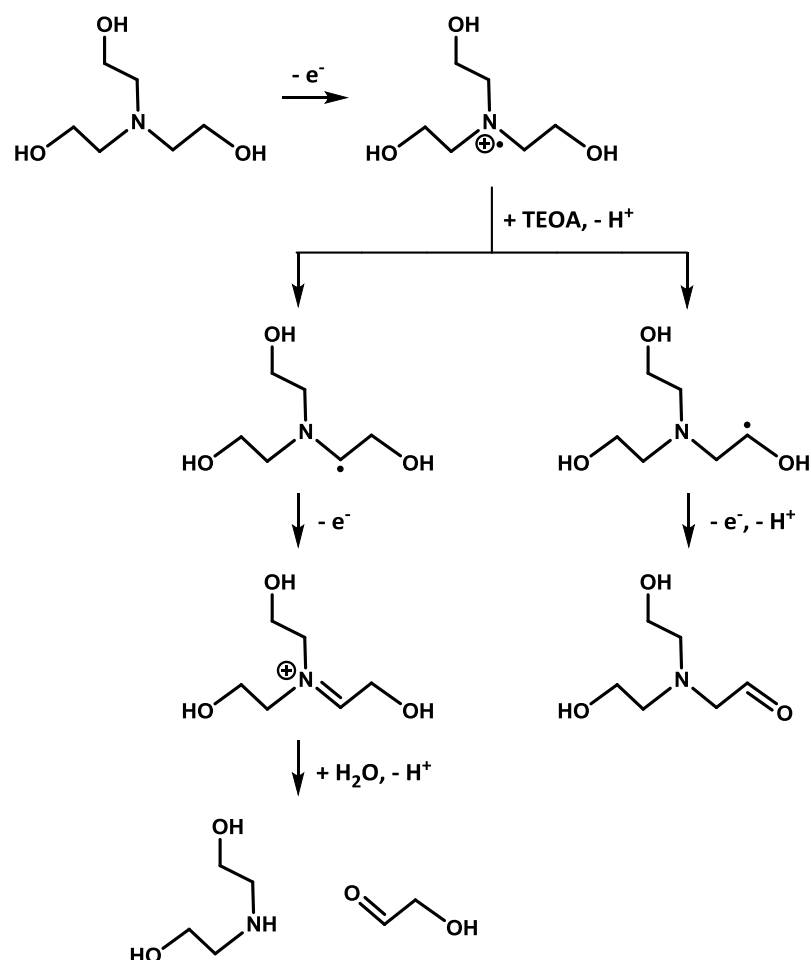


Figure 4.16 - TEOA decomposition pathway after electron donation.⁴⁹

4.5 Sustained light-driven H_2 -evolution by *Shewanella oneidensis* MR-1 from photo-produced MV^+

Irradiation of samples over extended periods of time was achieved using light supplied by a photosynthetic growth lamp within a shaker-incubator (see section 2.2). The module allowed uniform irradiation of multiple samples, complete temperature control and high experimental throughput compared to assays performed within the chamber of the H_2 -sensing electrode. To prepare samples, MR-1 was cultured under acceptor-limited conditions for 24 hr then washed and re-suspended in anaerobic 50 mM HEPES, 50 mM NaCl, pH 7. Bacterial suspensions (1.7 mL, $OD_{590nm} \approx 0.25$) were transferred to clear glass vials and then supplemented with 60 mM TEOA, 0.3 mM MV and 0.11 mM of either eosin Y or $Ru(bpy)_3^{2+}$. The glass vials provided a 3.3 mL gaseous headspace above samples

to allow photo-produced H_2 to escape the solution and avoid re-oxidation by the bacterium, as seen in **Fig. 3.4** and **Fig. 4.11A**. Glass vials were tightly sealed within the N_2 -filled chamber then suspensions were irradiated at an intensity of 0.02 kW m^{-2} for 96 hr at $25 \text{ }^\circ\text{C}$ with periodic quantification of headspace H_2 using GC (see section 2.4.1). Parallel assays were performed in the absence of MR-1. Results from the experiments are shown in **Fig. 4.17**. With no bacteria, trace amounts of H_2 ($\leq 96 \text{ nmol}$) were detected with both photosensitisers showing that eosin Y and $\text{Ru}(\text{bpy})_3^{2+}$ can directly reduce aqueous protons in the buffer. However, the quantities of H_2 produced in abiotic experiments remained below the levels detected when MR-1 was included in the sample. In the presence of MR-1, significantly more H_2 was generated with eosin Y compared to $\text{Ru}(\text{bpy})_3^{2+}$ which correlates with the relative performances of the photosensitisers observed when irradiation was provided by the cold light source (see **Fig. 4.9A** and **4.11**). With eosin Y, the amount of headspace H_2 decreased after 18 hr whereas with $\text{Ru}(\text{bpy})_3^{2+}$ the amount of H_2 continued to increase such that the final quantities after 96 hr were nearly identical with both photosensitisers.

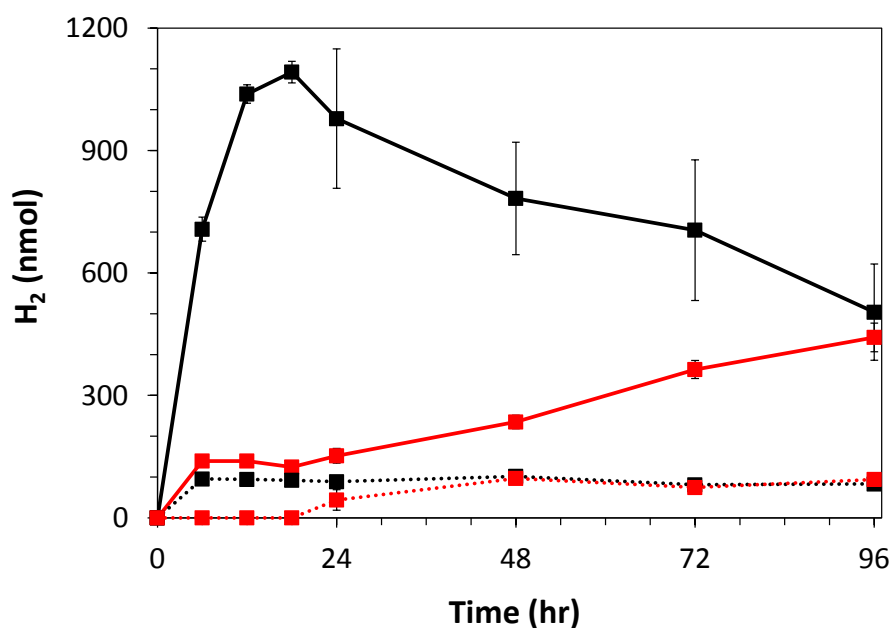


Figure 4.17 - Light-driven H_2 production by MR-1 over 96 hr. Headspace H_2 with 0.11 mM eosin Y (black) or $\text{Ru}(\text{bpy})_3^{2+}$ (red) for irradiated (0.02 kW m^{-2}) samples containing MR-1 (solid lines) or no bacteria (dashed lines). With MR-1, mean values from 2 (0-18 hr), 7 (24-48 hr) or 5 biological replicates (72-96 hr), error bars indicate standard error. With no bacteria, mean values from technical duplicates (0-96 hr), error bars indicate maximum and minimum. Anaerobic samples (1.7 mL) with MR-1 at $\text{OD}_{590\text{nm}} \approx 0.25$, 0.3 mM MV and 60 mM TEOA in 50 mM HEPES, 50 mM NaCl, pH 7 at $25 \text{ }^\circ\text{C}$. Samples had 3.3 mL headspace (100% N_2 at inoculation). Lines serve as a guide to the eye, the majority of error bars are too small to resolve. Irradiation provided by the photosynthetic growth lamp.

To further quantify light-driven production of headspace H_2 by MR-1, quantum yields were determined based on the calculations described in section 4.3. For the analysis, reaction suspensions (1.7 mL) containing MR-1 ($OD_{590nm} \approx 0.25$), 60 mM TEOA, 0.3 mM MV and 0.11 mM photosensitiser in anaerobic 50 mM HEPES, 50 mM NaCl, pH 7 were prepared within clear glass vials as described above. Samples were then irradiated for 1 hr with light from the cold light source (0.01 kW m^{-2} , $2.3 \times 10^{-4} \text{ m}^2$ irradiation area) passing through a bandpass filter at 450 or 500 nm for experiments with $Ru(bpy)_3^{2+}$ or eosin Y, respectively. At the end of the irradiation period, the total number of electrons used in productive electron transfer (i.e. for the generation of H_2) was calculated using **Eq. 4.8**, where mol H_2 is the amount of headspace H_2 after 1 hr in mol (determined using GC), N_A is Avogadro's constant and multiplication by a factor of two accounts for the fact that two electrons are required to generate one molecule of H_2 .

$$\text{mol } H_2 \times N_A \times 2 = \text{total electrons} \quad \text{Eq. 4.8}$$

Based on the Beer-Lambert law (see **Eq. 2.1**) and the extinction coefficients of the photosensitisers (see **Table 4.2**), 0.11 mM eosin Y or $Ru(bpy)_3^{2+}$ would give an absorbance of 8.84 or 1.58, respectively, at λ_{max} . This corresponds to the absorption of > 99.99 or 97.37 % of incident light by eosin Y or $Ru(bpy)_3^{2+}$, respectively. Accordingly, it can be assumed that samples containing eosin Y absorb all incident photons and the external quantum yield equals the internal quantum yield whereas samples containing $Ru(bpy)_3^{2+}$ only absorb 97.37 % of incident photons such that the external and internal quantum yields are different. Using **Eq. 4.4**, **4.5**, **4.6** and **4.8** with the experimental parameters described above, the quantum yields for light-driven H_2 -evolution were 0.56 ± 0.01 % for eosin Y and 0.46 ± 0.08 (external) and 0.47 ± 0.09 (internal) % for $Ru(bpy)_3^{2+}$ (all mean values from four biological replicates with standard error).

To further investigate the lack of sustained H_2 production with eosin Y after 18 hr, spectrophotometric H_2 oxidation assays (see section 2.5.1) were performed on supernatants and re-suspended cell pellets harvested after centrifugation of MR-1 suspensions which had been irradiated for 0, 24, 48, 72 or 96 hr as described in **Fig. 4.17**. Results from the analysis are presented in **Fig. 4.18** for samples previously containing eosin Y or $Ru(bpy)_3^{2+}$ as the photosensitiser. The results show that H_2 oxidation activity is predominantly associated with re-suspended cell pellets over 96 hr and that if bacteria lyse

during the experiment then they do not release significant quantities of active hydrogenases into solution. The considerable decrease in activity associated with cell pellets between 0 and 24 hr may be due to toxicity of the light-harvesting reagents (see section 4.4.4) causing a loss of bacterial viability (with the potential for subsequent cell lysis) and/or inhibition of the hydrogenases by O_2 .⁶⁰ In the latter case, gradual exposure to O_2 is a result of irradiating samples with the photosynthetic growth lamp outside the N_2 -filled chamber where headspace gases can slowly exchange with the surrounding air. This is illustrated in **Fig. 4.19** by the increase in GC peak area corresponding to headspace O_2 (see **Fig. 2.5**) recorded during light-driven H_2 -evolution experiments over 96 hr (as described in **Fig. 4.17**). To summarise, the results show that MR-1 hydrogenases remain active and associated with the pelletable cellular material over 96 hr. As a consequence, it is most likely that sustained H_2 -evolution with eosin Y is not possible due to photo-degradation of the photosensitiser (see **Fig. 4.5**) and, with no driving force for proton reduction, the amount of headspace H_2 decreases due to re-oxidation by the bacterium and/or slow leakage from the reaction vessel.

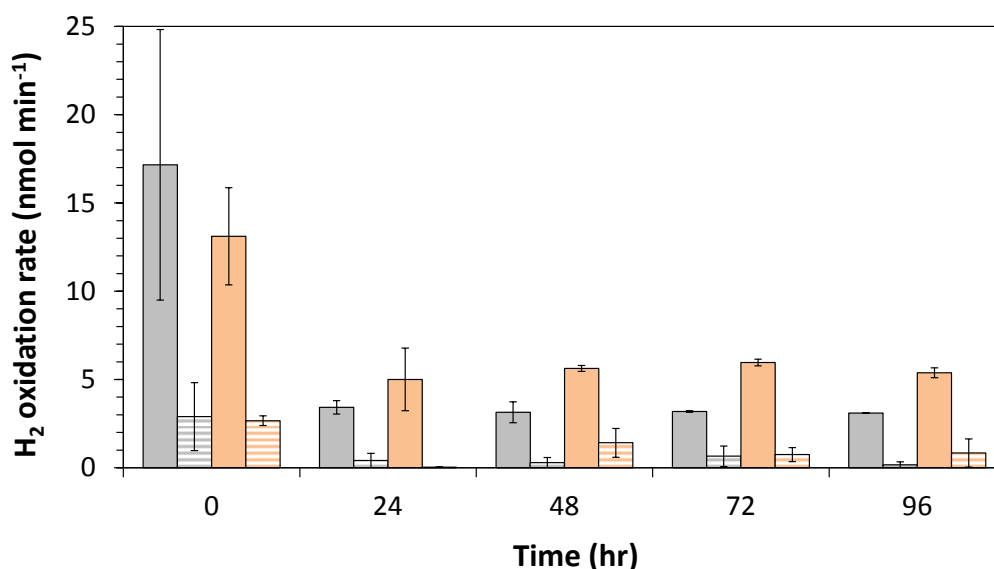


Figure 4.18 - Initial rates of H_2 oxidation coupled to BV reduction by MR-1 hydrogenases over 96 hr. Initial rates of H_2 oxidation associated with cell pellets (solid bars) and supernatants (striped bars) recovered after centrifugation of MR-1 suspensions irradiated for 0, 24, 48, 72 or 96 hr with eosin Y (grey) or $Ru(bpy)_3^{2+}$ (orange) as described in **Fig. 4.17**. Mean values for biological duplicates, error bars indicate maximum and minimum. Anaerobic samples in 50 mM HEPES, 50 mM NaCl, pH 7.

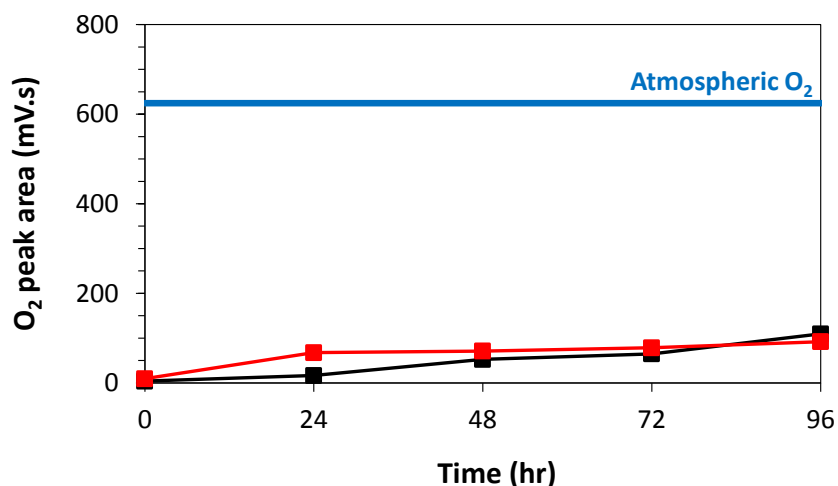


Figure 4.19 - Increase in headspace O₂ within glass vials over 96 hr. Representative data showing the increase in O₂ peak area for MR-1 suspensions irradiated by the photosynthetic growth lamp with eosin Y (black) or Ru(bpy)₃²⁺ (red) as described in **Fig. 4.17**. O₂ peak area for atmospheric O₂ is indicated, lines serve as a guide to the eye.

To assess whether light-driven H₂-evolution with eosin Y could be restored after photo-degradation of the photosensitiser, MR-1 cell pellets were harvested and then re-suspended in a fresh solution of TEOA, MV and eosin Y after 24 hr irradiation. For the experiments, MR-1 was first cultured under acceptor-limited conditions for 24 hr then harvested and re-suspended in 50 mM HEPES, 50 mM NaCl, pH 7 (1.7 mL, MR-1 OD_{590nm} ≈ 0.25) supplemented with 60 mM TEOA, 0.3 mM MV and 0.11 mM eosin Y. Reaction suspensions were irradiated (0.02 kW m⁻²) for 24 hr with the photosynthetic growth lamp as described in **Fig. 4.17** and then headspace H₂ was quantified by GC before samples were taken into a N₂-filled chamber. Cell pellets were harvested by centrifugation and then re-suspended in a fresh solution of TEOA, MV and eosin Y with an identical composition to the one described above. The new reaction suspensions were irradiated for a further 24 hr and headspace H₂ was quantified at the end of the experiment. The process of harvesting cell pellets, re-suspending in a fresh solution of TEOA, MV and eosin Y, and then irradiating for 24 hr was carried out a further two times using the same cellular material. Results from the analysis are presented in **Fig. 4.20** with data from parallel experiments performed with the HydA⁻/HyaB⁻ strain in place of MR-1. With the HydA⁻/HyaB⁻ strain, only trace amounts of headspace H₂ (≤ 99 nmol) were detected throughout all experiments corresponding to the lack of functional hydrogenases in the bacterium. In this case, the generation of H₂ is likely due to abiotic proton reduction as seen in **Fig. 4.17**. With MR-1, 1575 ± 87 nmol H₂ was produced after the first period of 24 hr irradiation. After the second, third and fourth periods of 24 hr irradiation, H₂-evolution was

restored to 20, 14 and 12 %, respectively, of that seen during the first period of irradiation. It is likely that full restoration of the original activity is not possible due to loss of cellular material during repeated processing of biological samples or inhibition of the hydrogenases as a result of decreased cell viability and exposure to O₂ (see above).

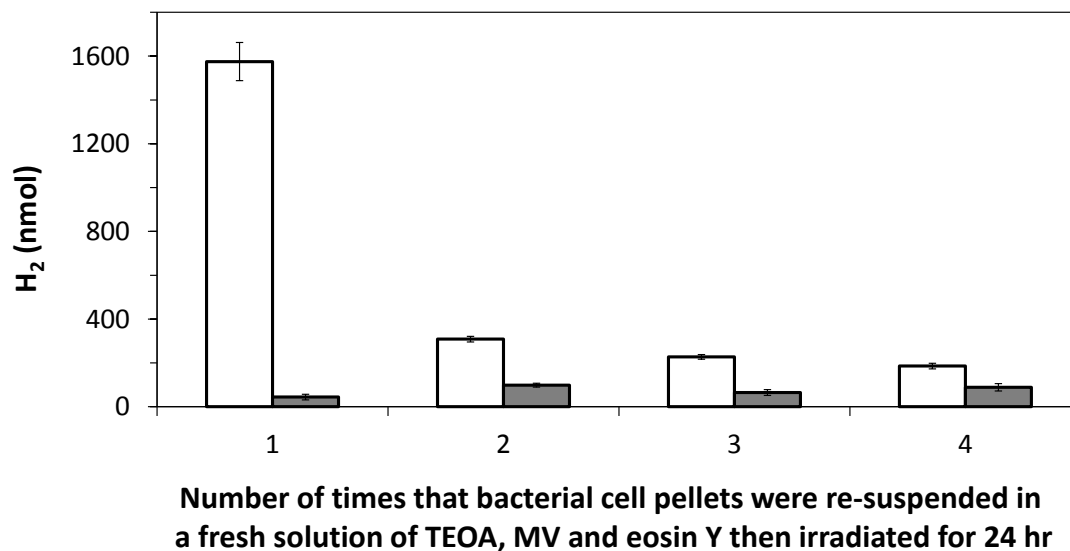


Figure 4.20 - Restoration of light-driven H₂-evolution by MR-1 through replacement of light-harvesting reagents after 24 hr irradiation. Headspace H₂ for MR-1 (white) or HydB/HyaB (grey) suspensions (OD_{590nm} ≈ 0.25) containing 60 mM TEOA, 0.3 mM MV and 0.11 mM eosin Y with 24 hr irradiation (0.02 kW m⁻²) by the photosynthetic growth lamp. Numerical label corresponds to the number of times that bacterial cell pellets were harvested and re-suspended in a fresh solution of light-harvesting reagents, see text for details. Mean values for technical triplicates, error bars indicate standard error. Anaerobic samples (1.7 mL) in 50 mM HEPES, 50 mM NaCl, pH 7.

The results presented in this section show that there is potential for sustained light-driven H₂-evolution with MR-1 due to the robustness of the hydrogenases which remain active over 96 hr despite decreases in bacterial viability (see section 4.4.4). However, the longevity of the system is compromised by the susceptibility of eosin Y to photo-degradation under extended periods of irradiation, although it is possible to partially restore light-driven H₂-evolution by replenishing the light-harvesting reagents. Under the same experimental conditions, photo-degradation of Ru(bpy)₃²⁺ did not occur to such an extent that the system stopped functioning but the rate of light-driven H₂-evolution was significantly lower than that seen with eosin Y. Overall, the results suggest that the system is predominantly influenced by the photosensitiser and photoreduction of MV²⁺ as opposed to the hydrogenases, similar to the findings in section 4.4.3. In the next section, results are shown from experiments that aimed to further understand the pathways by which electrons are transferred from MV⁺ to MR-1 hydrogenases for light-driven H₂-evolution.

4.6 Investigation of the possible role of outer membrane porin:cytochrome complexes in light-driven H₂-evolution by *Shewanella oneidensis* MR-1 from photo-produced MV⁺

In sections 4.4 and 4.5, light-driven H₂-evolution was achieved by performing photoreduction of MV²⁺ in the presence of anaerobically grown MR-1. The approach is underpinned by the presence of MV to effectively transfer photo-energised electrons to hydrogenases which are predominantly associated with pelletable cellular material. However, there are two main routes by which MV could transfer electrons into the periplasm (assuming the pelletable cellular material is largely comprised of intact cells). It is possible that MV crosses the outer membrane and interacts with MR-1 redox partners directly but it has also been reported that electrons can enter MR-1 via porin:cytochrome complexes spanning the outer membrane (see section 1.6.2).^{130,131} As a consequence, it was of interest to determine whether these protein complexes are involved in light-driven electron transfer across the outer membrane for the reduction of protons to H₂. For the experiments, a mutant strain of MR-1 was used where the genes encoding the entire *mtr* cluster have been deleted (referred to as Mtr⁻, see section 2.3.2).¹⁴⁰ To allow a direct comparison with the wild-type bacterium, the Mtr⁻ strain was cultured under anaerobic, acceptor-limited conditions then assessed for its hydrogenase activity using GC and spectrophotometric H₂ oxidation assays. Changes in OD_{590nm} and headspace H₂ during anaerobic growth with an excess of lactate to fumarate are shown in **Fig. 4.21** with the equivalent data for MR-1 and HydA⁻/HyaB⁻. The growth curve for Mtr⁻ is similar to the profile seen with the HydA⁻/HyaB⁻ strain but the Mtr⁻ strain displayed a decrease in OD_{590nm} between 12 and 20 hr corresponding to a decrease in the size and/or amount of bacteria. Headspace H₂ was detected 6 hr after inoculation confirming that the Mtr⁻ strain can produce hydrogenases active in proton reduction (coupled to lactate oxidation). However, Mtr⁻ produced approximately 2.5-fold and 3-fold more H₂ than MR-1 after 24 and 48 hr anaerobic growth, respectively. This may be due to increased hydrogenase content or increased electron delivery to the hydrogenases as a result of there being fewer cytochromes (i.e. MtrCAB, MtrDEF and OmcA) within the bacterium to accept electrons.

Spectrophotometric H₂ oxidation assays were performed using Mtr⁻ which had been harvested after 24 hr anaerobic growth then washed and re-suspended in anaerobic

50 mM HEPES, 50 mM NaCl, pH 7. Initial rates of H₂ oxidation were normalised to total protein content of samples using a BCA assay (see section 2.3.4) to better compare the responses of different strains. The results are presented in **Table 4.4** with the equivalent data for MR-1, HydA/HyaB⁻ and no bacteria. The mean H₂ oxidation rates for Mtr⁻ are approximately 2-fold greater than those seen with MR-1 under identical conditions suggesting increased hydrogenase content in Mtr⁻ compared to the wild-type bacterium.

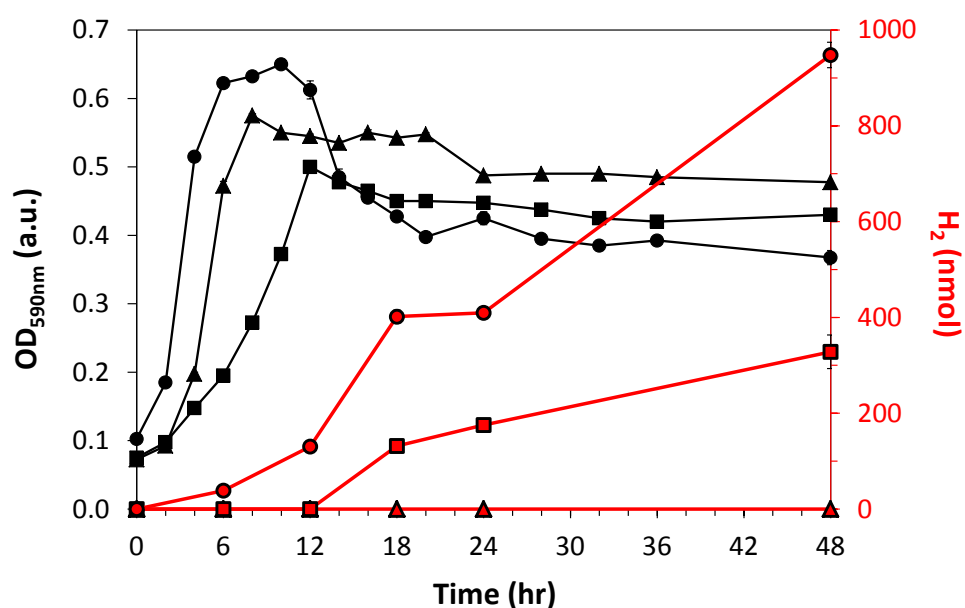


Figure 4.21 - Anaerobic growth of MR-1, HydA⁻/HyaB⁻ and Mtr⁻ with 37.5 mM lactate as electron donor and 18.8 mM fumarate as electron acceptor. Optical density at 590 nm (black, left axis) and headspace H₂ (red, right axis) for MR-1 (squares), HydA⁻/HyaB⁻ (triangles) and Mtr⁻ (circles). Inoculation at 0 hr of M72 medium (10 mL) supplemented with anaerobic growth additions. Samples had 7 mL headspace (100 % N₂ at inoculation). Optical densities are mean values from 4 biological replicates, error bars indicate standard error. Headspace H₂ data are mean values from biological duplicates, error bars indicate maximum and minimum. Lines serve as a guide to the eye, the majority of error bars are too small to resolve.

Table 4.4 - Initial rates of H₂ oxidation coupled to BV reduction by MR-1, HydA⁻/HyaB⁻, Mtr⁻ and no bacteria. Rates with MR-1, HydA⁻/HyaB⁻ and Mtr⁻ are mean values from technical duplicates of 4 biological replicates with standard error (normalised to total protein). Rate with no bacteria is the mean value from technical duplicates, error indicates maximum and minimum. Anaerobic samples in 1 mM BV, 50 mM HEPES, 50 mM NaCl, pH 7.

Strain	H ₂ oxidation rate
MR-1	138 ± 34 nmol min ⁻¹ mg ⁻¹
HydA ⁻ /HyaB ⁻	2 ± 2 nmol min ⁻¹ mg ⁻¹
Mtr ⁻	262 ± 47 nmol min ⁻¹ mg ⁻¹
No bacteria	0.06 ± 0.02 nmol min ⁻¹

In addition to experiments confirming the production of active hydrogenases, protein gels and Western blotting (see section 2.3.6) were used to determine whether bacteria cultured under acceptor-limited conditions had produced the MtrCAB complex (see **Fig. 1.16**). For the analysis, MR-1, HydA⁻/HyaB⁻ and Mtr⁻ were harvested after 24 hr anaerobic growth, re-suspended in loading buffer (32 μ L) and heated at 90 °C to lyse cells. Samples were then loaded on a 10 % SDS-PAGE gel and proteins in the cell lysates were resolved using gel electrophoresis. On separate gels, a Coomassie staining protocol was used to visualise all proteins within the sample and a heme-staining protocol was used to specifically visualise heme-containing proteins within the sample. Results from the visualisation protocols are presented in **Fig. 4.22** (top). The Coomassie stain did not establish whether MtrCAB has been produced because proteins are stained indiscriminately but the analysis confirmed that sample loading was equivalent for all three strains. The heme stain showed two clear bands for MR-1 (lane 2) and HydA⁻/HyaB⁻ (lane 3) which matched those seen for purified MtrCAB (lane 1). These bands most likely correspond to the presence of MtrA and MtrC in the samples. The Mtr⁻ strain did not stain under these conditions, presumably because the sample did not contain a sufficient amount of heme-containing protein. To specifically visualise MtrB and MtrC via Western blotting, cell lysates were prepared as described above then proteins in the sample were resolved by gel electrophoresis and transferred to a PVDF membrane for immunoblotting. Results from the visualisation of MtrB and MtrC are shown in **Fig. 4.22** (bottom). On both membranes, protein bands were seen around 75 kDa showing that anaerobic growth of MR-1 (lane 2) and HydA⁻/HyaB⁻ (lane 3) with an excess of lactate to fumarate leads to production of MtrB and MtrC. The bands match those seen for samples of the purified MtrCAB complex (lane 5). As expected, no protein bands were seen for Mtr⁻ (lane 4) confirming that the strain cannot produce MtrB or MtrC. It should be noted that the bands around 250 kDa, particularly visible in lanes 2 and 3 on the anti-MtrB membrane, are likely due to the fully associated MtrCAB complex which was not denatured during sample preparation.

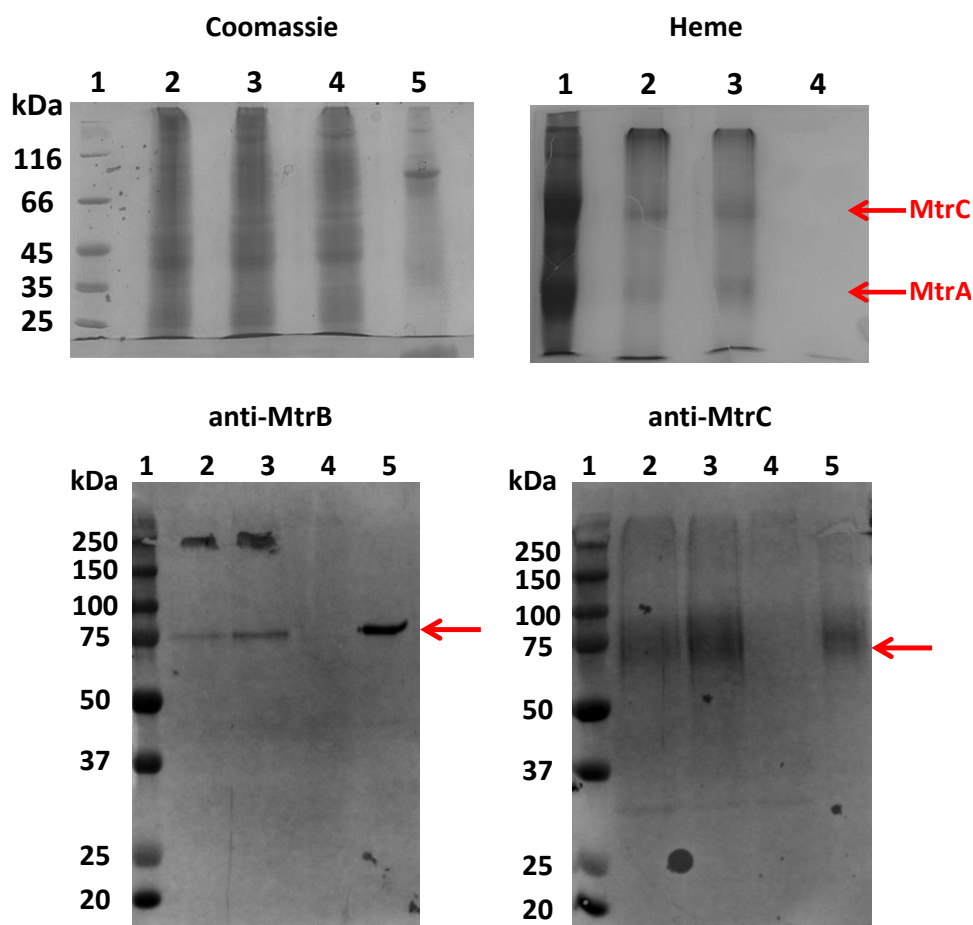


Figure 4.22 - MtrCAB content of MR-1, HydA⁻/HyaB⁻ and Mtr⁻ after 24 hr anaerobic growth with 37.5 mM lactate as electron donor and 18.8 mM fumarate as electron acceptor. Top left: protein visualisation by Coomassie staining. Lanes: 1] molecular weight markers, 2] MR-1, 3] HydA⁻/HyaB⁻, 4] Mtr⁻ and 5] purified MtrCAB. Top right: protein visualisation by heme staining. Lanes: 1] purified MtrCAB, 2] MR-1, 3] HydA⁻/HyaB⁻ and 4] Mtr⁻. Bottom: protein visualisation by Western blotting to anti-MtrB (residues 23-42) and anti-MtrC (residues 399-410) as indicated. Lanes: 1] molecular weight markers, 2] MR-1, 3] HydA⁻/HyaB⁻, 4] Mtr⁻ and 5] purified MtrCAB. Arrows indicate bands of interest. Theoretical masses of MtrA, MtrB and MtrC are 35, 85 and 75 kDa, respectively.⁸⁵

Taken together, the results presented above show that the Mtr⁻ strain can produce hydrogenases and not MtrCAB, the HydA⁻/HyaB⁻ strain can produce MtrCAB and not hydrogenases whilst MR-1 can produce both hydrogenases and MtrCAB, when cultured under acceptor-limited growth conditions. The findings confirm that the three strains can be assessed in parallel to determine the role of porin:cytochrome complexes in light-driven H₂-evolution. The assessment was performed by culturing MR-1, HydA⁻/HyaB⁻ and Mtr⁻ anaerobically for 24 hr then harvesting and re-suspending bacteria in 50 mM HEPES, 50 mM NaCl, pH 7. Samples (1.7 mL) were supplemented with 60 mM TEOA, 0.3 mM MV and 0.11 mM of either eosin Y or Ru(bpy)₃²⁺, transferred to the chamber of the H₂-sensing

electrode and then irradiated (0.7 kW m^{-2}) with the cold light source continuously for 30 min. The amounts of dissolved H_2 (normalised to total protein content) present in reaction suspensions at the end of the experiments are shown in **Table 4.5**. Similar trends were seen with both photosensitisers. Only negligible quantities of H_2 were produced with the $\text{HydA}^-/\text{HyaB}^-$ strain and approximately 3-fold or 3.5-fold more H_2 was produced with Mtr^- compared to MR-1 in experiments containing eosin Y or $\text{Ru}(\text{bpy})_3^{2+}$ as the photosensitiser, respectively. The differences between Mtr^- and MR-1 likely reflect the increased hydrogenase content of Mtr^- compared to MR-1 as shown by GC analysis (see **Fig. 4.21**) and spectrophotometric H_2 oxidation assays (see **Table 4.4**). The findings reveal that porin:cytochrome complexes are not required for light-driven H_2 -evolution, although it is possible that MtrCAB can contribute to electron transfer into the periplasm when present. Instead, the system is underpinned by the well-reported ability of MV to deliver electrons to bacterial enzymes.^{82,170} In particular, the results show the versatility of the approach to light-driven chemical synthesis as it may be possible to use MV to deliver photo-excited electrons to enzymes in bacteria lacking porin:cytochrome complexes.

Table 4.5 - Light-driven H_2 -evolution by MR-1, $\text{HydA}^-/\text{HyaB}^-$ and Mtr^- . Dissolved H_2 produced after 30 min continuous irradiation (0.7 kW m^{-2}) of the indicated strain with 0.11 mM eosin Y or $\text{Ru}(\text{bpy})_3^{2+}$. Mean values from 3 biological replicates with standard error (normalised to total protein). Anaerobic samples (1.7 mL) with 60 mM TEOA and 0.3 mM MV in 50 mM HEPES, 50 mM NaCl, pH 7 at room temperature. Irradiation provided by the cold light source.

Strain	Dissolved H_2 (nmol mg^{-1})	
	Eosin Y	$\text{Ru}(\text{bpy})_3^{2+}$
MR-1	584 ± 137	75 ± 18
$\text{HydA}^-/\text{HyaB}^-$	9 ± 9	10 ± 10
Mtr^-	1689 ± 182	271 ± 19

4.7 Discussion

The work presented in this chapter showed the development and assessment of a system for light-driven H_2 -evolution with MR-1. The results build upon those presented in chapter 3 where anaerobically grown MR-1 was exploited for reductive catalysis by combining the bacterium with DT and MV. Here, the requirement for DT as a chemical reductant was avoided by generating MV^+ with a SED and a photosensitiser under

irradiation by visible light. Photo-production of MV^+ was achieved with five water-compatible photosensitisers in the presence of TEOA as the optimal SED (see **Fig. 4.6** and **4.7**). Interestingly, the extent of light-driven MV^+ generation was not a simple reflection of the spectral properties of the photosensitisers. For example, eosin Y and proflavine gave similar performances despite the cold light source emitting more light around the λ_{max} of the former compared to the latter (see **Fig. 2.1** and **4.3**). Additionally, fluorescein was significantly less effective than eosin Y and proflavine despite all three photosensitisers having similar ϵ_{max} (see **Table 4.2**). Therefore, it is likely that light-driven electron transfer is also influenced by the (photo-)reduction potentials of the photosensitisers which affect the feasibility of reductive and oxidative quenching of the photo-excited state (see **Fig. 4.2**). A full mechanistic study was beyond the scope of this thesis but the relevant (photo-)reduction potentials of eosin Y, fluorescein, proflavine, $Ru(bpy)_3^{2+}$ and RuP have been reported previously for comparable systems (see **Table 4.1**).^{184,185,187,188,190–192} The presence of excess TEOA clearly increased the extent of MV^{2+} photoreduction with eosin Y, fluorescein and proflavine. This may be due to the fact that reduction of PS^+ (formed during oxidative quenching of the excited state, see **Fig. 4.1**) to regenerate PS^0 is facilitated by TEOA oxidation rather than MV^+ re-oxidation (i.e. non-productive electron transfer) or that reductive quenching is also possible with these photosensitisers. For the Ru(II)-dyes, assignment of a particular pathway is difficult because the rate of MV^{2+} photoreduction is slow in the presence and absence of TEOA, although both quenching mechanisms would generate reductants with $E_m \leq -0.84$ V for the $PS^{+/*}$ and $PS^{0/-}$ couples. Again, the effectiveness of each photosensitiser did not simply correlate with the predicted driving force meaning that additional factors such as the rate of electron exchange with TEOA (determined by the $PS^{+/0}$ and $PS^{*-/}$ couples) and/or the prevalence of futile side reactions are likely to be responsible for the relative extents of MV^{2+} photoreduction. Furthermore, the values quoted in **Table 4.1** and **4.3** may not reflect those for the system described here due to differences in the experimental conditions under which they were measured. Slight changes to the (photo-)reduction potentials of the photosensitisers and SEDs could significantly affect the likelihood of particular quenching mechanisms being in operation and may account for the fact that particular SEDs are more effective than others under the conditions described in this chapter (see **Fig. 4.7**).

After carrying out photoreduction of MV^{2+} in the presence of MR-1 which had been cultured under acceptor-limited conditions, H_2 production was quantified using a

H₂-sensing electrode and GC (see Fig. 4.9A and 4.17). The system is underpinned by the simultaneous presence of irradiation, TEOA, a photosensitiser, MV and MR-1 hydrogenases, and removal of any component significantly compromises the generation of H₂ (see Fig. 4.11 and Fig. 4.12). Additionally, it was confirmed that proton reduction is predominantly catalysed by hydrogenases associated with pelletable cellular material in the sample (see Fig. 4.18) and that electron transfer to these enzymes is not reliant on the presence of porin:cytochrome complexes (see section 4.6). Taken together, the results allow construction of a general schematic for light-driven H₂-evolution with MR-1, as shown in Fig. 4.23. Photoreduction of MV²⁺ may take place extracellularly and/or in the periplasm with the possibility of electron transfer proceeding via CymA for redox cycling of MK and MKH₂. The scheme also highlights decomposition of TEOA⁺ (see Fig. 4.16) as well as re-oxidation of H₂ which can occur at high cell densities in the absence of high intensity irradiation (see Fig. 4.11).

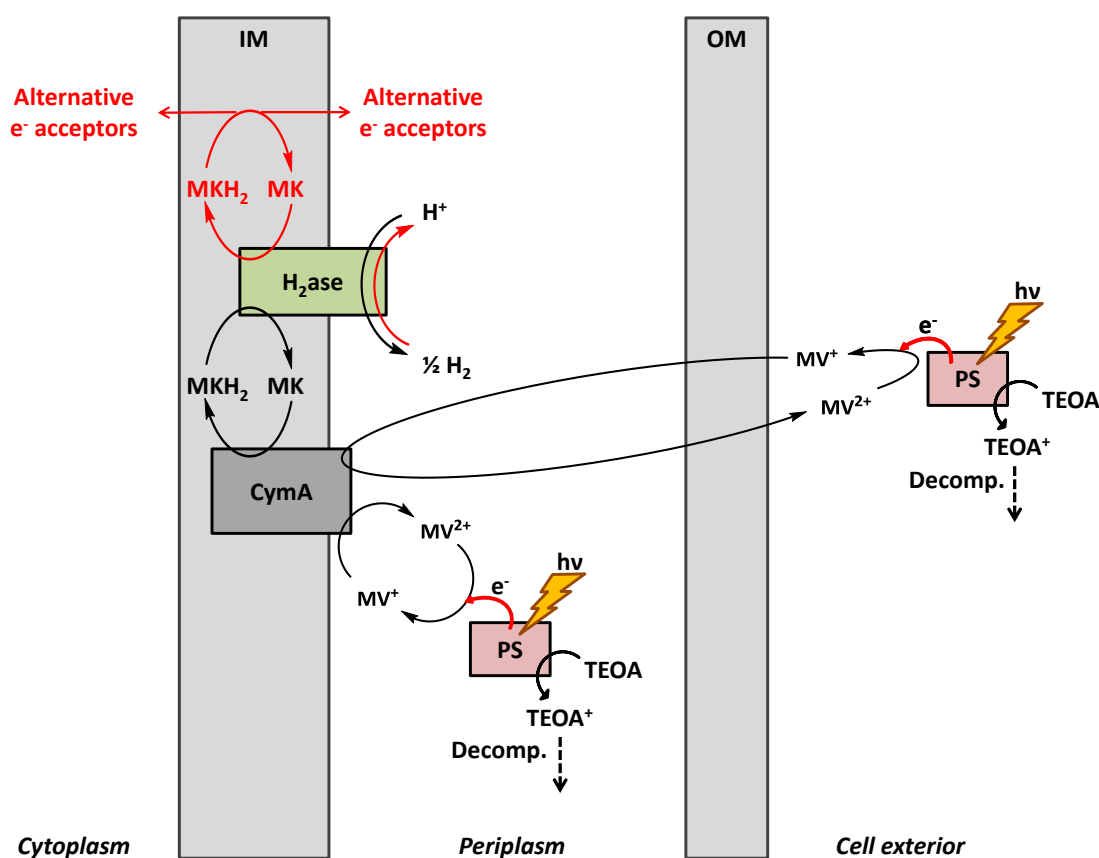


Fig. 4.23 - General schematic for light-driven H₂-evolution with MR-1. Photon (hv) absorption by a photosensitiser in the presence of TEOA leads to the reduction of MV²⁺ to MV⁺ which can subsequently transfer electrons to MR-1 hydrogenases for proton reduction. IM = inner membrane, OM = outer membrane, H₂ase = hydrogenase, MK = menaquinone, MKH₂ = menaquinol, MV = methyl viologen, TEOA = triethanolamine.

For the majority of work in this chapter, reaction suspensions for light-driven H₂-evolution contained 187 nmol photosensitiser meaning that a single turnover (i.e. photo-excitation followed by reductive or oxidative quenching to regenerate PS⁰) of the entire system would generate 187 nmol photo-excited electrons and 93.5 nmol H₂ (if all photo-excited electrons were delivered to the hydrogenases for proton reduction). As such, turnover numbers (TONs) with respect to the amount of photosensitiser can be estimated for experiments by dividing the amount of H₂ produced after a period of continuous irradiation by 93.5. Over 30 min irradiation with the cold light source (see **Fig. 4.11**, 100 % values), the TONs were approximately 2.6 and 0.4 with eosin Y and Ru(bpy)₃²⁺, respectively, showing that the system is not catalytic with respect to Ru(bpy)₃²⁺ under these conditions. For irradiation with the photosynthetic growth lamp (see **Fig. 4.17**), the TONs were approximately 11.7 with eosin Y (after 18 hr) and 4.7 with Ru(bpy)₃²⁺ (after 96 hr), showing that both systems are catalytic. Importantly, it should be noted that the TONs above are lower limits with respect to the generation of photo-excited electrons by the photosensitisers because there is an accumulation of MV⁺ under irradiation (see **Fig. 4.10**) and it is likely that electrons are transferred to alternative bacterial electron acceptors. This is corroborated by the fact that quantum yields for MV²⁺ photoreduction were 4-fold and 2-fold higher than those for light-driven H₂-evolution with eosin Y and Ru(bpy)₃²⁺, respectively (see sections 4.3 and 4.5), suggesting that electron transfer from the photosensitiser to MV²⁺ is more efficient than electron transfer from MV⁺ to the hydrogenases. However, it must be noted that the quantum yields for photoreduction of MV²⁺ by eosin Y and Ru(bpy)₃²⁺ are significantly lower than values reported previously under comparable experimental conditions: 30 and 19 % for eosin Y and Ru(bpy)₃²⁺, respectively, in the presence of TEOA.^{198,200} This shows that the efficiency of the system described in this chapter is not optimised and is most likely limited by processes involving photo-production of MV⁺ by the photosensitisers (e.g. light-harvesting, productive electron exchange with MV²⁺ and/or TEOA). This is also supported by the results presented in sections 4.4.3 and 4.5 which suggest the rate-defining events are photosensitiser-dependent rather than hydrogenase-dependent.

Comparable systems with whole-cell bacteria and purified enzymes have been reported previously and provide a benchmark for the work in this chapter.^{82,218} For example, Honda et al. (2016) (see **Table 1.5**, example A) reported the generation of 117 μmol H₂ using *E. coli* (containing recombinant [FeFe]-hydrogenase), ascorbate as SED, titanium

dioxide as photosensitiser and MV as electron transfer mediator with 5 hr irradiation by UV light.⁸² This corresponded to a quantum yield of 0.3 %. Although significantly more H₂ was produced by the system in Honda et al. (2016) compared to the one reported in this chapter, the quantum yields for both systems are very similar. Additionally, the approach used here has the advantage of functioning under irradiation by visible light and the potential to operate over 96 hr with a suitable photosensitiser due to the robustness of MR-1 hydrogenases (see **Fig. 4.17** and **4.18**). In Sakai et al. (2013), 5 μmol H₂ was produced after 24 hr irradiation by visible light using purified *Desulfomicrobium baculatum* [NiFeSe]-hydrogenase in the presence of TEOA as SED and eosin Y as photosensitiser.²¹⁸ This corresponded to a quantum yield of 1.5 % at low light intensity (0.015 kW m⁻²). Again, greater quantities of H₂ were generated by the system in Sakai et al. (2013) compared to the work in this chapter but the quantum yields for both systems are similar. Notably, the system in Sakai et al. (2013) did not require MV for effective electron transfer from eosin Y to the purified hydrogenase. This highlights the added complexity of cell-based approaches to light-driven chemical synthesis where there is competition between various metabolic pathways and bacterial electron acceptors. As shown in this chapter, the use of MV as electron shuttle overcomes this challenge but there is a corresponding loss of bacterial viability due to the toxicity of the reagent (see section 4.4.4). However, the result most likely reflects the fact that light-driven electron transfer is not directly linked to natural bacterial metabolism and no substrates for cell maintenance or growth were included in reaction suspensions. Indeed, if MR-1 was incubated with TEOA, MV and a photosensitiser in M72 growth medium, the samples contained ≈5 x 10⁶ CFU mL⁻¹ after 30 min incubation in the dark (i.e. considerably more than for equivalent experiments performed in buffer only). This shows that it is possible to reduce the toxicity of the light-harvesting reagents, although it is likely that this would also affect the yields of photo-produced H₂ due to changes in light absorption and/or quenching of the photo-excited state.

The loss of bacterial viability in the presence of the light-harvesting reagents means that the current system is unlikely to be self-regenerating over extended periods of time. However, despite samples predominantly containing non-viable bacteria, light-driven H₂ production could still be performed over 96 hr with Ru(bpy)₃²⁺ as photosensitiser and the use of MV renders the system highly versatile because it is likely that photo-energised electrons can be transferred to enzymes associated with micro-organisms

that cannot produce porin:cytochrome complexes. Another major advantage of the system developed in this thesis is the potential to drive multiple chemical transformations using a single bacterium, as shown by the work in chapter 3 which confirmed that acceptor-limited growth leads to the simultaneous presence of active hydrogenases, fumarate reductase, lactate dehydrogenases and formate dehydrogenases. As such, it was of interest to assess whether the approach to light-driven H₂-evolution described in this chapter could also be used for the photoreduction of fumarate, pyruvate and CO₂ to succinate, lactate and formate, respectively. In the next chapter, results are shown from experiments that evaluated how light-driven H₂-evolution is affected by the presence of carbon substrates and from ¹H-NMR analysis that quantified the extents of the desired reductive transformations.

CHAPTER 5

Light-driven reduction of
fumarate, pyruvate and CO₂
by *Shewanella oneidensis* MR-1

Chapter 5 - Light-driven reduction of fumarate, pyruvate and CO₂ by *Shewanella oneidensis* MR-1

5.1 Introduction

In chapter 4, light-driven H₂-evolution was achieved by carrying out the photoreduction of MV²⁺ in the presence of MR-1 which had been cultured under anaerobic, acceptor-limited conditions for production of active hydrogenases. From the work in chapter 3, it is known that the growth conditions also lead to the production of active fumarate reductase, lactate dehydrogenases and formate dehydrogenases by MR-1. As such, it was of interest to extend the use of the light-driven system for the reduction of fumarate, pyruvate and CO₂ by inclusion of the chosen carbon substrate in reaction suspensions. Eosin Y was selected as photosensitiser for the experiments due to its superior rates of MV²⁺ photoreduction compared to Ru(bpy)₃²⁺. First, results from the assessment of light-driven H₂-evolution in the presence of fumarate, pyruvate or CO₂ are shown to evaluate how MR-1 enzymes compete for electrons provided to the bacterium by photo-produced MV⁺. Next, data are presented from ¹H-NMR analysis that was used to quantify the formation of succinate, lactate and formate. Lastly, results are shown from experiments that aimed to improve light-driven CO₂-reduction and assess the longevity of the periplasmic fumarate reductase. The work presented below demonstrates the advantages of using MV to achieve cell-based photocatalysis then describes how MR-1 could be used to overcome the drawbacks of the approach by exploiting porin:cytochrome complexes to transfer electrons from the outside to the inside of the bacterium. Preliminary results for the development of such a system that operates in the absence of MV are shown in the next chapter.

5.2 Effect of fumarate, pyruvate and CO₂ on light-driven H₂-evolution by *Shewanella oneidensis* MR-1 from photo-produced MV⁺

Based on the results shown in section 3.3.2, it was predicted that the presence of fumarate, pyruvate and CO₂ would decrease the yields of photo-produced H₂ due to competition

between MR-1 enzymes for electrons provided to the bacterium by MV^+ . Furthermore, it was predicted that the relative decreases in H_2 production with each carbon substrate would correlate with the relative yields of succinate, lactate and formate. To test this, MR-1 was cultured under acceptor-limited conditions for 24 hr then harvested and re-suspended in anaerobic 50 mM HEPES, 50 mM NaCl, pH 7 (see sections 2.3.3 and 2.3.7). From the work in chapter 3, processing the bacterium as described above leads to the simultaneous presence of hydrogenases, fumarate reductase, lactate dehydrogenases and formate dehydrogenases which can all be exploited for reductive catalysis. Bacterial suspensions (1.7 mL, MR-1 $OD_{590nm} \approx 0.25$) were supplemented with 0.11 mM eosin Y, 60 mM TEOA, 0.3 mM MV and 1.5 or 3 mM fumarate, pyruvate or CO_2 then transferred to the chamber of a H_2 -sensing electrode which was sealed with minimal gaseous headspace above samples. Reaction suspensions were then irradiated for 30 min with the cold light source at an intensity of 0.7 kW m^{-2} (see sections 2.2 and 2.4.2). The H_2 -sensing electrode was used to quantify H_2 -evolution because formation of the product can be monitored in real-time and the initial concentrations of carbon substrates were chosen to best demonstrate the different trends over 30 min. Results from the experiments are shown in **Fig. 5.1**.

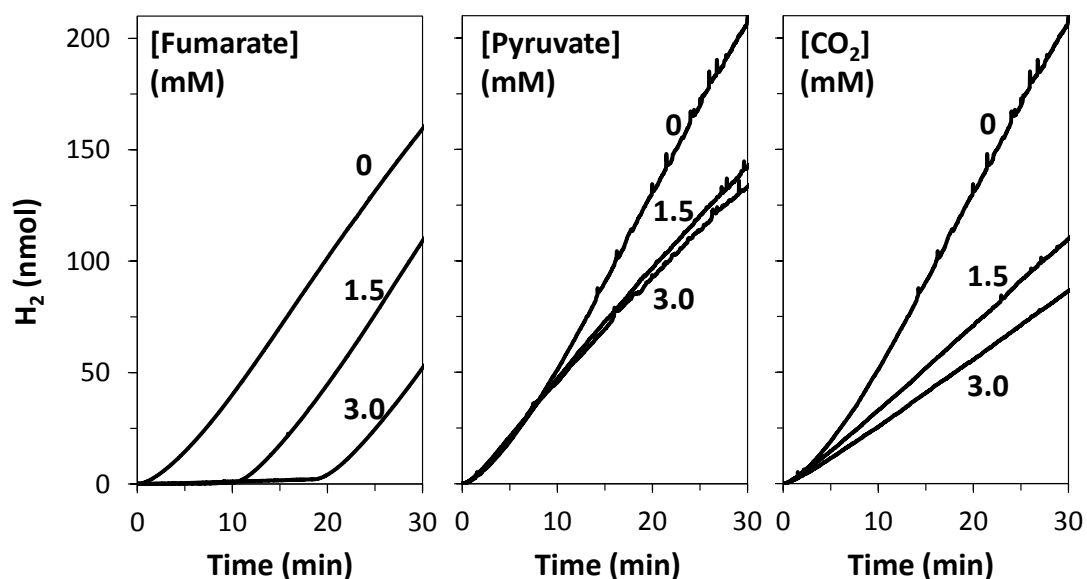


Figure 5.1 - Light-driven H_2 -evolution by MR-1 in the presence of fumarate, pyruvate or CO_2 . Dissolved H_2 in MR-1 suspensions ($OD_{590nm} \approx 0.25$) with 0.11 mM eosin Y, 60 mM TEOA, 0.3 mM MV and the indicated concentration of fumarate (left), pyruvate (middle) or CO_2 (right). Irradiation (0.7 kW m^{-2}) provided by the cold light source throughout. Anaerobic samples (1.7 mL) in 50 mM HEPES, 50 mM NaCl, pH 7 at room temperature.

In the presence of fumarate, light-driven H_2 -evolution was completely suppressed during the first part of the experiment. After approximately 10 or 20 min with an initial

concentration of 1.5 or 3 mM fumarate, respectively, production of H₂ then resumed at an identical rate to that seen in the absence of fumarate. This suggests that MR-1 hydrogenase activity does not change significantly over the course of the experiment. Assuming that fumarate was completely consumed before H₂-evolution took place, the rate of consumption was approximately 255 nmol fumarate min⁻¹. On the other hand, the rate of H₂-evolution in the absence of fumarate was approximately 5 nmol H₂ min⁻¹. The difference between the apparent rates most likely reflects the high abundance of the fumarate reductase and the more accessible redox cofactors compared to the hydrogenases, as discussed in section 3.4.^{91,106,176,177} When pyruvate or CO₂ were included in reaction suspensions, there were less substantial decreases in light-driven H₂ production compared to those seen in the presence of fumarate. However, increasing the concentration of CO₂ from 1.5 to 3 mM gave a further decrease in H₂ production whereas increasing the concentration of pyruvate in this way had little effect on the system. In general, the results are in agreement with those seen for comparable experiments with DT as the electron source where pyruvate and CO₂ were less effective than fumarate at re-directing electrons away from the hydrogenases (see **Fig. 3.5** and **Table 3.2**).

To standardise the analysis, light-driven H₂ production with MR-1 was carried out in the presence of 10 mM fumarate, pyruvate or CO₂ and irradiation was provided by either the cold light source (0.7 kW m⁻² light intensity, 30 min, room temperature) or the photosynthetic growth lamp (0.02 kW m⁻² light intensity, 24 hr, 25 °C) to compare the distinct irradiation regimes used in chapter 4. Reaction suspensions were prepared as described above. Dissolved H₂ was quantified with the H₂-sensing electrode and headspace H₂ was quantified with GC (see section 2.4.1) for experiments performed over 30 min and 24 hr, respectively. Representative data collected with the H₂-sensing electrode are presented in **Fig. 5.2** and mean values for dissolved and headspace H₂ are presented in **Table 5.1**. The pH of samples containing the light-harvesting reagents and 10 mM fumarate, pyruvate or CO₂ was also measured after 24 hr to confirm there were no changes which may impact the results. There were negligible pH changes in the presence of fumarate or pyruvate and an increase of 0.2 pH units in the presence of CO₂ after 24 hr showing the reagents do not significantly compromise the buffering capacity of the solution. To summarise, the results in **Fig. 5.2** reflect the trends shown in **Fig. 5.1** and the relative differences in H₂ production in **Table 5.1** correlate with those seen for DT-driven reactions (see **Table 3.2**).

Overall, the findings in this section show that there is competition between bacterial enzymes during light-driven experiments performed in the presence of exogenous carbon substrates. Additionally, the results suggest that the reduction of fumarate, pyruvate and CO_2 by MR-1 can be driven using photo-produced MV^+ and that the reduction of fumarate proceeds to a greater extent than the reduction of pyruvate and CO_2 . In the next section, data are presented from $^1\text{H-NMR}$ analysis that quantified the generation of succinate, lactate and formate by the system described above.

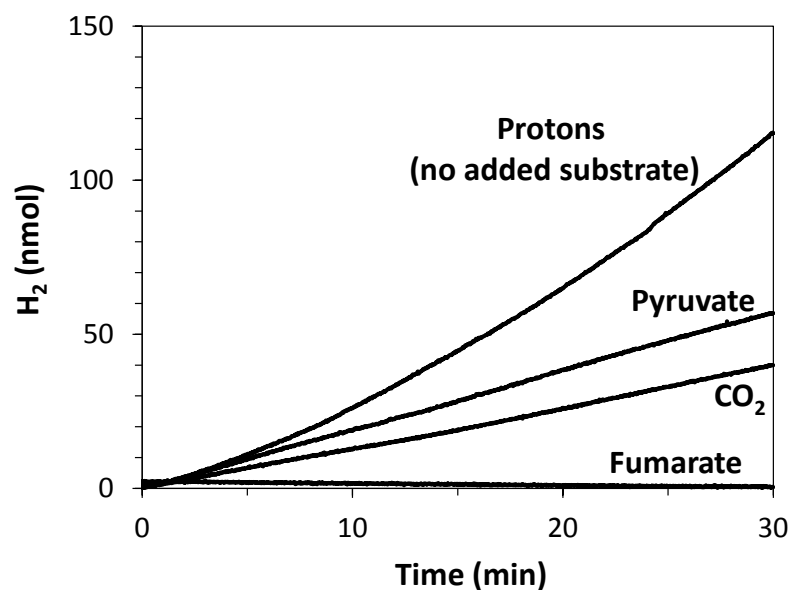


Figure 5.2 - Light-driven H_2 -evolution by MR-1 in the presence of 10 mM fumarate, pyruvate or CO_2 . Representative data for dissolved H_2 in MR-1 suspensions ($\text{OD}_{590\text{nm}} \approx 0.25$) with 0.11 mM eosin Y, 60 mM TEOA and 0.3 mM MV. Irradiation (0.7 kW m^{-2}) provided by the cold light source throughout. Anaerobic samples (1.7 mL) in 50 mM HEPES, 50 mM NaCl, pH 7 at room temperature.

Table 5.1 - Light-driven H_2 -evolution by MR-1 in the presence of 10 mM fumarate, pyruvate or CO_2 . Dissolved or headspace H_2 for samples incubated with 0.11 mM eosin Y, 60 mM TEOA and 0.3 mM MV. Assays performed with MR-1 ($\text{OD}_{590\text{nm}} \approx 0.25$) and either 30 min irradiation (0.7 kW m^{-2} , room temperature) by the cold light source or 24 hr irradiation (0.02 kW m^{-2} , 25°C) by the photosynthetic growth lamp. Mean values from technical duplicates, error indicates maximum and minimum. Anaerobic samples (1.7 mL) in 50 mM HEPES, 50 mM NaCl, pH 7.

Added substrate	Dissolved H_2 after 30 min (nmol)	Headspace H_2 after 24 hr (nmol)
None	121 ± 6	812 ± 62
Fumarate	0	180 ± 10
Pyruvate	56 ± 2	566 ± 8
CO_2	48 ± 8	582 ± 7

5.3 Light-driven reduction of fumarate, pyruvate and CO₂ by *Shewanella oneidensis* MR-1 from photo-produced MV⁺

To quantify the photoreduction of carbon substrates, MR-1 was cultured under acceptor-limited conditions for 24 hr then harvested and re-suspended in anaerobic 50 mM HEPES, 50 mM NaCl, pH 7. Bacterial suspensions (1 mL, MR-1 OD_{590nm} ≈0.25) were supplemented with 0.08 mM eosin Y, 50 mM TEOA, 0.5 mM MV and fumarate, pyruvate or CO₂ (initial concentrations between 8.1 and 11.7 mM, see below) then transferred to clear glass vials (4 mL gaseous headspace, initially 100 % N₂) which were tightly sealed within the N₂-filled chamber. Irradiation was provided by the cold light source (0.7 kW m⁻² light intensity, 30 min, room temperature) or the photosynthetic growth lamp (0.02 kW m⁻² light intensity, 24 hr, 25 °C). Parallel control experiments were performed with no added carbon substrate, no irradiation and/or no bacteria. After incubation for the required time period, samples containing MR-1 were centrifuged to remove cellular material and supernatants were analysed by ¹H-NMR to determine their composition (see section 2.6).

Representative ¹H-NMR spectra for the light-driven reduction of fumarate, pyruvate and CO₂ are shown in **Fig. 5.3**. The peaks for TSP, MV,¹⁷² residual H₂O¹⁷³ and the carbon-based compounds (see section 2.6 and **Table 2.4**) match the positions of those seen in **Fig. 3.6** for equivalent reactions driven by DT as electron source. The broad series of peaks between 2.8 and 4.0 ppm in **Fig. 5.3A** corresponds to buffer components including HEPES,¹⁷⁴ TEOA, trace metabolites produced by MR-1 (Human Metabolome Database, <http://www.hmdb.ca/>) and other small molecules resulting from the degradation of light-harvesting reagents (see section 4.4.4).^{49,227} The predicted peaks for eosin Y between 7 and 8 ppm²²⁹ were not observed, presumably due to an insufficiently high concentration of the reagent in samples. Quantification of carbon-based compounds was performed as described in section 3.3.2. Supernatant compositions are shown in **Table 5.2** for 30 min incubations and in **Table 5.3** for 24 hr incubations. The next sections describe and compare results with the different irradiation sources then introduce experiments which aimed to improve light-driven CO₂-reduction and assess the longevity of the fumarate reductase.

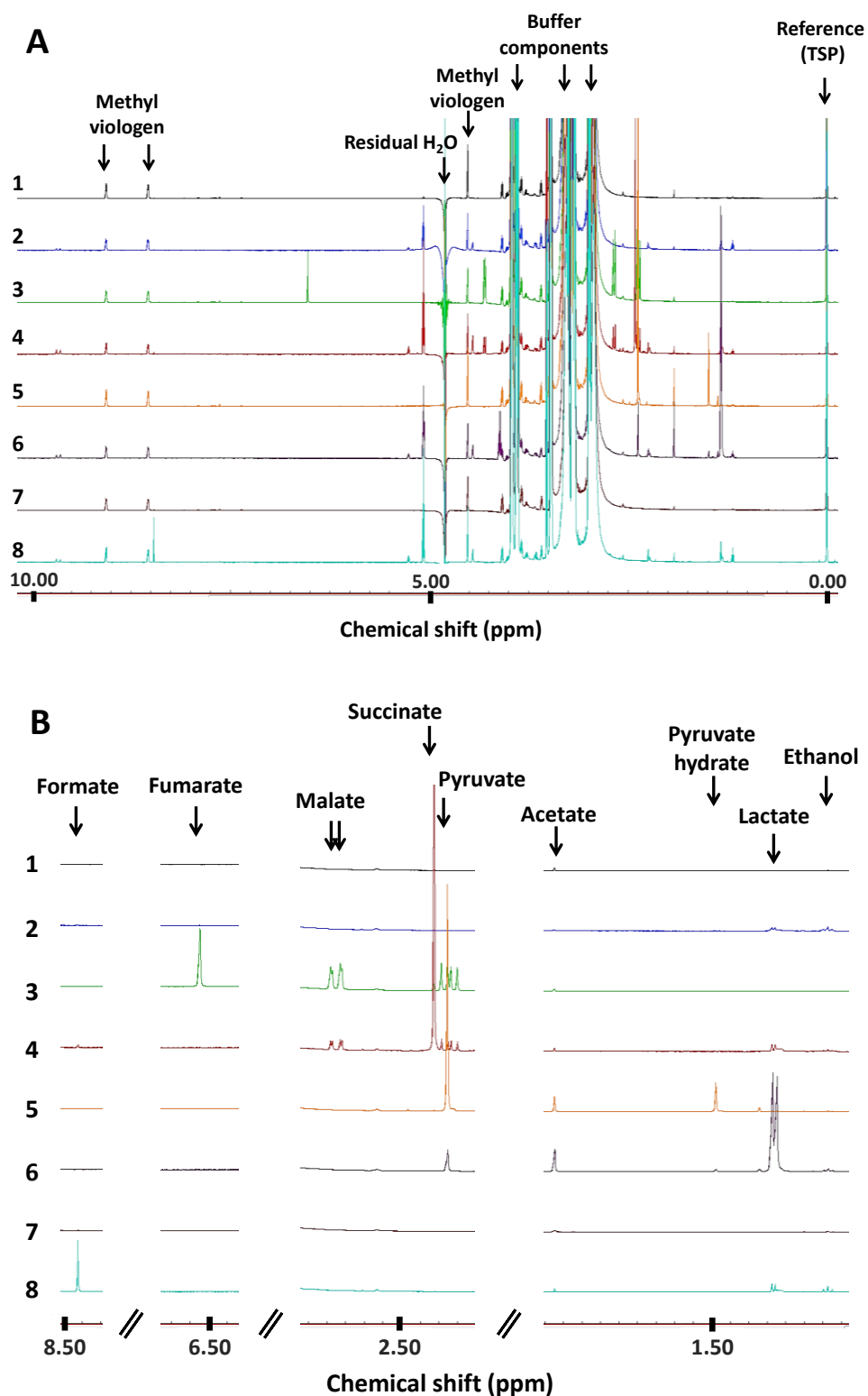


Figure 5.3 - Representative ^1H -NMR spectra for light-driven reduction of fumarate, pyruvate and CO_2 by MR-1. A) Full spectra showing peak positions of buffer components and sodium 3-(trimethylsilyl)-propionate- d_4 (TSP) reference. B) Expanded view of spectra highlighting peaks used to quantify carbon-based compounds (see section 2.6). Numerical label for each spectrum refers to a set of conditions described in **Table 5.3**.

Table 5.2 - Light-driven reduction of fumarate, pyruvate and CO₂ by MR-1 over 30 min irradiation with the cold light source at an intensity of 0.7 kW m⁻². ¹H-NMR derived quantification of the named compounds in supernatants recovered from samples (1 mL) incubated for 30 min with fumarate, pyruvate or CO₂ as indicated and 0.08 mM eosin Y, 0.5 mM MV and 50 mM TEOA. Assays performed with or without MR-1 (OD_{590nm} ≈ 0.25) in the dark or irradiated (0.7 kW m⁻²). Mean values from technical duplicates, error indicates maximum and minimum. Anaerobic samples in 50 mM HEPES, 50 mM NaCl, pH 7 at room temperature. Samples had 4 mL headspace (initially 100% N₂). nd = not detected; pyruvate is reported as the sum of pyruvate and pyruvate hydrate.

Added substrate	MR-1	Light	Supernatant component (nmol)									
			Fumarate	Succinate	Malate	Pyruvate	Lactate	Formate	Acetate	Ethanol		
None	No	Yes	nd	nd	nd	nd	nd	18 ± 1	8 ± 2	24		
	Yes	No	nd	8 ± 1	nd	nd	14 ± 1	9 ± 1	34 ± 2	28 ± 7		
	Yes	Yes	nd	7	nd	nd	27 ± 1	12 ± 5	21 ± 3	71 ± 3		
Fumarate	No	Yes	9466 ± 187	nd	nd	nd	nd	22 ± 1	7	22 ± 1		
	Yes	No	5868 ± 34	48 ± 1	4917 ± 103	528 ± 6	12 ± 2	nd	33 ± 1	22 ± 1		
	Yes	Yes	2229 ± 55	4337 ± 812	4249 ± 78	455 ± 5	nd	37 ± 5	34 ± 1	25 ± 2		
Pyruvate	No	Yes	nd	nd	nd	8057 ± 192	nd	7 ± 1	358 ± 4	25 ± 2		
	Yes	No	nd	7	nd	7936 ± 24	21 ± 3	nd	151 ± 4	26 ± 4		
	Yes	Yes	nd	nd	nd	7379 ± 208	594 ± 48	3 ± 3	214 ± 15	68 ± 2		
CO ₂	No	Yes	nd	nd	nd	nd	nd	20 ± 1	8 ± 1	22 ± 1		
	Yes	No	nd	7 ± 1	nd	nd	10 ± 1	12 ± 1	32 ± 1	24 ± 2		
	Yes	Yes	nd	7	nd	nd	26 ± 2	113 ± 23	20 ± 1	49 ± 3		

Table 5.3 - Light-driven reduction of fumarate, pyruvate and CO₂ by MR-1 over 24 hr irradiation with the photosynthetic growth lamp at an intensity of 0.02 kW m⁻². ¹H-NMR derived quantification of the named compounds in supernatants recovered from samples (1 mL) incubated for 24 hr with fumarate, pyruvate or CO₂ as indicated and 0.08 mM eosin Y, 0.5 mM MV and 50 mM TEOA. Assays performed with or without MR-1 (OD_{590nm} ≈0.25) in the dark or irradiated (0.02 kW m⁻²). Mean values from technical duplicates, error indicates maximum and minimum. Anaerobic samples in 50 mM HEPES, 50 mM NaCl, pH 7 at 25 °C. Samples had 4 mL headspace (initially 100 % N₂). nd = not detected; pyruvate is reported as the sum of pyruvate and pyruvate hydrate.

NMR spectra ref.	Added substrate	MR-1	Light	Supernatant component (nmol)							
				Fumarate	Succinate	Malate	Pyruvate	Lactate	Formate	Acetate	Ethanol
		No	Yes	nd	nd	nd	nd	nd	159 ± 6	52 ± 3	41 ± 3
1	None	Yes	No	nd	8 ± 4	nd	nd	nd	25 ± 1	92 ± 7	37 ± 7
2		Yes	Yes	nd	6 ± 1	nd	nd	nd	55 ± 3	80 ± 8	733 ± 15
		No	Yes	11727 ± 273	nd	nd	nd	nd	231 ± 12	37 ± 4	26 ± 6
3	Fumarate	Yes	No	2607 ± 1041	161 ± 1	11363 ± 1818	nd	nd	14 ± 14	80 ± 10	38 ± 10
4		Yes	Yes	nd	8289 ± 194	3451 ± 31	nd	nd	142 ± 17	88 ± 2	125 ± 19
		No	Yes	nd	nd	nd	9774 ± 1755	nd	71 ± 10	2439 ± 558	37 ± 9
5	Pyruvate	Yes	No	nd	8 ± 8	nd	11565 ± 1672	nd	nd	496 ± 54	47 ± 7
6		Yes	Yes	nd	8 ± 8	nd	1382 ± 757	9136 ± 3909	59 ± 17	1600 ± 866	292 ± 5
		No	Yes	nd	nd	nd	nd	nd	177 ± 26	57	34 ± 9
7	CO ₂	Yes	No	nd	3 ± 3	nd	nd	nd	30 ± 6	79 ± 9	44 ± 10
8		Yes	Yes	nd	5 ± 2	nd	nd	nd	1561 ± 194	88 ± 8	325 ± 11

5.3.1 Irradiation at an intensity of 0.7 kW m^{-2} for 30 min

The key results from experiments performed over 30 min (see **Table 5.2**) are presented in **Fig. 5.4A** to compare the extents of each reductive transformation. With no added fumarate, pyruvate or CO_2 , the supernatants analysed after 30 min contained negligible amounts of carbon-based compounds regardless of the presence of MR-1 or irradiation. This confirms that the light-harvesting reagents and their predicted (photo-)degradation products (see section 4.4.4) do not contribute to signals used for quantification of the compounds of interest. When MR-1 was incubated with fumarate (≈ 9466 nmol initially) and irradiated for 30 min, the supernatants contained ≈ 4337 nmol succinate (46 % yield) and ≈ 4249 nmol malate (45 % yield) at the end of the experiment. In the absence of MR-1, the transformation of fumarate did not occur whereas hydrolysis of fumarate to malate took place to a similar extent (52 % yield) in the presence of MR-1 in the dark. Formation of malate was also observed for DT-driven reactions (see **Table 3.3**) and is likely a result of fumarate hydration which can be catalysed by the cytoplasmic fumarate hydratase.^{102,175} When MR-1 was incubated with pyruvate (≈ 8057 nmol initially) under irradiation there was ≈ 594 nmol lactate (7 % yield) present after 30 min. Negligible quantities of lactate were produced when MR-1 or irradiation were omitted from parallel assays. Lastly, incubation of MR-1 with CO_2 (≈ 10000 nmol initially) under irradiation gave ≈ 113 nmol formate (1 % yield) after 30 min. This is 5-fold more than the quantities detected in parallel experiments performed in the absence of MR-1 or irradiation. In all cases, MR-1 and irradiation were required for formation of the desired compounds and the distribution of products corresponded to the presence of a particular carbon substrate. Complete consumption of the starting carbon substrate was not seen during any of the experiments, presumably due to the relatively short irradiation time. Interestingly, the yields of lactate and formate were considerably different despite the presence of pyruvate and CO_2 causing similar decreases to light-driven H_2 production (see section 5.2).

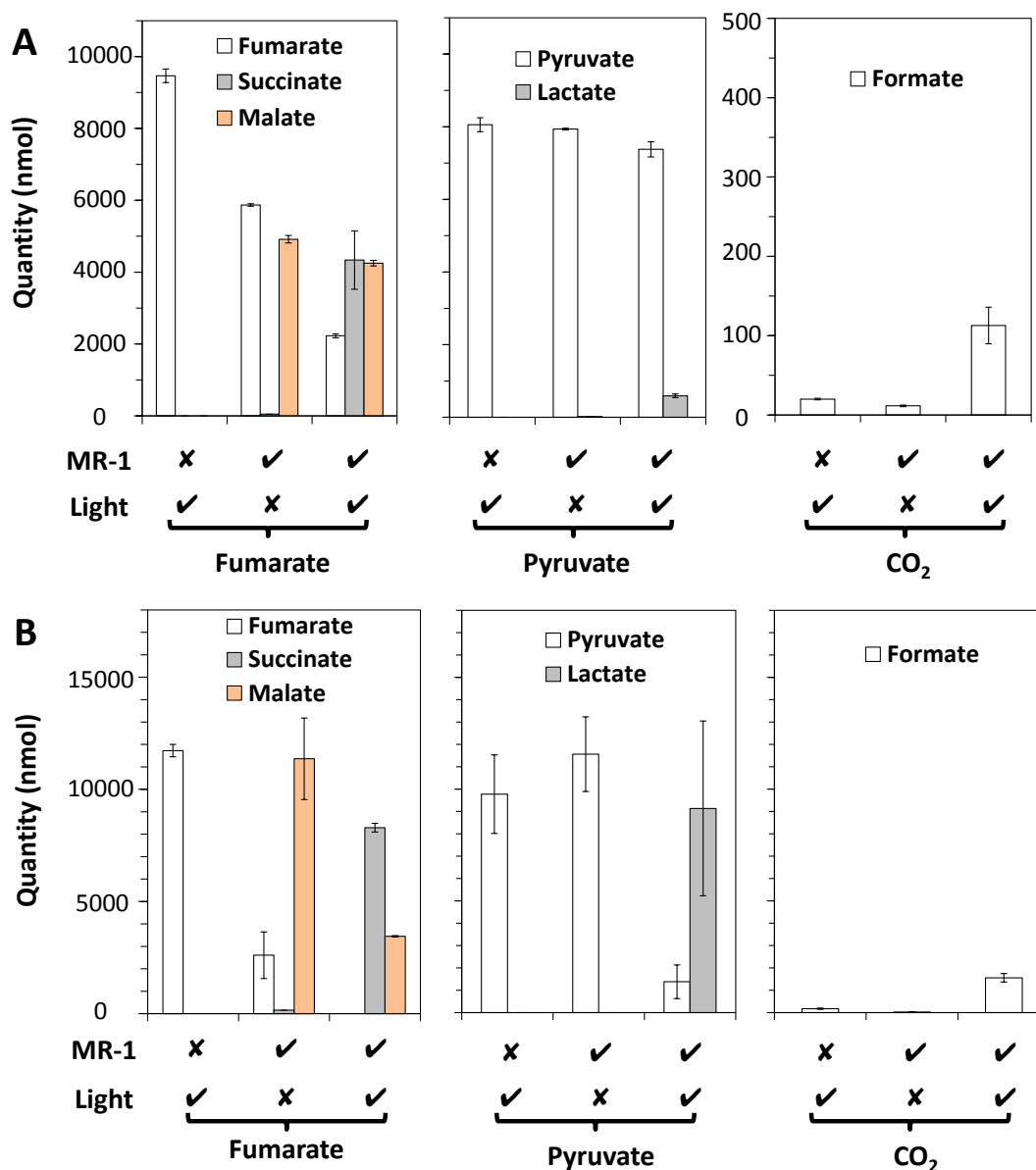


Figure 5.4 - Light-driven reduction of fumarate, pyruvate and CO₂ by MR-1. A) Composition of supernatants recovered from samples incubated for 30 min with 0.08 mM eosin Y, 0.5 mM MV, 50 mM TEOA and fumarate (left), pyruvate (middle) or CO₂ (right). Assays performed with or without MR-1 ($OD_{590nm} \approx 0.25$) in the dark or irradiated (0.7 kW m^{-2}) by the cold light source. B) As for A) but with 24 hr incubations and irradiation provided by the photosynthetic growth lamp at an intensity of 0.02 kW m^{-2} as required. Mean values from technical duplicates, error bars indicate maximum and minimum. Anaerobic samples (1 mL) in 50 mM HEPES, 50 mM NaCl, pH 7 at room temperature.

5.3.2 Irradiation at an intensity of 0.02 kW m^{-2} for 24 hr

The key results from experiments performed over 24 hr (see **Table 5.3**) are presented in **Fig. 5.4B** to compare the extents of each reductive transformation. With no added carbon substrate, there were negligible quantities of carbon-based compounds in supernatants

after 24 hr, similar to the control experiments described in section 5.3.1. The only difference was a slight enrichment of ethanol in samples which contained MR-1 under 24 hr irradiation. This may be due to increased formation of ethanol through decomposition of TEOA over extended periods of irradiation. When MR-1 was incubated with fumarate (≈ 11727 nmol initially) under irradiation, supernatants contained ≈ 8289 nmol succinate (71 % yield) and ≈ 3451 nmol malate (29 % yield) after 24 hr with no remaining fumarate. Succinate and malate were not detected in parallel experiments with no bacteria but malate (97 % yield) was still produced in samples containing MR-1 in the dark. Incubation of MR-1 with pyruvate (≈ 9774 nmol initially) under irradiation led to the production of ≈ 9136 nmol lactate (93 % yield) after 24 hr. Reduction of pyruvate to lactate did not occur in parallel assays that omitted MR-1 or irradiation. Compared to the equivalent experiments containing pyruvate described in the previous section, the only difference was an enrichment of acetate in supernatants analysed after 24 hr. This may be due to increased oxidation of pyruvate to acetate via the phosphotransacetylase-acetate kinase pathway (see **Fig. 1.11**) and/or formation of acetate through (photo-)degradation of light-harvesting reagents over longer periods of time. Lastly, irradiation of samples containing MR-1 and CO_2 (≈ 10000 nmol initially) produced ≈ 1561 nmol formate (16 % yield) after 24 hr. This is 8-fold more than the quantities produced in parallel assays omitting MR-1 or irradiation. To confirm that the presence of formate did not result from the release of intracellular metabolite reserves by MR-1, the CO_2 -reduction experiments were repeated identically but with ^{13}C -carbonate used as a source of $^{13}\text{CO}_2$ (≈ 10000 nmol initially), making it possible to track the fate of this species using ^{13}C -NMR analysis (see section 2.6). Results from the assays are shown in **Fig. 5.5**. There was no evidence for the presence of ^{13}C -formate after 24 hr when samples containing MR-1 were incubated in the dark whereas 1790 ± 230 nmol ^{13}C -formate (18 % yield) was produced in parallel assays under 24 hr irradiation (0.02 kW m^{-2}) by the photosynthetic growth lamp. The results show that CO_2 is directly reduced to formate by MR-1 in the system described in this chapter. To summarise, the desired transformations only took place in the presence of MR-1 under irradiation and the distribution of products was well-defined with respect to the initial carbon substrate, as was seen for experiments performed over 30 min.

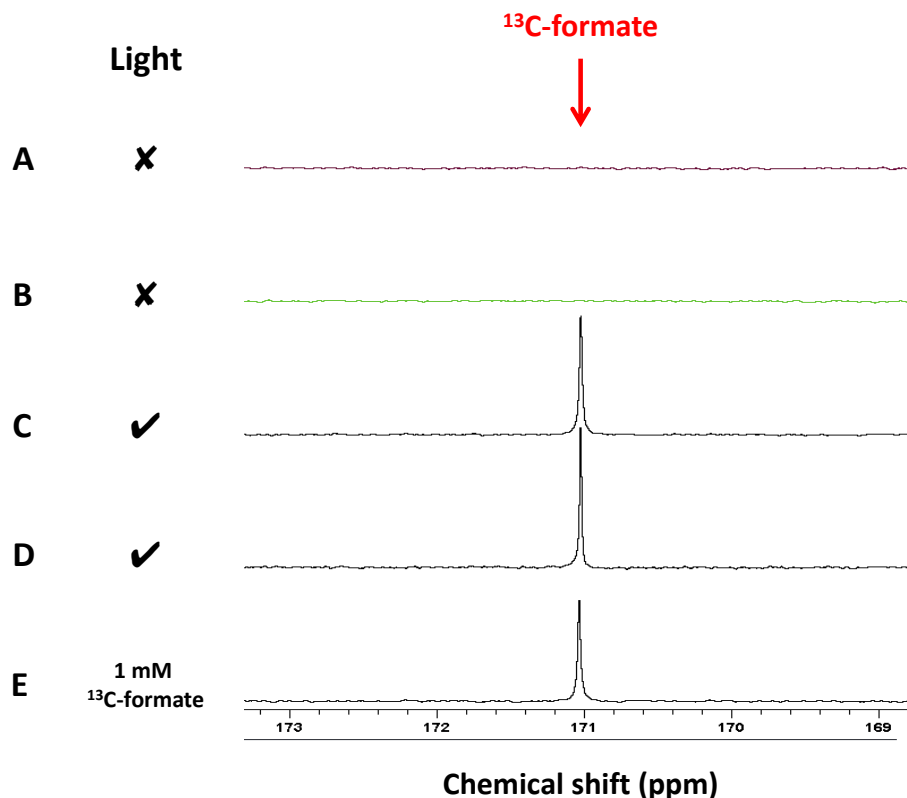


Figure 5.5 - Light-driven reduction of $^{13}\text{C}\text{O}_2$ by MR-1 over 24 hr irradiation. ^{13}C -NMR spectra for supernatants recovered from samples incubated for 24 hr with 0.08 mM eosin Y, 0.5 mM MV, 50 mM TEOA and 10 mM $^{13}\text{C}\text{O}_2$. Assays performed with MR-1 ($\text{OD}_{590\text{nm}} \approx 0.25$) in the dark (A and B) or irradiated (C and D). Anaerobic samples (1 mL) in 50 mM HEPES, 50 mM NaCl, pH 7 at 25 °C. Irradiation (0.02 kW m^{-2}) provided by the photosynthetic growth lamp. Peak for 1 mM ^{13}C -formate in 50 mM HEPES, 50 mM NaCl, pH 7 (E) is shown for comparison.

Overall, the results in section 5.3 confirm that MR-1 can be used to drive the reduction of fumarate, pyruvate and CO_2 to succinate, lactate and formate, respectively, from photo-produced MV^+ . Succinate was produced in high yield for experiments performed with 30 min or 24 hr irradiation which correlates with the ability of fumarate to significantly inhibit light-driven H_2 production (see **Fig. 5.1** and **5.2** and **Table 5.1**). Interestingly, less malate was produced over 24 hr irradiation compared to experiments where equivalent samples were irradiated for 30 min. This suggests that hydration of fumarate to malate by MR-1 is rapid over short periods of time but the transformation can be reversed once there is a sufficient driving force for reduction of fumarate to succinate. This is presumably achieved over 24 hr due to gradual accumulation of MV^+ in reaction suspensions, as discussed in section 4.4.1. Incubation of MR-1 with pyruvate and CO_2 under 24 hr irradiation gave far greater yields of lactate and formate, respectively, compared to experiments with 30 min irradiation. However, there were still considerable

differences between the yields of lactate and formate despite results in section 5.2 suggesting that the extents of each reaction would be similar. The reduction of pyruvate and CO₂ likely takes a longer time to proceed than the reduction of fumarate due to differences in enzyme accessibility, as discussed previously (see sections 1.6.1 and 3.4).

A notable result from the analysis in this section is that the extent of CO₂-reduction was significantly less than pyruvate-reduction under both irradiation regimes despite both compounds being equally effective at suppressing light-driven H₂-evolution (see **Fig. 5.1**, **5.2** and **Table 5.1**). Additionally, the yields of succinate were high over both the shorter and longer irradiation periods suggesting that the system is particularly suitable for facilitating the reduction of fumarate. However, it is possible that the longevity of the fumarate reductase is compromised after prolonged exposure to conditions required for photo-production of MV⁺ which affect bacterial viability and may cause cells to lyse (see sections 4.4.4 and 4.5). In the next sections, experiments were performed to address these matters and examine the wider properties of the system. Section 5.4 describes experiments that aimed to improve CO₂-reduction by varying the size of the gaseous headspace above samples during irradiation or by replacing MR-1 with the HydA⁻/HyaB⁻ strain. Section 5.5 describes experiments that assessed the activity of the fumarate reductase over 96 hr to compare with changes to the activity of the hydrogenases over the same time period.

5.4 Enhancement of light-driven CO₂-reduction by *Shewanella oneidensis* MR-1 from photo-produced MV⁺

An unexpected result from the ¹H-NMR analysis in the previous section was the production of approximately 6-fold less formate than lactate at the end of experiments even though the presence of pyruvate and CO₂ cause similar decreases to light-driven H₂-evolution (see section 5.2). As such, it was of interest to investigate whether experimental conditions could be changed to improve the extent of light-driven CO₂-reduction by MR-1. For example, it is possible that the presence of a gaseous headspace above samples allows dissolved CO₂ to escape solution, rendering it unavailable as a substrate for reductive catalysis. To test this, light-driven CO₂-reduction within glass vials was performed with minimal gaseous headspace in an attempt to increase the concentration of dissolved

CO₂ and improve photo-production of formate. For the assays, MR-1 was cultured for 24 hr under acceptor-limited conditions then harvested and re-suspended in 50 mM HEPES, 50 mM NaCl, pH 7. Bacterial suspensions (2 mL, MR-1 OD_{590nm} ≈0.25) were supplemented with 0.08 mM eosin Y, 0.5 mM MV, 50 mM TEOA and 10 mM CO₂ then transferred to clear glass vials with either 3 or 0.3 mL gaseous headspace (initially 100 % N₂) and irradiated (0.02 kW m⁻²) for 24 hr with the photosynthetic growth lamp. ¹H-NMR analysis of supernatants (technical duplicates for each condition) after 24 hr revealed the presence of 739 ± 17 (4 % yield) and 1609 ± 36 (8 % yield) nmol formate for assays with the larger and smaller headspaces, respectively. The yields of formate are less than those seen in section 5.3, presumably due to day-to-day variations of biological samples (see section 4.4.3), but the relative difference between the two values shows that decreasing the volume of gas above reaction suspensions improves the yield of formate by a factor of 2.

The discrepancy between the decrease of light-driven H₂-evolution in the presence of CO₂ and the overall yield of formate may also be a result of the requirement for H₂ to facilitate CO₂-reduction, as would occur with a formate-hydrogen lyase complex (see section 1.6.1.1)⁹¹ where a molecule of CO₂ and a molecule of H₂ are consumed to achieve formate production. If this is the case, electrons provided to the bacterium by photo-produced MV⁺ must also be delivered to the hydrogenases for proton reduction (with the evolved H₂ consumed for reduction of CO₂ to formate) such that fewer electrons are transferred directly to the formate dehydrogenases. Consequently, it may be possible to enhance the yields of formate by performing experiments with the HydA⁻/HyaB⁻ strain lacking functional hydrogenases to increase the flow of electrons to the formate dehydrogenases (assuming that CO₂-reduction can still occur in the absence of the hydrogenases). To test this, MR-1 and HydA⁻/HyaB⁻ were cultured and processed as described above then bacterial suspensions (1 mL, OD_{590nm} ≈0.25) were supplemented with 0.08 mM eosin Y, 0.5 mM MV, 50 mM TEOA and 10 mM CO₂. Samples were transferred to clear glass vials (4 mL gaseous headspace, initially 100 % N₂) and incubated for 24 hr in the dark or under irradiation (0.02 kW m⁻²) by the photosynthetic growth lamp. After 24 hr, the amount of formate in supernatants was quantified using ¹H-NMR analysis then normalised to total protein content determined using a BCA assay (see section 2.3.4). Results from the experiments are presented in **Table 5.4**.

Table 5.4 - Light-driven CO₂-reduction by MR-1 and HydA⁻/HyaB⁻. ¹H-NMR derived quantification of formate in supernatants recovered from samples incubated for 24 hr with 0.08 mM eosin Y, 0.5 mM MV, 50 mM TEOA and 10 mM CO₂. Assays performed with MR-1 or HydA⁻/HyaB⁻ (both at OD_{590nm} ≈0.25) in the dark or irradiated (0.02 kW m⁻²) with the photosynthetic growth lamp. Mean values from technical duplicates (normalised to total protein), error indicates maximum and minimum. Anaerobic samples (1 mL) in 50 mM HEPES, 50 mM NaCl, pH 7 at 25 °C.

Strain	Light	Formate (nmol mg ⁻¹)
MR-1	No	97 ± 10
	Yes	11373 ± 72
HydA ⁻ /HyaB ⁻	No	243 ± 54
	Yes	31285 ± 1068

Negligible amounts of formate were produced after 24 hr incubation in the dark with both strains whereas almost 3-fold more formate was produced by the HydA⁻/HyaB⁻ strain compared to MR-1 after 24 hr irradiation. To confirm that the latter result does not reflect significant differences in enzyme activity between the two strains, spectrophotometric CO₂-reduction assays were performed using MR-1 and HydA⁻/HyaB⁻ which had been cultured for 24 hr under acceptor-limited growth then harvested and re-suspended in 50 mM HEPES, 50 mM NaCl, pH 7. Samples were supplemented with 64.5 µg mL⁻¹ DT and 0.08 mM MV then the absorbance at 600 nm was recorded over 8 min with an aliquot (0.1 mL) of 100 mM CO₂ in 50 mM HEPES, 50 mM NaCl, pH 7 added after approximately 1 min (see section 2.5.2). Representative data from the assays are shown in **Fig. 5.6** with data from equivalent control experiments where the addition of CO₂ was omitted. The high absorbance at the start of the experiment is due to the presence of MV⁺, the sharp decrease in absorbance around 1 min is due to removal of the cuvette from the spectrophotometer for mixing and the differences in absorbance at the end of the experiment are due to differences in scattering caused by the presence of bacteria. It should also be noted that the gradual decrease in absorbance seen during the control experiments is likely due to electron transfer from MV⁺ to bacterial electron acceptors such as the MR-1 hydrogenases which can facilitate proton reduction. The background absorbance changes have been accounted for when calculating the CO₂-reduction rates quoted below.

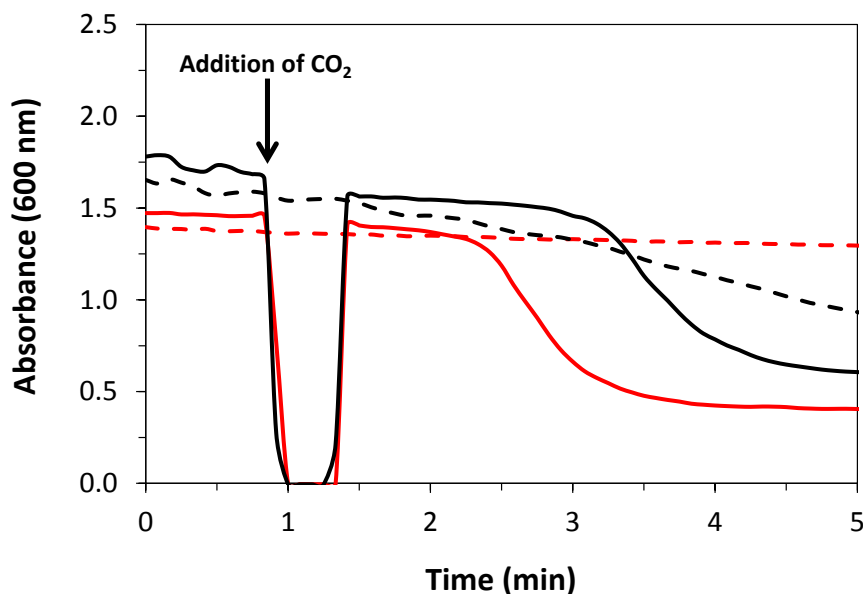


Figure 5.6 - Representative CO₂-reduction data for MR-1 and HyDA⁻/HydB⁻ after 24 hr acceptor-limited growth. Absorbance at 600 nm (pathlength 1 cm) for MR-1 (black) and HyDA⁻/HydB⁻ (red) cell pellets in 64.5 μg mL⁻¹ DT, 0.08 mM MV, 50 mM HEPES, 50 mM NaCl, pH 7 with an addition of CO₂ (to an initial concentration of 10 mM) after 1 min. Dashed lines correspond to equivalent experiments performed with no addition of CO₂.

Maximal CO₂-reduction rates were calculated from the change in absorbance over 0.5 min at the steepest part of the slope using **Eq. 5.1**, where ΔAbs_{600nm} is the change in absorbance at 600 nm over 0.5 min (minus the change in absorbance for an equivalent experiment with no addition of CO₂), the factor of 1.86 × 10³ accounts for the volume of the sample, ε_{MV+} is the extinction coefficient of MV⁺ (13.5 mM⁻¹ cm⁻¹),¹⁵⁹ and division by a factor of two accounts for the fact that two electrons are required to reduce one molecule of CO₂. The analysis gave CO₂-reduction rates of 172 ± 20 and 269 ± 21 nmol min⁻¹ mg⁻¹ (technical triplicates with standard error, normalised to total protein) for MR-1 and HyDA⁻/HydB⁻, respectively, showing that the photo-production of 3-fold more formate by HyDA⁻/HydB⁻ compared to MR-1 is not due to an increase in enzyme activity.

$$\frac{\Delta\text{Abs}_{600\text{nm}} \times 1.86 \times 10^3}{\epsilon_{\text{MV}^+} \times 2} = \text{nmol CO}_2 \text{ reduced min}^{-1} \quad \text{Eq. 5.1}$$

Overall, the results above indicate that H₂ is not required for light-driven CO₂-reduction and that the yields of photo-produced formate can be increased through the use of the HyDA⁻/HydB⁻ strain in place of MR-1, presumably because electrons are no longer lost to the hydrogenases for reduction of protons to H₂. The findings in this section do not fully account for there being less formate than anticipated at the end of experiments presented

in section 5.3 but showcase the ways in which CO₂-reduction could be enhanced and the potential benefits of genetically engineered *Shewanella* strains for cell-based photocatalysis. It is therefore possible that the formate dehydrogenases are unstable under the experimental conditions and lose activity during prolonged periods of irradiation and/or that photo-degradation of eosin Y permits the re-oxidation of formate to CO₂ due to the lack of a driving force for the reductive reaction. Similar observations were discussed in section 4.5 with respect to the longevity of the MR-1 hydrogenases.

Moving forward, it is also of interest to extend the analysis of reactions which resulted in the formation of the desired product in high yield, such as the light-driven reduction of fumarate to succinate by MR-1. High yields of succinate were seen over 30 min and 24 hr irradiation (see section 5.3) making it useful to evaluate the activity of the fumarate reductase over extended periods of time to see whether the current system could be used for sustained fumarate-reduction.

5.5 Longevity of the *Shewanella oneidensis* MR-1 fumarate reductase over 96 hr

The longevity of the MR-1 fumarate reductase was determined by measuring the activity of the enzyme in supernatants and re-suspended cell pellets harvested after centrifugation of MR-1 suspensions which had been irradiated for 0, 24, 48, 72 or 96 hr as described in **Fig. 4.17**. Such an analysis made it possible to compare the longevity of representative soluble and membrane-bound MR-1 enzymes because the activity of the hydrogenases was evaluated in an identical way in the previous chapter (see **Fig. 4.18**). For the experiments, MR-1 was cultured under acceptor-limited conditions for 24 hr then harvested and re-suspended in anaerobic 50 mM HEPES, 50 mM NaCl, pH 7. Bacterial suspensions (1.7 mL, MR-1 OD_{590nm} ≈0.25) were supplemented with 60 mM TEOA, 0.3 mM MV and 0.11 mM eosin Y then transferred to clear glass vials (3.3 mL headspace, initially 100 % N₂) and irradiated (0.02 kW m⁻²) with the photosynthetic growth lamp for 96 hr. Spectrophotometric fumarate-reduction assays were performed periodically on harvested supernatants and re-suspended cell pellets by supplementing samples with 64.5 μg mL⁻¹ DT and 0.08 mM MV then recording the absorbance at 600 nm over 8 min with an aliquot (0.1 mL) of 10 mM fumarate in 50 mM HEPES, 50 mM NaCl, pH 7 added after

approximately 1 min (see section 2.5.2). Representative data from the assays are shown in **Fig. 5.7A** with data from equivalent experiments performed with no addition of fumarate. Maximal fumarate-reduction rates were calculated from the change in absorbance over 0.5 min at the steepest part of the slope using **Eq. 5.1** and are presented in **Fig. 5.7B**. Control experiments where the addition of fumarate was omitted gave background reduction rates of ≤ 1.1 nmol min⁻¹ in all cases.

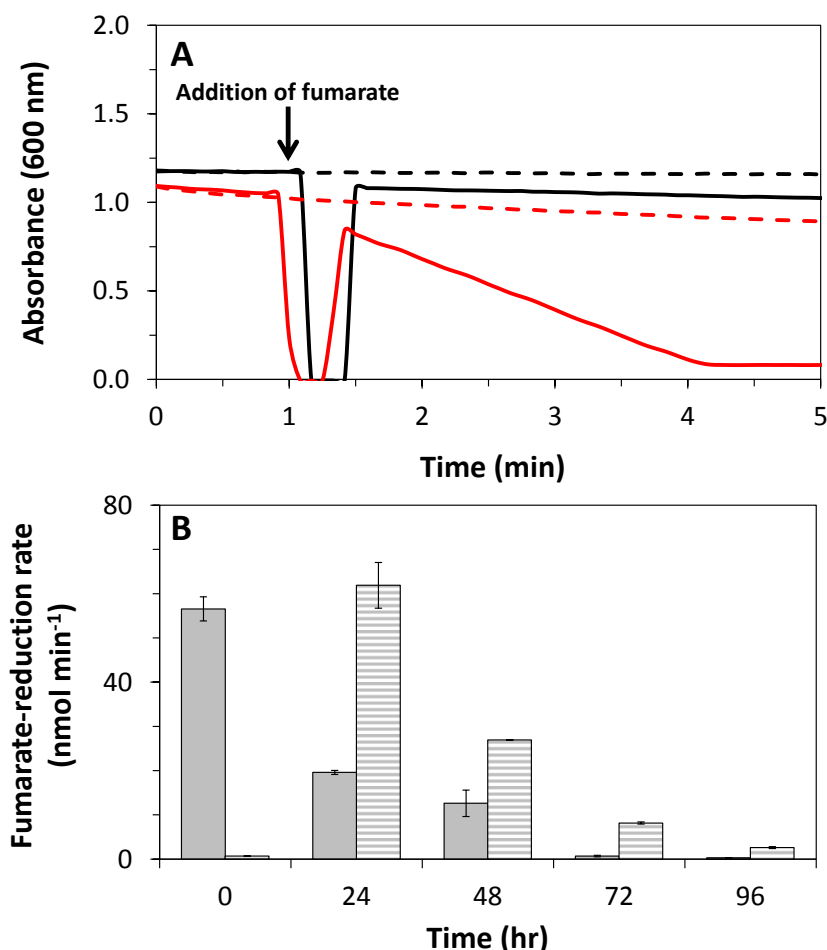


Figure 5.7 - Longevity of the MR-1 fumarate reductase. A] Representative fumarate-reduction data for cell pellets (black) and supernatants (red) recovered after centrifugation of MR-1 suspensions irradiated with eosin Y as described in **Fig. 4.17**. Absorbance at 600 nm (pathlength 1 cm) for samples in 64.5 $\mu\text{g mL}^{-1}$ DT, 0.08 mM MV, 50 mM HEPES, 50 mM NaCl, pH 7 with an addition of fumarate (to an initial concentration of 1 mM) after 1 min. Dashed lines correspond to equivalent experiments performed with no addition of fumarate. B] Maximal fumarate-reduction rates associated with cell pellets (solid bars) and supernatants (striped bars) recovered after centrifugation of MR-1 suspensions irradiated for 0, 24, 48, 72 or 96 hr with eosin Y. Mean values for technical duplicates, error bars indicate maximum and minimum. Anaerobic samples in 50 mM HEPES, 50 mM NaCl, pH 7.

At 0 hr, the majority of the fumarate reductase activity was associated with the re-suspended cell pellets but from 24 hr onwards the activity steadily decreased with

negligible rates of fumarate-reduction recorded after 72 hr. As the activity associated with the cell pellets decreased from 0 to 24 hr there was a corresponding increase in the activity associated with the supernatants. The rates of fumarate-reduction by supernatants then gradually decreased between 24 and 96 hr. The activity profile for the fumarate reductase over 96 hr is significantly different to that for the hydrogenases with respect to enzyme location and variation over time (see **Fig. 4.18**). H₂ oxidation activity was only associated with the re-suspended cell pellets and remained constant between 24 and 96 hr whereas fumarate-reduction activity varied significantly over the same time period and was also associated with supernatants. This is likely caused by exposure of MR-1 to conditions required for photo-production of MV⁺ which results in a loss of bacterial viability (see section 4.4.4) and, as evidenced here, cell lysis leading to a release of soluble periplasmic enzymes into solution. Despite the changes in enzyme location over 96 hr, fumarate reductase activity was detected in samples over the entire experiment. This suggests that MR-1 could be exploited for sustained light-driven fumarate-reduction but it is likely that the system could be improved if reagents and/or experimental conditions were found which facilitate rapid photocatalysis but avoid decreases in bacterial viability.

5.6 Discussion

The results in this chapter show that MR-1 can be used for light-driven hydrogenation of C=C and C=O bonds within simple carbon substrates. The work builds upon the findings presented in the two previous chapters where growth conditions were established for the production of four key enzymes by MR-1 then photoreduction of MV²⁺ was carried out in the presence of the bacterium to drive H₂-evolution. In this chapter, addition of an exogenous carbon substrate prior to irradiation successfully re-directed electrons away from the hydrogenases to yield a well-defined range of products. Based on the final amounts of succinate, lactate and formate, the rates of light-driven fumarate-, pyruvate- and CO₂-reduction over 30 min irradiation (0.7 kW m⁻²) with the cold light source were approximately 145, 20 and 4 nmol min⁻¹, respectively (see **Fig. 5.4A**). Determination of the corresponding rates over 24 hr irradiation (0.02 kW m⁻²) with the photosynthetic growth lamp is challenging because it is not known if or when the reactions reach completion. Compared to the rates observed with MR-1 in the presence of DT and MV (see section 3.4), the values here are slightly higher for fumarate-reduction and much lower for pyruvate- and CO₂-reduction. The lower rates of reduction with respect to pyruvate and

CO₂ likely reflect the fact that formation of MV⁺ and transfer of electrons to bacterial redox partners is slow during light-driven experiments relative to DT-driven experiments where MV²⁺ reduction is instantaneous. The slower formation of MV⁺ may also account for the greater yields of malate in light-driven experiments (see **Fig. 5.4**, left) compared to DT-driven experiments (see **Fig. 3.7**, left) because there is more time for hydration of fumarate to occur before there is a sufficient driving force for reduction of fumarate to succinate. Photocatalytic TONs with respect to the photosensitiser can be calculated based on the fact that reaction suspensions contained 80 nmol eosin Y and a single turnover of the system would generate 40 nmol product (see section 4.7 for more information). From the final quantities of succinate, lactate and formate, TONs for the system are approximately 108, 15 and 3, respectively, after 30 min irradiation and approximately 207, 228 and 39, respectively, after 24 hr irradiation. For both irradiation regimes, the yield of formate was lower than expected but could be improved through changes to the experimental setup or replacement of MR-1 with HydA⁻/HyaB⁻, presumably due to increased availability of dissolved CO₂ or increased electron transfer to the formate dehydrogenases, respectively. On the other hand, the yield of succinate was high under both irradiation regimes showing that electrons provided to the bacterium by photo-produced MV⁺ can be effectively delivered to the fumarate reductase. However, assays which examined the longevity of the fumarate reductase indicated that the enzyme is released from the bacterium and gradually becomes inactive over extended periods of irradiation. This suggests that the current system is more suitable for sustained photocatalysis with membrane-bound enzymes, such as the hydrogenases, that remain associated with cellular material and retain their activity over 96 hr despite decreases in bacterial viability caused by the light-harvesting reagents.

Enzymatic systems for the photocatalytic reduction of fumarate, pyruvate and CO₂ have been reported previously and can be compared with the work described in this chapter.^{65,110,135,230–232} For example, Bachmeier et al. (2014) reported fumarate-reduction under visible light irradiation (0.45 kW m⁻²) by co-adsorbing the purified fumarate reductase from *Shewanella frigidimarina* NCIMB400 and RuP on titanium dioxide nanoparticles.¹¹⁰ The system used MES as SED and generated 2.3 mM succinate (38 % yield) over 4 hr corresponding to a TON of approximately 5800 with respect to the amount of enzyme. Light-driven fumarate-reduction was also reported in Hutton et al. (2016) using the purified fumarate reductase from MR-1, cationic carbon dots as photosensitisers and

EDTA as SED.¹³⁵ The system produced 1.3 mM succinate (13 % yield) after 24 hr visible light irradiation (1 kW m^{-2}) corresponding to a TON of approximately 6000 with respect to the amount of enzyme. The examples in the literature display high TONs and operate with very little enzyme present. However, the absolute quantities of succinate being generated are in a similar range to those reported in this chapter where comparable yields were achieved over 30 min irradiation (see **Table 5.2**). An additional benefit of the cell-based approach developed in this thesis is that rapid photo-production of succinate takes place without the need for costly and time-consuming enzyme purification. With respect to light-driven pyruvate-reduction, Huang et al. (2014) reported the generation of 5 mM lactate (100 % yield) under 6 hr visible light irradiation using carbon nitride mesoporous spheres as photosensitisers, TEOA as SED and purified L-lactate dehydrogenase in a system that required exogenous NADH and a rhodium catalyst for regeneration of NADH from NAD^+ after hydride transfer.²³⁰ Miyatani et al. (2004) also reported photo-production of 0.17 mM lactate (17 % yield) after 4 hr visible light irradiation (0.2 kW m^{-2}) using a zinc porphyrin photosensitiser, TEOA as SED, MV as electron transfer mediator and purified L-lactate dehydrogenase from pig heart.²³¹ This corresponded to a quantum yield of 4 %. The examples with purified lactate dehydrogenases in the literature exhibit relatively high yields of lactate over short timescales. However, the cell-based approach developed in this chapter is beneficial because photo-produced MV^+ can effectively deliver electrons to intermediary MR-1 enzymes required for catalysis without the addition of exogenous cofactors such as NADH. Light-driven CO_2 -reduction was reported in Yadav et al. (2012) using a system comprised of a graphene-based photosensitiser with TEOA as SED, purified formate dehydrogenase, exogenous NADH and a rhodium catalyst for cofactor regeneration (see **Table 1.3**, example A).⁶⁵ After 2 hr irradiation with visible light and a continuous supply of gaseous CO_2 , approximately 111 μmol formate was generated in reaction solutions. Photo-production of formate was also reported in Ihara et al. (2013) with photosystem I as photosensitiser, exogenous NADPH, a genetically modified formate dehydrogenase and a range of electron transfer proteins including plastocyanin, ferredoxin and FNR.²³² After 2.5 hr irradiation by visible light with a CO_2 atmosphere, the final concentration of formate in reaction solutions was approximately 47 μM . Additionally, the mutant formate dehydrogenase could be produced by cyanobacteria to accelerate *in vivo* formate production under irradiation. The examples in the literature exhibit relatively fast rates of CO_2 -reduction but the systems are very complex and, in the latter case, require purification of four proteins as well as genetic manipulation of a formate dehydrogenase to

change its cofactor specificity from NADH to NADPH. The cell-based approach with MR-1 described here is advantageous because all the required enzymes, cofactors and redox partners are provided by the wild-type bacterium and can be accessed or surpassed by photo-produced MV⁺ without the need for enzyme purification.

To summarise, some of the examples in the literature likely display greater efficiencies than the system developed in this thesis due to improved enzyme accessibility and a lack of metabolic pathways found *in vivo* which can act as electron sinks. It is also likely that particular experimental conditions and/or combinations of SEDs and photosensitisers promote more effective photon absorption and generation of photo-excited electrons than the approach described here. However, a clear advantage of cell-based photocatalysis with MR-1 is the fact that four key reactions can be performed using a single set of growth conditions and without the need for genetic engineering. This is made possible through the use of MV which can rapidly deliver electrons from eosin Y to bacterial enzymes, including membrane-associated enzymes localised to the cytoplasm such as lactate dehydrogenases. MV also provides opportunities to exploit other micro-organisms for light-driven chemical synthesis as there is no barrier to electron transfer across the outer membrane (see section 4.6). As mentioned in the previous chapter, the major disadvantage of the approach is that successful photocatalysis comes at the expense of bacterial integrity and viability due to the intrinsic toxicity of MV and products from the (photo-)degradation of TEOA and/or the photosensitisers (see section 4.4.4).^{49,227,228} In the ideal case, MR-1 would remain viable during light-driven experiments to allow self-regeneration of enzymes for enhanced longevity. Accordingly, it is of interest to find more robust and biocompatible photosensitisers which can transfer electrons to bacterial enzymes in the absence of MV. For example, it may be possible to take advantage of porin:cytochrome complexes embedded in the outer membrane of MR-1 which act as electron conduits between the outside and the inside of the bacterium (see section 1.6.2).^{122,124} One such complex, MtrCAB, was produced by MR-1 after 24 hr anaerobic, acceptor-limited growth (see **Fig. 4.22**). In the next chapter, data are presented from assays that quantified light-driven H₂-evolution with MR-1 in the absence of MV using a range of carbon dots (CDs) as photosensitisers. The work included an evaluation of multiple *Shewanella* strains to take advantage of the different physicochemical properties associated with their outer surfaces,²³³ some of which may encourage productive interactions with CDs.

CHAPTER 6

Assessment of light-driven
H₂-evolution by *Shewanellaceae*
with carbon dot photosensitisers

Chapter 6 - Assessment of light-driven H₂-evolution by *Shewanellaceae* with carbon dot photosensitisers

6.1 Introduction

In chapters 3, 4 and 5, a system for cell-based photocatalysis was developed by combining anaerobically grown MR-1 with TEOA, water-compatible dyes and MV for generation of photo-energised electrons and subsequent electron transfer to bacterial enzymes. Four reductive transformations were achieved using eosin Y as photosensitiser but sustained irradiation led to photo-degradation of eosin Y and the toxicity of MV caused a significant decrease in bacterial viability. As a consequence, it was of interest to combine MR-1 with more robust photosensitisers that can deliver photo-energised electrons to bacterial enzymes in the absence of an exogenous electron shuttle, for example, by transferring electrons across the outer membrane via porin:cytochrome complexes. In this chapter, new-generation carbon dot (CD) photosensitisers were investigated as a replacement for eosin Y and MV to develop a more sustainable approach to cell-based photocatalysis with MR-1 and other species of *Shewanella*. Light-driven H₂-evolution was targeted for the preliminary work because the product can be rapidly quantified using GC to afford high experimental throughput. Furthermore, different species of *Shewanella* were used to assess whether variations in hydrogenase activity, the production of extracellular cytochromes and other extracellular polymeric substances (EPS), and cell surface physicochemistry (including charge, morphology and hydrophobicity) afford more effective electron exchange between CDs and bacteria. First, data are shown from spectrophotometric assays that evaluated photoreduction of MV²⁺, BV²⁺ and MtrC by three types of CDs under conditions compatible with MR-1 enzyme activity. Next, data are shown from an assessment of multiple *Shewanella* strains including their hydrogenase activity after acceptor-limited growth and ability to support light-driven H₂-evolution with CD photosensitisers. The results below display the potential for *Shewanellaceae* to be used in future photocatalytic systems that operate without exogenous electron mediators.

6.2 Carbon dot photosensitisers

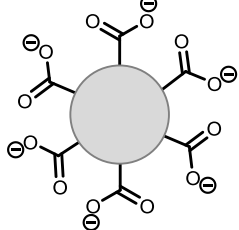
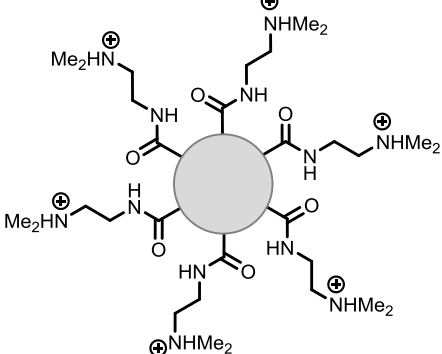
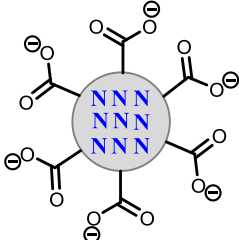
CDs (also known as carbon nanoparticles) have recently emerged as a stable, biocompatible and versatile allotrope of carbon with applications in light emitting devices and bio-imaging.^{234,235} Furthermore, their solubility in aqueous solutions and photochemical properties, including good absorption of light in the UV-visible region of the electromagnetic spectrum, have led to their use as photosensitisers for artificial photosynthesis with noble metals, transition metal complexes and purified enzymes as electrocatalysts.^{134,135,236} In this chapter, three types of CDs were evaluated: anionic CDs with terminal carboxylate groups (CD-CO_2^-), cationic CDs with terminal ammonium groups (CD-NHMe_2^+) and nitrogen-doped anionic CDs with terminal carboxylate groups (N-CD). All CDs were synthesised by Dr. Benjamin Martindale and Dr. Bertrand Reuillard (University of Cambridge, UK) and have been characterised previously using a variety of spectroscopic techniques.^{134–136,206} The next section provides an overview of their synthesis, key properties and use in recent photocatalytic systems.

6.2.1 Synthesis and physicochemical properties

CD-CO_2^- were synthesised by thermal decomposition (180 °C) of citric acid in air for 40 hr followed by dissolution in water, neutralisation with sodium hydroxide and freeze-drying to yield a solid product.¹³⁴ The nanoparticles are spherical with an average diameter of 6.8 nm as determined by high-resolution transmission electron microscopy and the terminal carboxylic acid groups are de-protonated at neutral pH to give a negative surface charge. CD-NHMe_2^+ were synthesised through surface modification of CD-CO_2^- .¹³⁵ Briefly, CD-CO_2^- were refluxed in thionyl chloride for 1 hr to form acyl chloride-capped CDs. These were then stirred in N,N-dimethylethylenediamine for 3 hr before the solid product was isolated through dissolution in acetone, filtration and freeze-drying. The nanoparticles have similar average diameters to CD-CO_2^- and the terminal amine groups are protonated at neutral pH to give a positive surface charge. N-CD were synthesised by thermal decomposition (320 °C) of aspartic acid in air for 100 hr followed by dissolution in water, neutralisation with sodium hydroxide and freeze-drying to yield a solid product.¹³⁶ The nanoparticles are quasi-spherical with an average diameter of 3.1 nm and the terminal carboxylic acid groups are deprotonated at pH 6 to give a negative surface charge.

CD-CO₂⁻ and CD-NHMe₂⁺ are predominantly composed of amorphous carbon with some graphitic regions whereas N-CDs are predominantly composed of graphitic carbon with nitrogen incorporated into the core of the nanoparticles.¹³⁴⁻¹³⁶ The properties of CD photosensitisers have been summarised in **Table 6.1** and the absorbance spectra for 0.3 mg mL⁻¹ CD in 50 mM HEPES, 50 mM NaCl, pH 7 are shown in **Fig. 6.1**.

Table 6.1 - Overview of CD photosensitisers used in this study. *Zeta potentials at pH 7 for CD-CO₂⁻ and CD-NHMe₂⁺ and at pH 6 for N-CD.

Photosensitiser	Precursor	Average particle diameter (nm)	Zeta potential (mV)*	Ref.
<p>CD-CO₂⁻</p> 	Citric acid	6.8 ± 2.3	-14	134
<p>CD-NHMe₂⁺</p> 	Citric acid	6.4 ± 1.2	+18	135
<p>N-CD</p> 	Aspartic acid	3.1 ± 1.1	-23	136

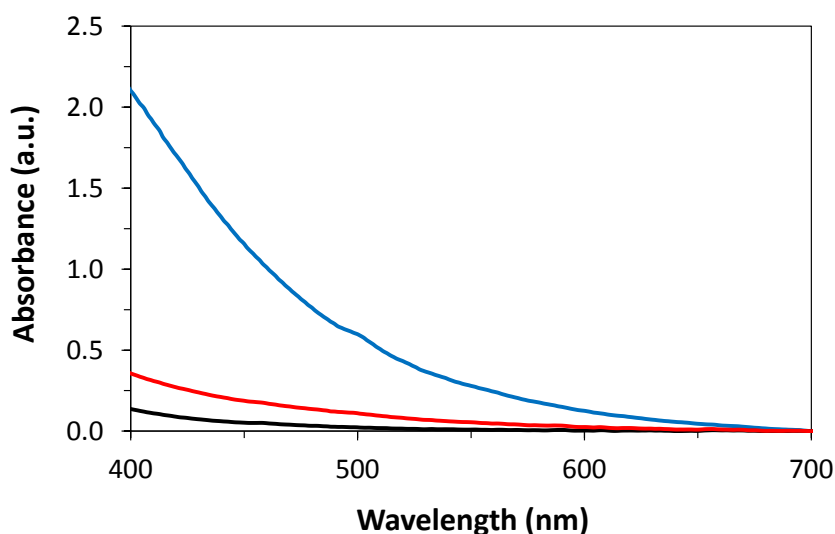


Figure 6.1 - Absorbance spectra of CD photosensitisers used in this study. 0.3 mg mL^{-1} CD-CO₂⁻ (black), CD-NHMe₂⁺ (red) and N-CD (blue) in 50 mM HEPES, 50 mM NaCl, pH 7 (pathlength 1 cm).

CD-CO₂⁻ and N-CD have been used as photosensitisers for light-driven H₂-evolution with a nickel bis(diphosphine) electrocatalyst in the presence of EDTA as SED.^{134,136} Under comparable conditions, quantum yields of approximately 1.4 and 5.3 % were reported with CD-CO₂⁻ and N-CD, respectively, using monochromatic light at 360 nm. The superior performance of N-CD compared to CD-CO₂⁻ was attributed to enhanced light absorption and electron transfer rates. CD-CO₂⁻ were also found to be compatible with a recyclable SED system comprised of TCEP and ascorbate for sustained light-driven H₂-evolution over 5 days.²⁰⁶ CD-NHMe₂⁺ have been used previously for light-driven reductive transformations with the purified fumarate reductase from MR-1 and the purified [NiFeSe]-hydrogenase from *Desulfomicrobium baculatum* as electrocatalysts and EDTA as SED.¹³⁵ Efficient electron transfer from CD-NHMe₂⁺ to the enzymes was afforded by favourable electrostatic interactions between the two components and TONs (with respect to the amount of enzyme) of approximately 6000 (for succinate production after 24 hr) and 50000 (for H₂ production after 48 hr) were reported with the fumarate reductase and the hydrogenase, respectively. Based on the success of the previously reported systems, it was predicted that the CDs would have sufficient reducing potential for proton reduction ($E_m = -0.41 \text{ V}$)¹⁰⁰ and electron transfer to outer membrane porin:cytochrome complexes such as MtrCAB ($E_m = -0.4$ to $+0.05 \text{ V}$).¹²⁴ To confirm this, a series of spectrophotometric assays were performed to assess light-driven electron transfer from the CDs to three different electron acceptors under conditions compatible with MR-1 enzyme activity. Results from the assays are presented in the next section.

6.2.2 Photoreduction of electron acceptors under conditions compatible with *Shewanella oneidensis* MR-1 enzyme activity

Spectrophotometric assays with CD photosensitisers were performed using MV^{2+} , BV^{2+} or purified MtrC (from MR-1) as electron acceptor with TEOA, EDTA or MES as SED. MV^{2+} and BV^{2+} (at final concentrations of 0.5 mM) were chosen as electron acceptors because they have reduction potentials comparable to those associated with chemical transformations of interest to this study (see Eq. 1.7 to 1.10).^{100,101,165} MtrC (at a final concentration of 0.6 μM = 6 μM heme) was chosen as an electron acceptor because it is produced by MR-1 after 24 hr acceptor-limited growth (see Fig. 4.22) and is localised to the outer surface of the bacterium (see section 1.6.2)¹¹⁹ so may be able to accept photo-excited electrons from CDs for subsequent electron transfer to bacterial enzymes. To prepare samples, anaerobic buffer (1 mL) was supplemented with the chosen CD, electron acceptor and SED within a N_2 -filled chamber and then irradiated (0.7 kW m^{-2}) with the cold light source for 30 min (see sections 2.2 and 2.5). The effectiveness of TEOA and EDTA was assessed in 50 mM HEPES, 50 mM NaCl, pH 7 and parallel control experiments without TEOA or EDTA reflected the ability of HEPES to act as SED. The effectiveness of MES was assessed in 150 mM MES, pH 6 where it may act as both a pH buffering component and SED. Representative spectra recorded after 0, 15 and 30 min irradiation for each electron acceptor with N-CD in the presence of TEOA as SED are presented in Fig. 6.2.

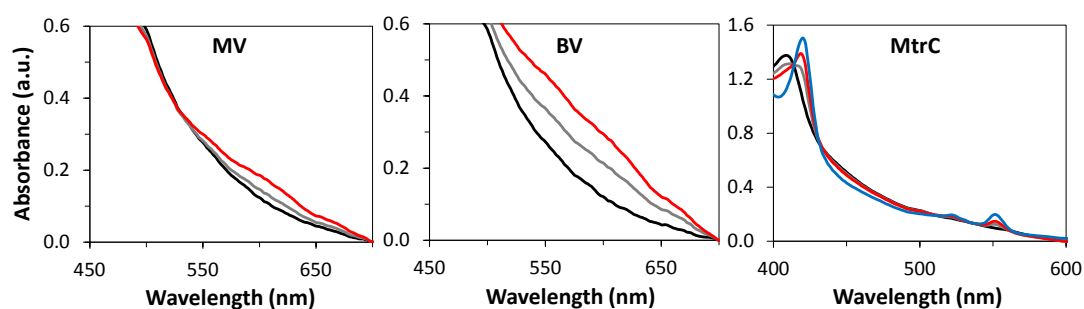


Figure 6.2 - Photoreduction of MV^{2+} , BV^{2+} and MtrC by N-CDs with TEOA as SED. MV and BV: Representative spectra for 0.3 mg mL^{-1} N-CD with 50 mM TEOA recorded after 0 (black), 15 (grey) and 30 min (red) irradiation (0.7 kW m^{-2}). Starting concentration of MV^{2+} and BV^{2+} was 0.5 mM. MtrC: Representative spectra for 0.13 mg mL^{-1} N-CD with 50 mM TEOA recorded after 0 (black), 15 (grey) and 30 min (red) irradiation (0.7 kW m^{-2}) and after an addition of excess DT (blue). Starting concentration of MtrC was 0.6 μM (= 6 μM heme). Anaerobic samples (1 mL) in 50 mM HEPES, 50 mM NaCl, pH 7 (pathlength 1 cm). Irradiation provided by the cold light source.

Upon irradiation, peaks appear around 600 nm (for assays with MV^{2+} and BV^{2+}) or 420, 523 and 552 nm (for assays with MtrC) corresponding to photoreduction of the electron

acceptors. The concentration of photo-produced MV^+ and BV^+ in samples was calculated using the Beer-Lambert law (see **Eq. 2.1**) with the known extinction coefficients at 600 nm (see section 2.5).^{157,159} MtrC heme photoreduction was quantified at 552 nm against the fully reduced cytochrome attained at the end of each experiment through the addition of excess DT. The extents of MV^{2+} , BV^{2+} and MtrC heme photoreduction with each combination of CD and SED are shown in **Fig. 6.3** and have been summarised below.

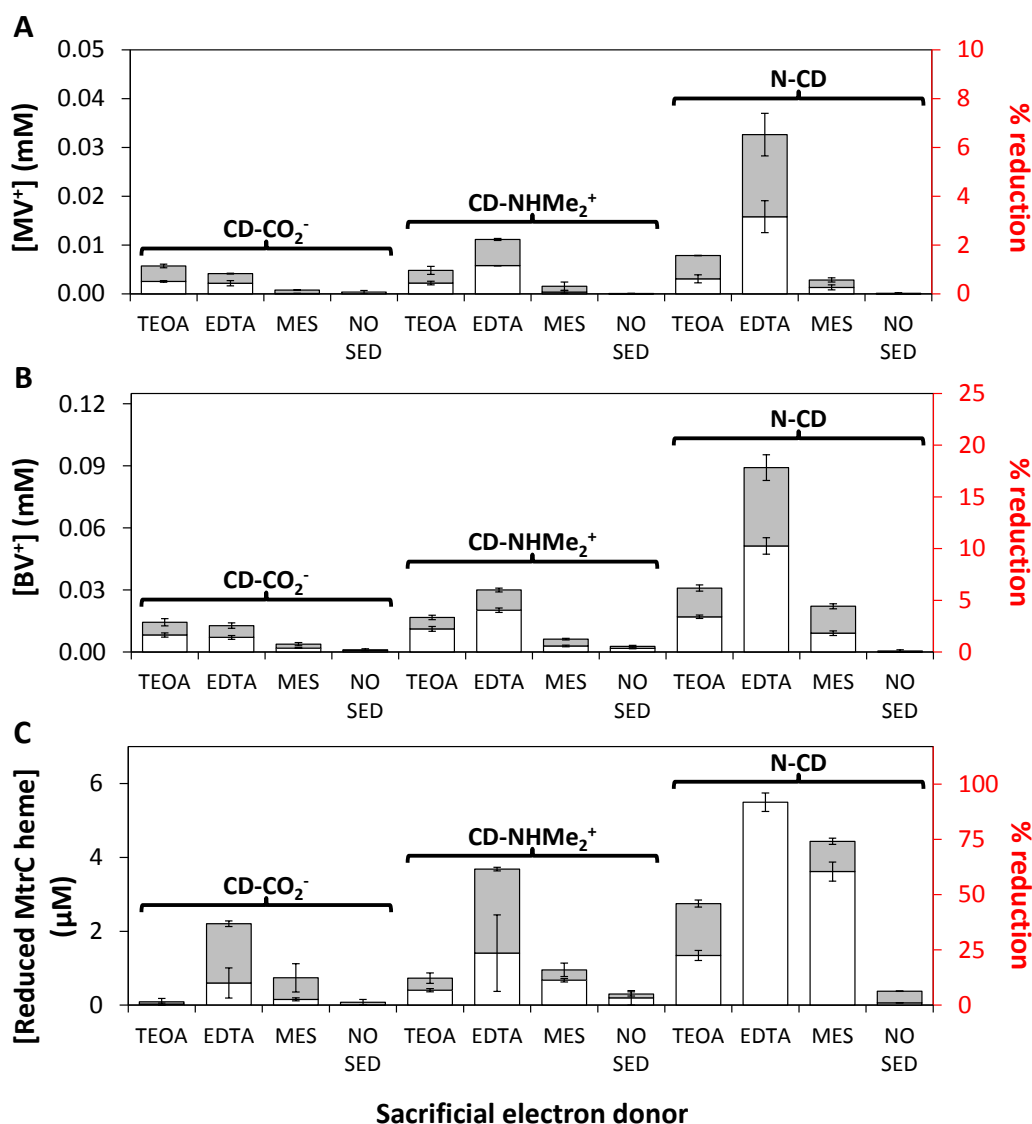


Figure 6.3 - Photoreduction of MV^{2+} , BV^{2+} and MtrC by CD photosensitisers with different SEDs. A] Concentration of MV^+ after 15 (white) and 30 min (grey) irradiation (0.7 kW m^{-2}) of the indicated CD (0.3 mg mL^{-1}) with either EDTA or TEOA at 50 mM or 150 mM MES. Starting concentration of MV^{2+} was 0.5 mM. B] As for A] but with BV^{2+} as electron acceptor. C] Concentration of reduced MtrC heme after 15 (white) and 30 min (grey) irradiation (0.7 kW m^{-2}) of the indicated CD (0.13 mg mL^{-1}) with either EDTA or TEOA at 50 mM or 150 mM MES. Starting concentration of MtrC was 0.6 μM (= 6 μM heme). Mean values from technical duplicates, error bars indicate maximum and minimum. Some error bars are too small to resolve. Anaerobic samples (1 mL) in 50 mM HEPES, 50 mM NaCl, pH 7 or 150 mM MES, pH 6. Irradiation provided by the cold light source.

Very little photoreduction was observed for any electron acceptor in the 50 mM HEPES, 50 mM NaCl, pH 7 buffer with no added SED. With added TEOA or EDTA as SED, the N-CD photosensitisers were most effective at photoreduction of all three electron acceptors. MES was not able to act as SED with MV^{2+} as electron acceptor and could only act as SED with BV^{2+} as electron acceptor in combination with N-CD. On the other hand, MES was able to act as SED for all CDs with MtrC as electron acceptor, which may reflect the lower concentration of MtrC in samples compared to MV^{2+} and BV^{2+} .

Overall, the results from spectrophotometric assays show that different combinations of CDs and SEDs can facilitate photoreduction of relevant electron acceptors under conditions compatible with MR-1 enzyme activity. This suggests that CD photosensitisers have sufficient reducing potential to achieve proton reduction in the presence of anaerobically grown MR-1 and other species of *Shewanella*. In the next section, results are presented from an evaluation of 12 wild-type *Shewanella* strains including a comparison of their genomes and quantification of hydrogenase activity after acceptor-limited growth. Particular strains were then chosen for further experiments that assessed light-driven H_2 -evolution with CD photosensitisers.

6.3 Evaluation of *Shewanella oneidensis* MR-1 and other species of *Shewanella* for light-driven H_2 -evolution with carbon dot photosensitisers

6.3.1 Genomic comparison of *Shewanellaceae*

A variety of *Shewanella* strains (see **Table 2.2**), for which the genomes have been sequenced, were evaluated for their hydrogenase activity and ability to facilitate light-driven H_2 -evolution with CD photosensitisers. Based on their genomes, the bacteria differ in their capacity to produce particular sets of extracellular cytochromes and hydrogenases, as illustrated in **Table 6.2** where comparison of the relevant genes was achieved using SyntTax software (<http://archaea.u-psud.fr/synttax/>)²³⁷ and Fredrickson et al. (2008).¹²⁰ The genes encoding MtrCAB and the [NiFe]-hydrogenase are common to

all 12 strains whereas the genes encoding other extracellular cytochromes and the [FeFe]-hydrogenase are only present in the genomes of certain bacteria.

Table 6.2 - Genomic comparison of *Shewanellaceae* showing the presence (✓) or absence (-) of genes encoding the indicated proteins.

<i>Shewanella</i> strain	MtrCAB	MtrDEF	OmcA1	OmcA2	UndA	HydA [FeFe]	HyaB [NiFe]
<i>oneidensis</i> MR-1	✓	✓	✓	-	-	✓	✓
<i>oneidensis</i> MR-4	✓	✓	✓	-	-	✓	✓
<i>oneidensis</i> MR-7	✓	✓	✓	-	-	-	✓
<i>amazonensis</i> SB2B	✓	✓	✓	✓	-	-	✓
ANA-3	✓	✓	✓	-	-	✓	✓
<i>baltica</i> OS185	✓	✓	✓	-	-	-	✓
<i>baltica</i> OS195	✓	✓	✓	-	-	-	✓
<i>baltica</i> OS223	✓	✓	-	-	✓	-	✓
<i>loihica</i> PV-4	✓	✓	✓	✓	-	-	✓
<i>putrefaciens</i> CN-32	✓	-	-	-	✓	-	✓
<i>putrefaciens</i> 200	✓	-	-	-	✓	-	✓
<i>putrefaciens</i> W3-18-1	✓	-	-	-	✓	-	✓

Differences in the production of extracellular cytochromes and other EPS (such as lipopolysaccharides) during growth (as well as sequence variations between protein homologs and the presence of bound metal ions) likely afford bacteria with distinct outer surfaces (with respect to their charge, morphology and hydrophobicity),^{137,233,238–240} some of which may promote productive interactions with CD photosensitisers for light-driven H₂-evolution. For example, it was reported in Korenevsky et al. (2002) that the cell surface of aerobically grown *Shewanella putrefaciens* CN-32 (CN-32) is not capsulated and lacks

fibrous material (i.e. does not possess extensive arrays of long-branched lipopolysaccharides), in contrast to MR-1, *Shewanella oneidensis* MR-4 (MR-4) and *Shewanella amazonensis* SB2B (SB2B), which may support adhesion of the bacterium to inanimate surfaces such as iron oxides.²³⁸ It was also shown in Korenevsky et al. (2007) that aerobically grown CN-32 has a more positive zeta potential and is more hydrophobic than other *Shewanella* strains such as MR-1 and MR-4.²³³ Furthermore, it is likely that the strains differ in their hydrogenase content and activity as well as their ability to produce natural electron shuttles such as flavins and soluble periplasmic cytochromes, including the small tetraheme cytochrome (STC),^{109,127} which may aid or hinder electron transfer to the hydrogenases. To quantify the differences in hydrogenase activity between the strains, spectrophotometric H₂ oxidation assays were performed after culturing bacteria under acceptor-limited conditions. Results from the assays are presented in the next section.

6.3.2 Hydrogenase activity of *Shewanellaceae* after anaerobic, acceptor-limited growth

To assess hydrogenase activity, the *Shewanella* strains were first cultured under anaerobic conditions with an excess of lactate to fumarate and the OD_{590nm} of bacteria was measured periodically to monitor growth (see section 2.3.3). Results from the analysis are shown in **Fig. 6.4** (data were obtained by Mr. Jack Day [University of East Anglia, UK]). The OD_{590nm} was not recorded during overnight incubations so data points have only been connected on consecutive hours and the growth curves have been grouped based on the OD_{590nm} measured at the end of the experiment. The results with MR-1 are comparable to those shown in chapter 3 (see **Fig. 3.1**). For the majority of the other strains, the OD_{590nm} increased following inoculation then plateaued after approximately 4 to 7 hours. After overnight incubation, the OD_{590nm} decreased (to a significant extent in some cases) suggesting a reduction in the amount and/or size of bacteria. The OD_{590nm} then remained relatively stable up to 48 hr. Spectrophotometric H₂ oxidation assays (see section 2.5.1) were performed using bacteria which had been cultured under acceptor-limited conditions for 20 hr then harvested from growth medium and re-suspended in 50 mM HEPES, 50 mM NaCl, pH 7 to an OD_{590nm} between 0.18 and 0.24. Mean H₂ oxidation rates (normalised to total protein using a BCA assay, see section 2.3.4) for all strains are shown in **Fig. 6.5** (data were obtained by Mr. Jack Day [University of East Anglia, UK]). All bacterial strains were able to oxidise H₂ but there were significant differences in the initial oxidation

rates suggesting variations in hydrogenase content and/or activity. However, there was no clear correlation between the H₂ oxidation rates and the relative OD_{590nm} endpoint during anaerobic growth (see Fig. 6.4) or the capacity for bacteria to produce the [FeFe]-hydrogenase in addition to the [NiFe]-hydrogenase (see Table 6.2).

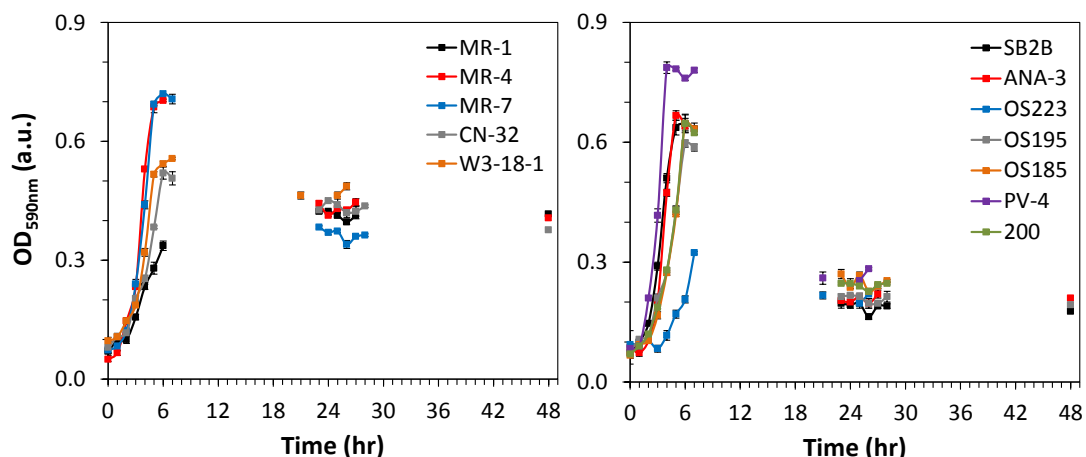


Figure 6.4 - Anaerobic growth of *Shewanellaceae* with 37.5 mM lactate as electron donor and 18.8 mM fumarate as electron acceptor. Optical density at 590 nm for strains which exhibit a higher (left) or lower (right) relative endpoint. Inoculation at 0 hr of M72 medium (10 mL) supplemented with anaerobic growth additions. Samples had 7 mL headspace (100 % N₂ at inoculation). Optical densities are mean values from 3 biological replicates, error bars indicate standard error. Lines serve as a guide to the eye, the majority of error bars are too small to resolve. Data obtained by Mr. Jack Day (University of East Anglia, UK).

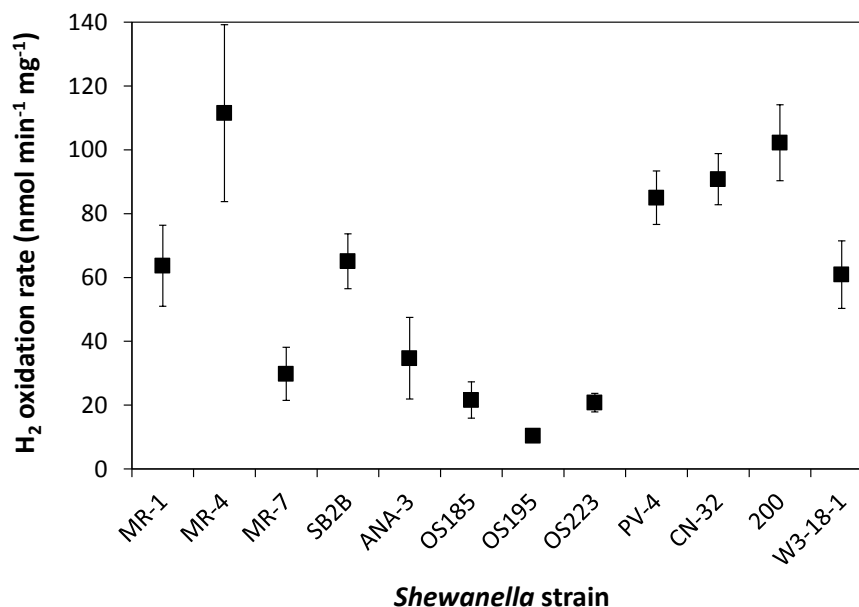


Figure 6.5 - Initial rates of H₂ oxidation coupled to BV reduction by *Shewanellaceae* after 20 hr acceptor-limited growth. Rates are mean values from 4 (MR-1, MR-4, ANA-3 OS223, CN-32), 3 (SB2B, OS185, 200) or 2 (MR-7, OS195, PV-4, W3-18-1) biological replicates with standard error (normalised to total protein). Anaerobic samples in 0.5 mM BV, 50 mM HEPES, 50 mM NaCl, pH 7. Data obtained by Mr. Jack Day (University of East Anglia, UK).

Overall, the findings in this section show that multiple species of *Shewanella* can be cultured under acceptor-limited conditions to produce hydrogenases active in H₂ oxidation. Based on the results, MR-4, SB2B, *Shewanella loihica* PV-4 (PV-4), CN-32 and *Shewanella putrefaciens* 200 (200) are of interest to be assessed for light-driven H₂-evolution with CD photosensitisers because they display faster rates of H₂ oxidation relative to MR-1, suggesting increased hydrogenase content. Furthermore, MR-4 and CN-32 (in addition to MR-1) are of particular interest because they grow to a relatively high OD_{590nm} after 24 hr acceptor-limited growth meaning the yields of cellular material for subsequent experiments are greater than for the other strains. In the next section, results are presented from a preliminary assessment of light-driven H₂-evolution by MR-1, MR-4 and CN-32 with CD photosensitisers.

6.3.3 Preliminary assessment of light-driven H₂-evolution by *Shewanellaceae*

To assess light-driven H₂-evolution by MR-1, MR-4 and CN-32 with CD photosensitisers, bacteria were cultured under acceptor-limited conditions for 24 hr then headspace H₂ in Hungate tubes was quantified using GC (see section 2.4.1) to provide confirmation that hydrogenases active in proton reduction had been produced. Next, bacteria were harvested and re-suspended in anaerobic 50 mM HEPES, 50 mM NaCl, pH 7 in a N₂-filled chamber (see section 2.3.7) then samples (1 mL, OD_{590nm} ≈0.3) were supplemented with 0.5 mg mL⁻¹ N-CD and 50 mM TEOA. For the experiments, N-CD were used as photosensitisers because they showed faster rates of MV²⁺, BV²⁺ and MtrC heme photoreduction compared to CD-CO₂⁻ and CD-NHMe₂⁺ (see **Fig. 6.3**) and TEOA was used as SED to allow a direct comparison with results presented in chapter 4. Reaction suspensions were transferred to clear glass vials with 4 mL gaseous headspace (initially 100 % N₂) and irradiated (0.7 kW m⁻²) for 4 hr with the cold light source. At the end of the irradiation period, headspace H₂ was quantified using GC. Results from the analysis (normalised to total protein) are shown in **Fig. 6.6** with equivalent data for samples that contained no bacteria, HydA⁻/HyaB⁻ or Mtr⁻ (prepared as described above). Each data point corresponds to H₂ production by a different biological sample. The amount of headspace H₂ produced after 24 hr acceptor-limited growth is plotted against the left axis (black squares) and the amount of headspace H₂ produced after 4 hr irradiation in the presence of N-CD and TEOA is plotted against the right axis (red crosses). No headspace H₂ was detected for parallel

control experiments containing *Shewanellaceae* ($OD_{590nm} \approx 0.3$), 0.5 mg mL^{-1} N-CD and 50 mM TEOA in 50 mM HEPES, 50 mM NaCl, pH 7 after 4 hr incubation in the dark.

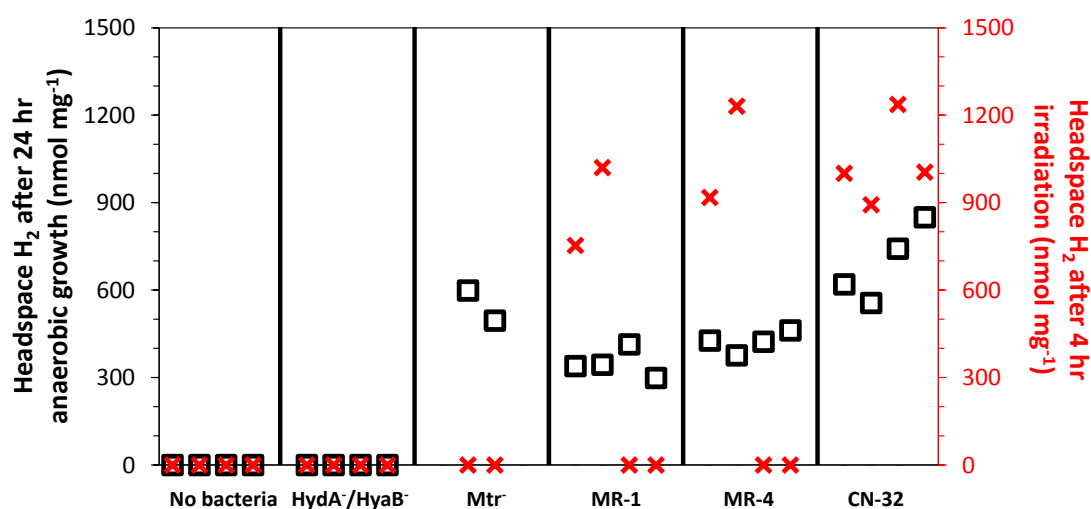


Figure 6.6 - Assessment of light-driven H₂-evolution by *Shewanellaceae* with N-CD. Left axis (black squares): Headspace H₂ (normalised to total protein) for the indicated strain after 24 hr anaerobic growth in Hungate tubes with 37.5 mM lactate as electron donor and 18.8 mM fumarate as electron acceptor. Right axis (red crosses): Headspace H₂ (normalised to total protein) after 4 hr continuous irradiation (0.7 kW m^{-2}) for the indicated strain ($OD_{590nm} \approx 0.3$) with 50 mM TEOA and 0.5 mg mL^{-1} N-CD. Anaerobic samples (1 mL) in 50 mM HEPES, 50 mM NaCl, pH 7 at room temperature. Irradiation provided by the cold light source.

In general, the results from the assessment of light-driven H₂-evolution with N-CD photosensitisers were variable. With MR-1 and MR-4, only two out of the four samples facilitated light-driven H₂-evolution (see **Fig. 6.6**, red crosses) despite the detection of headspace H₂ in all Hungate tubes after 24 hr acceptor-limited growth (see **Fig. 6.6**, black squares), confirming the production of active hydrogenases. In contrast, all samples containing CN-32 were found to facilitate light-driven H₂-evolution. These observations may reflect the fact that different biological samples of MR-1 and MR-4 vary significantly with respect to the production of extracellular cytochromes, EPS and/or periplasmic redox partners. These changes may impact the system if a particular cell surface physicochemistry affords close interactions with N-CD for photoreduction of bacterial electron acceptors or if specific bacterial redox partners are essential for electron transfer across the outer membrane and periplasmic space to the hydrogenases. Alternatively, it is possible that CN-32 is particularly suitable for light-driven H₂-evolution with N-CD photosensitisers. For example, CN-32 produced approximately 2-fold more headspace H₂ after 24 hr acceptor-limited growth compared to MR-1 and MR-4 suggesting increased hydrogenase content for proton reduction. It is also possible that the outer surface of CN-32 is more

accessible to N-CD for photoreduction of bacterial electron acceptors due to a lack of fibrous material extending from the outer membrane, in contrast to MR-1 and MR-4 (see section 6.3.1).²³⁸ Overall, the preliminary results in this section are encouraging, particularly with CN-32, because light-driven H₂-evolution can be achieved using TEOA and N-CD in the absence of MV. However, more work clearly needs to be done to assess the determinants of the system and to understand the variability between biological samples of *Shewanella* strains. Some proposals for future experiments are discussed in the next section.

6.4 Discussion

In this chapter, N-CD were revealed as superior photosensitisers to CD-CO₂⁻ and CD-NHMe₂⁺ in spectrophotometric assays that quantified the photoreduction of MV²⁺, BV²⁺ and purified MtrC (see **Fig. 6.3**). The results most likely reflect enhanced light absorption at wavelengths > 400 nm (see **Fig. 6.1**) and/or more efficient electron transfer via reductive or oxidative quenching of the excited state (see **Fig. 4.2**) for N-CD compared to the other CDs. However, the relevant (photo-)reduction potentials for CDs have not been determined experimentally at the time of writing. The rate of MV²⁺ photoreduction by N-CD in the presence of TEOA was slow compared to analogous experiments performed with eosin Y or proflavine as photosensitiser but correlated well with assays containing fluorescein, Ru(bpy)₃²⁺ or RuP (see **Fig. 4.6**). On the other hand, the extent of MtrC heme photoreduction by N-CD was comparable to experiments performed with eosin Y as described in Ainsworth et al. (2016).¹³² Overall, the results showed that N-CD should have sufficient reducing potential to drive proton reduction by *Shewanellaceae*.

12 wild-type *Shewanella* strains were screened in this chapter to take advantage of variations in the charge, morphology and hydrophobicity of their outer surfaces which may support close and stable interactions with N-CD for light-driven H₂-evolution. Some of these variations have been investigated previously (see section 6.3.1) and were attributed to differences in the production of extracellular cytochromes and lipopolysaccharides.^{233,238,239} All species of *Shewanella* showed hydrogenase activity after 20 hr acceptor-limited growth but only MR-1, MR-4 and CN-32 displayed fast rates of H₂ oxidation coupled with high yields of cellular material during anaerobic growth (see **Fig. 6.4** and **6.5**). However, light-driven H₂-evolution with N-CD photosensitisers in the presence of TEOA as SED gave variable results with both MR-1 and MR-4 under identical

experimental conditions whereas results with CN-32 were more reproducible (see **Fig. 6.6**). An analysis of headspace gases after 24 hr acceptor-limited growth confirmed that these observations did not reflect a lack of hydrogenase activity. Instead, it is possible that different biological samples of MR-1 and MR-4 vary with respect to their surface physicochemistry and/or the production of periplasmic redox partners such as STC or the fumarate reductase (which have both been shown to interact with MtrA and CymA *in vitro*)¹⁰⁹ required for productive electron transfer from N-CD to the hydrogenases. To test this, the zeta potential of anaerobically grown *Shewanella* strains could be measured to evaluate differences related to the charge of cell surfaces and the variations in bacterial EPS production could be monitored using microscopy after staining bacteria with a ruthenium red dye, as reported in Kouzuma et al. (2010).²⁴¹ Additionally, Western blotting could be used to quantify production of extracellular cytochromes and STC after 24 hr acceptor-limited growth and spectrophotometric assays could be used to quantify the activity of the fumarate reductase. Taken together, results from the assays described above may indicate that variations of *Shewanella* samples hinder light-driven H₂-evolution with N-CD due to differences in cell surface properties and/or the production of bacterial redox partners.

To extend the analysis, additional experiments could be performed to determine the routes by which photo-energised electrons are transferred from N-CD to bacterial hydrogenases. Two predominant pathways can be envisioned for this process, as shown in **Fig. 6.7**. On the one hand, it is possible that N-CD closely associate with the outer surface of bacteria and transfer electrons into the periplasm via MtrC and MtrA (or other porin:cytochrome complexes if present). Electrons could then be delivered to CymA via periplasmic redox partners for cycling of MK and MKH₂ which results in proton reduction. This mechanism is feasible because N-CD have an average diameter (see **Table 6.1**)¹³⁶ comparable to the size of MtrC (approximately 4 x 7 x 9 nm)¹³⁷ making them less likely to cross the outer membrane than small molecules such as eosin Y and MV. On the other hand, the size distribution of N-CD is relatively broad¹³⁶ meaning that smaller nanoparticles may be able to enter the periplasm and transfer electrons directly to CymA, particularly if the experimental conditions affect the integrity of the outer membrane or cause bacteria to lyse. To experimentally determine the mechanism(s) for light-driven electron transfer, a series of CN-32 mutants systematically lacking extracellular cytochromes and/or periplasmic redox partners could be produced to see whether the absence of particular

proteins completely inhibits electron transfer to the hydrogenases. The system could also be directly compared with the MV-mediated approach by irradiating samples with the cold light source over 96 hr and periodically performing spectrophotometric enzyme assays on re-suspended cellular material and supernatants, similar to the work described in sections 4.5 and 5.5. This would reveal whether the localisation of membrane-bound and soluble enzymes varies under extended periods of irradiation.

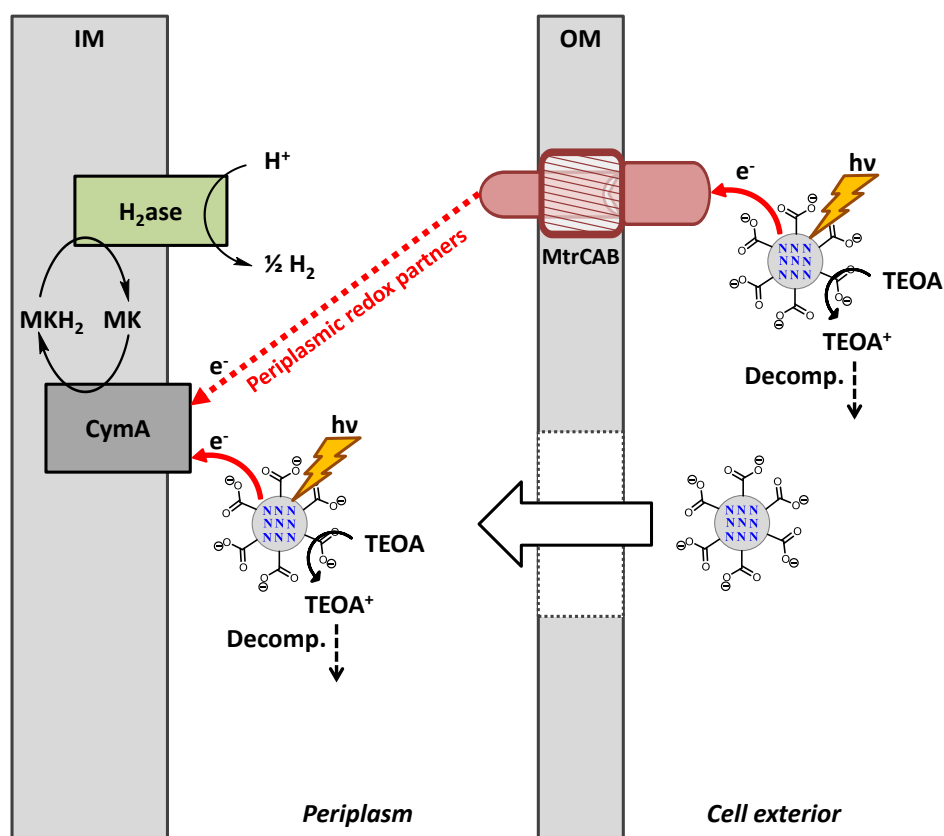


Fig. 6.7 - General schematic for light-driven H_2 -evolution by *Shewanellaceae* with N-CD photosensitisers. Photon ($h\nu$) absorption by N-CD in the presence of TEOA leads to direct or indirect electron transfer to CymA for subsequent proton reduction by the hydrogenases. See text for details. IM = inner membrane, OM = outer membrane, H_2ase = hydrogenase, MK = menaquinone, MKH_2 = menaquinol, TEOA = triethanolamine.

To conclude, the preliminary findings in this chapter provide a basis for sustainable cell-based photocatalysis with MR-1 and other species of *Shewanella* but further experiments are required to understand the variability of the system and elucidate the pathways for light-driven electron transfer from N-CD to bacterial hydrogenases. In the next chapter, a summary of the work in this thesis is presented to highlight key accomplishments and future experiments are discussed to showcase the opportunities for light-driven chemical synthesis with *Shewanellaceae* and other species of bacteria.

CHAPTER 7

Summary and Future Perspectives

Chapter 7 - Summary and Future Perspectives

To avoid the harmful environmental impacts of accessing fossil reserves, new technologies that harness solar energy must be developed for the sustainable production of valuable chemicals including fuels (see sections 1.2 and 1.3). Plants and photosynthetic micro-organisms can drive the production of complex chemicals using sunlight and have provided inspiration for research into artificial systems that aim to mimic and improve upon natural photosynthesis using a SED and photosensitiser to generate photo-energised electrons and an electrocatalyst to perform a reductive chemical transformation (see sections 1.4 and 1.5). In particular, whole-cell bacteria have emerged as effective electrocatalysts for artificial photosynthesis because they provide opportunities for sustained chemical synthesis and the formation of multiple products (see section 1.6). In this thesis, a system for cell-based photocatalysis was developed with the non-photosynthetic bacterium MR-1 where MV shuttles photo-energised electrons from water-compatible dyes to bacterial enzymes for the reduction of protons, fumarate, pyruvate and CO₂ to H₂, succinate, lactate and formate, respectively. Preliminary work was also carried out to assess the possibility of light-driven H₂-evolution with MR-1 and other species of *Shewanella* using N-CD photosensitisers in the absence of MV. The key findings from this work are summarised below and further experiments are discussed to show how these results could be expanded upon in the future.

The results in chapter 3 provided a platform for the subsequent work in the thesis by confirming that MR-1 could be cultured under a single growth condition to afford the simultaneous presence of active hydrogenases, fumarate reductase, lactate dehydrogenases and formate dehydrogenases. In addition, spectrophotometric enzyme assays, GC, H₂-evolution assays within the chamber of a H₂-sensing electrode and ¹H-NMR analysis were all established as effective techniques for quantification of enzyme activity and formation of the desired products. The work also revealed that MV was a suitable electron shuttle for MR-1 enzymes, including those localised to the cytoplasm. In chapter 4, TEOA was shown to be an effective SED in combination with water-compatible dyes for photoreduction of MV²⁺ and light-driven H₂-evolution in the presence of anaerobically grown MR-1. An assessment of the determinants of the system suggested the rate-defining events were photosensitiser-dependent rather than hydrogenase-dependent and highlighted a major advantage and disadvantage of the MV-mediated approach to

cell-based photocatalysis, namely, that the use of MV affords versatility because electrons can be transferred across the outer membrane of bacteria lacking porin:cytochrome complexes but that photocatalysis comes at the detriment of cell viability. The results in chapter 5 showed that MR-1 could drive the reduction of carbon substrates from photo-produced MV⁺ to give a well-defined distribution of products in relatively high yields. The work also demonstrated that photo-production of formate could be enhanced through changes to the experimental set-up or genetic manipulation of MR-1. Overall, the MV-mediated system represents an interesting proof-of-principle approach to light-driven chemical synthesis because a selectable product range can be accessed using bacteria cultured under a single growth condition without the need for costly and time-consuming enzyme purification. The loss of cell viability during photocatalysis is undesirable because soluble enzymes are released from the periplasm (see **Fig. 5.7**) and bacteria are rendered incapable of self-regeneration but, significantly, this did not prevent the desired reductive transformations from taking place. Consequently, it should be possible to develop the system further in a number of ways, as detailed below.

First, it may be possible to improve the efficiency of light-driven reductive transformations by optimising conditions for photoreduction of MV²⁺, where the quantum yield was low with both eosin Y and Ru(bpy)₃²⁺ compared to results reported previously (see sections 4.3 and 4.7).^{198,200} For example, the concentrations of TEOA, the photosensitiser and/or MV could be changed or experiments could be performed in a different buffer. Alternatively, new photosensitisers such as Rose Bengal (or other xanthene-dyes)^{242,243} or metal porphyrins and phthalocyanines²⁴⁴ could be screened with each SED (see **Table 4.3**). A similar optimisation of reaction conditions was reported recently in Honda et al. (2017) to enhance light-driven H₂-evolution by a hydrogenase-producing *E. coli* strain (see **Table 1.5**, example A) where changing the photosensitiser from anatase titanium dioxide to P-25 titanium dioxide increased the quantum yield from 0.3 to 26.4 % (with monochromatic light at 300 nm).²⁴⁵ Another way to improve the efficiency of photocatalysis could be to vary the growth conditions (e.g. growth medium, incubation time, concentrations of electron donor and acceptor) to favour production of particular enzymes by MR-1. This could include culturing MR-1 under acceptor-limited conditions for > 24 hr before harvesting bacteria for increased formation of the [FeFe]-hydrogenase, as reported in Kreuzer et al. (2014),⁹⁷ or using formate as electron donor instead of lactate to evaluate whether expression of the genes encoding the formate dehydrogenases is increased.

Whilst it is advantageous that wild-type MR-1 can be used to drive four reductive transformations, there are opportunities to develop the MV-mediated system further using genetically modified MR-1 strains or different species of bacteria. For example, it may be possible to knockout multiple genes encoding proteins that act as undesirable electron acceptors to direct electrons towards particular enzymes, as shown in section 5.4 for photo-production of formate using the $\text{HydA}^-/\text{HyaB}^-$ variant. The use of arabinose-inducible over-expression strains (such as the MR-1 mutant reported in Shi et al. (2011) capable of over-expressing the genes encoding the [NiFe]-hydrogenase)⁹⁸ may also represent a way to significantly increase production of the enzymes of interest by the bacterium. Alternatively, it may be possible to engineer mutant strains of MR-1 that can produce non-native (recombinant) enzymes to evaluate whether they display faster rates of photocatalysis than MR-1 enzymes. An example of a potential strain for this work was reported in Sybirna et al. (2008) where the [FeFe]-hydrogenase from *Chlamydomonas reinhardtii* was produced by MR-1.¹³⁸ Another possibility would be to generate mutant MR-1 strains capable of producing cytochrome P450s for stereospecific mono-oxygenation reactions. A comparable approach was reported previously in Park et al. (2015) where *E. coli* was engineered to produce a range of bacterial and human cytochrome P450s for light-driven transformations of drugs and steroids.⁷⁸ To avoid recombinant gene expression, the MV-mediated system could be used in combination with different species of bacteria because porin:cytochrome complexes are not required for electron transfer across the outer membrane (see section 4.6). As an example, the native nitrous oxide reductase in *Paracoccus denitrificans* (a model bacterium for denitrification)^{246,247} could be targeted for the reduction of nitrous oxide to N_2 , which represents removal of a potent greenhouse gas from the atmosphere.

An alternative way to develop the MV-mediated system further would be to find experimental conditions that do not cause a significant decrease in bacterial viability during photocatalysis (see section 4.4.4). This would afford a more sustainable, self-regenerating system where living bacteria can replace or repair enzymes as necessary. This could be achieved by performing experiments in M72 medium rather than buffer (see section 4.7) or by using different combinations of photosensitisers and SEDs (see **Table 4.1** and **4.3**). However, a balance would have to be found between the rates of light-driven electron transfer and the impact on cell viability. On the other hand, photo-production of MV^+ could be achieved with a (photo-)cathode to avoid using a vast excess of TEOA which generates

radical species upon oxidation (see **Fig. 4.16**). It would also be interesting to assess different electron transfer mediators to see whether they have less of an impact on cell viability than MV. Potential reagents include common soluble mediators added to microbial fuel cells such as neutral red or anthraquinone-2,6-disulfonate (AQDS)²⁴⁸ and membrane-intercalating mediators such as those based on the ferrocene moiety.²⁴⁹ However, if the mediator has a more positive reduction potential than the MV^{2+/+} couple then it may not be able to facilitate thermodynamically demanding reactions such as H₂-evolution and CO₂-reduction. In the ideal case, it would be possible to perform light-driven reductive transformations without an exogenous electron shuttle to reduce complexity and avoid any issues with toxicity caused by mediators. The possibility for such a strategy was assessed in chapter 6 using new-generation CD photosensitisers which can be synthesised using cheap and abundant precursors.^{134–136} The preliminary work revealed that N-CD were particularly effective photosensitisers because they showed relatively fast rates of MV²⁺, BV²⁺ and MtrC heme photoreduction in combination with a range of SEDs. Furthermore, it was found that different species of *Shewanella* can be cultured under acceptor-limited conditions for the production of active hydrogenases. Light-driven H₂-evolution was reproducibly facilitated by CN-32 but inconsistent results were seen with MR-1 and MR-4, which may be due to the variations of biological samples. As such, further experiments are required to investigate the variability and determinants of the system, as discussed in section 6.4. Once a better understanding of the system has been realised, the biocompatibility of this approach to cell-based photocatalysis could be assessed by measuring CFU mL⁻¹ (or using a live/dead bacterial viability stain)²⁵⁰ after incubating bacteria with TEOA and N-CD under irradiation. Furthermore, it would be useful to calculate quantum yields through the irradiation of samples with a fixed wavelength of light (see sections 4.3 and 4.5) and investigate the (sustained) photocatalytic reduction of carbon substrates to provide a comprehensive comparison with the MV-mediated system.

Finally, there are future opportunities to directly exploit porin:cytochrome complexes for cell-based photocatalysis with *Shewanellaceae* by covalently attaching a photosensitiser to an extracellular cytochrome. This approach could use photosensitisers such as Ru(bpy)₃²⁺ or fluorescein derivatives linked to the surface of extracellular cytochromes via thiol, amine or carboxylic acid groups.^{67,251,252} This may allow for rapid electron transfer across the bacterial outer membrane due to the close proximity of the photosensitiser to the hemes of the extracellular cytochrome. If the photosensitisers cannot be directly attached to

bacteria *in vivo*, photosensitiser-modified cytochromes could be produced *in vitro* and then combined with bacteria to form functional, light-harvesting porin:cytochrome complexes, as illustrated in **Fig. 7.1** with the MtrCAB complex. To aid in the attachment of photosensitisers (or photosensitiser-modified extracellular cytochromes) to the outer surface of bacteria, experimental protocols are available for the removal of EPS from *Shewanellaceae* with little impact on cell viability (e.g. by using heat treatment at 40 °C).²⁵³ Additionally, it was reported in De Windt et al. (2005) that MR-1 can couple the oxidation of electron donors to the reduction of soluble palladium (II), resulting in the formation of palladium (0) nanoparticles localised to the outer surface of the bacterium and the periplasm.²⁵⁴ Such a process may provide an additional, biologically-produced surface which exogenous photosensitisers could be attached to.

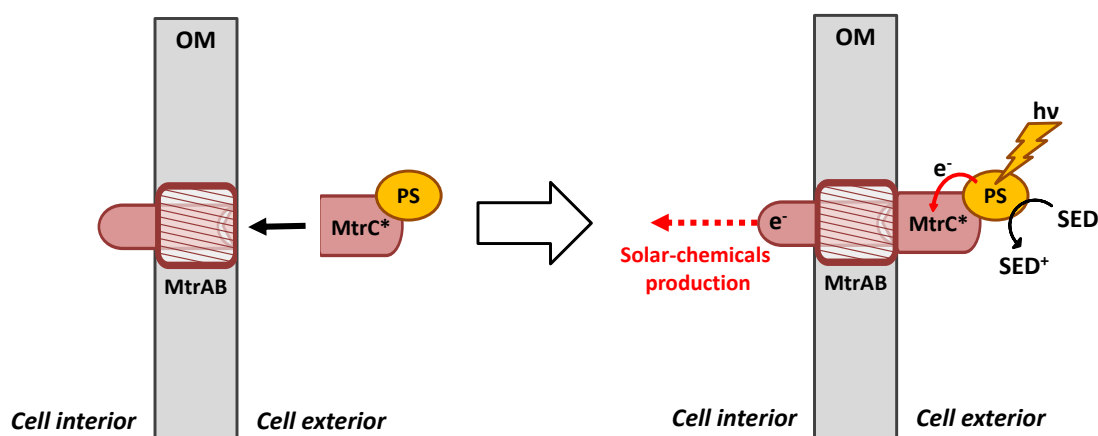


Figure 7.1 - General schematic for solar-chemicals production with *Shewanellaceae* using a photosensitiser-modified MtrC. Left: Combination of a photosensitiser-modified MtrC with a mutant *Shewanella* strain lacking native MtrC. Right: Photon ($h\nu$) absorption by the photosensitiser in the presence of a SED drives electron transfer into the periplasm. OM = outer membrane, PS = photosensitiser, SED = sacrificial electron donor.

Overall, it is envisioned that this type of approach to cell-based photocatalysis would be inherently biocompatible because it is designed to take advantage of the native electron transfer capabilities of *Shewanellaceae*. Work in this area of research is ongoing at the University of East Anglia, UK for the development of bespoke and sustainable approaches to light-driven chemical synthesis with whole-cell bacteria.

References

1. Tran, P. D., Wong, L. H., Barber, J. & Loo, J. S. C. Recent advances in hybrid photocatalysts for solar fuel production. *Energy Environ. Sci.* **5**, 5902–5918 (2012).
2. Frischmann, P. D., Mahata, K. & Würthner, F. Powering the future of molecular artificial photosynthesis with light-harvesting metallocsupramolecular dye assemblies. *Chem. Soc. Rev.* **42**, 1847–1870 (2013).
3. Barber, J. & Tran, P. D. From natural to artificial photosynthesis. *J. R. Soc. Interface* **10**, 1–16 (2013).
4. Armaroli, N. & Balzani, V. Solar electricity and solar fuels: status and perspectives in the context of the energy transition. *Chem. Eur. J.* **22**, 32–57 (2016).
5. British Petroleum, BP statistical review of world energy: June 2016. <http://www.bp.com> 1–44 (2015).
6. Speight, J. G. *Petroleum chemistry and refining*. (Taylor & Francis, 1997).
7. Miller, R. G. & Sorrell, S. R. The future of oil supply. *Phil. Trans. R. Soc. A* **372**, 1–27 (2014).
8. Abas, N., Kalair, A. & Khan, N. Review of fossil fuels and future energy technologies. *Futures* **69**, 31–49 (2015).
9. Hardy, J. T. *Climate change: causes, effects and solutions*. (Wiley, 2003).
10. Schobert, H. *Chemistry of fossil fuels and biofuels*. (Cambridge University Press, 2013).
11. McAllister, S., Chen, J.-Y. & Fernandez-Pello, A. C. *Fundamentals of combustion processes*. (Springer-Verlag New York, 2011).
12. Höök, M. & Tang, X. Depletion of fossil fuels and anthropogenic climate change - a review. *Energy Policy* **52**, 797–809 (2013).
13. MacFarling Meure, C. *et al.* Law Dome CO₂, CH₄ and N₂O ice core records extended to 2000 years BP. *Geophys. Res. Lett.* **33**, 1–4 (2006).
14. Dr. Pieter Tans, NOAA/ESRL (www.esrl.noaa.gov/gmd/ccgg/trends/) and Dr. Ralph Keeling, Scripps Institution of Oceanography (scrippsco2.ucsd.edu/).
15. Etheridge, D.M., *et al.* 2010. Law Dome Ice Core 2000-Year CO₂, CH₄, and N₂O Data. IGBP PAGES/World Data Center for Paleoclimatology Data Contribution Series #2010-070. NOAA/NCDC Paleoclimatology Program, Boulder CO, USA.
16. Church, J. A. & White, N. J. Sea-level rise from the late 19th to the early 21st century. *Surv. Geophys.* **32**, 585–602 (2011).
17. Hansen, J., Ruedy, R., Sato, M. & Lo, K. Global surface temperature change. *Rev. Geophys.* **48**, 1–29 (2010).
18. Cook, J. *et al.* Consensus on consensus: a synthesis of consensus estimates on human-caused global warming. *Environ. Res. Lett.* **11**, 1–7 (2016).
19. Wheeler, T. & Braun, J. Von. Climate change impacts on global food security. *Science* **341**,

-
- 508–513 (2013).
20. Cleaveland, M. K. Plain facts about anthropogenic global climate change and warming: a review. *J. Ark. Acad. Sci.* **70**, 64–76 (2016).
 21. Thomas, C. D. *et al.* Extinction risk from climate change. *Nature* **427**, 145–148 (2004).
 22. Doney, S. C., Fabry, V. J., Feely, R. A. & Kleypas, J. A. Ocean acidification: the other CO₂ problem. *Annu. Rev. Mar. Sci.* **1**, 169–192 (2009).
 23. Schobert, H. H. & Song, C. Chemicals and materials from coal in the 21st century. *Fuel* **81**, 15–32 (2002).
 24. Roddy, D. J. Biomass in a petrochemical world. *Interface Focus* **3**, 1–8 (2013).
 25. Vennestrøm, P. N. R., Osmundsen, C. M., Christensen, C. H. & Taarning, E. Beyond petrochemicals: the renewable chemicals industry. *Angew. Chem. Int. Ed.* **50**, 10502–10509 (2011).
 26. *International energy outlook 2016, US Energy Information Association (EIA)*. (2016).
 27. Ellabban, O., Abu-Rub, H. & Blaabjerg, F. Renewable energy resources: current status, future prospects and their enabling technology. *Renew. Sustain. Energy Rev.* **39**, 748–764 (2014).
 28. Kruse, O., Rupprecht, J., Mussgnug, J. H., Dismukes, G. C. & Hankamer, B. Photosynthesis: a blueprint for solar energy capture and biohydrogen production technologies. *Photochem. Photobiol. Sci.* **4**, 957–970 (2005).
 29. Royal Society of Chemistry (RSC). *Solar fuels and artificial photosynthesis: science and innovation to change our future energy options*. (2012).
 30. Deibel, C. & Dyakonov, V. Polymer–fullerene bulk heterojunction solar cells. *Rep. Prog. Phys.* **73**, 1–39 (2010).
 31. Liu, F., Gu, Y., Jung, J. W., Jo, W. H. & Russell, T. P. On the morphology of polymer-based photovoltaics. *J. Polym. Sci. Pol. Phys.* **50**, 1018–1044 (2012).
 32. Wright, M. & Uddin, A. Organic-inorganic hybrid solar cells: a comparative review. *Sol. Energy Mater. Sol. Cells* **107**, 87–111 (2012).
 33. Su, J. & Vayssieres, L. A place in the sun for artificial photosynthesis? *ACS Energy Lett.* **1**, 121–135 (2016).
 34. Kannan, N. & Vakeesan, D. Solar energy for future world: - a review. *Renew. Sustain. Energy Rev.* **62**, 1092–1105 (2016).
 35. Green, M. A., Emery, K., Hishikawa, Y., Warta, W. & Dunlop, E. D. Solar cell efficiency tables (version 38). *Prog. Photovoltaics* **19**, 565–572 (2011).
 36. Saga, T. Advances in crystalline silicon solar cell technology for industrial mass production. *NPG Asia Mater.* **2**, 96–102 (2010).
 37. Son, H. J., Carsten, B., Jung, I. H. & Yu, L. Overcoming efficiency challenges in organic solar cells: rational development of conjugated polymers. *Energy Environ. Sci.* **5**, 8158 (2012).
 38. Bian, L., Zhu, E., Tang, J., Tang, W. & Zhang, F. Recent progress in the design of narrow bandgap conjugated polymers for high-efficiency organic solar cells. *Prog. Poly. Sci.* **37**,

-
- 1292–1331 (2012).
39. Yilmaz, F., Balta, M. T. & Selbaş, R. A review of solar based hydrogen production methods. *Renew. Sustain. Energy Rev.* **56**, 171–178 (2016).
 40. Dunn, B., Kamath, H. & Tarascon, J.-M. Electrical energy storage for the grid: a battery of choices. *Science* **334**, 928–935 (2011).
 41. Chen, H. *et al.* Progress in electrical energy storage system: a critical review. *Prog. Nat. Sci.* **19**, 291–312 (2009).
 42. Reisner, E. Solar hydrogen evolution with hydrogenases: from natural to hybrid systems. *Eur. J. Inorg. Chem.* 1005–1016 (2011).
 43. Bren, K. L. Multidisciplinary approaches to solar hydrogen. *J. R. Soc. Interface* **5**, 1–12 (2015).
 44. Blankenship, R. E. *et al.* Comparing photosynthetic and photovoltaic efficiencies and recognizing the potential for improvement. *Science* **332**, 805–809 (2011).
 45. Eroglu, E. & Melis, A. Microalgal hydrogen production research. *Int. J. Hydrog. Energy* **41**, 12772–12798 (2016).
 46. Hemschemeier, A., Melis, A. & Happe, T. Analytical approaches to photobiological hydrogen production in unicellular green algae. *Photosynth. Res.* **102**, 523–540 (2009).
 47. Oey, M., Sawyer, A. L., Ross, I. L. & Hankamer, B. Challenges and opportunities for hydrogen production from microalgae. *Plant Biotechnol. J.* **14**, 1487–1499 (2016).
 48. Torzillo, G., Scoma, A., Faraloni, C. & Giannelli, L. Advances in the biotechnology of hydrogen production with the microalga *Chlamydomonas reinhardtii*. *Crit. Rev. Biotechnol.* **35**, 1–12 (2014).
 49. Pellegrin, Y. & Odobel, F. Sacrificial electron donor reagents for solar fuel production. *Comptes Rendus Chim.* (2016).
 50. Crabtree, G. W., Dresselhaus, M. S. & Buchanan, M. V. The hydrogen economy. *Phys. Today* **57**, 39–44 (2004).
 51. Shi, J. *et al.* Enzymatic conversion of carbon dioxide. *Chem. Soc. Rev.* **44**, 5981–6000 (2015).
 52. Casci, J. L., Lok, C. M. & Shannon, M. D. Fischer-Tropsch catalysis: the basis for an emerging industry with origins in the early 20th Century. *Catal. Today* **145**, 38–44 (2009).
 53. Moret, S., Dyson, P. J. & Laurency, G. Direct synthesis of formic acid from carbon dioxide by hydrogenation in acidic media. *Nat. Commun.* **5**, 1–7 (2014).
 54. Singh, A. K., Singh, S. & Kumar, A. Hydrogen energy future with formic acid: a renewable chemical hydrogen storage system. *Catal. Sci. Technol.* **6**, 12–40 (2016).
 55. Pérez-Fortes, M., Schöneberger, J. C., Boulamanti, A., Harrison, G. & Tzimas, E. Formic acid synthesis using CO₂ as raw material: techno-economic and environmental evaluation and market potential. *Int. J. Hydrog. Energy* **41**, 16444–16462 (2016).
 56. Obert, R. & Dave, B. C. Enzymatic conversion of carbon dioxide to methanol: enhanced methanol production in silica sol-gel matrices. *J. Am. Chem. Soc.* **121**, 12192–12193 (1999).
 57. Kiwi, J. & Graetzel, M. Projection, size factors, and reaction dynamics of colloidal redox

-
- catalysts mediating light induced hydrogen evolution from water. *J. Am. Chem. Soc.* **101**, 7214–7217 (1979).
58. Miller, D. S., Bard, A. J., McLendon, G. & Ferguson, J. Catalytic water reduction at colloidal metal ‘microelectrodes’. 2. Theory and experiment. *J. Am. Chem. Soc.* **103**, 5336–5341 (1981).
59. Reda, T., Plugge, C. M., Abram, N. J. & Hirst, J. Reversible interconversion of carbon dioxide and formate by an electroactive enzyme. *P. Natl. Acad. Sci. USA* **105**, 10654–10658 (2008).
60. Fontecilla-Camps, J. C., Volbeda, A., Cavazza, C. & Nicolet, Y. Structure/function relationships of [NiFe]- and [FeFe]-hydrogenases. *Chem. Rev.* **107**, 4273–4303 (2007).
61. Soboh, B. *et al.* The respiratory molybdo-selenoprotein formate dehydrogenases of *Escherichia coli* have hydrogen: benzyl viologen oxidoreductase activity. *BMC Microbiol.* **11**, 1–10 (2011).
62. Sultana, S., Chandra Sahoo, P., Martha, S. & Parida, K. A review of harvesting clean fuels from enzymatic CO₂ reduction. *RSC Adv.* **6**, 44170–44194 (2016).
63. Ghosh, S. *et al.* Hydrogenase biomimetics: Fe₂(CO)₄(μ-dppf)(μ-pdt) (dppf = 1,10-bis(diphenylphosphino)ferrocene) both a proton-reduction and hydrogen oxidation catalyst. *Chem. Commun.* **50**, 945–947 (2014).
64. Sugimoto, H. *et al.* A new series of bis(ene-1,2-dithiolato)tungsten(IV), -(V), -(VI) complexes as reaction centre models of tungsten enzymes: preparation, crystal structures and spectroscopic properties. *Dalt. Trans.* **42**, 3059–3070 (2013).
65. Yadav, R. K. *et al.* A photocatalyst–enzyme coupled artificial photosynthesis system for solar energy in production of formic acid from CO₂. *J. Am. Chem. Soc.* **134**, 11455–11461 (2012).
66. Lubner, C. E. *et al.* Wiring an [FeFe]-hydrogenase with photosystem I for light-induced hydrogen production. *Biochemistry* **49**, 10264–10266 (2010).
67. Zadvornyy, O. A. *et al.* Photo-induced H₂ production by [NiFe]-hydrogenase from *T. roseopersicina* covalently linked to a Ru(II) photosensitizer. *J. Inorg. Biochem.* **106**, 151–155 (2012).
68. Bachmeier, A. & Armstrong, F. Solar-driven proton and carbon dioxide reduction to fuels - lessons from metalloenzymes. *Curr. Opin. Chem. Biol.* **25**, 141–151 (2015).
69. Jones, A. K., Sillery, E., Albracht, S. P. J. & Armstrong, F. A. Direct comparison of the electrocatalytic oxidation of hydrogen by an enzyme and a platinum catalyst. *Chem. Commun.* 866–867 (2002).
70. Kim, J. H., Nam, D. H. & Park, C. B. Nanobiocatalytic assemblies for artificial photosynthesis. *Curr. Opin. Biotech.* **28**, 1–9 (2014).
71. O’Reilly, E., Köhler, V., Flitsch, S. L. & Turner, N. J. Cytochromes P450 as useful biocatalysts: addressing the limitations. *Chem. Commun.* **47**, 2490–501 (2011).
72. Wang, F. *et al.* A highly efficient photocatalytic system for hydrogen production by a robust hydrogenase mimic in an aqueous solution. *Angew. Chem. Int. Ed.* **123**, 3251–3255 (2011).

-
73. Lakadamyali, F. & Reisner, E. Photocatalytic H₂ evolution from neutral water with a molecular cobalt catalyst on a dye-sensitised TiO₂ nanoparticle. *Chem. Commun.* **47**, 1695–1697 (2011).
 74. Sato, S., Morikawa, T., Saeki, S., Kajino, T. & Motohiro, T. Visible-light-induced selective CO₂ reduction utilizing a ruthenium complex electrocatalyst linked to a p-type nitrogen-doped Ta₂O₅ semiconductor. *Angew. Chem. Int. Ed.* **49**, 5101–5105 (2010).
 75. Utschig, L. M., Soltau, S. R. & Tiede, D. M. Light-driven hydrogen production from photosystem I-catalyst hybrids. *Curr. Opin. Chem. Biol.* **25**, 1–8 (2015).
 76. Amao, Y. Solar fuel production based on the artificial photosynthesis system. *ChemCatChem* **3**, 458–474 (2011).
 77. Sakimoto, K. K., Wong, A. B. & Yang, P. Self-photosensitization of nonphotosynthetic bacteria for solar-to-chemical production. *Science* **351**, 74–77 (2016).
 78. Park, J. H. *et al.* Cofactor-free light-driven whole-cell cytochrome P450 catalysis. *Angew. Chem. Int. Ed.* **54**, 969–973 (2015).
 79. Torella, J. P. *et al.* Efficient solar-to-fuels production from a hybrid microbial–water-splitting catalyst system. *P. Natl. Acad. Sci. USA* **112**, 2337–2342 (2015).
 80. Liu, C., Colón, B. C., Ziesack, M., Silver, P. A. & Nocera, D. G. Water splitting – biosynthetic system with CO₂ reduction efficiencies exceeding photosynthesis. *Science* **352**, 1210–1213 (2016).
 81. Liu, C. *et al.* Nanowire-bacteria hybrids for unassisted solar carbon dioxide fixation to value-added chemicals. *Nano Lett.* **15**, 3634–3639 (2015).
 82. Honda, Y., Hagiwara, H., Ida, S. & Ishihara, T. Application to photocatalytic H₂ production of a whole-cell reaction by recombinant *Escherichia coli* cells expressing [FeFe]-hydrogenase and maturases genes. *Angew. Chem. Int. Ed.* **55**, 8045–8048 (2016).
 83. Myers, C. R. & Nealson, K. H. Bacterial manganese reduction and growth with manganese oxide as the sole electron acceptor. *Science* **240**, 1319–1321 (1988).
 84. Hartshorne, R. S. *et al.* Characterization of *Shewanella oneidensis* MtrC: a cell-surface decaheme cytochrome involved in respiratory electron transport to extracellular electron acceptors. *J. Biol. Inorg. Chem.* **12**, 1083–1094 (2007).
 85. Breuer, M., Rosso, K. M., Blumberger, J. & Butt, J. N. Multi-haem cytochromes in *Shewanella oneidensis* MR-1: structures, functions and opportunities. *J. R. Soc. Interface* **12**, 1–27 (2015).
 86. Burns, J. L. & Dichristina, T. J. Anaerobic respiration of elemental sulfur and thiosulfate by *Shewanella oneidensis* MR-1 requires *psrA*, a homolog of the *phsA* gene of *Salmonella enterica* Serovar Typhimurium LT2. *Appl. Environ. Microbiol.* **75**, 5209–5217 (2009).
 87. Gralnick, J. A., Vali, H., Lies, D. P. & Newman, D. K. Extracellular respiration of dimethyl sulfoxide by *Shewanella oneidensis* strain MR-1. *P. Natl. Acad. Sci. USA* **103**, 4669–4674 (2006).
 88. Nealson, K. H. & Saffarini, D. Iron and manganese in anaerobic respiration: environmental

-
- significance, physiology, and regulation. *Annu. Rev. Microbiol.* **48**, 311–343 (1994).
89. Marritt, S. J. *et al.* The roles of CymA in support of the respiratory flexibility of *Shewanella oneidensis* MR-1. *Biochem. Soc. Trans.* **40**, 1217–1221 (2012).
 90. Cruz-García, C., Murray, A. E., Klappenbach, J. A., Stewart, V. & Tiedje, J. M. Respiratory nitrate ammonification by *Shewanella oneidensis* MR-1. *J. Bacteriol.* **189**, 656–662 (2007).
 91. Meshulam-Simon, G., Behrens, S., Choo, A. D. & Spormann, A. M. Hydrogen metabolism in *Shewanella oneidensis* MR-1. *Appl. Environ. Microbiol.* **73**, 1153–1165 (2007).
 92. Liu, C., Gorby, Y. A., Zachara, J. M., Fredrickson, J. K. & Brown, C. F. Reduction kinetics of Fe(III), Co(III), U(VI), Cr(VI), and Tc(VII) in cultures of dissimilatory metal-reducing bacteria. *Biotechnol. Bioeng.* **80**, 637–649 (2002).
 93. Pinchuk, G. E. *et al.* Pyruvate and lactate metabolism by *Shewanella oneidensis* MR-1 under fermentation, oxygen limitation, and fumarate respiration conditions. *Appl. Environ. Microbiol.* **77**, 8234–8240 (2011).
 94. Kane, A. L. *et al.* Formate metabolism in *Shewanella oneidensis* generates proton motive force and prevents growth without an electron acceptor. *J. Bacteriol.* **198**, 1337–1346 (2016).
 95. Kouzuma, A., Kasai, T., Hirose, A. & Watanabe, K. Catabolic and regulatory systems in *Shewanella oneidensis* MR-1 involved in electricity generation in microbial fuel cells. *Front. Microbiol.* **6**, 1–11 (2015).
 96. Marritt, S. J. *et al.* A functional description of CymA, an electron-transfer hub supporting anaerobic respiratory flexibility in *Shewanella*. *Biochem. J.* **444**, 465–474 (2012).
 97. Kreuzer, H. W. *et al.* Contributions of the [NiFe]- and [FeFe]-hydrogenase to H₂ production in *Shewanella oneidensis* MR-1 as revealed by isotope ratio analysis of evolved H₂. *FEMS Microbiol. Lett.* **352**, 18–24 (2014).
 98. Shi, L. *et al.* Purification and characterization of the [NiFe]-hydrogenase of *Shewanella oneidensis* MR-1. *Appl. Environ. Microbiol.* **77**, 5584–5590 (2011).
 99. Myers, C. R. & Myers, J. M. Fumarate reductase is a soluble enzyme in anaerobically grown *Shewanella putrefaciens* MR-1. *FEMS Microbiol. Lett.* **98**, 13–20 (1992).
 100. Reeve, H. A. *et al.* Enzymes as modular catalysts for redox half reactions in H₂-powered chemical synthesis: from biology to technology. *Biochem. J.* **474**, 215–230 (2017).
 101. Berg, J. M., Tymoczko, J. L. & Stryer, L. *Biochemistry, 5th Edition*. (W. H. Freeman & Co. Ltd., 2002).
 102. Heidelberg, J. F. *et al.* Genome sequence of the dissimilatory metal ion-reducing bacterium *Shewanella oneidensis*. *Nat. Biotech.* **20**, 1118–1123 (2002).
 103. Cruz-García, C. *et al.* Fnr (EtrA) acts as a fine-tuning regulator of anaerobic metabolism in *Shewanella oneidensis* MR-1. *BMC Microbiol.* **11**, 1–14 (2011).
 104. Le Laz, S., Kpebe, A., Lorquin, J., Brugna, M. & Rousset, M. H₂-dependent azoreduction by *Shewanella oneidensis* MR-1: involvement of secreted flavins and both [Ni-Fe] and [Fe-Fe]

-
- hydrogenases. *Appl. Microbiol. Biotechnol.* **98**, 2699–2707 (2014).
105. Brigé, A. *et al.* Bacterial decolorization of textile dyes is an extracellular process requiring a multicomponent electron transfer pathway. *Microb. Biotechnol.* **1**, 40–52 (2008).
 106. Leys, D. *et al.* Structure and mechanism of the flavocytochrome *c* fumarate reductase of *Shewanella putrefaciens* MR-1. *Nat. Struct. Biol.* **6**, 1113–1117 (1999).
 107. Paquete, C. M., Saraiva, I. H. & Louro, R. O. Redox tuning of the catalytic activity of soluble fumarate reductases from *Shewanella*. *Biochim. Biophys. Acta* **1837**, 717–725 (2014).
 108. Pessanha, M. *et al.* Tuning of functional heme reduction potentials in *Shewanella* fumarate reductases. *Biochim. Biophys. Acta* **1787**, 113–120 (2009).
 109. Fonseca, B. M. *et al.* Mind the gap: cytochrome interactions reveal electron pathways across the periplasm of *Shewanella oneidensis* MR-1. *J. Biochem.* **449**, 101–108 (2013).
 110. Bachmeier, A., Murphy, B. J. & Armstrong, F. A. A multi-heme flavoenzyme as a solar conversion catalyst. *J. Am. Chem. Soc.* **136**, 12876–12879 (2014).
 111. Koninger, K. *et al.* Recombinant Cyanobacteria for the asymmetric reduction of C=C bonds fueled by the biocatalytic oxidation of water. *Angew. Chem. Int. Ed.* **55**, 5582–5585 (2016).
 112. Cao, Y. *et al.* Fermentative succinate production: an emerging technology to replace the traditional petrochemical processes. *Biomed. Res. Int.* **723412**, 1–12 (2013).
 113. Bozell, J. J. & Petersen, G. R. Technology development for the production of biobased products from biorefinery carbohydrates - the US Department of Energy's 'Top 10' revisited. *Green Chem.* **12**, 539–554 (2010).
 114. Pinchuk, G. E. *et al.* Genomic reconstruction of *Shewanella oneidensis* MR-1 metabolism reveals a previously uncharacterized machinery for lactate utilization. *P. Natl. Acad. Sci. USA* **106**, 2874–2879 (2009).
 115. Brutinel, E. D. & Gralnick, J. A. Preferential utilization of D-lactate by *Shewanella oneidensis*. *Appl. Environ. Microbiol.* **78**, 8474–8476 (2012).
 116. Hu, Y., Daoud, W. A., Cheuk, K. K. L. & Lin, C. S. K. Newly developed techniques on polycondensation, ring-opening polymerization and polymer modification: focus on poly(lactic acid). *Materials (Basel)*. **9**, 1–14 (2016).
 117. Ghaffar, T. *et al.* Recent trends in lactic acid biotechnology: a brief review on production to purification. *J. Radiat. Res. Appl. Sci.* **7**, 222–229 (2014).
 118. Beliaev, A. S. *et al.* Global transcriptome analysis of *Shewanella oneidensis* MR-1 exposed to different terminal electron acceptors. *J. Bacteriol.* **187**, 7138–7145 (2005).
 119. White, G. F. *et al.* Mechanisms of bacterial extracellular electron exchange. *Adv. Microb. Physiol.* **68**, 87–138 (2016).
 120. McLean, J. S. *et al.* Oxygen-dependent autoaggregation in *Shewanella oneidensis* MR-1. *Environ. Microbiol.* **10**, 1861–1876 (2008).
 121. Ross, D. E. *et al.* Characterization of protein-protein interactions involved in iron reduction by *Shewanella oneidensis* MR-1. *Appl. Environ. Microbiol.* **73**, 5797–5808 (2007).

-
122. Richardson, D. J. *et al.* The 'porin-cytochrome' model for microbe-to-mineral electron transfer. *Mol. Microbiol.* **85**, 201–212 (2012).
 123. Richardson, D. J. *et al.* Exploring the biochemistry at the extracellular redox frontier of bacterial mineral Fe(III) respiration. *Biochem. Soc. Trans.* **40**, 493–500 (2012).
 124. Hartshorne, R. S. *et al.* Characterization of an electron conduit between bacteria and the extracellular environment. *P. Natl. Acad. Sci. USA* **106**, 22169–22174 (2009).
 125. White, G. F. *et al.* Development of a proteoliposome model to probe transmembrane electron-transfer reactions. *Biochem. Soc. Trans.* **40**, 1257–1260 (2012).
 126. White, G. F. *et al.* Rapid electron exchange between surface-exposed bacterial cytochromes and Fe(III) minerals. *P. Natl. Acad. Sci. USA* **110**, 6346–6351 (2013).
 127. Brutinel, E. D. & Gralnick, J. A. Shuttling happens: soluble flavin mediators of extracellular electron transfer in *Shewanella*. *Appl. Microbiol. Biotechnol.* **93**, 41–48 (2012).
 128. Marsili, E. *et al.* *Shewanella* secretes flavins that mediate extracellular electron transfer. *P. Natl. Acad. Sci. USA* **105**, 3968–3973 (2008).
 129. Pirbadian, S. *et al.* *Shewanella oneidensis* MR-1 nanowires are outer membrane and periplasmic extensions of the extracellular electron transport components. *P. Natl. Acad. Sci. USA* **111**, 12883–12888 (2014).
 130. Ross, D. E., Flynn, J. M., Baron, D. B., Gralnick, J. A. & Bond, D. R. Towards electrosynthesis in *Shewanella*: energetics of reversing the Mtr pathway for reductive metabolism. *PLoS One* **6**, e16649 (2011).
 131. Hsu, L., Masuda, S. A., Nealson, K. H. & Pirbazeri, M. Evaluation of microbial fuel cell *Shewanella* biocathodes for treatment of chromate contamination. *RSC Adv.* **2**, 5844 (2012).
 132. Ainsworth, E. V. *et al.* Photoreduction of *Shewanella oneidensis* extracellular cytochromes by organic chromophores and dye-sensitized TiO₂. *ChemBioChem* **17**, 2324–2333 (2016).
 133. Gillaizeau-Gauthier, I. *et al.* Phosphonate-based bipyridine dyes for stable photovoltaic devices. *Inorg. Chem.* **40**, 6073–6079 (2001).
 134. Martindale, B. C. M., Hutton, G. A. M., Caputo, C. A. & Reisner, E. Solar hydrogen production using carbon quantum dots and a molecular nickel catalyst. *J. Am. Chem. Soc.* **137**, 6018–6025 (2015).
 135. Hutton, G. A. M. *et al.* Carbon dots as versatile photosensitizers for solar-driven catalysis with redox enzymes. *J. Am. Chem. Soc.* **138**, 16722–16730 (2016).
 136. Martindale, B. C. M. *et al.* Enhancing light absorption and charge transfer efficiency in carbon dots through graphitization and core nitrogen doping. *Angew. Chem. Int. Ed.* **56**, 6459–6463 (2017).
 137. Edwards, M. J. *et al.* Redox linked flavin sites in extracellular decaheme proteins involved in microbe-mineral electron transfer. *Sci. Rep.* **5**, 1–11 (2015).
 138. Sybirna, K. *et al.* *Shewanella oneidensis*: a new and efficient system for expression and maturation of heterologous [Fe-Fe] hydrogenase from *Chlamydomonas reinhardtii*. *BMC*

-
- Biotechnol.* **8**, 1–8 (2008).
139. Marshall, M. J. *et al.* Hydrogenase- and outer membrane *c*-type cytochrome-facilitated reduction of technetium(VII) by *Shewanella oneidensis* MR-1. *Environ. Microbiol.* **10**, 125–136 (2008).
 140. Liu, J. *et al.* Identification and characterization of MtoA: a decaheme *c*-type cytochrome of the neutrophilic Fe(II)-oxidizing bacterium *Sideroxydans lithotrophicus* ES-1. *Front. Microbiol.* **3**, 1–11 (2012).
 141. Nealson, K. H., Myers, C. R. & Wimpee, B. B. Isolation and identification of manganese-reducing bacteria and estimates of microbial Mn(IV)-reducing potential in the Black Sea. *Deep Sea Res. A* **38**, S907–S920 (1991).
 142. Venkateswaran, K., Dollhopf, M. E., Aller, R., Stackebrandt, E. & Nealson, K. H. *Shewanella amazonensis* sp. nov., a novel metal-reducing facultative anaerobe from Amazonian shelf muds. *Int. J. Syst. Bacteriol.* **48**, 965–972 (1998).
 143. Saltikov, C. W., Cifuentes, A., Venkateswaran, K. & Newman, D. K. The *ars* detoxification system is advantageous but not required for As(V) respiration by the genetically tractable *Shewanella* species strain ANA-3. *Appl. Environ. Microbiol.* **69**, 2800–2809 (2003).
 144. Brettar, I., Moore, E. R. B. & Höfle, M. G. Phylogeny and abundance of novel denitrifying bacteria isolated from the water column of the Central Baltic Sea. *Microb. Ecol.* **42**, 295–305 (2001).
 145. Gao, H. *et al.* *Shewanella loihica* sp. nov., isolated from iron-rich microbial mats in the Pacific Ocean. *Int. J. Syst. Evol. Microbiol.* **56**, 1911–1916 (2006).
 146. Fredrickson, J. K. *et al.* Biogenic iron mineralization accompanying the dissimilatory reduction of hydrous ferric oxide by a groundwater bacterium. *Geochim. Cosmochim. Acta.* **62**, 3239–3257 (1998).
 147. Obuekwe, C. O. & Westlake, D. W. S. Effects of medium composition on cell pigmentation, cytochrome content, and ferric iron reduction in a *Pseudomonas* sp. isolated from crude oil. *Can. J. Microbiol.* **28**, 989–992 (1982).
 148. Murray, A. E. *et al.* DNA/DNA hybridization to microarrays reveals gene-specific differences between closely related microbial genomes. *P. Natl. Acad. Sci. USA* **98**, 9853–9858 (2001).
 149. Smith, P. K. *et al.* Measurement of protein using bicinchoninic acid. *Anal. Biochem.* **150**, 76–85 (1985).
 150. Steinberg, T. H. *Guide to protein purification: protein gel staining methods, an introduction and overview (chapter 31).* *Methods Enzymol.* **463**, (Elsevier Inc., 2009).
 151. Goodhew, C. F., Brown, K. R. & Pettigrew, G. W. Haem staining in gels, a useful tool in the study of bacterial *c*-type cytochromes. *Biochim. Biophys. Acta* **852**, 288–294 (1986).
 152. Thomas, P. E., Ryan, D. & Levin, W. An improved staining procedure for the detection of the peroxidase activity of cytochrome P-450 on sodium dodecyl sulfate polyacrylamide gels. *Anal. Biochem.* **75**, 168–176 (1976).

-
153. Guo, Y., Ma, Q., Cao, F., Zhao, Q. & Ji, X. Colorimetric detection of hypochlorite in tap water based on the oxidation of 3,3',5,5'-tetramethyl benzidine. *Anal. Methods* **7**, 4055–4058 (2015).
 154. McGadey, J. A tetrazolium method for non-specific alkaline phosphatase. *Histochemie* **23**, 180–184 (1970).
 155. Sinha, P. Detection of alkaline phosphatase activity after conventional isoelectric focusing by an indoxyl-tetrazolium salt technique. *J. Biochem. Biophys. Meth.* **11**, 327–340 (1985).
 156. Sander, R. Compilation of Henry's law constants (version 4.0) for water as solvent. *Atmos. Chem. Phys.* **15**, 4399–4981 (2015).
 157. Jones, R. W. The topography of the membrane-bound hydrogenase of *Escherichia coli* explored by non-physiological electron acceptors. *Biochem. Soc. Trans.* **7**, 724–725 (1979).
 158. Watanabe, T. & Honda, K. Measurement of the extinction coefficient of the methyl viologen cation radical and the efficiency of its formation by semiconductor photocatalysts. *J. Phys. Chem.* **86**, 2617–2619 (1982).
 159. Torche, F. & Marignier, J. L. Direct evaluation of the molar absorption coefficient of hydrated electron by the isosbestic point method. *J. Phys. Chem. B* **120**, 7201–7206 (2016).
 160. Ala-Korpela, M. ¹H-NMR spectroscopy of human blood plasma. *Prog. Nucl. Magn. Reson. Spectrosc.* **27**, 475–554 (1995).
 161. Keeler, J. & Wothers, P. *Chemical structure and reactivity: an integrated approach*. (Oxford University Press (OUP), 2008).
 162. Alkins, P. & Paula, J. D. *Atkins' physical chemistry*. (Oxford University Press (OUP), 2006).
 163. Matulova, M. *et al.* NMR study of cellulose and wheat straw degradation by *Ruminococcus albus* 20. *FEBS J.* **275**, 3503–3511 (2008).
 164. Lourenço, A. B., Roque, F. C., Teixeira, M. C., Ascenso, J. R. & Sá-Correia, I. Quantitative ¹H-NMR-metabolomics reveals extensive metabolic reprogramming and the effect of the aquaglyceroporin *FPS1* in ethanol-stressed yeast cells. *PLoS One* **8**, 1–12 (2013).
 165. Michaelis, L. & Hill, E. S. The viologen indicators. *J. Gen. Physiol.* **16**, 859–873 (1933).
 166. Pinske, C. *et al.* Physiology and bioenergetics of [NiFe]-hydrogenase 2-catalysed H₂ consuming and H₂ producing reactions in *Escherichia coli*. *J. Bacteriol.* **197**, 296–306 (2015).
 167. Peck, H. D. & Gest, H. Hydrogenase of *Clostridium butylicum*. *J. Bacteriol.* **73**, 569–580 (1957).
 168. Yang, H. *et al.* Isotopic fractionation associated with [NiFe]- and [FeFe]-hydrogenases. *Rapid Commun. Mass Spectrom.* **30**, 285–292 (2016).
 169. Mayhew, S. G. The redox potential of dithionite and SO₂⁻ from equilibrium reactions with flavodoxins, methyl viologen and hydrogen plus hydrogenase. *Eur. J. Biochem.* **85**, 535–547 (1978).
 170. Jones, R. W. & Garland, P. B. Sites and specificity of the reaction of bipyridylum compounds with anaerobic respiratory enzymes of *Echerischia coli*. *Biochem. J.* **164**, 199–211 (1977).

-
171. Pismenskaya, N. *et al.* Dependence of composition of anion-exchange membranes and their electrical conductivity on concentration of sodium salts of carbonic and phosphoric acids. *J. Memb. Sci.* **181**, 185–197 (2001).
 172. Kim, H.-J., Jeon, W. S., Ko, Y. H. & Kim, K. Inclusion of methylviologen in cucurbit[7]uril. *P. Natl. Acad. Sci. USA* **99**, 5007–5011 (2002).
 173. Gottlieb, H. E., Kotlyar, V. & Nudelman, A. NMR chemical shifts of common laboratory solvents as trace impurities. *J. Org. Chem.* **62**, 7512–7515 (1997).
 174. Martins, A. F. *et al.* Spectroscopic, radiochemical, and theoretical studies of the Ga³⁺-N-2-hydroxyethyl piperazine-N'-2-ethanesulfonic acid (HEPES buffer) system: evidence for the formation of Ga³⁺-HEPES complexes in ⁶⁸Ga labeling reactions. *Contrast Media Mol. Imaging* **8**, 265–273 (2013).
 175. Rosenbaum, M. A. *et al.* Transcriptional analysis of *Shewanella oneidensis* MR-1 with an electrode compared to Fe(III)citrate or oxygen as terminal electron acceptor. *PLoS One* **7**, 1–13 (2012).
 176. Tsapin, A. I. *et al.* Identification of a small tetraheme cytochrome *c* and a flavocytochrome *c* as two of the principal soluble cytochromes *c* in *Shewanella oneidensis* strain MR1. *Appl. Environ. Microbiol.* **67**, 3236–3244 (2001).
 177. Schuetz, B., Schicklberger, M., Kuermann, J., Spormann, A. M. & Gescher, J. Periplasmic electron transfer via the *c*-type cytochromes MtrA and FccA of *Shewanella oneidensis* MR-1. *Appl. Environ. Microbiol.* **75**, 7789–7796 (2009).
 178. Josefsen, L. B. & Boyle, R. W. Photodynamic therapy and the development of metal-based photosensitisers. *Met.-Based Drugs* **276109**, 1–24 (2008).
 179. Tucker, J. W. & Stephenson, C. R. J. Shining light on photoredox catalysis: theory and synthetic applications. *J. Org. Chem.* **77**, 1617–1622 (2012).
 180. Romero, N. A. & Nicewicz, D. A. Organic photoredox catalysis. *Chem. Rev.* **116**, 10075–10166 (2016).
 181. Jones, W. E. & Fox, M. A. Determination of excited-state redox potentials by phase-modulated voltammetry. *J. Phys. Chem.* **98**, 5095–5099 (1994).
 182. Heelis, P. F. The photophysical and photochemical properties of flavins (isoalloxazines). *Chem. Soc. Rev.* **11**, 15–39 (1982).
 183. Song, S. H., Dick, B. & Penzkofer, A. Photo-induced reduction of flavin mononucleotide in aqueous solutions. *Chem. Phys.* **332**, 55–65 (2007).
 184. Pileni, M.-P. & Grätzel, M. Light-induced redox reactions of proflavin in aqueous and micellar solution. *J. Phys. Chem.* **84**, 2402–2406 (1980).
 185. Ghosh, T., Slanina, T. & König, B. Visible light photocatalytic reduction of aldehydes by Rh(III)-H: a detailed mechanistic study. *Chem. Sci.* **6**, 2027–2034 (2015).
 186. Kalyanasundaram, K. & Dung, D. Role of proflavin as a photosensitizer for the light-induced hydrogen evolution from water. *J. Phys. Chem.* **84**, 2551–2556 (1980).

-
187. Lazarides, T. *et al.* Making hydrogen from water using a homogeneous system without noble metals. *J. Am. Chem. Soc.* **131**, 9192–9194 (2009).
188. Mau, A. W.-H., Johansen, O. & Sasse, W. H. F. Xanthene dyes as sensitizers for the photoreduction of water. *Photochem. Photobiol.* **41**, 503–509 (1985).
189. Okamoto, A., Hashimoto, K., Nealon, K. H. & Nakamura, R. Rate enhancement of bacterial extracellular electron transport involves bound flavin semiquinones. *P. Natl. Acad. Sci. USA* **110**, 7856–7861 (2013).
190. Bock, C. R. *et al.* Estimation of excited-state redox potentials by electron-transfer quenching. Application of electron-transfer theory to excited-state redox processes. *J. Am. Chem. Soc.* **101**, 4815–4824 (1979).
191. Park, H., Bae, E., Lee, J.-J., Park, J. & Choi, W. Effect of the anchoring group in Ru-bipyridyl sensitizers on the photoelectrochemical behavior of dye-sensitized TiO₂ electrodes: carboxylate versus phosphonate linkages. *J. Phys. Chem.* **110**, 8740–8749 (2006).
192. Gross, M. A., Reynal, A., Durrant, J. R. & Reisner, E. Versatile photocatalytic systems for H₂ generation in water based on an efficient DuBois-type nickel catalyst. *J. Am. Chem. Soc.* **136**, 356–366 (2014).
193. Koziol, J. Fluorometric analyses of riboflavin and its coenzymes. *Methods Enzym.* **18B**, 253–285 (1971).
194. Hernandez, M. E. & Newman, D. K. Extracellular electron transfer. *Cell. Mol. Life Sci.* **58**, 1562–1571 (2001).
195. Von Canstein, H., Ogawa, J., Shimizu, S. & Lloyd, J. R. Secretion of flavins by *Shewanella* species and their role in extracellular electron transfer. *Appl. Environ. Microbiol.* **74**, 615–623 (2008).
196. Edwards, M. J. *et al.* The crystal structure of the extracellular 11-heme cytochrome UndA reveals a conserved 10-heme motif and defined binding site for soluble iron chelates. *Structure* **20**, 1275–1284 (2012).
197. Gurunathan, K., Maruthamuthu, P. & Sastri, M. V. C. Photocatalytic hydrogen production by dye-sensitized Pt/SnO₂ and Pt/SnO₂/RuO₂ in aqueous methyl viologen solution. *Int. J. Hydrog. Energy* **22**, 57–62 (1997).
198. Crutchley, R. J. & Lever, A. B. P. Ruthenium(II) tris(bipyrazyl) dication - a new photocatalyst. *J. Am. Chem. Soc.* **102**, 7128–7129 (1980).
199. Reisner, E., Powell, D. J., Cavazza, C., Fontecilla-Camps, J. C. & Armstrong, F. A. Visible light-driven H₂ production by hydrogenases attached to dye-sensitized TiO₂ nanoparticles. *J. Am. Chem. Soc.* **131**, 18457–18466 (2009).
200. Islam, S. D.-M. *et al.* Photosensitized reduction of methyl viologen using eosin-Y in presence of a sacrificial electron donor in water-alcohol mixture. *Photochem. Photobiol.* **71**, 675–680 (2000).
201. Pal, U., Ghosh, S. & Chatterjee, D. Effect of sacrificial electron donors on hydrogen

-
- generation over visible light-irradiated nonmetal-doped TiO₂ photocatalysts. *Transit. Met. Chem.* **37**, 93–96 (2011).
202. Neshvad, G. & Hoffman, M. Z. Reductive quenching of the luminescent excited state of tris(2,2'-bipyrazine)ruthenium(2+) ion in aqueous solution. *J. Phys. Chem.* **93**, 2445–2452 (1989).
203. Woolerton, T. W., Sheard, S., Pierce, E., Ragsdale, S. W. & Armstrong, F. A. CO₂ photoreduction at enzyme-modified metal oxide nanoparticles. *Energy Environ. Sci.* **4**, 2393–2399 (2011).
204. Peng, S. Q., Peng, Y. J., Li, Y. X., Lu, G. X. & Li, S. B. Photocatalytic hydrogen generation using glucose as electron donor over Pt/Cd_xZn_{1-x}S solid solutions. *Res. Chem. Intermed.* **35**, 739–749 (2009).
205. Taylor, S., Mehta, M. & Samokhvalov, A. Production of hydrogen by glycerol photoreforming using binary nitrogen-metal-promoted N-M-TiO₂ photocatalysts. *ChemPhysChem* **15**, 942–949 (2014).
206. Martindale, B. C. M., Joliat, E., Bachmann, C., Alberto, R. & Reisner, E. Clean donor oxidation enhances the H₂ evolution activity of a carbon quantum dot-molecular catalyst photosystem. *Angew. Chem. Int. Ed.* **55**, 9402–9406 (2016).
207. Prasad, D. R., Hoffman, M. Z., Mulazzani, Q. G. & Rodgers, M. A. J. Pulsed-laser flash and continuous photolysis of aqueous solutions of methyl viologen, oxalate, and their ion-pair complexes. *J. Am. Chem. Soc.* **108**, 5135–5142 (1986).
208. Norena, L. E., Wang, J.-A., Yu, S. & Zhou, Y. *Advanced catalytic materials - photocatalysis and other current trends*. (InTech, 2016).
209. Limburg, B., Bouwman, E. & Bonnet, S. Effect of liposomes on the kinetics and mechanism of the photocatalytic reduction of methyl viologen. *J. Phys. Chem. B* **120**, 6969–6975 (2016).
210. Natali, M. & Deponi, E. Photocatalytic hydrogen evolution with ruthenium polypyridine sensitizers: unveiling the key factors to improve efficiencies. *Dalt. Trans.* **45**, 9136–9147 (2016).
211. Grady, J. K., Chasteen, N. D. & Harris, D. C. Radicals from Good's buffers. *Anal. Biochem.* **173**, 111–115 (1988).
212. Surdhar, P. S. & Armstrong, D. A. Redox potentials of some sulfur-containing radicals. *J. Phys. Chem.* **90**, 5915–5917 (1986).
213. Habib, A., Tabata, M. & Wu, Y. G. Formation of gold nanoparticles by Good's buffers. *Bull. Chem. Soc. Jpn.* **78**, 262–269 (2005).
214. Manke, A.-M., Geisel, K., Fetzer, A. & Kurz, P. A water-soluble tin(IV) porphyrin as a bioinspired photosensitizer for light-driven proton-reduction. *Phys. Chem. Chem. Phys.* **16**, 12029–12042 (2014).
215. Yamada, Y., Miyahigashi, T., Ohkubo, K. & Fukuzumi, S. Photocatalytic hydrogen evolution from carbon-neutral oxalate with 2-phenyl-4-(1-naphthyl)quinolinium ion and metal

-
- nanoparticles. *Phys. Chem. Chem. Phys.* **14**, 10564–10571 (2012).
216. Chang, A. C., Pfeiffer, W. F., Guillaume, B., Baral, S. & Fendler, J. H. Preparation and characterization of selenide semiconductor particles in surfactant vesicles. *J. Phys. Chem.* **94**, 4284–4289 (1990).
217. Das, T. N., Huie, R. E. & Neta, P. Reduction potentials of $\text{SO}_3^{\cdot-}$, $\text{SO}_5^{\cdot-}$, and $\text{S}_4\text{O}_6^{\cdot-}$ radicals in aqueous solution. *J. Phys. Chem. A* **103**, 3581–3588 (1999).
218. Sakai, T., Mersch, D. & Reisner, E. Photocatalytic hydrogen evolution with a hydrogenase in a mediator-free system under high levels of oxygen. *Angew. Chem. Int. Ed.* **52**, 1–5 (2013).
219. Yalloway, G. N., Mayhew, S. G., Malthouse, J. P. G., Gallagher, M. E. & Curley, G. P. pH-dependent spectroscopic changes associated with the hydroquinone of FMN in flavodoxins. *Biochem.* **38**, 3753–3762 (1999).
220. McLaughlin, M. P., McCormick, T. M., Eisenberg, R., Patrick, L. & Holland, P. L. A stable molecular nickel catalyst for the homogeneous photogeneration of hydrogen in aqueous solution. *Chem. Commun.* **47**, 7989–7991 (2011).
221. Bird, C. L. & Kuhn, A. T. Electrochemistry of the viologens. *Chem. Soc. Rev.* **10**, 49–82 (1981).
222. Lerman, L. S. The structure of the DNA-acridine complex. *P. Natl. Acad. Sci. USA* **49**, 94–102 (1963).
223. Wainwright, M. Acridine - a neglected antibacterial chromophore. *J. Antimicrob. Chemother.* **47**, 1–13 (2001).
224. Franklin, T. J. & Snow, G. A. *Biochemistry and molecular biology of antimicrobial drug action.* (Springer, 2006).
225. Hau, H. H., Gilbert, A., Coursolle, D. & Gralnick, J. A. Mechanism and consequences of anaerobic respiration of cobalt by *Shewanella oneidensis* strain MR-1. *Appl. Environ. Microbiol.* **74**, 6880–6886 (2008).
226. Vincent, K. A., Parkin, A. & Armstrong, F. A. Investigating and exploiting the electrocatalytic properties of hydrogenases. *Chem. Rev.* **107**, 4366–4413 (2007).
227. Bhattacharjee, A. & Ahmaruzzaman, M. CuO nanostructures: facile synthesis and applications for enhanced photodegradation of organic compounds and reduction of p-nitrophenol from aqueous phase. *RSC Adv.* **6**, 41348–41363 (2016).
228. Vaidyalingam, A. & Dutta, P. K. Analysis of the photodecomposition products of $\text{Ru}(\text{bpy})_3^{2+}$ in various buffers and upon zeolite encapsulation. *Anal. Chem.* **72**, 5219–5224 (2000).
229. Okuom, M. O., Wilson, M. V, Jackson, A. & Holmes, A. E. Intermolecular interactions between eosin Y and caffeine using ^1H -NMR spectroscopy. *Int. J. Spectrosc.* **245376**, 1–6 (2013).
230. Huang, J., Antonietti, M. & Liu, J. Bio-inspired carbon nitride mesoporous spheres for artificial photosynthesis: photocatalytic cofactor regeneration for sustainable enzymatic synthesis. *J. Mater. Chem. A* **2**, 7686–7693 (2014).
231. Miyatani, R. & Amao, Y. Lactic acid production with lactate dehydrogenase using the visible

-
- light sensitization of zinc porphyrin. *Photochem. Photobiol. Sci.* **3**, 681–683 (2004).
232. Ihara, M., Kawano, Y., Urano, M. & Okabe, A. Light driven CO₂ fixation by using Cyanobacterial photosystem I and NADPH-dependent formate dehydrogenase. *PLoS One* **8**, 1–8 (2013).
233. Korenevsky, A. & Beveridge, T. J. The surface physicochemistry and adhesiveness of *Shewanella* are affected by their surface polysaccharides. *Microbiology* **153**, 1872–1883 (2007).
234. Wang, F., Chen, Y., Liu, C. & Ma, D. White light-emitting devices based on carbon dots' electroluminescence. *Chem. Commun.* **47**, 3502–3504 (2011).
235. Cao, L. *et al.* Carbon dots for multiphoton bioimaging. *J. Am. Chem. Soc.* **129**, 11318–11319 (2007).
236. Cao, L. *et al.* Carbon nanoparticles as visible-light photocatalysts for efficient CO₂ conversion and beyond. *J. Am. Chem. Soc.* **133**, 4754–4757 (2011).
237. Oberto, J. SyntTax: a web server linking synteny to prokaryotic taxonomy. *BMC Bioinformatics* **14**, 1–10 (2013).
238. Korenevsky, A. A., Vinogradov, E., Gorby, Y. & Beveridge, T. J. Characterization of the lipopolysaccharides and capsules of *Shewanella* spp. *Appl. Environ. Microbiol.* **68**, 4653–4657 (2002).
239. Dague, E., Duval, J., Jorand, F., Thomas, F. & Gaboriaud, F. Probing surface structures of *Shewanella* spp. by microelectrophoresis. *Biophys. J.* **90**, 2612–2621 (2006).
240. Edwards, M. J., Fredrickson, J. K., Zachara, J. M., Richardson, D. J. & Clarke, T. A. Analysis of structural MtrC models based on homology with the crystal structure of MtrF. *Biochem. Soc. Trans.* **40**, 1181–1185 (2012).
241. Kouzuma, A., Meng, X.-Y., Kimura, N., Hashimoto, K. & Watanabe, K. Disruption of the putative cell surface polysaccharide biosynthesis gene SO3177 in *Shewanella oneidensis* MR-1 enhances adhesion to electrodes and current generation in microbial fuel cells. *Appl. Environ. Microbiol.* **76**, 4151–4157 (2010).
242. Mills, A., Lawrence, C. & Douglas, P. Photoreduction of water sensitised by Rose Bengal. *J. Chem. Soc., Faraday Trans. 2* **82**, 2291–2303 (1986).
243. Lee, S. H., Nam, D. H. & Park, C. B. Screening xanthene dyes for visible light-driven nicotinamide adenine dinucleotide regeneration and photoenzymatic synthesis. *Adv. Synth. Catal.* **351**, 2589–2594 (2009).
244. Darwent, J. R., Douglas, P., Harriman, A., Porter, G. & Richoux, M.-C. Metal phthalocyanines and porphyrins as photosensitisers for reduction of water to hydrogen. *Coord. Chem. Rev.* **44**, 83–126 (1982).
245. Honda, Y., Watanabe, M., Hagiwara, H., Ida, S. & Ishihara, T. Inorganic/whole-cell biohybrid photocatalyst for highly efficient hydrogen production from water. *Appl. Catal. B* **210**, 400–406 (2017).

-
246. Zumft, W. G. Cell biology and molecular basis of denitrification. *Microbiol. Mol. Biol. Rev.* **61**, 533–616 (1997).
 247. Torres, M. J. *et al.* Nitrous oxide metabolism in nitrate-reducing bacteria: physiology and regulatory mechanisms. *Adv. Microb. Physiol.* **68**, 353–432 (2016).
 248. Du, Z., Li, H. & Gu, T. A state of the art review on microbial fuel cells: a promising technology for wastewater treatment and bioenergy. *Biotechnol. Adv.* **25**, 464–482 (2007).
 249. Kirchhofer, N. D., Rengert, Z. D., Dahlquist, F. W., Nguyen, T.-Q. & Bazan, G. C. A ferrocene-based conjugated oligoelectrolyte catalyzes bacterial electrode respiration. *Chem* **2**, 240–257 (2017).
 250. Berney, M., Hammes, F., Bosshard, F., Weilenmann, H. U. & Egli, T. Assessment and interpretation of bacterial viability by using the LIVE/DEAD BacLight kit in combination with flow cytometry. *Appl. Environ. Microbiol.* **73**, 3283–3290 (2007).
 251. Kokhan, O. *et al.* Bidirectional photoinduced electron transfer in ruthenium(II)-tris-bipyridyl-modified PpcA, a multi-heme *c*-type cytochrome from *Geobacter sulfurreducens*. *J. Phys. Chem. B* **119**, 7612–7624 (2015).
 252. Toseland, C. P. Fluorescent labeling and modification of proteins. *J. Chem. Biol.* **6**, 85–95 (2013).
 253. Dai, Y.-F. *et al.* Effective methods for extracting extracellular polymeric substances from *Shewanella oneidensis* MR-1. *Water Sci. Technol.* **74**, 2987–2996 (2016).
 254. De Windt, W., Aelterman, P. & Verstraete, W. Bioreductive deposition of palladium (0) nanoparticles on *Shewanella oneidensis* with catalytic activity towards reductive dechlorination of polychlorinated biphenyls. *Environ. Microbiol.* **7**, 314–325 (2005).